

University of Southampton Research Repository

Copyright © and Moral Rights for this thesis and, where applicable, any accompanying data are retained by the author and/or other copyright owners. A copy can be downloaded for personal non-commercial research or study, without prior permission or charge. This thesis and the accompanying data cannot be reproduced or quoted extensively from without first obtaining permission in writing from the copyright holder/s. The content of the thesis and accompanying research data (where applicable) must not be changed in any way or sold commercially in any format or medium without the formal permission of the copyright holder/s.

When referring to this thesis and any accompanying data, full bibliographic details must be given, e.g.

Thesis: Pattarinee White (2025) "The Investigation of Energy Harvesting from Electrospun Fibres", University of Southampton, Faculty of Engineering and Physical Sciences, School of Electronics and Computer Science, PhD Thesis, pagination.

Data: Pattarinee White (2025) The Investigation of Energy Harvesting from Electrospun Fibres. URI [dataset]

University of Southampton

Faculty of Engineering and Physical Sciences

School of Electronics and Computer Science

The Investigation of Energy Harvesting from Electrospun Fibres

DOI

by

Pattarinee White

ORCID ID <u>0000-0001-6341-6378</u>

Thesis for the degree of Doctor of Philosophy

April 2025

University of Southampton Abstract

Faculty of Engineering and Physical Sciences
School of Electronics and Computer Science

<u>Doctor of Philosophy</u>

The Investigation of Energy Harvesting from Electrospun Fibres

by

Pattarinee White

Wearable technology is a growing and evolving market. Advanced materials that harvest energy can reduce the need for constant device recharging. In this respect, piezoelectric polymers have great potential for use in wearable technology devices and have many advantages compared to traditional ceramic piezoelectric materials. However, the energy harvesting performance of piezoelectric polymers is not as proficient as that of ceramic piezoelectric polymers.

Triboelectric and ferroelectret energy harvesters are optional for polymer-based energy harvesting devices with higher efficiency compared to piezoelectric energy harvesters.

Triboelectric nanogenerators (TENGs) require materials with a high surface area to improve their efficiency in converting mechanical energy into electrical energy. The increased surface area promotes a greater contact area between the materials, which is essential for maximising charge transfer during the triboelectric effect. This improvement in charge transfer is directly related to the power production and efficiency of the TENGs.

Electrospinning is widely recognised as a highly efficient method for fabricating polymer structures with nanofibrous morphology. This leads to a significant surface area for the confined charge in the electret polymer, which is advantageous for energy harvesting applications. Polyvinylidene Fluoride (PVDF) electrospun fibre is recognised as an excellent performance piezoelectric and triboelectric polymer. The thermal stability of polytetrafluoroethylene (PTFE) ranks among the highest in the negative triboelectric materials series. Polystyrene (PS) increases charge storage in the electret material and exhibits positive surface potential when using the electrospinning technique.

This thesis investigates the development of advanced electrospun fibre structures for energy harvesting applications, focusing on wearable and flexible technology. Energy harvesting devices have gained significant attention as alternatives to conventional batteries, enabling sustainable and lightweight solutions for wearable electronics. The research explores the fabrication and performance evaluation of composite, hollow, and coaxial electrospun fibres, with an emphasis on their triboelectric and ferroelectret properties.

Composite electrospun fibres of PTFE/PVDF were fabricated using a one-step electrospinning technique. The optimised composition demonstrated a substantial enhancement in triboelectric energy harvesting performance, achieving a power density of 348.5 mW/m². Practical applications, such as shoe insoles and book-shaped energy harvesters, showcased the material's potential in wearable technology.

Hollow structure PVDF fibres were produced using a novel one-step coaxial electrospinning method. This design significantly improved piezoelectric properties, achieving a maximum

power density of 2.18 mW/m² compared to the solid structure of electrospun PVDF. However, the experimental results might be insufficient to indicate the working principle of ferroelectret-based energy harvesters.

Coaxial fibres with PS as the core and PVDF as the shell were developed using a single-nozzle technique. This structure exhibited remarkable triboelectric performance, achieving a power density of 6.27 W/m². Practical demonstrations included efficient capacitor charging and the illumination of LEDs, underscoring the feasibility of this approach for scalable energy harvesting systems.

The research contributes to the growing field of energy harvesting by introducing innovative materials and structures, enhancing power densities, and expanding the applicability of electrospun fibres. These findings lay the groundwork for further advancements in sustainable, high-performance energy harvesting technologies for wearable devices.

Table of Cont	ents4
Table of Table	s9
Table of Figur	es 10
Research The	sis: Declaration of Authorship17
Acknowledge	ments 18
Definitions an	d Abbreviations19
Chapter 1 In	troduction 21
1.1 Introduc	tion and Research Motivation21
1.2 The rese	arch objectives24
1.3 Thesis s	tructure25
1.4 Stateme	ent of novelty25
1.5 Publicat	ions and conferences26
-	terature reviews, background theory of harvesting energy from
el	ectrospun fibres 28
2.1 Introduc	tion28
2.2 Mechan	ical energy harvesting from polymers28
2.2.1 Piez	oelectric effect29
2.2.1	.1 Piezoelectric effect in polymer30
2.2.1	.2 Piezoelectric properties of Ferroelectrets/ theory of Ferroelectret
	and mechanism31
2.2.1	.3 Typical ferroelectret material and applications34
2.2.2 Trib	oelectric effect34
2.2.2	2.1 Typical triboelectric effect and fundamental operation mode of
	TENGs34
2.2.2	2.2 Triboelectric series35
2.2.2	2.3 Triboelectrification in polymer44
2.3 Electros	pinning techniques and parameters46

	2.3.1	Effect of electrospinning parameters4!
		2.3.1.1 Polymer solution parameters49
		2.3.1.2 Processing conditions52
		2.3.1.3 Ambient parameters54
	2.3.2	Coaxial electrospinning and control parameters54
		2.3.2.1 Technology and Control for the Coaxial or Core-Shell Structures .5.
	2.3.3	The compound Taylor cone and the parameter for coaxial electrospinning.5
	2.3.4	Hollow fibre preparation5
		2.3.4.1 Template coaxial electrospinning approach5
		2.3.4.2 One-step hollow fibre approach62
	2.3.5	Co-electrospinning of core-shell fibres using a single-nozzle technique64
	2.3.6	Charge trapped behaviour in electrospun fibre mechanism6
2.4	Pol	mers used in this work6
	2.4.1	Polyvinylidene fluoride (PVDF)6
	2.4.2	Polystyrene (PS)70
	2.4.3	Polytetrafluoroethylene, (PTFE)7
2.5	The	state-of-the-art72
	2.5.1	Nature of TENG research72
	2.5.2	Energy harvesting from composite fibre79
	2.5.3	Ferroelectret from electrospun hollow fibre83
	2.5.4	Energy harvesting from the core-shell structure fibre8
2.6	Cor	clusion8
Cha	pter 3	Experimental process, materials, and methods 89
3.1	Intr	duction89
3.2		erials, equipment and fabrication89
		Materials and chemicals for electrospinning preparation89
		Electrospinning setup9
		Equipment for characterisation9

		3.2.3.1	Fourier-transform infrared spectroscopy (FTIR)	90
		3.2.3.2	Scanning electron microscope (SEM)	91
		3.2.3.3	Transmission electron microscopy (TEM)	92
		3.2.3.4	X-ray diffraction (XRD)	92
		3.2.3.5	Surface potential testing	92
		3.2.3.6	Piezometer	94
		3.2.3.7	Tapping test setup	95
		3.2.3.8	Voltage and current measurement for Triboelectric mode	95
3.3	Со	nclusion.		96
Cha	pter 4	4 Energ	y harvesting performance of composite electrospun f	ibre 98
4.1	Inti	roduction	· · · · · · · · · · · · · · · · · · ·	98
4.2			PTFE in the controlled PVDF fibre	
			etion	
			s and Methods	
		4.2.2.1	Electrospinning Preparation	99
		4.2.2.2	Test Assembly and Protocol	99
	4.2.3	Results	and Discussion	
	4.2.4	Conclus	sion of the additive PTFE in the controlled PVDF fibre	104
4.3	Со	ntrolling	the overall polymer concentration experiment	104
	4.3.1	Introduc	etion	104
	4.3.2	Material	s and Methods	105
		4.3.2.1	Electrospinning Preparation	105
		4.3.2.2	Fibre characterisation	106
		4.3.2.3	Electromechanical characterisation	106
	4.3.3	Results	and discussion	107
		4.3.3.1	Morphological analysis	107
		4.3.3.2	Structural analysis	109
		4.3.3.3	Electromechanical study	111

	4.3.4	Conclus	sion of controlling the overall polymer concentration experiment.	117
4.4	Coi	nclusion	S	119
Cha	pter	5 Energ	y harvesting performance from the hollow and coaxial	
		electi	rospun fibres	120
5.1	Inti	oduction	1	120
5.2	. The	energy l	narvesting from the hollow structure electrospun fibre	120
	5.2.1	Introduc	ction and research motivation of hollow PVDF electrospun fibre	120
	5.2.2	Experim	ents	122
		5.2.2.1	Fabrication of electrospun hollow fibre structure	122
		5.2.2.2	Geometrical and structural characteristics	124
		5.2.2.3	Electromechanical characteristics	125
	5.2.3	Results	and discussion	125
		5.2.3.1	The geometrical characteristics	125
		5.2.3.2	The electromechanical characteristics	126
	5.2.4	Conclus	sion from the energy harvesting from the hollow fibre structure	129
5.3	Ene	ergy harv	esting performance from the coaxial electrospun fibres	130
	5.3.1	Introduc	ction and research motivation	130
	5.3.2	Experim	ental procedure	131
		5.3.2.1	Electrospun fibre preparation	131
		5.3.2.2	Electrospun fibre characteristics	132
		5.3.2.3	The electromechanical study	132
	5.3.3	Results	and discussion	133
		5.3.3.1	Morphology and structure characterisation	133
		5.3.3.2	Electromechanical properties and energy harvesting performance	се
				142
		5.3.3.3	Surface potential results from the distinguished charges	4.40
	E 0.4	Const	experiment	146
	ა.ა. 4		sion of the energy harvesting performance from the core-shell re PS/PVDF electrospun fibre	148
				-

5.4	4 Cor	nclusion	. 149
Cha	apter 6	6 Conclusion and Future Works	.150
6.	l Cor	nclusion	. 150
6.2	2 Fut	ure works	. 152
	6.2.1	Further investigation of the energy harvesting performance	152
	6.2.2	Further work on wearable devices	153
App	endix	A Publications	.154
Glo	ssary	of Terms	.178
Bib	liogra	phy	.179

Table of Tables

Table of Tables

Table 1.1	The comparison of energy narvesting technology from mechanical energy 23
Table 1.2	List of publications and conferences
Table 2. 1	Triboelectric series of materials and their triboelectric charge density (TECD) proposed by Zou et al. (2019) [63] . Copyright 2019, Nature Research37
Table 2. 2	A summary of the production of the produced electrospun hollow fibres.60
Table 2. 3	A summary of the production of the electrospun hollow fibres63
Table 2. 4	A summary of the research using a single nozzle technique to produce the coaxial electrospun fibres
Table 2.5	The summary of TENG using electrospinning techniques73
Table 2. 6	Summary of the filler used in electrospinning technique for TENGs76
Table 2. 7	The comparison of the electrospun fibre of non-polar polymers85
Table 4. 1	Crystallinity index obtained from XRD110
Table 4. 2	Summary of the electromechanical characteristics of the sample 115
Table 5. 1	Summary of the average diameter, core and shell layer of the coaxial PS/PVDF fibres
Table 5. 2	The crystallinity index of β -phase PVDF as calculated from XRD and FTIR spectra
Table 5. 3	Summary of the electromechanical characteristics of the samples 145

Figure 1.1	Amount of power generated by human activity. Reproduced from Zeng et al.,
	2014 [27]. Copyright 2014, John Wiley & Sons, Inc
Figure 2. 1	Schematic diagram showing the piezoelectric effect in different types of
	polymers; bulk piezopolymers: are divided into amorphous and semi-
	crystalline polymers, piezoelectric particles in polymer or polymer composites
	31
Figure 2. 2	a) the schematic of ferroelectret material where $P_{\text{\tiny S}}$ is the polarisation direction,
	b) the hysteresis loop in a single pore ferroelectret. Reproduced from Zhang et
	al. (2019) [56]. Reprinted with permission from Šutka et al. (2023) [57].
	Copyright 2017, Elsevier32
Figure 2. 3	a) Ferroelectric PVDF and b) a simple model for piezoelectricity in ferroelectric
	materials (positively and negatively charged particles that are connected by
	springs having force constants of k_1 and k_2) in the unit of N/m and c)
	ferroelectret PP (the clear ellipsoidal areas are gas bubbles and the dark area is
	the polymer matrix). Reproduced from Mohebbi et al. (2018) [55], Copyright
	2016, John Wiley & Sons, Inc
Figure 2. 4	A commonly used Triboelectric series based on Diaz et al.'s work, reproduced
	by Lee et al. [63]. Reprinted © Copyright 2023 AIP36
Figure 2. 5	TENG in contact mode - TENG in sliding mode a) and b) dielectric to dielectric
	contact mode TENG, c) and d) conductor to dielectric sliding mode.
	Reproduced from Zhang et al. (2020) [66] under CC BY and Copyright 2023
	Walter de Gruyter GmbH39
Figure 2. 6	the design of partial elastic bellow–type triboelectric nanogenerator as a partial
	book-shaped like model a) Schematic illustrating a simplified structure of
	book-shaped TENGs b) the working mechanism of the book-shaped like model
	c) simulation results for the electrical potential distribution for the different
	angles between two electrodes, using COMSOL as studied by J. Chung et al.
	2016 [68] Copyright Elsevier Ltd. 2015
Figure 2. 7	Illustration demonstrating the simplified electrical arrangement when different
	materials come into contact. a) The first scenario involves two metals, where
	the lower energy metal can accommodate an electron from the higher energy

- Figure 2. 10 Four main factors that can affect the electrospinning process................48
- Figure 2. 12 A schematic of coaxial electrospinning......55
- Figure 2. 14 SEM image of the electrospun TiO₂ fibres fabricated by D. Li and Y. Xia 2004. a) the TiO₂/PVP hollow fibres prepared by a coaxial electrospinning technique, b) the TiO₂/PVP fibres with the oil phase inside the bead formation. Reprinted from

	Li and Xia (2004) [92]. Copyright 2006-2023 Scientific Research Publishing Inc.
Figure 2. 15	5 A model of a) single fibre, b) coaxial fibre, c) hollow fibre, and d) a technique for
	producing hollow fibre61
Figure 2. 16	Schematic illustration of Li and Xia setup, the SEM images proved the obtained
	hollow structure. Reprinted from Li and Xia (2004) [92]. Copyright 2023 American Chemical Society61
	·
Figure 2. 17	The SEM image of the hollow nanotubes produced by the one-step hollow fibre
	approach in the random orientation. The first was proposed by Loscertales et
	al. in 2004. Reprinted from Loscertales et al. (2004) [93]. Copyright by 2023
	American Chemical Society62
Figure 2. 18	Coaxial electrospinning using a single-nozzle technique. Reproduced based on
	Bazilevsky et al.'s work [99]. Copyright 2023 American Chemical Society.65
Figure 2. 19	Schematics describe the type of charge in corona charged and electrospun
	fibre explained by Gao et al. (2020). Reprinted from Gao et al. (2020) [112],
	Copyright 2020 Elsevier B.V68
Figure 2. 20	The main phase of PVDF and the beta phase are induced by stretching and a
	high-voltage poling process69
Figure 2. 21	Energy harvesting from mechanical energy regime in PVDF69
Figure 2. 22	Polystyrene chemical structure. Reproduced from Merrington (2017) Copyright
	by 2017 Elsevier Inc70
Figure 2. 23	The polymer structure of PTFE. Reprinted from Keng et al. (2022) [126].
	Copyright by 2023 Elsevier B.V71
Figure 2. 24	Schematics of the theoretical energy harvesting model of the as-electrospun
	polystyrene fibre mat setup of Yuya led research group, a) $h=h_0$, b) $h>0$, and C)
	$h{\le}~0$ d)- f) Schematic of the measurement flow of $\Delta Qouthand~h:$ d) h=h0 e) h>0,
	and f) h \leq 0, g) Microscope image of the electrospun PS. Reprinted from Ishii
	and Kurihara, 2019 [175], Copyright 2023 AIP84
Figure 2. 25	The proposed concept of the bead-like lens hollow fibre for ferroelectret fibre
	applications a) bead-less fibres with a perfectly rearranged model b) a bead
	lens-like shape fibre model86

Figure 2. 26	S Schematic show the idea of coaxial PS/PVDF electrospun fibre87
Figure 3. 1	a) The photograph and, b) the schematic of the electrospinning setup used in this work90
Figure 3. 2	Working principle of FTIR. Reprinted from Introduction to Fourier Transform Infrared Spectrometry (2001) [186]. Copyright 2001 Thermo Nicolet Corporation
Figure 3. 3	The setup for static potential testing, a) the corona charge equipment, b) the setup of static measurement before and after the corona charge in the study of the hollow PVDF electrospun fibre under the assumption of being ferroelectret-based
Figure 3. 4	Discharge chamber setup94
Figure 3. 5	The schematic of assembling the cell for the tapping test95
Figure 3. 6	a) The experimental setup for the tapping test b) diagram of voltage divider circuit96
Figure 4. 1	SEM images of the single PTFE/PVDF electrospun fibre with the diameter distribution curve prepared by control PVDF at 18% a) PTFE 0%, b) PTFE 1 %wt, c) PTFE 2 %wt, d) PTFE 3%wt, e) PTFE 4%wt
Figure 4. 2	a) PTFE/PVDF fibre mats after the electrospinning process of the 4%wt PTFE in the PVDF sample; b) the schematic of the book-shaped assembly for the testing cell PTFE/PVDF fibre sandwich with electrodes; c) the compression test rig; d) voltage output from constantly tapping the booked-shaped PTFE/PVDF fibre assembly at different PTFE concentrations of 0, 1, 2, 3, and 4%wt., respectively
Figure 4. 3	a) The schematic of the improved triboelectric harvester design with added nylon fabric, b) 95 LED lights were illuminated via tapping the harvester with the PTFE/PVDF electrospun fibres as the acceptor and nylon fabric as the donor material, c) the voltage output of the triboelectric assembly without nylon fabric, d) the voltage output of the triboelectric assembly after introducing nylon fabric the charging profile, e) voltage vs. time of the PTFE/PVDF fibre device without nylon fabric, f) the charging profile after introducing nylon fabric.
	103

Figure 4. 4 The flow chart describes the PTFE/PVDF electrospun fibre preparation.105

Figure 4. 5	a) Schematic of PTFE/PVDF triboelectric assembly and testing, b) working
	principle in contact standing mode and c) corresponding with the
	measurement of short circuit current107
Figure 4. 6	The SEM images (operated at 10 kV) of the single PTFE/PVDF fibre with fibre size
	distribution curve prepared by different PTFE/PVDF ratios a) PTFE0/PVDF100, b)
	PTFE5/PVDF95, c) PTFE10/PVDF90, d) PTFE15/PVDF85, e) PTFE20/PVDF80, f)
	PTFE25/PVDF75, g) PTFE30/PVDF70 and h) PTFE35/PVDF65108
Figure 4. 7	TEM images were measured at acceleration voltage of 100 kV, filament voltage
	of 25 kV for a single PTFE20/PVDF80 fibre, which was coated on the mesh
	copper grids at magnification a) 7000x, b) 25000x109
Figure 4. 8	a) FTIR-ATR spectra of PTFE/PVDF electrospun fibre. The measurements were
	carried out at room temperature over the range of 600-1400 cm ⁻¹ b) XRD
	spectra of the single PTFE/PVDF electrospun fibre. The analyses were
	conducted on samples using Cu- $K\alpha_1$ radiation 1.5406 Å, 40 kV and 25 mA, Step
	size 0.5111
Figure 4. 9	a) open circuit voltage was tested over 100 $M\Omega$ resistor and b) short circuit
	current of the PTFE/PVDF electrospun fibre prepared at different
	concentrations112
Figure 4. 10	a) peak open circuit voltage (V_{oc}) and peak to peak short circuit current (I_{sc}) v.s.
	load resistance test, b) calculated power and power density of the
	PTFE20/PVDF80 over different resistances, c) V_{oc} and, d) I_{sc} of PTFE20/PVDF80
	at different tapping frequencies
Figure 4. 11	a) Schematic of the book-shaped triboelectric energy harvester used to charge
	the capacitors; b) the voltage across 0.1, 0.47, and 1, capacitors, when
	charged by the book-shaped energy harvester at 6 Hz over a 90s period; c)
	schematic of the hand tapping test during the testing of the 100 LED lights
	experiment; d) the 100 LED lights illuminated via hand tapping of the book-
	shaped PTFE/PVDF energy harvester116
Figure 4. 12	The triboelectric insole for a demonstration of human gait energy harvesting a)
	the photo and schematic of the shoe insole used in this study b) the photo
	when charging the capacitor when running on the treadmill c) the voltage
	across the 1 μF capacitor, when charged by running on the PTFE20/PVDF80
	insole over a 60s period d) the comparison of the voltage across the 1 µF

capacitor, when running and walking on PTFE20/PVDF80 and PVDF insole over

	a 60s period117
Figure 5. 1	The schematic of electrospinning apparatus to fabricate hollow fibre structure
Figure 5. 2	Hollow structure formation in a one-step electrospun hollow fibre technique
Figure 5. 3	a) and b) the SEM images of the electrospun partial hollow PVDF fibre c) the FTIR spectra of the solid and partial hollow PVDF electrospun fibres d) the XRD pattern of the partial hollow PVDF electrospun fibre
Figure 5. 4	Surface potential of hollow structure PVDF after electrospinning, after left in the environment for 14 days, and after corona charge for 14 days 127
Figure 5. 5	The maximum absolute piezoelectric coefficient value of the coaxial PVDF measured from PiezoMeter PM-300
Figure 5. 6	a) Schematic of the testing sample for tapping test, b) the setup of tapping rig during tapping test, c) the open circuit output voltage of solid PVDF and partial hollow PVDF electrospun fibres
Figure 5. 7	a) The flow chart of coaxial PS/PVDF electrospun fibre preparation, b) model of the coaxial PS/PVDF electrospun fibre where PS is the core and PVDF is the shell fibre
Figure 5. 8	SEM images show the structure and morphology of the PS/PVDF electrospun fibres
Figure 5. 9	TEM images of the coaxial PS/PVDF electrospun fibre136
Figure 5. 10	PS-PVDF solutions and colloid layer138
Figure 5. 11	The FTIR result of the suspended layer in PS/PVDF solution
Figure 5. 12	Chemical composition of the Coaxial PS/PVDF fibre141
Figure 5. 13	3 XRD pattern of the coaxial PS/PVDF electrospun fibre at various ratios of polymer solutions
Figure 5. 14	a) Schematic of PS/PVDF triboelectric assembly and testing, b) working principle in contact standing mode, c) corresponding with the measurement of short circuit current, d) open circuit voltage and e) short circuit current of the

	coaxial PS/PVDF electrospun fibre at various concentrations during the tapping
	test. The result was collected at the tapping frequency of 6 Hz143
Figure 5. 15	ia) open circuit voltage (V_{oc}) and b) short circuit current (I_{sc}) obtained from the
	book-shaped PS16/PVDF12 assembly c) V_{oc} and I_{sc} v.s. load resistance test, d))
	V_{oc} and I_{sc} of the book-shaped PS16/PVDF12 assembly at different tapping
	frequencies144
Figure 5. 16	a) Schematic of book-shaped triboelectric energy harvester on charging
	capacitor testing b) the voltage output over the capacitor 0.22, 0.47, 1, 10, 33
	and 100 μF , respectively, during the charging capacitor testing of the
	PS16/PVDF12 assembled with the book shaped energy harvester c) the
	schematic of the hand tapping test during the testing of the 100 LED lights
	experiment d) the 100 LED lights illuminated via hand tapping of the book
	shaped like PS16/PVDF12 energy harvester146
Figure 5. 17	the bar charge presents the surface potential after electrospinning of sample
	PS10/PVDF18, PS12/PVDF16, PS14/PVDF14, PS16/PVDF12, and PS18/PVDF10
	147
Figure 5. 18	The bar chart presents the surface potential before discharge in the discharge
	chamber and after the rubbing test to build up a triboelectric charge of the
	electrospun PVDF, PS and coaxial PS/PVDF, respectively

Research Thesis: Declaration of Authorship

Research Thesis: Declaration of Authorship

Print name: Pattarinee White

Title of thesis: The Investigation of Energy Harvesting from Electrospun Fibres

I declare that this thesis and the work presented in it are my own and has been generated by me as the result of my own original research.

I confirm that:

- This work was done wholly or mainly while in candidature for a research degree at this University;
- 2. Where any part of this thesis has previously been submitted for a degree or any other qualification at this University or any other institution, this has been clearly stated;
- 3. Where I have consulted the published work of others, this is always clearly attributed;
- 4. Where I have quoted from the work of others, the source is always given. With the exception of such quotations, this thesis is entirely my own work;
- 5. I have acknowledged all main sources of help;
- 6. Where the thesis is based on work done by myself jointly with others, I have made clear exactly what was done by others and what I have contributed myself;
- 7. Parts of this work have been published as listed in Section 1.5:

Signatura	
oignature.	

Acknowledgements

First and foremost, I would like to express my deepest appreciation to my PhD project supervisor, Professor Steve Beeby, for this opportunity. It is such a great honour to be a student under his supervision. I learned a lot from his research vision and life experience. Dr Mohamed Torbati and Dr Dmitry Bavykin, the second supervisors, for organising the experiments in the laboratory, including the electrospinning machine. In addition, their research ideas and coaching are always excellent. Without their assistance, trust and understanding during hard times and through the pandemic, this research project would never have been accomplished. Furthermore, this endeavour would not have been possible without Prof. Neil White and Prof. Sohini Kar-Narayan, the examiners, for an intellectually stimulating viva.

I would like to acknowledge the Royal Thai Government Scholarship and Rajamangala University of Technology Krungthep for providing me with an academic scholarship to fund all my expenses while I was studying.

Also, all of the SEMS group members, especially Dr Abiodun Komolafe, Dr Sheng Yong and Dr Junjie Shi, for their support, insights and general discussions.

I sincerely thank Dr Piyapong Pankaew for his assistance with the scanning electron microscope and X-ray diffraction analyses during the pandemic lab closure in the UK and for all the backup equipment for measurement in Thailand.

I want to thank my parents and sister for their understanding and emotional support.

The White family members made my life in the UK feel like home because of all their support, pleasure, and joy.

In appreciation of his sacrifice, maturity, patience, kindness, and support, I dedicate this degree to my beloved husband, Dr Alan White. My journey without him would have never been meaningful—special thanks for the brilliant mechanical work and academic proofreading.

Definitions and Abbreviations

AgNW Silver Nanowire

BTO Barium titanate

CNT Carbon Nanotube

CB Carbon Black

CE Contact electrification

CS Contact-Separation mode

DMAc...... Dimethylacetamide

DMF...... Dimethylformamide

DMSO Dimethyl sulfoxide

DOS...... Density of states

EC Ethyl cellulose

FEGs..... Ferroelectret generators

FT Free standing

GO...... Graphene Oxide

HFIP Hexafluoroisopropano

I_{sc}......Short circuit current

LS Lateral sliding

LUMO Lowest unoccupied molecular orbital

MoS₂..... Molybdenum disulfide

MWCNT Multi-walled carbon nanotubes

Nylon 6 Polycaprolactam

PA6......Polyamide-6

PAN Polyacrylonitrile

PEG Polyethylene glycol

PEGs..... Piezoelectric generators

PEO Polyethylene oxide

Definitions and Abbreviations

PET Polyethylene terephthalate PHBV Poly(3-hydroxybutyrate-co-3-hydroxyvalerate) PI..... Polyimide PLA..... Polylactic Acid PLLA Poly(L-lactic acid) PMMA Poly(methyl methacrylate) POPolyolefin PP......Polypropylene PS......Polystyrene PTFEPolytetrafluoroethylene PU Polyurethane PVA..... Polyvinyl alcohol PVC Polyvinyl chloride PVDF Polyvinylidene fluoride PVDF-HFP......Poly(vinylidene fluoride-co-hexafluoropropylene) PVDF-TrFE Poly(vinylidene fluoride-co-trifluoroethylene PVP......Polyvinylpyrrolidone SEBS......Styrene-Ethylene-Butylene-Styrene SE......Single electrode SF......Silk Fibroin SWCNTs Single-walled carbon nanotubes THF..... Tetrahydrofuran TPU......Thermoplastic Polyurethane

Chapter 1 Introduction

1.1 Introduction and Research Motivation

Wearable technology relates to an electronic device that can be worn, embedded, or implanted in the user. Wearable technology devices are a rapidly growing market predicted to be worth \$70 billion (55.6 billion GBP) by 2025 [1]. This rapid adoption amongst users has placed wearable technology at the cutting edge of the Internet of Things (IoTs). Such technology can include clothing, watches, hats, and glasses. These devices work through the cooperation and relationship between materials, electronics, and computers. Advances in technology, resulting in greater functionality, have created a situation whereby various mobile devices require charging on an almost daily basis. Smart electronic devices with a self-powered sensor or their own energy source can make life easier for the user by avoiding the need to recharge in the absence of a power outlet [2]. The alternative of a larger battery may cause issues for users who need to carry various electronic devices for long periods of time. For example, military personnel, hikers, climbers, and trail runners need to keep weight to a minimum and may find larger batteries to be an added burden. Therefore, energy harvesting devices have been studied as an energy substitute for batteries or other primary energy sources for self-powered sensors [3-4].

Energy harvesting is a promising area that attempts to capture and transform ambient energy from a variety of sources into useful electricity. This technique is especially useful for powering low-energy equipment like wireless sensors and communication systems, such as when battery replacement is impossible. The basic sources of energy for harvesting include kinetic [5-7], solar [8-9], thermal [10-13], and chemical [14], energy, each with unique properties and potential power outputs [15].

Mechanical energy appears to be a suitable power source for wearable devices connected to the human body. This type of energy creation is possible through foot, knee, hip, and elbow movements in active people. Energy captured from mechanical movement has been shown to be an effective source for conversion to electrical energy. The amount of energy captured from the human body can be seen in Figure 1.1. Piezoelectric [16-17], electromagnetic [18-19], and triboelectric [20-24], approaches are among the most promising, with each offering distinct benefits in terms of efficiency and scalability. These technologies transform mechanical energy from human motion into electrical energy, ensuring a constant power supply for wearable devices. Table 1.1 reviews the comparison of energy harvesting technology from mechanical

energy for piezoelectric, electromagnetic and triboelectric devices in terms of mechanism, efficiency and scalability from the human body.

Piezoelectric and triboelectric devices are often more efficient than electromagnetic systems, especially in small-scale applications [25-26]. Research and development of piezoelectric polymer material have played a significant role in harvesting energy from mechanical movement. Piezoelectric polymer is breathable, flexible and lightweight, making it suitable for wearable technology applications. In addition, it is easier to recycle when compared to ceramic piezoelectric materials.

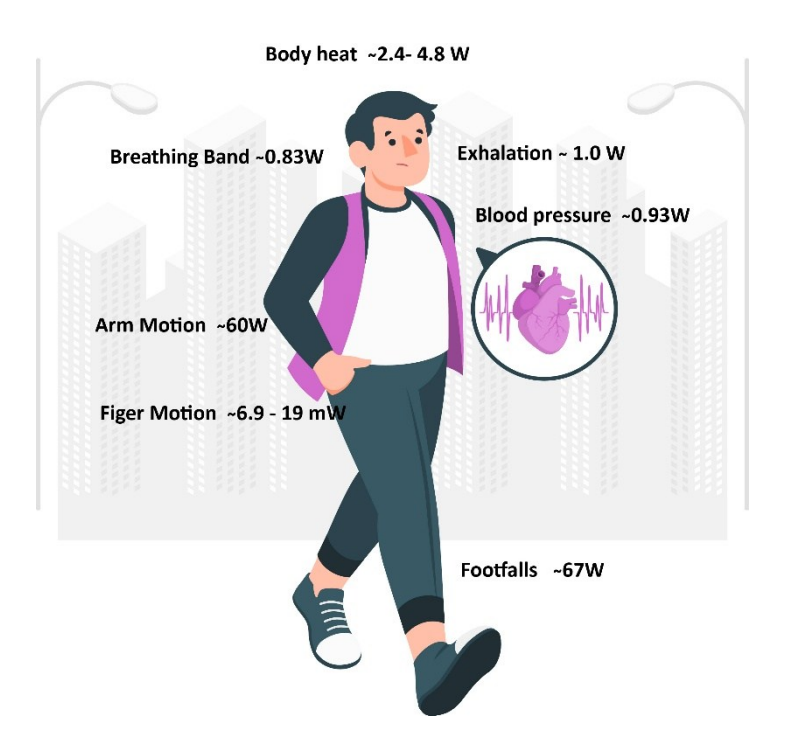


Figure 1.1 Amount of power generated by human activity. Reproduced from Zeng et al., 2014 [27]. Copyright 2014, John Wiley & Sons, Inc.

Table 1.1 The comparison of energy harvesting technology from mechanical energy

	Piezoelectric	Electromagnetic	Triboelectric
	[25-26], [28]	[26], [29-30]	[25], [31]
Mechanism	Uses piezoelectric	Uses the movement of a	Using the triboelectric
	material to convert	magnet across a coil to	effect, electricity is
	mechanical force into	produce electricity	generated by contacting
	electrical charge		and separating various
			materials
Efficiency	High efficiency in	Generally lower than	High potential efficiency
	converting mechanical	piezoelectric	due to a variety of
	energy, particularly in	technologies, but can be	material combinations
	dynamic contexts like	optimised with improved	and surface area
	walking or running	coil designs	increases
Scalability	Thin-film piezoelectric	More challenging to	Highly scalable, with the
	materials are available,	miniaturise than	potential for
	making them suitable for	piezoelectric systems,	incorporation into
	incorporation into	but provides solid	numerous wearable
	compact, flexible	performance in larger	forms, thanks to flexible
	devices	devices	material possibilities

Triboelectric devices offer the most potential for scalability due to their adaptable material alternatives and ease of integration into various wearable designs [25], [32]. This makes triboelectric energy harvesters gain interest among researchers around the world. The outstanding output and easy assembly mean triboelectric generators can be applied to small devices, especially with wearable technology. This technology is highly dependent on the triboelectric charge transfer from the different types of triboelectric material. The surface modification of such technology plays an important role and has recently gained interest among researchers [33-34], in order to enhance the surface area of the material.

Electrospinning is well known as an effective technique for producing a nanofibrous polymer structure. The strong electric field during the electrospinning process could arrange dipole moment in polar polymers such as poly(vinylidene fluoride) PVDF [35], poly(vinylidene fluoride-co-trifluoroethylene) PVDF-TrFE [23], and poly(L-lactic acid) PLLA [36]. This results in a high surface area for the trapped charge in the electret polymer, which can be useful for various

energy harvesting applications based on piezoelectric, ferroelectret, and triboelectric energy harvesters.

Significant electrospinning techniques in developing triboelectric nanogenerator for wearable devices

Electrospinning techniques have become important in further developing triboelectric nanogenerators (TENGs) for wearable devices, offering a diverse and efficient approach to producing nanofibers with excellent features. These strategies increase the performance and utility of TENGs in wearable electronics by enhancing flexibility, surface area, and energy conversion efficiency. Incorporating electrospinning in TENG production is essential for the next phase of wearable technology, allowing the development of functional and adaptive materials for human motion. The electrospinning technique produces nanofibres with a large specific surface area, enhancing the contact area and, consequently, the energy output of TENGs [37]. The technique can integrate various materials, including polyvinylidene fluoride (PVDF) and barium titanate (BTO), to improve triboelectric performance via enhanced polarisation and phase content [38]. Electrospun fibres demonstrate excellent elasticity and mechanical resilience. This is crucial for wearable applications that require materials that can survive repeated mechanical stress [39]. In addition, it can convert low-frequency mechanical energy into electrical energy, hence addressing the power supply issues of wearable electronics [38]. Although electrospinning presents several benefits in advancing TENGs for wearable devices, issues persist in optimising material combinations and structural designs to enhance energy production and efficiency. Ongoing research and innovation in this field are essential to overcome these challenges and fully exploit the potential of electrospun TENGs in sustainable, high-performance wearable technologies.

This research aims to fabricate, demonstrate, and investigate energy harvesting using electrospinning techniques such as composite, core-shell structure, and hollow structure fibre. The findings of this research will aid the study of energy harvesting for wearable technology, where a flexible, lightweight, biocompatible, and environmentally friendly material is required.

1.2 The research objectives

- 1. To fabricate the composite structure of PTFE/PVDF using an electrospinning technique
- 2. To demonstrate energy harvesting potential from the composite PTFE/PVDF electrospun fibre
- 3. To fabricate the hollow structure of PVDF using an electrospinning technique

- 4. To demonstrate energy harvesting potential from the hollow PVDF electrospun fibre
- 5. To fabricate the coaxial structure of PS/PVDF using an electrospinning technique
- 6. To demonstrate energy harvesting potential from the electrospun PS/PVDF fibre
- 7. To investigate, analyse, and study the possibility of fabricating wearable devices by using the composite PTFE/PVDF, hollow structure PVDF and PS/PVDF coaxial structure electrospun fibres as an energy harvesting part

1.3 Thesis structure

This thesis is structured into 6 chapters; Chapter 1 provides an overview of the research motivation, objectives, and scope and introduces the importance of wearable technology and energy harvesting solutions. The outlines of the thesis objectives, novelty, and the broader implications of the research are also shown in this chapter.

Chapter 2 discusses the theoretical background of mechanical energy harvesting and key concepts such as piezoelectric, ferroelectret, and triboelectric effects. It reviews the state-of-the-art electrospinning techniques and polymers used for energy harvesting to highlight research gaps and sets the stage for experimental investigations.

Chapter 3 details the materials, experimental setups, and characterisation techniques used to fabricate and evaluate the electrospun fibres. This also introduces methods for analysing fibre properties.

Chapter 4 presents the fabrication of PTFE/PVDF composite fibres and evaluates their triboelectric performance, demonstrates practical applications, including book-shaped energy harvesters and shoe insoles.

Chapter 5 explores the fabrication and characterisation of hollow PVDF fibres and coaxial PS/PVDF fibres and their superior triboelectric energy harvesting capabilities.

Chapter 6 summarises the key findings and contributions of the thesis. The idea of future work to enhance material performance and expand practical applications in wearable technology is proposed.

1.4 Statement of novelty

This study presents novel methods and materials for energy harvesting through electrospun fibres in Chapters 4 and 5. This study examines the practical uses of the new materials, focusing

on wearable and flexible energy harvesters that exhibit enhanced power densities and compatibility with lightweight, biocompatible designs. The innovations of each work can be described as follows:

- 1. The composite electrospun PTFE/PVDF fibres were fabricated using a one-step electrospinning process, resulting in improved triboelectric energy harvesting capabilities. This method simplifies the manufacturing process while enhancing the material's electromechanical properties.
- 2. Production of hollow PVDF electrospun fibres: A unique one-step coaxial electrospinning technique was utilised to fabricate hollow PVDF fibres. This design markedly improves the piezoelectric efficacy and energy harvesting capability of the material, especially for wearable applications.
- 3. This study introduces the manufacturing of coaxial fibres comprising a PS core and a PVDF shell by a single-nozzle electrospinning technique. This method illustrates the capacity to enhance energy harvesting efficiency by utilising the unique triboelectric characteristics of the two materials.

Publications and conferences 1.5

Table 1.2 List of publications and conferences

Title

Publication/conference

The Energy Harvesting Performance of	White, P.; Bavykin, D.; Moshrefi-Torbati, M.; Beeby, S.
a Flexible Triboelectric-based	The Energy Harvesting Performance of a Flexible
Electrospun PTFE/PVDF Fibre [40]	Triboelectric-Based Electrospun PTFE/PVDF Fibre.
	Eng. Proc. 2023, 30, 8.

The Fabrication of the Electrospun Structure Fibre for Energy Harvesting Applications [41]

White, P.; Pankaew, P.; Bavykin, D.; Moshrefi-Torbati, Polyvinylidene Fluoride (PVDF) Hollow M.; Beeby, S. The Fabrication of the Electrospun Polyvinylidene Fluoride (PVDF) Hollow Structure Fibre for Energy Harvesting Applications. 2024 International Electrical Engineering Congress (iEECON 2024) March 6-8, 2024, Pattaya Chonburi, THAILAND https://doi.org/10.1109/iEECON60677.2024.10537826

https://doi.org/10.3390/engproc2023030008

Publication/conference

The Investigation of the Energy
Harvesting Performance Using
Electrospun PTFE/PVDF Based on a
Triboelectric Assembly [42]

White, P., Pankaew, P., Bavykin, D. V., Moshrefi-Torbati, M., & Beeby, S. P. (2024). The investigation of the energy harvesting performance using electrospun PTFE/PVDF based on a triboelectric assembly. *Smart Materials and Structures*. 33 075010

https://doi.org/10.1088/1361-665X/ad508d

Chapter 2 Literature reviews, background theory of harvesting energy from electrospun fibres

2.1 Introduction

The main purpose of this research is to investigate energy harvesting from electrospun fibre. To understand the mechanism of electrical energy from the material obtained from the electrospinning technique, the researcher must understand the nature of porous polymer film and the relevant charge effect/behaviour. Thus, this chapter examines and discusses relevant concepts related to this study. First, it discusses the parts utilised for mechanical energy harvesting and the significance of obtaining energy from a source. The use of piezoelectric material as an energy harvester is then discussed. Thirdly, the discussion turns to electret or ferroelectret energy and its mechanism. The triboelectric effect is presented as an energy harvester working concept. The basic electrospinning knowledge is presented, followed by the polymers used in the research. The literature review and research gap are then presented in the final part of the chapter.

2.2 Mechanical energy harvesting from polymers

Energy gathering from external sources, including mechanical, thermal, solar, wind, electromagnetic, and wave energy, and converting it to electrical power is called energy harvesting or energy scavenging. This energy can be collected and stored for wearable electronic devices and small gadgets. It provides an advantageous means of supplying electricity to mobile devices in isolated areas with access to traditional power sources.

Smart wearable technology is a combination of hardware and software that allows people to keep track of various elements of their lives. The lightweight design and comfort are important, as well as the flexibility and breathability of the gadget. Polymeric materials are exceptionally suitable for this purpose. There are a few phenomena involved in harvesting energy from polymer materials. It can be said that the majority of polymers are insulators, which show dielectric properties. The charge behaviour in dielectric materials is quite complicated, especially in polymeric materials. At a scale of wearable devices, three fundamental devices have played an important role in research and development in the last decade: Piezoelectric generators (PEGs), Ferroelectret generators (FEGs) and Triboelectric nanogenerators (TENGs). In the exceptional crystalline polymer poly(vinylidene difluoride) (PVDF), it is difficult to distinguish between these three phenomena in the output measurement. This is because the

deformation of charge is caused by the deformation of aligned polymer chains in a crystallite, which in turn deforms aligned dipole moments, resulting in a net electric field between parallel electrodes. Triboelectricity is a basic characteristic that occurs when two different materials come into contact, forming opposite charges on each surface. This phenomenon is known as contact electrification (CE) [43]. However, when PVDF is treated under a strong electric field, positive and negative charges build up inside the polymer close voids. Placing a parallel electrode over the polymer would produce the charge flow in the circuit as the void charges behave like dipole moments, called ferroelectret generators. This section discusses the working principles of piezoelectric, ferroelectret, and triboelectric energy harvesters.

2.2.1 Piezoelectric effect

When mechanical stress is applied, piezoelectric materials have the capacity to generate an electric current by pressing, tapping, bending, or twisting. It is recognised that a variety of substances, including proteins, crystals, and ceramics, have piezoelectric capabilities. It has been shown that piezoelectric materials have the potential to power or charge devices through mechanical movement [44].

The piezoelectric constant, d₃₃ is an important parameter in piezoelectric materials, indicating the ability of the material to transform mechanical stress into electrical charge along the identical axis. This quantifies the piezoelectric effect when the electric field and mechanical stress are applied collinearly, usually along the thickness of the material. This coefficient plays an important role in determining the efficiency and effectiveness of piezoelectric materials for various purposes, including sensors, actuators, and energy harvesters. The d₃₃ coefficient quantifies the piezoelectric response in the direction of applied stress and electric field, typically expressed in pico coulombs per Newton (pC/N).

Greater d₃₃ values are advantageous for applications requiring significant displacement or greater sensitivity, such as piezoelectric speakers and pressure sensors [45]. In energy harvesting, a high d₃₃ value improves the efficiency of converting mechanical energy into electrical energy. The composition and structure of piezoelectric materials substantially affect the d₃₃ value. Multilayer piezoelectric ceramics and polymer composites are capable of increased d₃₃ values, thus enhancing their functional characteristics [45]. Design advancements, like d₃₃ mode polarisation, enhance the performance of piezoelectric devices, making them more appropriate for particular applications such as gait rehabilitation systems [46]. Although the d₃₃ coefficient is a crucial indicator for piezoelectric materials, it is not the only factor that influences their performance. Other coefficients, including d₃₁ and g₃₃, are also significant in certain applications, requiring that material selection and design take into account

the specific requirements of the intended usage. However, this thesis exclusively concentrates on d_{33} .

In this field, ceramic and its composite piezoelectric materials, such as lead zirconate titanate (PZT) [47], barium titanate (BaTiO₃) [48], and zinc oxide (ZnO) [49], are of interest for their potential advantages in terms of low manufacturing cost and possess a high d₃₃ constant. However, the drawback of ceramic piezoelectric materials is their inflexibility and brittleness. In addition, PZT is not seen as an environmentally friendly material. The performance values of piezoelectric polymers, such as polyvinylidene fluoride or polyvinylidene difluoride are lower when compared with a ceramic piezoelectric such as PZT. However, these polymers are flexible and more suitable for wearable technology.

2.2.1.1 Piezoelectric effect in polymer

Synthetic polymers have inspired a vast range of applications due to their design flexibility, strong mechanical strength, and solution processability. Various polymer categories can be considered to show a piezoelectric effect. Figure 2.1 shows the different types of piezoelectric polymers that are available. The bulk polymer is the first category of piezoelectric polymers. These solid polymer films possess the piezoelectric mechanism through their arrangement and molecular structure. The second category includes piezoelectric composite polymers with an integrated piezoelectric ceramic structure that generates the piezoelectric effect. These composites are well recognised for having both the high electromechanical coupling of piezoelectric ceramics and the mechanical flexibility of polymers. Polymers with void charges belong to the third type. This is a vastly different type of piezoelectric polymer than those mentioned in the first two categories and is a cellular polymer film with a void structure. The film is charged in order to form the internal dipoles, which will then be confined within the voids. The polarisation of these dipoles changes when stress is applied to the polymer film (i.e. a piezoelectric response is produced). This type of polymer can be seen as being "Ferroelectret" [50].

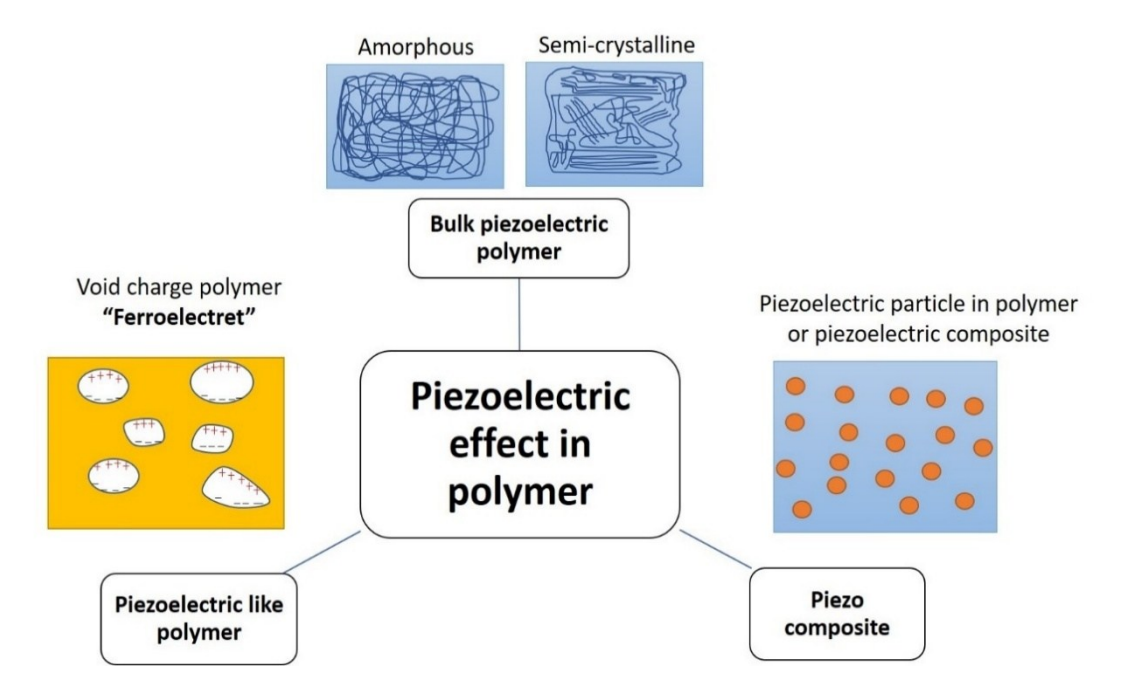


Figure 2. 1 Schematic diagram showing the piezoelectric effect in different types of polymers; bulk piezopolymers: are divided into amorphous and semi-crystalline polymers, piezoelectric particles in polymer or polymer composites

Cellular thermoplastic polymers may exhibit piezoelectric-like behaviour through internal charging. This is achieved by exposing the material to a high-level external electric field. Cellular charged polymers are being studied for various applications such as ferroelectret devices, vibration control, ultrasonic transducers, tactile sensors, shock sensors, energy conversion devices, speakers, microphones, keyboards, and thermal and optical property measurement devices [51]. Additionally, the ability to create very thin, flexible films with low density, as well as the inexpensive cost of the materials, make piezoelectric devices made from cellular polymer films of incredible significance [52].

2.2.1.2 Piezoelectric properties of Ferroelectrets/ theory of Ferroelectret and mechanism

Ferroelectrets are classified as a piezoelectrically active polymer foam. In relation to this class, a gas, such as air, within a macro-sized pore space (typically > 1 μ m) can be treated to electrical breakdown. The application of a high electric field through a corona poling process causes this to occur. The structure possesses some similarities with the atomic scale dipole configuration seen in ferroelectric materials, as shown in Figure 2.2 a). These originate from the asymmetric arrangement of the negative and positive atoms and the remnant polarisation that occurs after being subjected to an electric field above its coercive field during a similar poling process. In a similar manner to ferroelectrics, ferroelectret materials can also show polarity reversal and dipole switching, whereby the direction of the applied electric field is switched [12]. This leads

to a theoretical hysteresis loop formation, as shown in Figure 2.2 a). In this loop, the threshold voltage (as seen in Figure 2.2 b) for breakdown within a pore is comparable in certain respects to the coercive field for a ferroelectric. When the polarised pores form, the electrode of the cellular polymer attracts surface charges (see Figure 2.2 b). If the polarisation of the pores is changed through temperature changes or mechanical stress, then there is a redistribution of surface charge. This causes an electric current to flow. Therefore, ferroelectrets are both piezoelectric and pyroelectric (which generate voltage due to changing temperature). Recently, these properties have attracted interest in energy harvesting applications. Please note that ferroelectrets are also known as piezoelectrets or piezo(ferro) electrets [53-55].

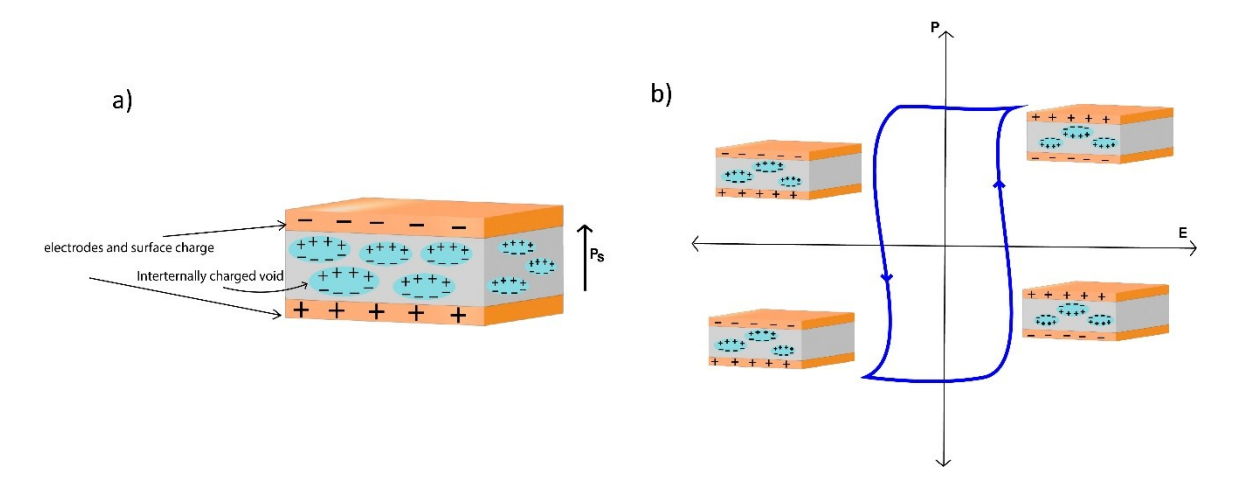


Figure 2. 2 a) the schematic of ferroelectret material where P_s is the polarisation direction, b) the hysteresis loop in a single pore ferroelectret. Reproduced from Zhang et al. (2019) [56]. Reprinted with permission from Šutka et al. (2023) [57]. Copyright 2017, Elsevier.

Figure 2.3 reveals the formation of dipoles in PVDF (a) as a piezoelectric material. This is in comparison to PP (c), which is a ferroelectret material. In addition, Figure 2.3 b) shows a basic piezoelectric model in relation to ferroelectric materials. In this model, positively and negatively charged particles are connected by springs possessing force constants of k_1 and k_2 . It has been approximately calculated that in cellular space-charged materials, like PP, the point of symmetry is broken on a macroscopic order of around 10⁵ µm³ (or 10¹⁴ nm³) (estimated cell dimensions: $100 \times 100 \times 10 \,\mu\text{m}^3$). As for PVDF, a piezoelectric material, this is on a nanoscale order of around 0.1 nm³ (with unit cell dimensions $0.858 \times 0.49 \times 0.256$ nm³ for PVDF, β -phase). Therefore, the cell volume for symmetry breakup in PP is around a factor of 10¹⁵ times larger than the unit cell volume of PVDF. The piezoelectric property for cellular nonpolar polymers, such as PP, is therefore viewed as being different when compared to polar polymers such as PVDF. Furthermore, this behaviour in ferroelectrets originates from the deformation of charged cells. The source of this behaviour in polar piezoelectric materials is considered to be ion displacement in a lattice. Ferroelectric polymers show a moderate electromechanical d₃₃ coefficient, which ranges from 10 to 20 pC/N. Ferroelectrets show larger d₃₃ values vastly above 100 pC/N. The charging process of cellular polymers occurs through charge transfer across the cells, which begins at the surface of the sample [58].

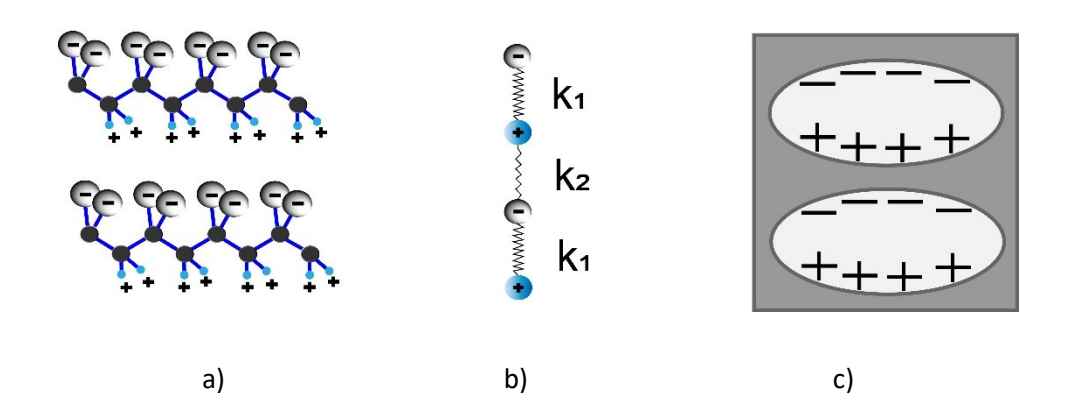


Figure 2. 3 a) Ferroelectric PVDF and b) a simple model for piezoelectricity in ferroelectric materials (positively and negatively charged particles that are connected by springs having force constants of k_1 and k_2) in the unit of N/m and c) ferroelectret PP (the clear ellipsoidal areas are gas bubbles and the dark area is the polymer matrix). Reproduced from Mohebbi et al. (2018) [55], Copyright 2016, John Wiley & Sons, Inc.

2.2.1.3 Typical ferroelectret material and applications

Polymer materials with ferroelectric properties, such as PVDF and its copolymers, have demonstrated the ability to generate piezoelectricity [59]. This is due to the ferroelectric orientation of the dipolar crystals. Currently, though, cellular ferroelectret polymers have increased their applications for nonpolar polymers as high-level performance piezoelectric materials. Thermoplastic and nonpolar polymers such as polyurethane (PU), and polyolefin (PO) have previously been used to produce ferroelectrets. Additionally, copolymers, polyvinyl chloride (PVC), fluoropolymer, poly (ethylene naphthalene) (PEN) and poly (ethylene terephthalate) (PET) have been utilised for this purpose. The polymer ferroelectret foam can be viewed as a composite that consists of a gas phase, dispersed in a solid polymer matrix, whereby the pore space has been generated through physical bonding or chemical blowing agents [60].

2.2.2 Triboelectric effect

Triboelectric nanogenerators (TENGs) have gained popularity and become a hot topic in energy harvesting research in the past few years. Since 2012, Professor Zhong Lin Wang has revealed outstanding performance based on the coupling of triboelectrification and electrostatic induction effect devices [61]. Although the concepts of contact electrification have been recognised for centuries, the research primarily concentrates on converting the static charge generated by friction at micro- or nano-scale contacts (contact electrification) into electrical energy by electrostatic induction. To understand its basic working principle, this section presents the necessary theory in the typical triboelectric effect, including the triboelectric series and the operating mode of TENGs. Furthermore, the triboelectrification in polymer, which is mainly related to this work, is discussed.

2.2.2.1 Typical triboelectric effect and fundamental operation mode of TENGs

The triboelectric effect refers to certain materials becoming electrically charged when they come into contact with another substance, resulting in their separation. Triboelectrification is a process in which two initially neutral bodies can acquire an electric charge when brought together and subsequently separated. This phenomenon occurs in all highly insulating materials due to their presence in polymers. Triboelectricity is a specific instance of the overall phenomenon of charge retention demonstrated by electrets. If polymers have sufficient insulation, they can retain electrical charges for a longer period of time. The stored charges can consist of either real charges (i.e., additional net charge) or polarisation charges, or a combination of both. The real charges consist of layers of positive or negative charges that are

either trapped at or near surfaces or spread across the whole volume. The real charges may also be unevenly distributed inside molecules or domain structures that resemble a dipole polarisation. Polarisation charges arise from the fixed orientation of dipoles, which can be attributed to the molecular arrangement [62].

2.2.2.2 Triboelectric series

Triboelectrification is a widely recognised phenomenon that frequently occurs on both a natural and a daily basis. The triboelectric series classifies different materials based on their propensity to collect or release electrons, indicating their natural physical characteristics. Recently, Zou et al. proposed the universal standard of a triboelectric series, which has been ranked in a qualitative manner based on triboelectric polarisation [63]. The triboelectric series classifies materials based on their propensity to gain or donate electrons, indicating their inherent physical characteristics. Static electricity arises from the accumulation of either positive or negative charges on the surface of an object through the process of rubbing certain materials together. The effectiveness of charge exchange is determined by the position of the material in the triboelectric series. Typically, the accumulation of static energy is undesirable due to its potential to cause product failure or pose a significant safety risk through electrostatic discharge and/or electrostatic attraction.

The creation of a triboelectric series involves measuring the surface charge of each triboelectric material after it comes into contact with several metals that have known work functions. The work function of each triboelectric material can be determined by interpolating the graph that relates the surface charge to the work function of different metals. Diaz et al. [64], produced data for the triboelectric series in 2014, which is frequently referred to. The series compares and combines other qualitative and quantitative triboelectric series, as shown in Figure 2.4.



Figure 2. 4 A commonly used Triboelectric series based on Diaz et al.'s work, reproduced by Lee et al. [63]. Reprinted © Copyright 2023 AIP

Zou et al. [63], evaluated the triboelectric properties of several materials by applying a layer of copper (Cu) to their back surfaces and immersing their front surfaces in liquid mercury at a temperature of 20 °C and a humidity level of 0.43% RH. Utilising liquid mercury enhances the contact area between the tested materials and the liquid metal, as the liquid metal readily conforms to the solid surfaces of the materials. Electrical outputs were measured, and the triboelectric charge density (TECD) σ was determined in contact-separation mode. The normalised triboelectric series α is defined as $\alpha = \sigma$ multiplied by the absolute value of $|\sigma PTFE|$. Table 2.1 presents the Triboelectric series, their triboelectric charge density (TECD), and the normalised triboelectric series as suggested by Zou et al.

Table 2. 1 Triboelectric series of materials and their triboelectric charge density (TECD) proposed by Zou et al. (2019) [63] . Copyright 2019, Nature Research

Materials	Abbr.	Average TECD (μCm ⁻²)	STDEV	α
Chemical-Resistant Viton® Fluoroelastomer Rubber		-148.20	2.63	-1.31
Acetal		-143.33	2.48	-1.27
Flame-retardant garolite		-142.76	1.49	-1.26
Garolite G-10		-139.89	1.31	-1.24
Clear cellulose		-133.30	2.28	-1.18
Clear polyvinyl chloride	PVC	-117.53	1.31	-1.04
Polytetrafluoroethylene	PTFE	-113.06	1.14	-1.00
Abrasion-resistant polyurethane rubber		-109.22	0.86	-0.97
Acrylonitrile butadiene styrene	ABS	-108.07	0.50	-0.96
Clear polycarbonate (Glossy)	PC	-104.63	1.79	-0.93
Polystyrene	PS	-103.48	2.48	-0.92
Ultem polyetherimide	PEI	-102.91	2.16	-0.92
Polydimethylsiloxane*	PDMS	-102.05	2.16	-0.91
Polvester fabric (Plain)	I DIVIS	-102.03	1.49	-0.90
Easy-to-machine electrical-insulating garolite		-101.46	1.79	-0.90
Food-grade high-temperature silicone rubber		-94.03	0.99	-0.83
Polvimide film	Vantan	-94.03 -92.88	2.58	-0.82
Polyimide ilim DuraLar polyester film	Kapton PET			-0.82 -0.79
	PVDF	-89.44	0.86 2.06	-0.79 -0.77
Polyvinylidene fluoride		-87.35		
Polyetheretherketone	PEEK	-76.25	1.99	-0.67
Polyethylene	PE	-71.20	1.71	-0.63
High-temperature silicone rubber		-69.95	0.50	-0.62
Wear-resistant garolite	LDDD	-68.51	1.99	-0.61
Low-density polyethylene	LDPE	-67.94	1.49	-0.60
High impact polystyrene		-67.37	1.79	-0.60
High-density polyethylene	HDPE	-59.91	1.79	-0.53
Weather-resistant EPDM rubber		-53.61	0.99	-0.47
Leather strip (Smooth)		-52.75	1.31	-0.47
Oil-filled cast nylon 6		-49.59	0.99	-0.44
Clear cast acrylic	PPMA	-48.73	1.31	-0.43
Silicone		-47.30	1.49	-0.42
Abrasion-resistant SBR rubber		-40.13	1.31	-0.35
Flexible leather strip (Smooth)		-34.40	0.86	-0.30
Noryl polyphenyl ether		-31.82	0.86	-0.28
Poly(phenylene Sulfide)	PPS	-31.82	0.86	-0.28
Pigskin (Smooth)		-30.10	0.86	-0.27
Polypropylene	PP	-27.23	1.31	-0.24
Slippery nylon 66		-26.09	0.50	-0.23
Weather- and chemical-resistant santoprene rubber		-25.23	0.50	-0.22
Chemical- and steam-resistant aflas rubber		-22.65	1.31	-0.20
Polysulfone		-18.92	0.86	-0.17
Cast nylon 6		-18.35	0.99	-0.16
Copy paper		-18.35	0.50	-0.16
Chemical-resistant and low-temperature fluorosilicone rubber		-18.06	0.86	-0.16
Delrin® Acetal Resin		-14.91	0.50	-0.13
Wood (marine-grade plywood)		-14.05	0.99	-0.12
Wear-resistant slippery garolite		-11.47	0.50	-0.10
Super-stretchable and abrasion-resistant natural rubber		-10.61	0.50	-0.09
Oil-resistant buna-N rubber		2.49	0.23	0.02
Food-grade oil-resistant buna-N/vinyl rubber		2.95	0.13	0.03

Note: STDEV refers to the standard deviation. The α refers to the measured triboelectric charge density of tested materials over the absolute value of the measured triboelectric charge density of the reference material. The material marked with an asterisk "*" means it has strong adhesion with mercury, a small drop of mercury is observed when it is separated with mercury. The measured TECD value may be a bit lower than its real value. Source data are provided as a Source Data file.

TENGs are devices that convert kinetic energy generated by the relative motion and frictional contact between two materials with varying electron affinities into electricity using the principles of the triboelectric effect and electrostatic induction. The external kinetic energy will periodically cause the charged surfaces to move, resulting in a relative displacement between the surfaces and electrodes. This, in turn, leads to a periodic change in the induced potential difference between the electrodes. When an electrical load is attached to the electrodes, electrons will flow continually between the electrodes to lower the potential difference and maintain electrostatic equilibrium. This principle allows for extracting an alternative power output at the load. The operational modes of TENG can be classified into four categories based on the various configurations of the triboelectric materials and electrodes and their relative movement.

In order to enhance the performance and expand the range of applications of a TENG, intensive efforts have been undertaken, with a specific emphasis on increasing the surface charge density and creating new structures/modes. Nowadays, four primary modes of TENG have been created: vertical contact-separation (CS) mode, lateral sliding (LS) mode, single-electrode (SE) mode, and freestanding triboelectric-layer (FT) mode. Four assembly modes can be produced to harvest energy from the triboelectric effect, as shown in Figure 2.5.

Each mode possesses its unique arrangement and selection of materials, along with distinct mechanical triggering mechanisms. In the case of the CS mode, it is initiated by a vertical periodic driving force that induces a repetitive contact separation cycle between two distinct materials, each having coated electrodes on their respective top and bottom surfaces. The LS mode is activated when there is a linear motion between two different materials that are aligned in parallel. To assess and contrast the efficiency of TENGs in various structures and modes, it is necessary to provide a general criterion for quantifying their performance, regardless of the specific mode of operation [65].

The parallel-plate capacitor model is applicable to TENGs that have planar designs. The parallel-plate capacitor model can be applied to TENGs due to their naturally capacitive behaviour. This model is based on two fundamental assumptions: (1) charges are uniformly distributed on the dielectric surfaces, and (2) the electric field inside the dielectric is merely perpendicular to the plates, disregarding any parallel component. The V–Q–x relationship is essential to the parallel-plate capacitor model used for TENGs. The V–Q–x relationship expresses the correlation between three significant parameters in TENGs: the output voltage V, the transferred charge quantity between the two electrodes Q, and the separation distance x. The following expression (Eq.2.1) represents this relationship as a triboelectric harvester equation.

$$V = -\frac{1}{C(x)}Q + V_{oc}(x)$$
 (2.1)

Q = amount of transferred charges between the two electrodes

x =separate distance

 $V_{oc}(x)$ = potential difference contributed by the polarised charges

 $-\frac{1}{C(x)}Q$ = potential difference contributed by the transferred charges

S = contact area of the tribo-pair

$$d_0$$
 = thickness = $\frac{d_1}{\varepsilon_{r1}} + \frac{d_2}{\varepsilon_{r2}}$

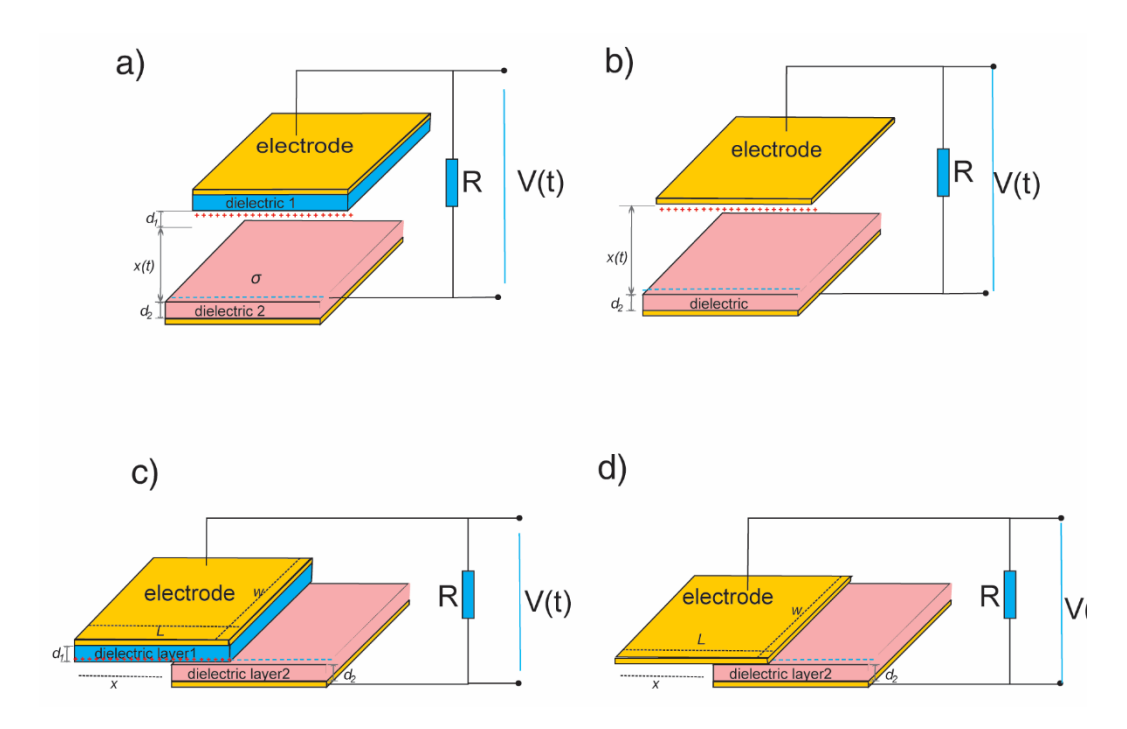


Figure 2. 5 TENG in contact mode - TENG in sliding mode a) and b) dielectric to dielectric contact mode TENG, c) and d) conductor to dielectric sliding mode. Reproduced from Zhang et al. (2020) [66] under CC BY and Copyright 2023 Walter de Gruyter GmbH

Figure 2.5 a) and b) demonstrate the Contact-Mode TENGs in vertical contact-separation (CS) mode and single-electrode (SE) mode, according to the materials used and device structures: dielectric-to-dielectric contact and conductor-to-dielectric contact (Figure 2.5 b) structures. Based on fundamental assumptions, the length and width of tribo-pairs should significantly exceed their thickness, while the area of the electrodes should be considerably higher than the distance between them.

 $V_{oc}(x)$ and C(x) of contact mode TENGs can be worked out based on electrodynamics as $V_{oc}(x) = \frac{\sigma x(t)}{\varepsilon_0}$ and $C(x) = \frac{\varepsilon_0 S}{(d_0 + x(t))}$, where ε_0 is the vacuum permittivity, σ is the charge density at the contact surface of the tribo-pair, and S is the contact area of the tribo-pair. The equivalent thickness d_0 is defined as $\frac{d_1}{\varepsilon_{r1}} + \frac{d_2}{\varepsilon_{r2}}$, and for conductor-to-dielectric contact TENGs, d_1 is equal to 0.

Substituting the expression of $V_{oc}(x)$ and C(x) into $V=-\frac{1}{C(x)}Q+V_{oc}(x)$, the relationship of the contact mode TENGs (in equation 2.2).

$$V = -\frac{Q}{S\varepsilon_0}(d_0 + x(t)) + \frac{\sigma x(t)}{\varepsilon_0}$$
 (2.2)

Figure 2.5 c) and d) present the sliding-mode TENGs, which is similar to the contact mode. They can be classified into two groups based on materials utilised as triboelectric layers- dielectric to dielectric, Figure 2.5 c) and conductor-to-dielectric, Figure 2.5 d). Regarding sliding mode TENGs, it is essential that the length l is significantly greater than both d_1 and d_2 . Failure to meet this condition would make the electric field component parallel to the plate insignificant. Furthermore, it is important that the separation distance x is less than 0.9l. If the overlapping area is too small, the capacitance of the device will not be accurately represented by the capacitance of the overlapping area. In addition, the distribution of electric charge on the electrodes and dielectric surfaces will also diverge from the fundamental assumption. If both of those meet the requirements, the effects of the edge effect can be disregarded, and the total capacitance can be expressed as (in equation 2.3).

$$C(x) = \varepsilon_0 w \frac{(l-x)}{d_0} \tag{2.3}$$

The expression of $V_{oc}(x)$ is dependent on the charge distribution on the electrodes. When the two dielectric plates separate laterally, there exist charges on the lower surface of dielectric 1 and the upper surface of dielectric 2 at the non-overlapped part. Under the above assumptions, the surface charge density for the overlapped region on the top and bottom electrodes is σ and $-\sigma$, respectively. The surface charge density for the non-overlapped region on the top and bottom electrodes is $\frac{\sigma x}{(l-x)}$ and $\frac{-\sigma x}{(l-x)}$. Combining the charge distribution Gauss theorem, $V_{oc} = \frac{\sigma x d_0}{\varepsilon_0(l-x)}$ can be obtained.

Substituting the expression of $V_{oc}(x)$ and C(x) into $V=-\frac{1}{C(x)}Q+V_{oc}(x)$, the relationship of the contact mode TENGs is

$$V = -\frac{d_0 Q}{w \varepsilon_0 (l - x)} + \frac{\sigma d_0 x}{\varepsilon_0 (l - x)}$$
(2.4)

Furthermore, despite their unique structures, the free-standing triboelectric-layer-based nanogenerators and single-electrode triboelectric nanogenerators can be accurately simulated using the capacitor model. This is because they can still be considered as capacitors, and their output can be expressed using equation $V = -\frac{1}{C(x)}Q + V_{oc}(x)$ [66].

This thesis employed the CS mode to demonstrate the energy performance of the electrospun fibre. The basic contact-separation structure was employed in the initial examination of electrospinning parameters because of the elimination of a requirement for a complicated setup. The research was extended by utilising the book-shaped structure to demonstrate the applicability of wearable technologies.

Book-Shaped TENGs design

TENGs utilise the triboelectric effect, which involves the generation of electric charge through the contact and subsequent separation of two materials. TENGs are offered in several configurations, including a book-shaped model. The fundamental design is a book-shaped triboelectric energy nanogenerator that enhances the performance of TENGs through incorporating unique structural characteristics resembling books. This design generally has two triboelectric layers arranged in a book-like configuration, with one layer stationary and the other capable of movement or flexing in response to external mechanical stimulation. The flexibility of the movable layer allows efficient charge separation and production, leading to enhanced energy harvesting capabilities in comparison with rigid ones [67].

J. Chung et al. [68] suggest the construction of an elastic bellow-type triboelectric nanogenerator (B-TENGs), as illustrated in Figure 2.6 a). The simplified model of the B-TENGs can be referred to as a book-shaped TENG. The B-TENG can operate independently as an elastic element, which is essential for sustaining the vertical contact-separation mechanism. A vertical contact-separation type TENG functions when an external force is exerted, with the magnitude dictated by the stiffness of the elastic material. The TENG may provide electrical output with minimal force by making contact between two surfaces possessing opposing triboelectric charges. Upon pressing the gadget, the electrodes of both TENGs make contact, generating electrical output. Figure 2.6 b) and c) show the working mechanism of the book-shaped like model c) simulation results for the electrical potential distribution for the different angles between two electrodes as studied by Chung et al. 2016. The $V_{\rm oc}$ and $I_{\rm sc}$ values can be measured independently due to the different $V_{\rm oc}$ values of the two TENGs, although being composed of the same material, as described by the equation.

Chapter 2

$$V_{oc} = V_A - V_B = \frac{\sigma}{\varepsilon_0} d = \frac{2\sigma lsin\left(\frac{\theta}{2}\right)}{\varepsilon_0}$$
 (2.5)

Where $V_A - V_B$ is the electrical potential difference between the two electrodes;

 σ is the surface charge density of the PTFE;

 \emph{d} is the distance between the two horizontal electrodes;

l is the length of the book-shaped model;

heta is the angle between the two electrodes; and

 ε_0 is the permittivity of vacuum.

From the equation, it can be seen that the V_{oc} depends on the angle between the two electrodes.

Thus, the maintained stiffness of the substrate directly affects the performance of the device.

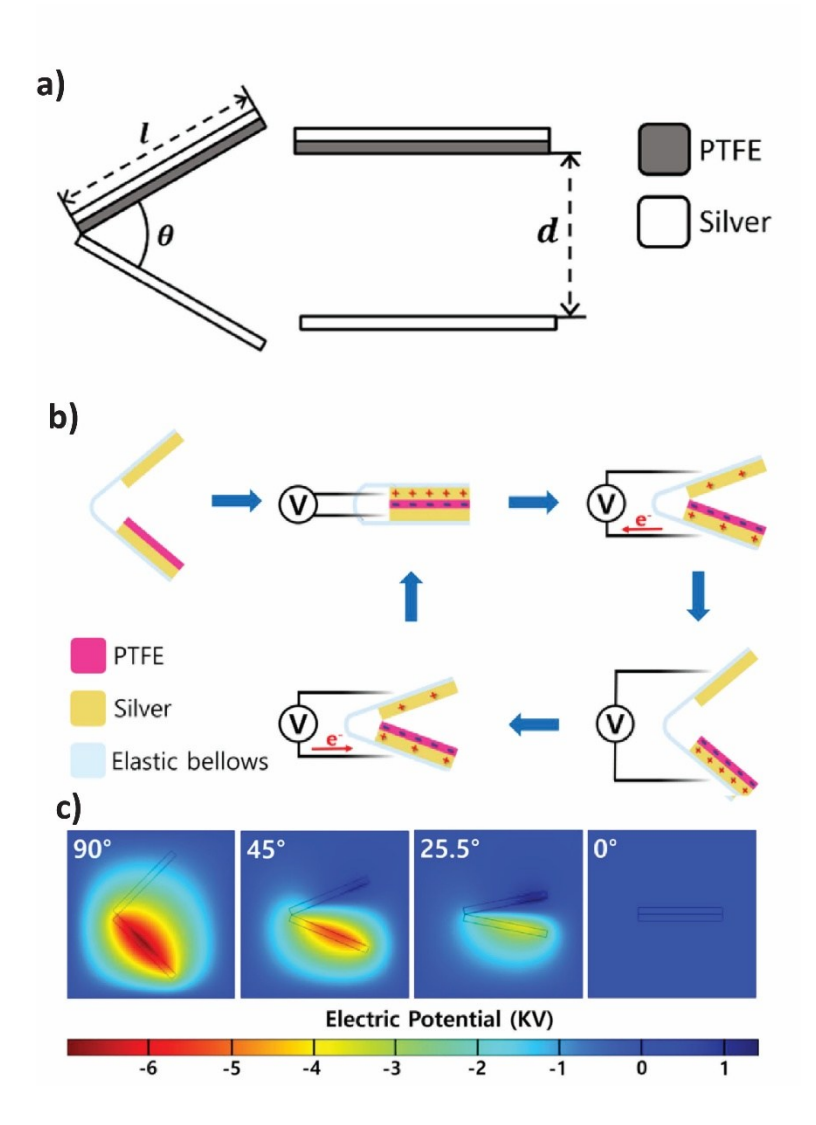


Figure 2. 6 the design of partial elastic bellow–type triboelectric nanogenerator as a partial book-shaped like model a) Schematic illustrating a simplified structure of book-shaped TENGs b) the working mechanism of the book-shaped like model c) simulation results for the electrical potential distribution for the different angles between two electrodes, using COMSOL as studied by J. Chung et al. 2016 [68] Copyright Elsevier Ltd. 2015.

TENGs require materials with a high surface area to enhance their efficiency in converting mechanical energy into electrical energy. The larger surface area increases surface charge density, which is necessary for increasing the performance output of TENGs. This is accomplished using diverse material optimisation techniques. This includes complex materials with higher porosity and specific surface area, alongside structural modifications. These approaches significantly enhance the performance of TENGs in energy harvesting applications. However, apart from surface area, other factors influence the surface charge of triboelectrification. Šutka et al. (2023) categorised the factors that can influence TENGs as follows [57], [69]:

- Surface Morphology: Surface roughness and patterns may significantly influence charge magnitude by modifying the contact area between materials [70].
- Adhesion and Fracture: In the process of contact separation, material adhesion, deformation, and fracture are crucial in charge creation. Adhesion increases interaction between surfaces, promoting charge transfer.
- 3. Material Properties: Chemical Composition: The existence of functional groups or additions can affect electron, ion, or mass transfer. Mechanical Properties: The stiffness or flexibility of materials influences deformation upon contact, thus affecting charge production.
- 4. Thermal Effects: Heat generated via contact or external sources can modify charge transfer dynamics by affecting material characteristics or charge carriers.
- 5. Bond Cleavage: The disruption of bonds in polymers (either homolytic or heterolytic) during contact separation can produce charged fragments that enhance surface charge.
- 6. Role of Additives: Additives can modify surface structure and enhance charge retention by altering local properties or increasing electron donor/acceptor sites.

These factors combine to affect triboelectric performance by modifying the mechanisms of electron, ion, or mass transfer that dominate in different systems

2.2.2.3 Triboelectrification in polymer

Despite being observed since ancient Greek times 2600 years ago, the origins of contact-electrification (CE) or triboelectrification are still subject to much debate. The primary question revolves around whether the charge transfer occurs through electrons or ions, and why the charges remain on the surface without disappearing quickly. Electron transfer has been broadly accepted in explaining the electrification of metal-metal and metal-semiconductor systems, as determined by the work function or contact potential difference. This concept can also be applied in explaining the electrification of metal-insulator systems by taking into account the presence of surface states. The phenomenon of electrification, particularly in relation to polymers, was also attributed to ion transfer. It was proposed that ions carrying functional groups played an essential part in contributing to CE. The continuous inconsistencies raised the question of whether electron or ion transfer is the predominant fundamental process in CE [57], [69].

Bidirectional material transfer occurs during polymer-polymer interaction; both materials are transported to opposing surfaces upon contact [71]. Thus, to enhance the triboelectric output, the induced charge separation between two materials can be developed in the form of generating more heterolysis bond cleavage and controlling cohesive energy density and

roughness [57]. The generation of heterolysis bond cleavage, cohesive energy density, and roughness can be induced.

The three main mechanisms suggested for polymer triboelectrification include 1) electron transfer, 2) transfer of ions or water, and 3) transfer of charged fragments from macromolecules. The identification of the mechanism is complicated because various factors can impact the formation of charges in polymer triboelectrification. These factors include the environment (temperature and humidity), contact duration and intensity, surface characteristics (roughness and pattern) [70], overall properties (macromolecular arrangement and crosslinking), fillers, and the chemical composition of the surface (functional groups).

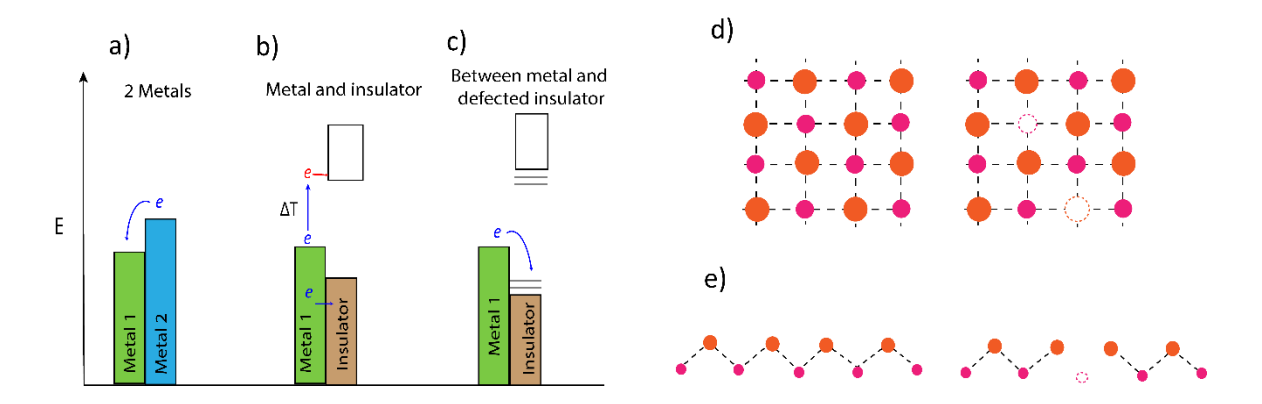


Figure 2.7 Illustration demonstrating the simplified electrical arrangement when different materials come into contact. a) The first scenario involves two metals, where the lower energy metal can accommodate an electron from the higher energy metal due to a difference in energy levels. b) The second scenario involves a metal and an insulator, where there are no available states for an electron to occupy. Therefore, electron transfer can only occur through a process called tunnelling or through thermal excitation processes. c) The third scenario occurs between a metal and a defective insulator, where the presence of atomic defects creates electronic states that allow for electron transfer to take place. d) The schematics show the bonding networks of ceramic materials, with the pristine lattice on the left and the generated lattice on the right. The ceramic network maintains its lattice structure through multiatom coordinated bonding networks. e) The schematics show the bonding networks of polymer materials, with the pristine lattice on the left and the defectinduced lattice on the right. In polymers, the one-dimensional bonding network is potentially broken, which can lead to mass transfer. Reproduced from Šutka et al. (2023) [57] Copyright 2023, Wiley-VCH GmbH

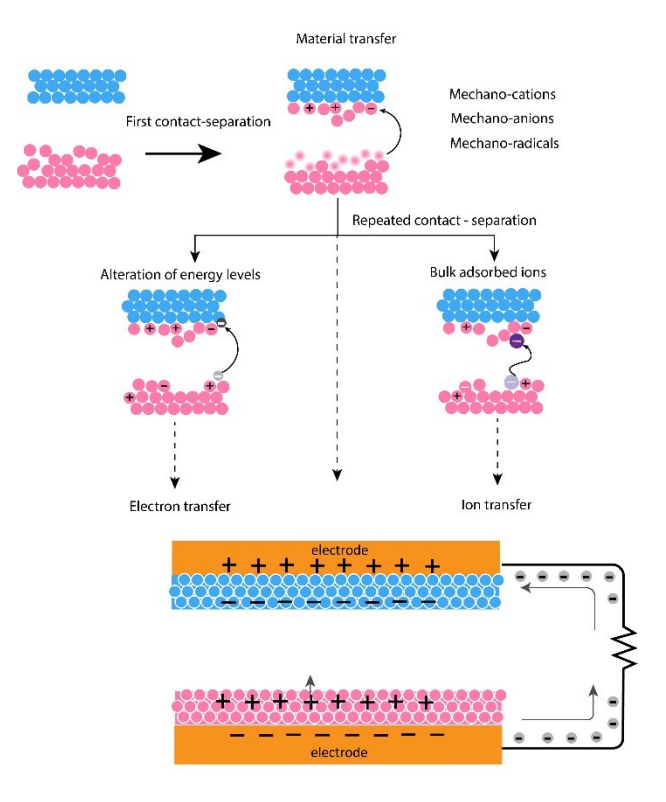


Figure 2. 8 Schematic of the suggested complicated contact electrification mechanism, involving initial charge generation through mechano-radical and ion creation, followed by subsequent transfer of adsorbed ions and electrons during ongoing contact separation. Reproduced based on Lapčinskis et al. (2019) [72]. Copyright 2023, Wiley-VCH GmbH

2.3 Electrospinning techniques and parameters

It has been shown that electrospinning is a simple but efficient and versatile technology for producing polymeric fibres with diameters controllable in the range of nanometres to micrometres. The produced fibres are within the submicron/micrometre range diameter. This process is possible for almost any soluble co/polymer as long as its molecular weight is high enough. Electrospun fibres possess a large surface area per unit mass, which is due to their small diameters. This means that the fibres have the potential for various applications, such as wound dressings [73], tissue engineering [74], filters [75], protective wearable devices [76-77], sensors [78], and batteries [79].

Electrospinning is a process where electrostatic forces draw a droplet of polymer solution into a fine fibre. This is followed by the deposition of the fibre onto a grounded collector. At a steady rate, the liquid polymer is extruded from the nozzle tip. This is achieved through the use of a syringe pump or through constant pressure from a header tank, which then forms a droplet at the tip (see Figure 2.9). When a small volume of polymer liquid is subjected to an electric field,

the formed droplet stretches toward the nearest lower potential point. A Taylor cone is then formed (see Figure 2.9). As the electric field reaches a critical value at the tip of the Taylor cone, the electrical forces overcome the surface tension of the formed droplet. This causes a charged fluid stream or jet of liquid polymer to be ejected. The jet of liquid is then partly elongated through "whipping instability" during the journey from the needle tip to the grounded collector.

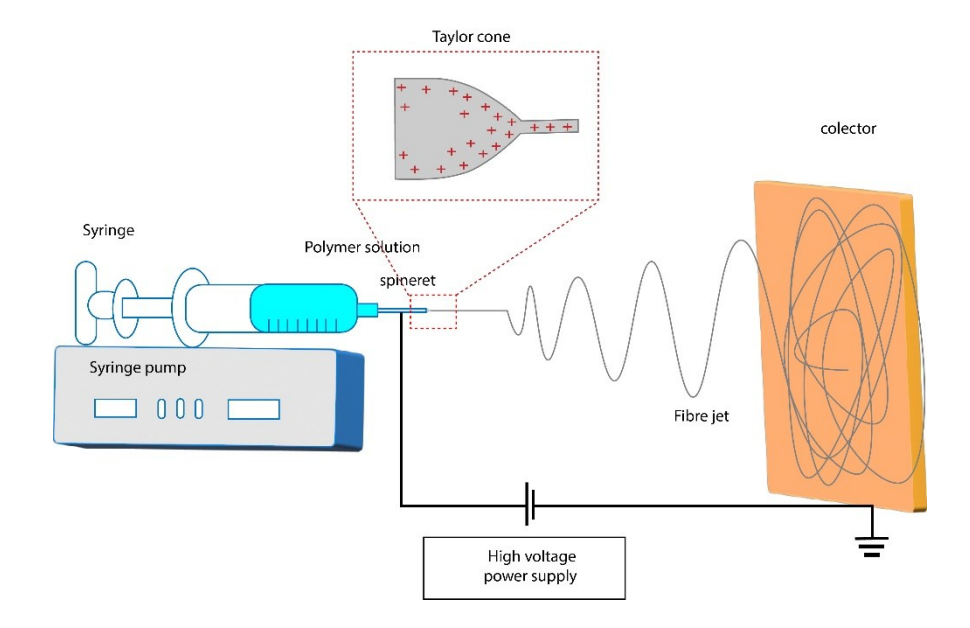


Figure 2. 9 Schematic of electrospinning setup with the basic electrospinning setup includes the syringe pump, conductive needle, collector and high voltage supply and the Taylor cone model.

Figure 2.10 shows the main considerations for the electrospinning parameters are solution properties, molecular weight and its concentration, solvent properties; vapour pressure, surface/interfacial tension, conductivity, dielectric constant, and viscosity; working parameters; electric potential, gap distance, flow rate of solution and needle dimensions, environmental conditions that includes temperature. The details and the effect of each factor are discussed in this section.

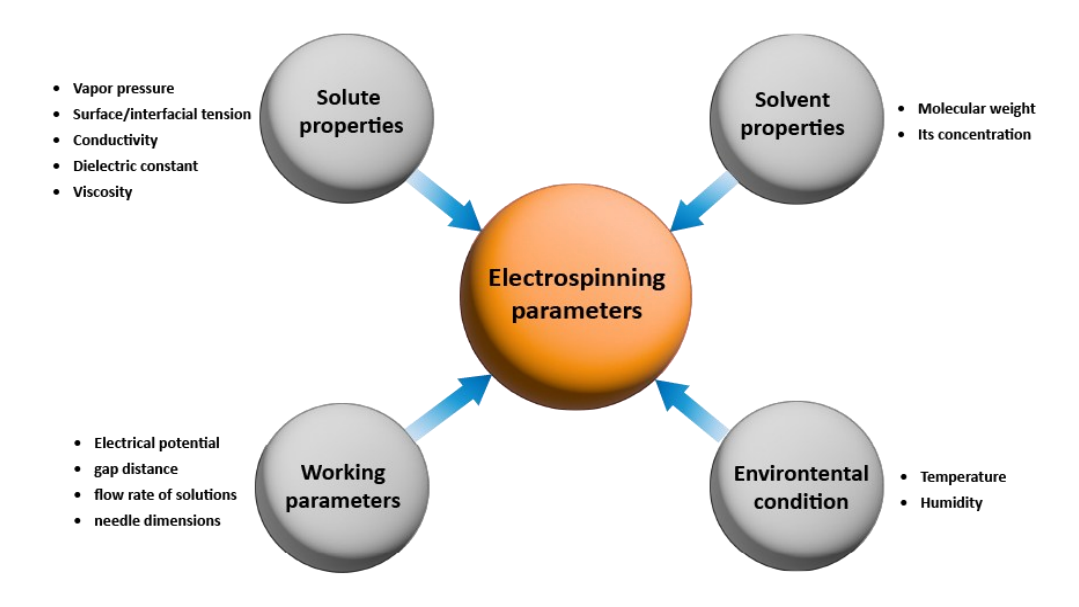


Figure 2. 10 Four main factors that can affect the electrospinning process

The molecular weight of the polymer and its concentration in solution are the two key elements to take into account when determining chain entanglement. In solution, polymer molecules are known to occupy a certain effective volume with an average radius of gyration (R_g). At low concentrations (dilute solutions), the polymer chains of the molecules in the solution do not overlap. The individual polymer chains govern the viscoelasticity of the solution. The chains start to overlap and become entangled with an increasing polymer concentration. The critical concentration (c^*) at which entanglement initially occurs is generally seen to be in proportion to the ratio of the polymer molecular weight (M_w) and the effective volume [Eq. (2.6)]:

$$c^* = \frac{3M_W}{4\pi R_g^3 N_A} \tag{2.6}$$

where N_A is the Avogadro's constant [80].

Taylor cone information

The formation of the Taylor cone when electrospraying or electrospinning is essential for achieving the micronisation, nanonisation and homogenisation of the particles [80-81]. The parameters for this important process are applied voltage, flow rate, working distance, environmental temperature, environmental pressure, spraying mode, nozzle gauge, collection method and environmental humidity. It has been shown that various evaporation rates and the compatibility of non-solvent, solvent and polymeric matrix, leads to phase separation, which results in highly porous particles being formed [82]. The electrohydrodynamic process is carried out under the cone-jet mode. This is achieved when the electrical conductivity of the working liquids is in the range of 10^{-11} to 10^{-1} S/m. For PCL, this is in the range of 8.0×10^{-10} to 3.2×10^{-2} S/m, and more specifically from 10^{-4} to 10^{-8} S/m. Increases occur with a rise in surface tension

and the viscosity of the solutions. High electrical conductivity of solvent systems is needed for high PCL concentrations.

If viscosity and surface tension are too high, an electrical conductivity of liquids exceeding the mentioned range is needed to balance the surface tension and viscoelastic forces. This is required to achieve the cone-jet mode [83].

2.3.1 Effect of electrospinning parameters

Many parameters influence the morphology of the electrospun fibre. Most electrospinning was carried out using a polymer solution. It is possible to design or create the electrospun fibre by varying the electrospinning parameters. Therefore, the parameters that affected electrospinning and fibre morphology will be discussed in this topic.

2.3.1.1 Polymer solution parameters

Molecular weight and solution viscosity

A polymer with a greater molecular weight dissolves in a solvent with a higher viscosity than a polymer solution with a lower molecular weight. In the electrospinning process, the solution must consist of a polymer of sufficient molecular weight and viscosity. When the jet leaves the needle tip during the electrospinning process, the polymer solution is stretched by the electrical force when moving towards the target collector (the opposite electrode). During the stretching, the polymer solution comprises the entanglement of the molecular chains that prevent the electrically driven jet from breaking up, thus maintaining a continuous flow of solution.

The molecular weight of the polymer influences the polymer chain length. This has an impact on the solution's viscosity since the length of the polymer will affect the extent to which its chains are entangled with the solvent. Increases in polymer concentration will, in turn, increase the viscosity of the solution. This will also increase the molecular weight of the polymer. The increased concentration will cause greater polymer chain entanglement in the solution. This is required to maintain the continuity of the jet during the electrospinning process. It has been shown that polymer chain entanglement controls whether the electrospinning jet splits into small drops or whether the final electrospun fibre contains beads. However, a dry solution may form in the needle tip if the viscosity is too high. This will stop the electrospinning process. At a low viscosity, the bead structure will commonly be found within the fibre. When the viscosity increases, the shape of the beads will gradually change from spherical to spindle-like until a smooth fibre is obtained. At the lower viscosity, the higher amount of the solvent molecule's surface tension has a dominant influence along the electrospinning jet. This results in beads forming along the fibre. When the viscosity is increased, the changes to the electrospinning jet

will cause the solution to fully stretch with the solvent molecules distributed among the polymer chains. The diameter of the fibre will also increase when the viscosity is increased. This is due to the greater resistance of the solution when being stretched by the charges on the jet.

Bead-like structure

It has been shown that the creation of the bead-like structure during the electrospinning process comes from the unsaturated polymer content in the polymer solution. The average diameter of electrospun fibres usually varies from about 5 nm to 10 µm. The distribution of fibre diameters is usually wider than that achieved using conventional fibre spinning processes. Structural defects in the webs can be present among the resultant fibres. Colloid beads, beads on string, or spindle morphologies are examples of these defects. These defects are dependent on the operating conditions and the material properties. The formation of beads and spindles is caused by the uneven thinning of the fibre during the drawing process. This is not caused by stress relaxation after the deposition of the fibres. Bead formation is observed in fibres that are not drawn by electrostatic force (e.g. glass fibres). It is widely recognised that the primary factors that influence bead formation are viscosity, surface tension of the polymer solution, and the net charge density carried by the jet. The applied electrostatic field and conductivity of the solution are known to influence the net charge density that is carried by the moving jet during the process. The beads become smaller and more spindle-like as the net charge density increases. This is the reason the diameter of the fibres becomes smaller. Nevertheless, it should be noted that bead or spindle formation is a phenomenon observed in non-electrostatic drawing out of the fibre. A decrease in surface tension will gradually make the beads disappear. Many of the previous studies have been concerned with producing smooth fibres. Beaded fibre is considered a defect in electrospun fibre that occurs from a low viscosity condition [81]. Several studies are interested in beaded fibres to embed a reservoir for drugs for medical therapeutics [84-86].

Chapter 2

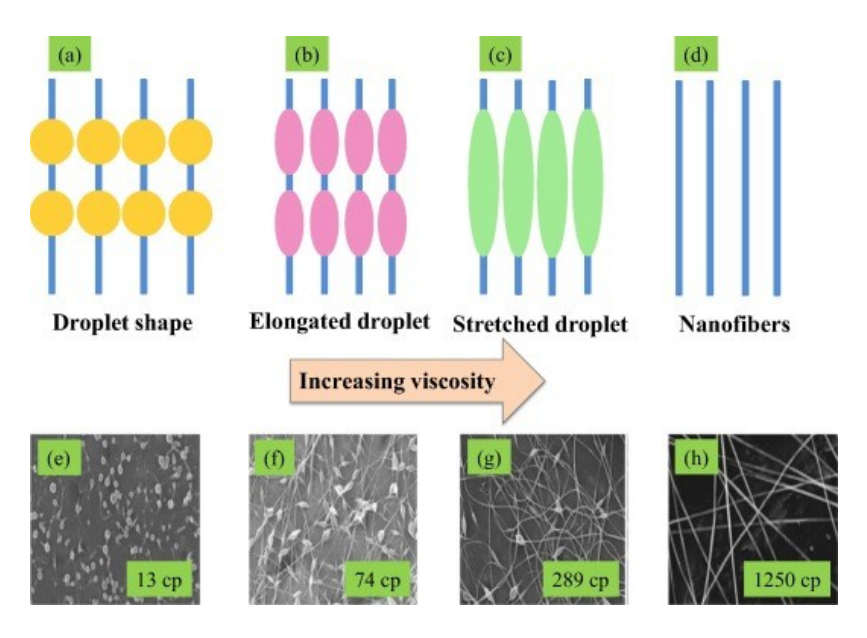


Figure 2. 11 The effect of increasing the solution viscosity on the morphology of the resulting electrospun fibres, Reprinted from Haider et al. (2018) [81]. Copyright by 2015 Elsevier B.V.

Surface tension

Initiation of the electrospinning process needs an altered solution to overcome the surface tension. Nevertheless, surface tension may result in the formation of beads along the jet as it travels towards the collector plate. A decrease in surface area per unit mass of fluid is caused by surface tension. When a high concentration of free solvent molecules is present, there is a greater tendency for the solvent molecules to congregate. These solvent molecules adopt a spherical shape as a result of the surface tension. Higher viscosity means greater interaction between the solvent and polymer molecules. Therefore, the solvent molecules will have a tendency to spread out over the entangled polymer molecules as the solution stretches under the influence of the charges. Ethanol has low surface tension and can be added to stimulate the formation of smooth fibres.

Solution conductivity

The electrospinning process involves stretching the solution. This is caused by the repulsion of the charges at its surface. The electrospinning jet can carry more charges as the solution's conductivity increases. The conductivity of the solution can be increased through the addition of ions. The solution will stretch more as its carrying charges increase. This is achieved through the addition of a small amount of salt or polyelectrolyte. Smooth fibre is formed as a result. An increase in the stretching of the solution will also tend to result in a smaller diameter fibre. As the ions increase the conductivity of the solution, the critical voltage for electrospinning is reduced. Increased charges will also result in greater bending instability. Due to this, the

deposition area of the fibres will be increased. This will also assist in forming finer fibre as the jet path has now increased.

Dielectric effect of solvent

It has been shown that the dielectric constant of a solvent significantly influences the electrospinning process. A solution with a higher dielectric property can decrease bead formation and the diameter of the resulting electrospun fibre. The dielectric characteristics of a solution can be improved by adding solvents such as DMF. This will improve the morphology of the fibre. A high dielectric constant increases the bending instability of the electrospinning jet. The addition of a solvent with a higher dielectric constant that improves the electrospinnability of the polymer will impact the morphology of the resulting fibres. Adding DMF to a polystyrene (PS) solution will cause beads to form. However, the electrospinnability should have improved due to the higher dielectric constant of DMF. This effect could be the result of the retraction of the PS molecule, which could be due to the pure interaction between PS and the solvent molecules. Liu et al. examined grooved texture on fabricated electrospun polystyrene fibre. They investigated the effect of the solvent system and relative humidity on the grooved PS fibre [87-88].

2.3.1.2 Processing conditions

Voltage

Voltage in the range of kilovolts is a crucial parameter in the electrospinning process. The high voltage will induce the charges in the solution with the external electric field. This results in the electrostatic force in the solution overcoming the surface tension. Generally, the high and negative (or positive) voltage of more than 6 kV is sufficient to distort the droplet at the needle tip into the shape of the Taylor cone for the initial jet. The feed rate of the solution depends on the voltage, and a higher voltage is required to maintain the stability of the Taylor cone. The Coulomb repulsive force in the droplet will then stretch the viscoelastic solution. The greater amount of charge will cause the jet to accelerate faster. In addition, a larger volume of solution will be drawn from the tip when the voltage is higher. A smaller and less sturdy Taylor cone might be a result of this.

Supplied voltage and electric field influence the stretching and acceleration of the jet. This affects the morphology of the obtained fibre and causes it to be smaller in diameter. The duration of the electrospinning jet's flight is another factor that directly influences the diameter of the fibre. Longer flight time allows more time for the fibre to be stretched and elongated before being deposited on the collector plate. Therefore, a lower voltage reduces the acceleration of the jet. A weaker electric field may increase the flight time, which causes a finer

fibre to form. However, a higher voltage has been found to cause a greater tendency for bead formation.

Feed rate/Flow rate

The voltage corresponds to the feed rate in order to maintain the stability of the Taylor cone. It is known that a greater volume of solution will require greater strength from the electric field to drive the jet. Due to the greater volume of the solution, the jet will take longer to dry. This results in the deposited fibre not having enough time to evaporate in the same flight time. The residual solvents may cause secondary corrosion to the fibre shell when they form on the collector [89]. This is the reason why the lower feed rate is more desirable for expanding the evaporation time.

Temperature

A solution's temperature affects the increase of its evaporation rate and reduces the polymer solution's viscosity. At lower viscosity, the Coulomb force can exert a greater stretching load on the solution, resulting in a smaller fibre diameter. Increased polymer molecule mobility due to the increased temperature allows the Coulomb force to stretch the solution further.

Effect of substrate

The type of substrate on the collector influences the electric force between the tip and the collector. Therefore, it is essential to design the collector correctly to enhance the electric field in the electrospinning process. The general material for covering the collector is aluminium foil, which is electrically grounded. When a nonconducting material is used as a collector, the charge on the electrospinning jet will quickly accumulate on the collector, resulting in less fibre deposited on the substrate. This can cause the formation of a 3D fibre structure due to the repulsive force of the like-charges. If sufficient charge density is present on the fibre mesh that is formed initially, repulsion on the subsequent fibres can cause honeycomb structures to form. However, even for a conductive substrate, if there is a high deposition rate and the fibre mesh is thick enough, a high residual charge on the fibre mesh will also be present as the polymer fibre is generally non-conductive.

Diameter of the needle

The smaller internal diameter of the needle was found to reduce clogging and the level of bead formation on the electrospun fibre.

Distance between tip and collector

Varying the distance between the tip and the collector results in a direct effect on flight time and electric field strength. During the electrospinning flight, the jet must be allowed enough time for most of the solvent to evaporate before reaching the collector. Furthermore, a shorter distance will increase the electric field strength at the same time and increase the acceleration of the jet to the collector.

2.3.1.3 Ambient parameters

There has been little investigation into the effect of the electrospinning jet's surroundings. Any interaction between the surroundings and the polymer solution may alter the electrospun fibre's morphology. As the electrospinning process is influenced by the external electric field and, any changes in the environment will also have an effect.

Ambient temperature and humidity

Recently, studies on ambient temperature and humidity in regard to electrospinning have been reported [90]. Szewczyk et al.'s study showed the enhanced piezoelectric properties for PVDF electrospun fibre of up to 74% when the ambient environment was controlled under 60% humidity at 25 °C when compared to 30% humidity. This can be explained because at higher ambient humidity, the evaporation rate of the solvent during the electrospinning process is decreased.

2.3.2 Coaxial electrospinning and control parameters

Coaxial electrospinning, which is an extension of the electrospinning technique, has been developed to produce multi-layered nanofibre structures.

2.3.2.1 Technology and Control for the Coaxial or Core-Shell Structures

The setup of the coaxial electrospinning process is practically the same as for the traditional electrospinning process. The main modification of the technique relates to the spinneret, which consists of a couple of capillary tubes. The smaller one is inserted (inner) concentrically inside the bigger (outer) capillary to produce a coaxial configuration. Both of the capillary tubes are connected to their reservoir. This is independently supplied by an air pressure system or syringe-pump arrangement. This system (two syringe pumps placed in parallel) sends dual solutions to the coaxial spinneret. Inside the coaxial spinneret, both of the fluids flow. In the tip of the device, the injection of one solution into another is produced, and both solutions can be

seen to be coaxial. A schematic of the coaxial electrospinning process can be seen in Figure 2.12.

The flow of the shell fluid drags and causes the inner fluid to flow and form as a co-fluid or compound Taylor cone of the electrospinning jet. If the fluids are immiscible, a core-shell structure can be seen. In the other situation (miscible solutions), a fibre/droplet with distinct phases is produced.

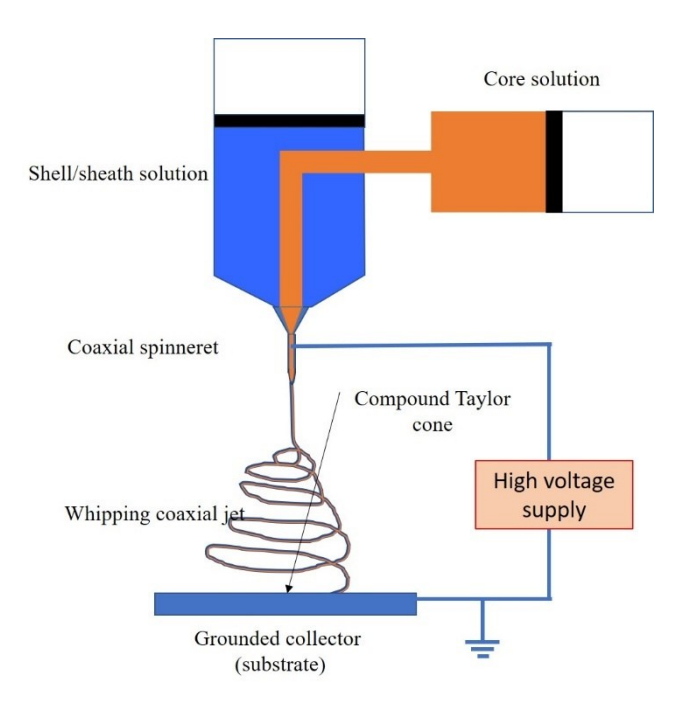


Figure 2. 12 A schematic of coaxial electrospinning

2.3.3 The compound Taylor cone and the parameter for coaxial electrospinning

The flow of the shell fluid drags the inner fluid to flow and form a co-fluid or compound Taylor cone of the electrospinning jet. If the fluids are immiscible, a core-shell structure can be seen. In the other situation (miscible solutions), a fibre/droplet with distinct phases is produced.

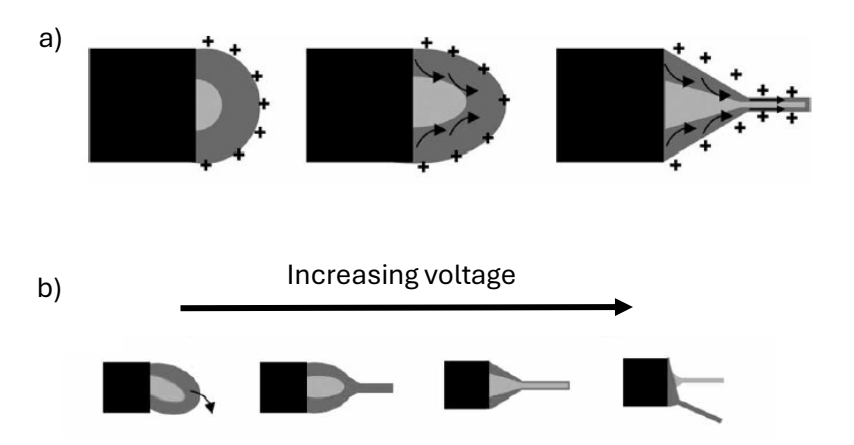


Figure 2. 13 a) the compound Taylor cone formation and b) the effect of the increased voltage on the formation of the compound Taylor cone. Reprinted from Moghe & Gupta (2008) [91]. Copyright 2023 Informa UK Limited.

As mentioned, the coaxial electrospinning process is not too different to single electrospinning. Both polymer solutions are connected to a high voltage, and charge accumulation is evident on the shell liquid's surface. The shape of the Taylor cone is widely used to indicate the directions for adjusting the parameters. Voltage is the main parameter that can be observed from the stability of the compound Taylor cone. Figure 2.13 a) shows the surface charges on the shell solution, which drag the core solution to flow as a compound Taylor cone. Figure 2.13 b) shows the tendency for a compound Taylor cone shape when the voltage increases. When the charge accumulation reaches a certain threshold value, a fine jet extends from the cone. Stresses generated in the shell solution result in the shearing of the core solution. This is through "viscous dragging" and "contact friction." The core liquid deforms into a conical shape, and a compound jet is produced at the tip of the cone. If the compound cone is stable, the core is uniformly incorporated into the shell for core-shell fibre formation. During the journey to the collector plate, the jet undergoes bending instability and follows a back-and-forth whipping trajectory. This causes the two solvents to evaporate and the core-shell nanofibers to form. The variables that control the process and the morphology of the resulting fibres/spheres affect the behaviour in the former. Furthermore, the degree of dissimilarity between them, in terms of composition and physical and rheological properties, plays an important role in the formation of the composite fibre. This is due to the shell and core solutions being in contact and undergoing the same bending instability and whipping motion.

Control Parameters

Solution Viscosities: The viscosity of the shell solution must be adequate to create sufficient viscous stress in the core to overcome the interfacial tension between the two solutions. The correct viscosity will allow the formation of a compound Taylor cone and a jet. Therefore, the viscosity of the shell solution is critical. The chosen shell solution system needs to generate core-shell structures and be electrospinnable. The spinnability requirements for the core solution are not critical due to the jet break-up of the core fluid, which has a tendency to be prevented by the shell. This is because of strain hardening of the interface between the shell and the lesser surface forces that act upon the core solution surrounded by the shell, which otherwise would be higher. The core fluid should possess a certain minimum viscosity if it is to continuously travel without breaking up.

Solution Concentration: An increase in the core solution concentration would increase the core and overall fibre diameters and decrease the thickness of the shell. This is due to the same mass of the shell being distributed over a larger core.

Solvent/Solution Miscibility and Incompatibility: An important parameter to consider before choosing the desired set of solvents for coaxial electrospinning is the interaction between the core and the shell solutions (polymers or solvents). When the solutions encounter the capillary's tip, the solvent in either one must not build up precipitation of the polymer from another solution for electrospinning to be successful. Furthermore, the interfacial tension between the shell and the core should be low for the stable compound Taylor cone to generate.

Solvent Vapor Pressure: The resulting morphology of the core-shell structure will be affected by the type of solvent used in the core solution. Solvents with high vapour pressure that evaporate rapidly, such as chloroform and acetone, create a thin layer at the core-shell interface when used in the core. This has a tendency to trap the interior solvent, which then diffuses out more slowly due to the barrier that has been newly created. When it fully leaves the solidified structure, a vacuum is created. This causes the core structure to collapse and go from being round to a ribbon-like configuration under atmospheric pressure. High vapour pressure solvents cannot be used in the shell solution due to a stable compound Taylor cone and an initial jet being required for coaxial electrospinning. This scenario may produce an unstable Taylor cone and lead to multiple jets forming due to rapid solvent evaporation. Unstable Taylor cones can result in the formation of irregular core-shell structures as well as resulting in separate fibres from the two solutions.

Solution Conductivities: Solutions with high conductivity have high surface charge density. This causes an increase in the elongational force on the jet due to self-repulsion of the excess

charges under a given electrical field. Enhancing the whipping action makes it possible to produce smaller diameter fibres. Conductivity differences between the core-shell solutions can also have an effect on the core-shell fibre formation. A more conductive core solution can be pulled at a higher rate through the applied electric field and cause discontinuity in the core-shell structure. On the other hand, higher shell conductivity would not hinder the process of core-shell fibre formation. However, it would result in higher shear stress on the core material and its subsequent elongation to form a thinner core. It is clear from previous studies that even non-conductive or less conductive liquids can be successfully used as the core in a higher-conducting shell.

2.3.4 Hollow fibre preparation

Up to the present, the hollow fibre structure has been fabricated using electrospinning techniques using two approaches. As mentioned, the first approach is based on the coaxial fibre template, removing the core fibre after the electrospinning process by heat treatment or by the use of solvent solution treatment of the core. This method requires two steps of preparation. This traditional method is popular among ceramic or metal shell fibre fabrication. In this instance, the shell fibre has a much higher melting point than the core fibre. The second approach is based on the different evaporation rates of the core and shell solutions. This method seems to work on the polymeric shell fibre, where its melting point is not much higher than that of the core fibre.

2.3.4.1 Template coaxial electrospinning approach

The production of hollow nanofibres or nanotubes from ceramic-polymer composites is a unique technique that has been developed in relation to coaxial electrospinning. In this technique, the core is selectively removed, instead of the shell, from the assembly to produce the hollow nanofibres. This method of producing nanotubes using coaxial electrospinning was first reported in 2004 by Li et al. and by Loscertales et al. [92-93]. Both studies resulted in the production of composite and ceramic hollow nanofibres. Non-polymeric liquid was employed as the core solution. This was either olive oil or glycerin, as used by Loscertales et al., or a heavy mineral oil, as used by Li and Xia. The oil was extracted using octane after hydrolysis of the precursor through a prolonged exposure to air. In order to obtain pure titania nanotubes, the structure was further calcinated (see Figure 2.14). The study showed that the dimensions of the hollow nanofibres that were produced, in terms of inner diameter and wall thickness, could be varied by the feeding rate of the oil. The hollow fibres that were produced had an inner diameter of 200–370 nm and a wall thickness of 20–50 nm. Loscertales et al. prepared the silica nanotubes in a similar manner by using tetraethyl orthosilicate (TEOS) as the shell.

The direct coaxial electrospinning method for forming hollow fibre structures requires mineral oil as a core material [92]. Li et al. prepared a Poly (vinyl pyrrolidone) (PVP) solution, which contained the precursor of $Ti(O_iPr)_4$ as a shell material. The hollow PVP/ $Ti(O_iPr)_4$ was obtained after the core oil was removed by octane.

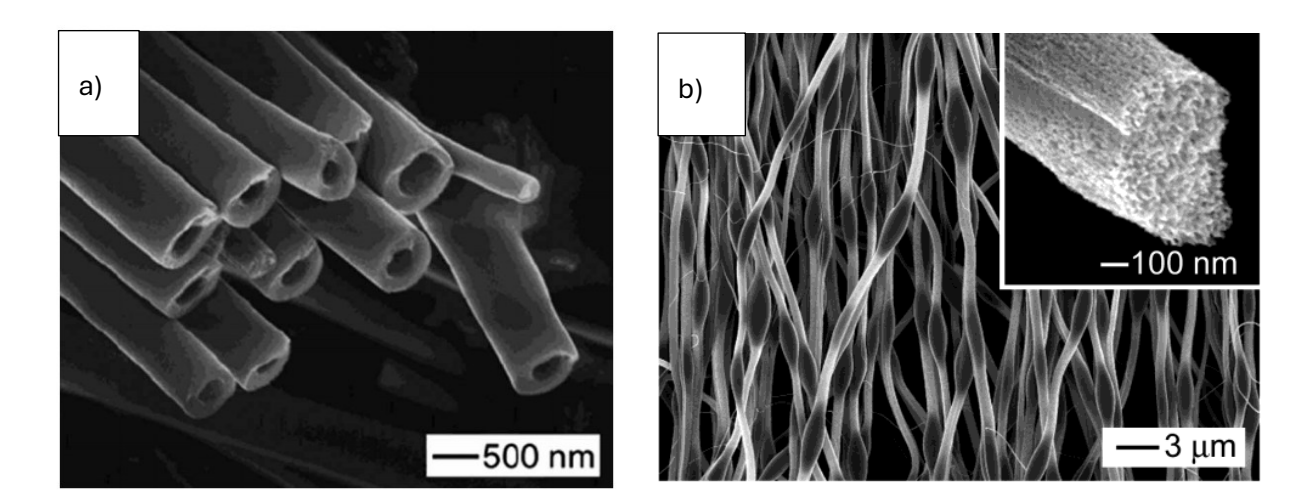


Figure 2. 14 SEM image of the electrospun TiO₂ fibres fabricated by D. Li and Y. Xia 2004. a) the TiO₂/PVP hollow fibres prepared by a coaxial electrospinning technique, b) the TiO₂/PVP fibres with the oil phase inside the bead formation. Reprinted from Li and Xia (2004) [92]. Copyright 2006-2023 Scientific Research Publishing Inc.

There are several studies that report the methodology for producing electrospun hollow fibre, as shown in Table 2.2. Interestingly, the majority of the existing research used the same techniques to produce hollow fibres. This was done by using paraffin oil as a core fibre while using the alternative material mix with electrospun precursor, and then calcining the core fibre out at temperatures above 500 °c.

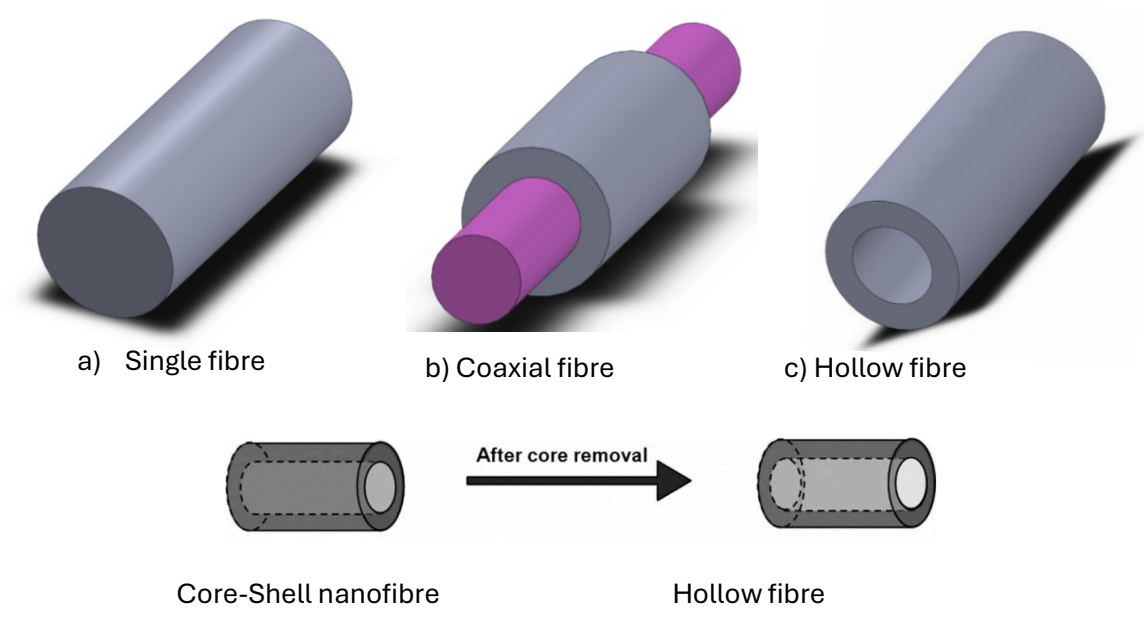
Table 2. 2 A summary of the production of the produced electrospun hollow fibres.

Hollow fibre	Solutions/Precursors	Electrospinning condition	Ref
TiO ₂	PVP/Tetra-butyl titanate (TBT)/ethanol/acetic acid	V = 30kV, D = 15 cm Inner = paraffin oil Treatment = 500 °c, t= 4 h	[94]
	PVP/tetrabutyl titanate $(Ti(OC_4H_9)_4)$ /ethanol/paraffin oil	V = 20-30kV, D = 15-25 cm Inner = paraffin oil Treatment = 500 °c, t= 8 h	[95]
	Titanium isopropoxide/PVP/acetic acid/ethanol	V = 30kV, D = 20 cm Inner = paraffin oil Treatment = 600 °c, t= 2 h	[96]

Figure 2.15 shows the different models of fibre: a) single fibre produced from the single needle/spinneret, b) and c) are coaxial or core-shell structure fibre, and hollow fibre produced from a coaxial spinneret. The hollow fibre is a coaxial fibre with the core removed by different techniques, as can be seen in d). Ga Hyoung Lee presented the technique for controlling the wall thickness and porosity of the PMMA hollow electrospun fibre using the template coaxial electrospinning [97]. The silicon oil was used to be a core template solution and extracted by soaking overnight in n-hexane solution.

This technique became the main method for the production of electrospun hollow fibre.

However, the disadvantage of this technique is the damage to the shell polymer after calcination. The usage in an application that requires a closed shell cavity is not suited to this specific technique.



d) technique for producing hollow fibre

Figure 2. 15 A model of a) single fibre, b) coaxial fibre, c) hollow fibre, and d) a technique for producing hollow fibre

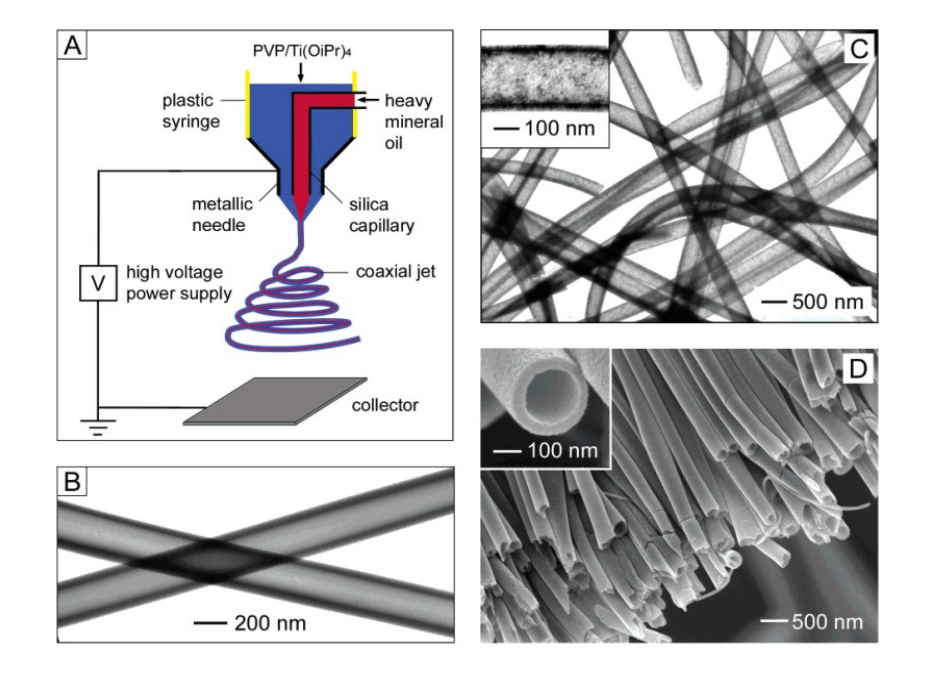


Figure 2. 16 Schematic illustration of Li and Xia setup, the SEM images proved the obtained hollow structure. Reprinted from Li and Xia (2004) [92]. Copyright 2023 American Chemical Society.

2.3.4.2 One-step hollow fibre approach

In 2004, a Spanish team led by Loscertales et al proposed the one-step coaxial electrospinning approach. This was the same year as the hollow structure for metal shell electrospun fibre was first presented [93]. The research group had been examining the compound Taylor cone since 2002. The researchers later introduced the idea of a one-step hollow fibre approach for producing a form of nanotube ceramic material ZrO₂. This novel method is based on the compound Taylor cone's immiscibility (or poorly miscible) for the two solutions. The core solution must be poorly miscible with the shell solution in the compound Taylor cone. During the electrospinning process, the shell solution receives a prior charge, while the layer between the core and shell solution forms the gel layer, which behaves like a gel template for the shell jet. The gel and shell jet then travel to the target by overcoming the electrostatic force. The gel layer evaporates during the electrospinning flight, resulting in a solid and hollow structure inside the shell polymer. When the outer liquid solidifies, it results in the formation of a shell fibre or a liquid-filled hollow fibre. There is no chemical requirement for this process.

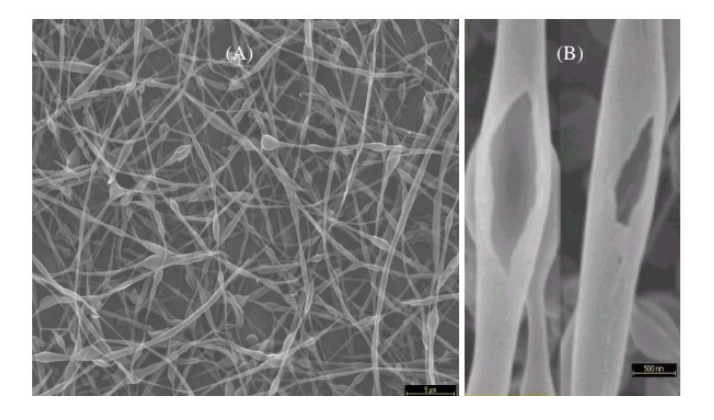


Figure 2. 17 The SEM image of the hollow nanotubes produced by the one-step hollow fibre approach in the random orientation. The first was proposed by Loscertales et al. in 2004. Reprinted from Loscertales et al. (2004) [93]. Copyright by 2023 American Chemical Society

Figure 2.16 shows hollow nanotubes collected from a compound electrospray of an aged formulation based on zirconium acetate acid-mediated hydrolysis (outer fluid) and olive oil (inner). The materials were post-treated at 110 °c. Figure 2.17 a) shows the shape, and b) shows the details of the fibres. Figure 2.17 b) reveals that the fibres were intentionally broken so that the hollow inner structure could be viewed. The diameter of the nanotubes was found to be around 500 nm. The thickness of the shell was approximately 60 nm. The scale bar in Figure 2.17 is shown at 500 nm. The results of the study suggested variations in the shapes of the collected fibres. This can be explained by the solidification of the outer shell occurring at the onset of the compound jet instabilities. Dror et al. 2007 demonstrated the fabrication of the polymer shell

solution using a one-step hollow fibre approach. This was achieved with a PCL shell fibre and 4 different core solutions; PEO in ethanol/water, PVA in ethanol/water, PEO in DMF, and PEO in ethanol/water + PBS. The operating parameters are summarised in Table 2.3. The study suggests that it is necessary to have faster solidification of the core than the shell solvent to achieve a hollow structure. In 2012, H. Na et al. presented the fabrication technique for PVDF hollow fibre by using PVA as a core solution. It was found that the high boiling point solvent DMSO and acetone caused secondary corrosion on the shell's skin. This can be eliminated, though, by placing part of the electrospinning collector plate in water. The collected fibres were soaked in H_2O for 24 hours to remove the solvents. Table 2.3 compares the one-step hollow fibre approaches from the existing research.

Table 2. 3 A summary of the production of the electrospun hollow fibres.

Authors, year	Polymer Solution					Ambient temperature	Wall thickness	
	Shell			Core			-	(micron)
	Polymer	Solvent	Flow rate (mL/h)	Polyme r	Solvent	Flow rate (mL/h)		
Loscertales et al., 2004 [93]	Tetraethyl orthosilicate (TEOS) Hydrous Zirconia tube	Not reported	Not reported	Olive oil glycerin	Not reported	Not reported	23 °C Require post- drying at 500 C	0.07
Dror et al., 2007 [98]	PCL 10% Chlorofor m/DMF 80:20	m/DMF	4, 3	PEO 4%	Ethanol/ water, 40:60	0.5, 0.3	Room temperature, humidity 50- 60%	0.5-1.0
		80:20	Not reported	PVA 9%	Ethanol/ water, 50:50	Not reported		
		Not reported	PEO 4%	DMF	Not reported			
			3	PEO 4%	Ethanol/ water, 40:60 1 mL PEO solution+50 mL PBS	0.3		
Na et al., 2012 [89]	PVDF 17%	DMSO/Ace tone 4:6	1.7	PVA 19%	DMSO: Ethanol 9:1	0.1 - 1.5	Not reported	1.5-2.7

To date, there are only two studies related to hollow polymer shell research. Both of these studies examined the fabrication process. There are no known studies regarding the further characterisation or applications of electrospun hollow polymer fibres.

2.3.5 Co-electrospinning of core-shell fibres using a single-nozzle technique

To produce a core-shell structure of polymer on a microscale using electrospinning techniques, the coaxial nozzle is typically used for this purpose. The co-electrospinning setup consists of 2 syringe pumps to push the polymer solutions through the inner and outer needles, as can be seen in Figure 2.12. As discussed in section 2.3.2, the flow rate of the polymer solution is the main working factor in the electrospinning process, which is quite challenging when two or more polymer solutions are flown simultaneously at the micro-scale. Regarding mass production, the small changes in electrospinning parameters affect the entire system. Obtaining satisfactory concentration between the core and shell materials in the as-spun fibres is challenging, which can lead to the emergence of extended sections of the core material from the shell. Core entrainment cannot be assured without assistance. To enhance core entrainment, it has been discovered that protruding the inner nozzle from the outer shell nozzle is beneficial.

Thus, this section discusses the technique of using a single nozzle to produce a core-shell structure of the electrospun fibre. This technique was first demonstrated by Bazilevsky et al. in 2007 [99]. The technique relies on the precipitation of the polymer solution in the form of droplets after leaving the solution for a day. The team found that the 1-day-old poly(methyl methacrylate) (PMMA)/polyacrylonitrile (PAN) solutions in dimethylformamide (DMF) were precipitated. After electrospinning using the single nozzle, the PMMA droplet was trapped inside the base PAN solution in the Taylor cone. An analysis based on theory demonstrates that the flow of the outer shell is sufficient to stretch the inner droplet into the shape of a Taylor cone, resulting in the formation of a jet with a core-shell structure, as seen in Figure 2.18. In the conventional electrospinning process, the jet is subjected to simultaneous pulling, stretching, elongation, and bending due to the electric forces. The rapid evaporation of the solvent leads to the solidification of the shell jet, resulting in the formation of compound core-shell nano/micro fibres. In order to create hollow tubes, it is necessary to remove the inner core after coelectrospinning. This can be achieved by selectively eliminating the core material using solvents or heat treatment, as can be seen in Figure 2.14

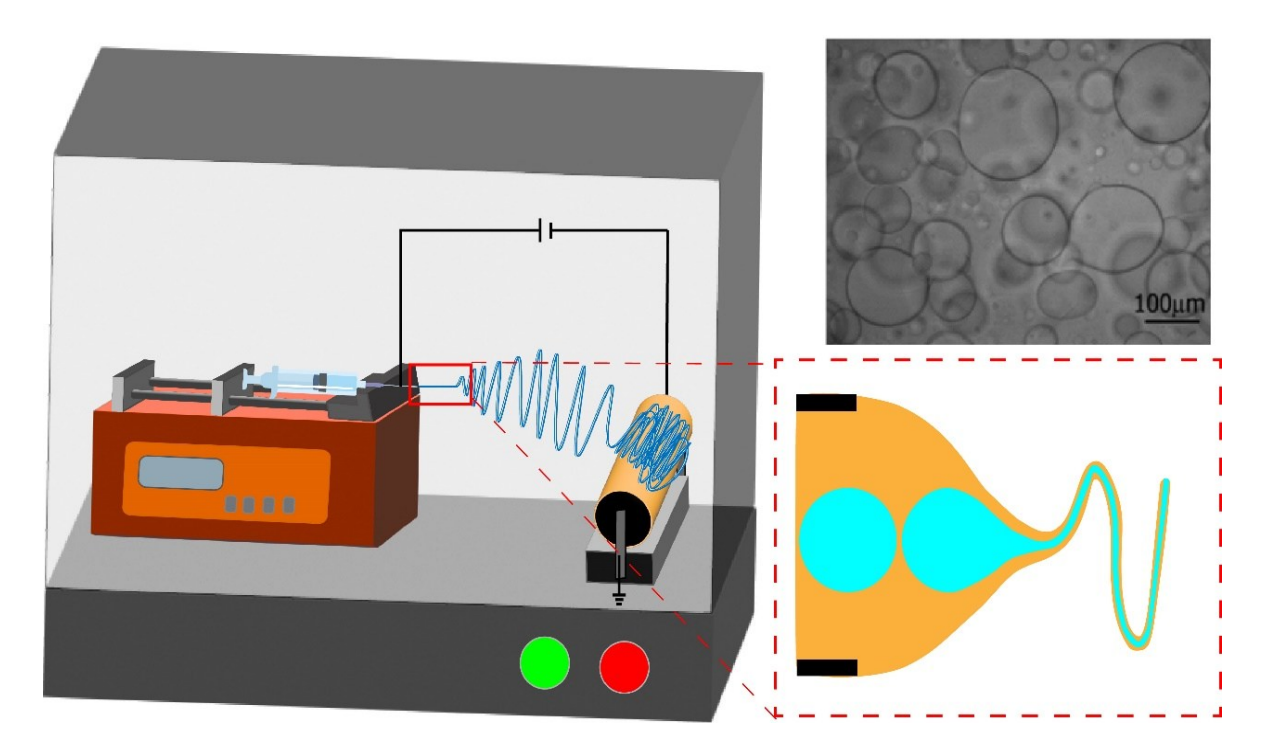


Figure 2. 18 Coaxial electrospinning using a single-nozzle technique. Reproduced based on Bazilevsky et al.'s work [99]. Copyright 2023 American Chemical Society.

Table 2. 4 A summary of the research using a single nozzle technique to produce the coaxial electrospun fibres

Authors, year	F	Polymer	Solvent	Applications	
	Shell	Core			
Bazilevsky et al.	PAN	PMMA	DMF	Study theory	
2007 [99]				and principles	
Wang et al.,	Water	Oil	-	Study theory	
2014 [100]	phosphate	poly(lactic-co-	-	and principles	
	buffer saline	glycolic acid)			
	(PBS)	(PLGA) solution			
Wang et al.,	(PEDOT:	sodium alginate	Acetone and IPA	Wearable	
2020 [101]	PSS)	(SA)	LiCl and CaCl2	Sensor	
Mirmohammad	PAN	Epoxy resin	N, N-	Study theory	
et al., 2020			dimethylbenzylamine	and principles	
[102]			(BDMA)		
			as the catalyst and N ,		
			N-		
			dimethylformamide		
			(DMF)		
Zaidi et al.,	CNF	Fe(NO ₃) ₃ :9H ₂ O/PAN	DMF	Anode for a	
2020 [103]	MoS ₂ /PMMA			battery	

2.3.6 Charge trapped behaviour in electrospun fibre mechanism

The electret material has been used in various applications, especially in energy harvesting, such as ferroelectret, piezoelectric, and triboelectric generators. The corona discharge is one of the most popular techniques to fabricate charge generation and store charge in the electret material. The capacity to store charge primarily relies on the qualities of the polymer. Furthermore, the charge stability is significantly affected by factors such as the architecture of the membrane, the type of chemicals used, and the processing circumstances. Various techniques can be employed to prolong the lifespan of a charge and prevent its degradation. One effective approach involves introducing a porous structure to the fibres, which enhances

the stability of the charge and the incorporation of additives that have been functionalised as charge traps into the polymer matrix is achieved by integration. However, the manufacture of porous fibres is complicated, and the choice of additives is highly dependent on the properties of the polymer and must be customised to suit the polymer matrix.

Electrospinning, a creative method for producing nanofibers, offers an effective way that overcomes the limitations of the traditional corona discharge by using charge injection during the fabrication process [104-107]. The charge retention capability is dependent on the dielectric characteristic of the polymer, the strength of the electric field, and, notably, the specific locations inside the material where the charges become trapped. Sessler's research classifies the charges in the polymer as either surface trapped charges or volume trapped charges [108]. Surface trapped charges arise from surface defects, fractured chains, and contaminants, which are present in shallow traps and dissipate rapidly as the potential barrier is reduced. Trapped charges of volume are confined to lower energy levels, such as atomic sites, molecule chains, crystalline regions, and crystalline-amorphous interfaces. These charges are released gradually due to a higher energy barrier. In comparison to other electret approaches, electrospinning facilitates the formation of volume charges in deeper traps more readily. This is achieved by utilising a conductive capillary as the electrode and generating charges through field-enhanced dissociation and field emission processes [109]. The solution jets transport charges in the liquid phase, and once solidified, the charges become trapped both on the surface and within the fibres. In addition to charges related to volume, charges related to dipoles are also generated as a result of dipole alignment in response to an electric force. The verification of dipolar orientation was conducted by Dipankar et al. [110], using the technique of infrared spectroscopy. Catalani et al. [111], also found a current signal near the glass transition temperature by thermally triggered depolarisation current measurements. The charges increased the electrostatic interaction between particles and fibres, enhancing particle capture efficiency. Conversely, the charges that build up on the deposited fibres would impact the deposition of subsequent fibres and lead to an uneven membrane structure. Gao et al. [112], present the electret mechanism and charge trapped in the electrospun fibre compared to the corona charge in the form of surface potential. It was found that the characteristics of the discharge time in the electrospun fibre of both PMMA and PI are higher than in the corona discharge approach, as seen in Figure 2.19.

Corona: surface charges Electrospinning: surface and volume charges

Figure 2. 19 Schematics describe the type of charge in corona charged and electrospun fibre explained by Gao et al. (2020). Reprinted from Gao et al. (2020) [112], Copyright 2020 Elsevier B.V.

2.4 Polymers used in this work

This section provides the background to the polymers used in this research. To investigate the effect of the hollow structure of electrospun fibre, polar and nonpolar polymers were chosen to present the piezoelectric properties.

2.4.1 Polyvinylidene fluoride (PVDF)

Polyvinylidene fluoride (PVDF) is popular in many ferroelectric polymer applications due to its polar structure, stability, light weight form and flexibility. PVDF possesses unique electroactive properties and has piezo-, pyro and ferroelectric properties. The chemical inert thermoplastic fluoropolymer obtained from the polymerisation of vinylidene fluoride is lightweight, flexible, has high purity, is resistant to solvents and is stable under an electric field. As PVDF is naturally a crystalline polymer or polar polymer, it is widely used in several applications, including energy harvesting, sensors and transducers. PVDF consists of repeated monomer units such as (-CH₂-CF₂-)_n with a 50% crystallinity embedded in the amorphous domain at a low melting point (177 C) [113]. PVDF exists in four different crystalline forms. These are α , β , γ , and δ phases when based on the chain formation (order of polymer chains in the unit cell) as gauche or trans linkages. The polymorph that shows piezoelectric nature is β and γ phases. The material has oriented hydrogen and fluoride unit cells in conjunction with a carbon backbone. Therefore, it is seen as useful in many applications related to nanofibre materials. The structure of PVDF in α , β , γ is shown in Figure 2.20. Typically, PVDF is found in the form of a nonpolar α -phase. To achieve the piezoelectric phases, an electrical field or a mechanically applied force is needed.

Electrospinning has been shown to be a versatile and promising technique for using electrostatic force to induce the β and γ phases. The basic principle behind this technique is the uniaxial stretching of a viscoelastic polymer solution, which is applied through electrostatic force. The nanofibre will then be continually extruded onto the substrate, attached to the other side of the electrode. As a result, the evaporated polymer solution will pole and lay on top of the substrate in a solid fibre. The randomly aligned fibre is shown to exhibit the piezoelectric phase after the electrospinning process [114].

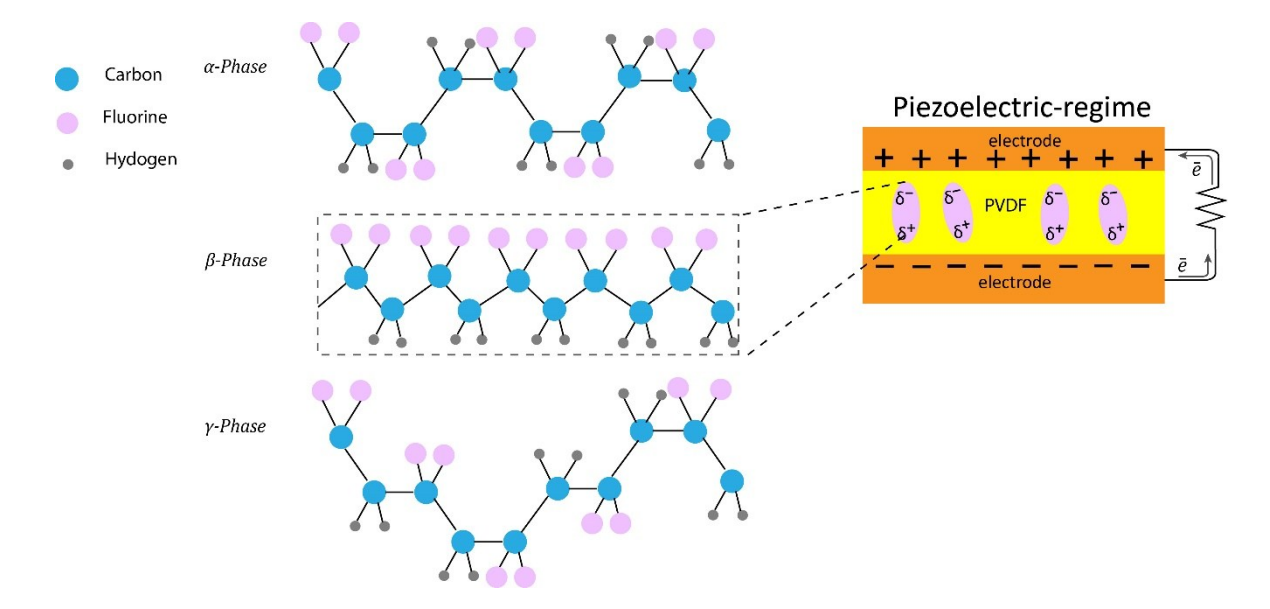


Figure 2. 20 The main phase of PVDF and the beta phase are induced by stretching and a high-voltage poling process.

Several studies have shown electrospinning to be the most effective method for producing a β -phase [115-118]. In addition, the porous structure of electrospun PVDF has been found desirable for energy harvesting applications. In general, PVDF has d₃₁ of around 20 pC/N and - $20>d_{33}>-30$ pC/N [119].

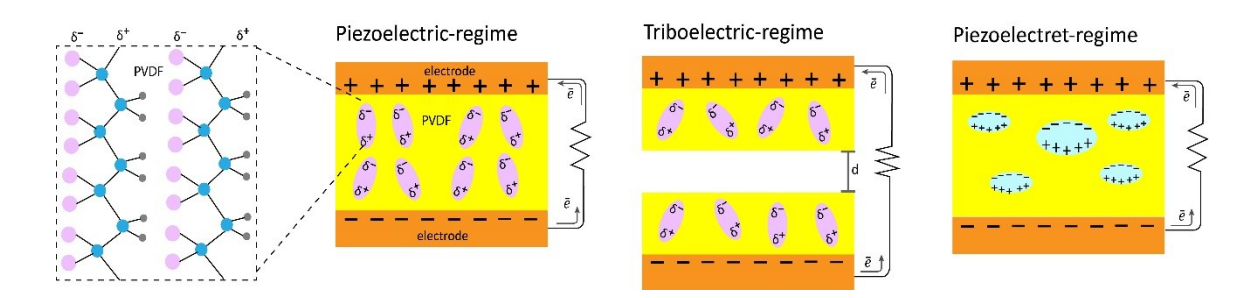


Figure 2. 21 Energy harvesting from mechanical energy regime in PVDF

2.4.2 Polystyrene (PS)

Polystyrene is a widely used low-cost thermoplastic polymer that is easy to recycle when compared to thermoset and elastomer polymers. Its intrinsic hydrophobicity has been extensively investigated and improved upon for various applications [120]. The material consists of many ("poly") styrenes. Styrene is a clear, colourless liquid and small organic compound that is also known as vinylbenzene. Its chemical formula is C₆H₅CH=CH₂ and it possesses a vinyl (-CH=CH₂) functional group attached to a benzene ring (C₆H₆). When heat is applied to the material, the individual molecules (monomers) join and form long chains. An abundance of mixed styrene chains can tangle and form a strong, interconnected mesh. Polystyrene can be found in two main forms: a solid and a foam. The foam exists as extruded polystyrene (XPS) and expanded polystyrene (EPS). A common use for extruded polystyrene is in architectural modelling, and expanded polystyrene is used for packing. Polystyrene has a low weight in relation to its strength, is thermoplastic, and easy to model. When a thermoplastic reaches its melting point, it will become a liquid; however, on cooling, it returns to a solid state. This process can be repeated a number of times. In general, polystyrene (PS) is used in foam, solid and expanded forms. Many of the materials are used for disposable or single-use items. Unfortunately, there are several barriers to recycling polystyrene and very little from food packaging is reused. Recycling involves the basic wash, dry and pelletize routes. Expanded polystyrene usually requires a densification process that removes air through grinding. The recycled plastic is often used in low-cost applications [121].

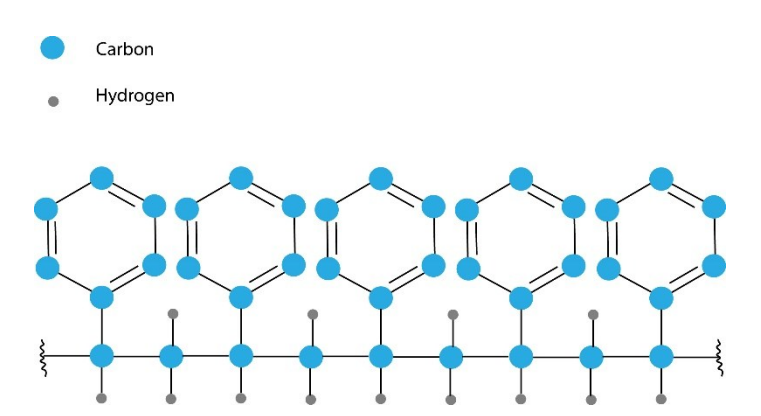


Figure 2. 22 Polystyrene chemical structure. Reproduced from Merrington (2017) Copyright by 2017 Elsevier Inc.

In electrospinning, PS is used as the precursor in many applications, as it is one of the base polymers for electrospinning. Previously, PS has been used in the study of electrospinning parameters, as it is considered to be a low-cost polymer that possesses a high electrospinning rate [122-124]. Datsyuk et al. [121] used electrospun recycled expanded PS as an insulating material for conventional wall-building in construction. It was found that a highly porous PS

possesses excellent thermal insulation conductivity of up to 30% more when compared to traditional materials.

In comparison to PVDF, the polymer structure of PS is considered to be an amorphous, non-polar polymer. The polymer structure of PS remains unchanged under an electric field, thermal treatment or mechanical stretching. Therefore, it does not show ferroelectric properties. In 2019, though, Yuya Ishii and his team reported the discovery of ferroelectric properties in electrospun fibre [125]. It was found that the electrostatic charge trapped in the PS fibre during the electrospinning process showed changes to the ferroelectric properties. This interesting discovery has motivated further research, which will be clarified in the state of the art section.

2.4.3 Polytetrafluoroethylene, (PTFE)

Polytetrafluoroethylene is a synthetic fluoropolymer of tetrafluoroethylene and a Polyfluoroalkyl substance (PFAS) with numerous applications. The commonly known brand name of PTFE-based composition is Teflon by Chemours, a spin-off from DuPont. The outstanding properties of polytetrafluoroethylene (PTFE) include remarkable thermal and chemical stability, high fracture toughness, reduced surface friction, and biocompatibility.

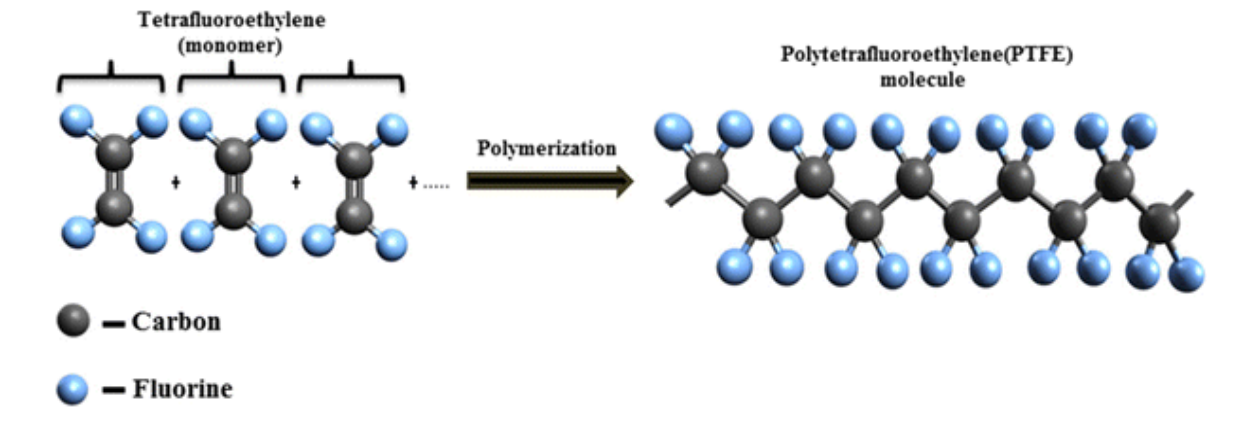


Figure 2. 23 The polymer structure of PTFE. Reprinted from Keng et al. (2022) [126]. Copyright by 2023 Elsevier B.V.

Polytetrafluoroethylene (PTFE) is a very favourable negative triboelectric material employed in high-performance triboelectric nanogenerators (TENGs). The outstanding properties of PTFE include remarkable thermal and chemical stability, high fracture toughness, reduced surface friction, and biocompatibility.

Triboelectric nanogenerators (TENGs) have undergone substantial research in recent years for their potential use in a range of electronic devices, including sensors, power sources, and biomedical devices. Fluoropolymers such as polytetrafluoroethylene (PTFE), perfluoroalkoxy alkanes (PFA), and fluorinated ethylene propylene (FEP) are utilised in high-performance TENGs

due to their exceptional surface charge and strongly negative triboelectric characteristics. PTFE has exceptional flexibility, chemical resistance, thermal resistance, non-stick characteristics, and high surface potential. As a result, it is well-suited for the development of high-performance and durable TENGs.

TENGs provide a contact force that induces molecular structure deformation and electronic structure modification. Carbon possesses electrically efficient states and a positive local dipole due to the strong electron attraction of bound fluorine. Enhancing the deformation of carbon leads to an improvement in its positive local dipole, allowing it to receive a greater number of electrons to compensate for this dipole. Furthermore, the band diagram, orbital distribution, and density of states (DOS) are used to reduce the energy level of the lowest unoccupied molecular orbital (LUMO). PTFE has the ability to receive a greater number of electrons when it is deformed. The immediate change in PTFE is an important factor in confirming the unknown process of charge transfer in contact electrification [126].

2.5 The state-of-the-art

This section is focused on the nature of current research to indicate the gap in knowledge in relation to energy harvesting based on electrospinning techniques.

2.5.1 Nature of TENG research

Dielectric polymers such as PTFE, PVDF, PDMS, nylon, and Kapton, together with metallic materials like Au, Cu, and Al, are extensively utilised as electrode layers. They significantly influence the conventional triboelectric series due to their flexibility and favourable triboelectric characteristics in the form of flexible films. The advancement of TENGs is severely limited by those materials due to their surface morphology, inspiring researchers to investigate new materials that can address this drawback. These investigations broaden the application range and enhance the output performance of TENGs. The use of electrospinning techniques is one of the important strategies to overcome this limitation. The summary of the research that used electrospinning to fabricate polymer for energy harvesting purposes based on TENG assembly can be seen in Table 2. 5.

Table 2. 5 The summary of TENG using electrospinning techniques

	Polymer	Solvent	Tribo-polar	Operating mode	TENG Negative layer	TENG Positive layer	Active Area (cm²)	V _{oc} (V)	I _{sc} (μΑ)	Peak power density (mW/m²)	Ref.
1	PVDF	DMF: acetone	Negative	CS	Electrospun PVDF	Nickel copper- coated PET fabric	30	210	45	21	[127]
2	Silk fibroin	Silk fibroin dissolved in a water-based solution	Positive	CS	PI film	Silk fibroin nanofiber	NA	22	NA	4.3	[128]
3	PVDF Nylon 6	DMF: acetone Formic: acetic acid	Negative Positive	CS	PVDF	Nylon6	100	1000	200	1717	[129]
4	PVDF PA6	DMF: acetone Acetic: formic acid	Negative Positive	CS	PVDF nanofiber	PA6 nanofiber	16	164	0.392	130	[130]
5	PI	DMAc	Negative	CS	PI nanofibers	Aluminium electrode	16	753	10.79	2610	[131]
6	PU	DMF: acetone	Negative	CS	Electrospun PU	Aluminium	N/A	2.3	0.35	0.002	[132]
7	PVDF	DMF: acetone	Negative	Sliding mode	Electrospun PVDF	Electrospun PA6	12	228	0.870	1800	[133]
	PA6	Formic: acetic acid	Positive								

Chapter 2

	Polymer	Solvent	Tribo-polar	Operating mode	TENG Negative layer	TENG Positive layer	Active Area (cm²)	V _{oc} (V)	Ι _{sc} (μΑ)	Peak power density (mW/m²)	Ref.
8	Nylon 66	Formic acid	Positive	CS	Copper electrode	Electrospun Nylon 6,6	16	350	300	550	[134]
9	PAN Nylon 66	DMF Formic acid	Negative Positive	CS	Electrospun PAN	Electrospun Nylon	1	15	0.300	62	[135]
10	PVDF	DMF: acetone	Negative	CS	Electrospun PVDF	Tempo-oxidised cellulose aerogel film	9 cm²	90	740	130	[136]
11	Nylon 66	Formic acid	Positive	CS	PVDF coating on PET	Electrospun Nylon 66 on silk	6.25	101	15.3	280	[137]

2.5.2 Energy harvesting from composite fibre

Electrostatic phenomena have long been known and also appear to occur on a regular basis. Wang's research group though have just recently observed the potential of electrostatic charge transfer in energy harvesting technologies [138]. This was the start of applying electrostatic phenomena in energy harvesting, and it is well known as a triboelectric nanogenerator (TENG). Enhancing surface area and adding ferroelectric material can improve triboelectrification. Increasing the speed or frequency of the electrostatic induction component of triboelectricity is a frequently reported process to develop TENG devices in order to increase their output performance [139-141]. Nevertheless, the approaches to enhance the contact electrification element of TENGs have been somewhat restricted. These have mostly involved three basic methods: modifying surface morphology, modifying surface chemistry, and integrating ferroelectric materials (via dipole-dipole induction) [57].

Table 2. 6 Summary of the filler used in electrospinning technique for TENGs

	Polymer	Filter	Solvent	Tribo- polar	Operating mode	TENG Negative layer	TENG Positive layer	Active Area (cm²)	V _{oc} (V)	I _{sc} (μΑ)	Peak power density (W/m²)	Ref.
1	PVDF PHBV	GO	DMF: acetone Trichloromethane	Negative Positive	CS book- shaped	PVDF - GO	PHBV	20	340	78	2.3	[142]
2	PVDF Nylon	AgNW	DMF: acetone Formic acid	Negative Positive	CS	PVDF/ AgNW-	Nylon fibres	4	240	33	3.5	[143]
3	PVDF	Pore creating by template electrospinning	DMSO: acetone	Negative	CS	Trimurti PVDF mat	Natural Rubber mat	20.25	1403	78	10.6	[144]
4	PVA	Mxene nanosheets	Water for PVA/MXene solution	Negative	CS	PVA/MXene nanofibers	Silk Fibroin	28.26	118.4	-	1.0876	[145]
	Silk Fibroin	-	HFIP	Positive								
5	PVDF	ZnO NWs	DMF: acetone	Negative	CS arch-shaped	PVDF-ZnO NWs	Nylon-ZnO NWs	10	330	10	3	[146]
	Nylon 11	ZnO NWs	1,1,1,3,3,3- Hexafluoro-2- propanol (HFIP)	Positive	TENG							

	Polymer	Filter	Solvent	Tribo-	Operating	TENG	TENG	Active	V _{oc}	I _{sc}	Peak power	Ref.
				polar	mode	Negative	Positive	Area	(V)	(µA)	density	
						layer	layer	(cm²)			(W/m²)	
6	PVDF	ВТ	PVDF in	Negative	CS	PDMS/BT-	PHBV	22	1020	29	2.2	[147]
			DMF/acetone		book shaped	PVDF	nanofibre					
			PDMS dissolved in			nanofibre						
			THF with BT 0.3-									
			3.6 wt%									
7	Nylon 6	PP combined	Nylon 6 in formic		CS	Nylon 6	Melt-blown PP	25	33.93	0.247	N/A	[148]
		with the	acid and acetic			nanofibre						
		electrospun	acid mixture									
		Nylon 6.										
8	PVDF-	Styrene-	PVDF-HFP in DMF:	Negative	CS	PVDF-	Aluminium or	4	160	7	0.222	[149]
	HFP	Ethylene-	acetone			HFP/SEBS	human skin					
		Butylene-Styrene				composite						
		(SEBS)	SEBS dissolved in			nanofibres						
		microspheres	Mesitylene: DMF									
9	PVDF	Polyethylene	PVDF in DMF:	Negative	CS	Hollow PVDF	PDMS valve	13.5	105.5	16.7	0.92	[150]
		glycol (PEG) to	acetone									
		form a hollow	PEG in THF									
		structure										
10	PVDF-	MXene	PVDF-TrFE in	Negative	CS	PVDF-	Nylon 11	3.14	270	140	4.02	[151]
	TrFE		ACT/DMF			TrFE/MXene				mA/m²		

	Polymer	Filter	Solvent	Tribo- polar	Operating mode	TENG Negative layer	TENG Positive layer	Active Area (cm²)	V _{oc} (V)	I _{sc} (μΑ)	Peak power density (W/m²)	Ref.
11	PVDF	MXene	DMF: acetone	Negative		PVDF/MXene fibre	PA6 fibre	4	46	2.42	0.290	[152]
	PA6	NA	Formic: acetic	Positive								
12	PVDF	Graphene	DMF	Negative	CS	PVDF/GNSs	PA6 film		1511 V	189	130.2	[153]
	PA6	nanosheets (GNSs)	Formic acid	Positive		fibres				mA/m²		
13	PVDF- TrFE	PI	PVDF-TrFE in DMF: acetone PI in DMAc	Negative	cs	PI/PVDF-TrFE composite nanofibre	PET	1.6	364	17.2	2.56	[154]
14	PVDF- TrFE	MXene	DMF: acetone	Negative	CS	Electrospun PVDF- TrFE/MXene	Electrospun Nylon-11	0.3	270	140 mA/m²	4.02	[155]
15	PVDF	PS as a charge storage layer	DMF: acetone	Negative	CS	Electrospun PVDF with PS	Electrospun Nylon 66	3	200	20	NA	[156]
	Nylon 66	AgNWs as electrodes	HFIP	Positive		intermediate layer for charge trapping						

	Polymer	Filter	Solvent	Tribo- polar	Operating mode	TENG Negative layer	TENG Positive layer	Active Area (cm²)	V _{oc} (V)	I _{sc} (μΑ)	Peak power density (W/m²)	Ref.
16	PVDF	KNN-ZS nanorods	DMF: acetone	Negative	CS	PVDF/KNN-ZS	PTFE tape	N/A	25	211	9.075	[157]
17	PVDF- HFP P3HT	P3HT as conductive filler	PVDF-HFP in THF P3HT in PVDF-HFP - THF	Positive	CS	Kapton	P3HT/PVDF- HFP nanofibre	6.25	78	7	0.45	[158]
18	PVDF	MoS ₂ /Carbon Nanotubes	DMF: acetone	Negative	CS	PVDF- MoS ₂ /CNT nanofibres	Nylon fabric	36	300 V at 50 N and 1.6 Hz	11.5	0.134	[159]
19	PVDF	РММА	PVDF/PMMA in DMAc	Negative	CS	PVDF/PMMA fibre film	Glass fibre fabric	9	810	70	13.8	[160]
20	PLLA	Cyclodextrin (CD)	DCM: DMF	Positive	CS	PLLA -CD		16	245	84.70	53.04	[161]

	Polymer	Filter	Solvent	Tribo-	Operating .	TENG	TENG	Active	V _{oc}	I _{sc}	Peak power	Ref.
				polar	mode	Negative	Positive	Area	(V)	(μ A)	density	
						layer	layer	(cm²)			(W/m²)	
21	PLA and	Carbon Black	DMF: acetone	Positive	CS	TPU/CB	PLA/CS/aloin	4	9.91			[162]
	Chitosan	(CB)				beaded	porous					
	(CS)	nanoparticles				nanofibre	nanofibre					
						membrane	membrane					
	polyureth			Negative		(TPU/CB	(PCA PNFM)					
	ane (TPU)					BNFM)						
22	PVDF-	MWCNTs and	DMF: acetone	Negative	CS	PVDF-TrFE	Aluminium foil	9	508	16.5	5.28	[163]
	TrFE	AgNWs				nanofibre						
						MWCNTs/PDM						
						S/AgNWs						
						composite						
23	PLA	Poly(ethylene	Chloroform/DMF	Positive	CS	: P(VDF–TrFE)	PLA-mPEG	4	342.8	38.5	116.21	[164]
		glycol)				nanofibrous	nanofibrous					
		monomethyl				films	films					
		ether (mPEG)										
24	PVDF	SWCNTs (in the	DMF	Negative	CS	PVDF/SWCNT	Doku spray	15	19.5	15	N/A	[165]
		piezoelectric				s nanofibres	(with or					
		part) and $\alpha\text{-Al}_2O_3$					without α-					
		nanoparticles in					Al₂O₃ NPs) on					
		the triboelectric					aluminum foil					
		part)										

	Polymer	Filter	Solvent	Tribo- polar	Operating mode	TENG Negative	TENG Positive	Active Area (cm²)	V _{oc} (V)	I _{sc} (μΑ)	Peak power density (W/m²)	Ref.
						layer	layer	(CIII)			((((((((((((((((((((
25	PVDF-	Thermoplastic	PVDF-TrFE in	Negative	CS	P(VDF-	Polylactic	4	49.29	N/A	0.054	[166]
	TrFE	polyurethane	DMF/acetone			TrFE)/TPU-CB	acid/chitosan/					
		blended with	(40:60 w/w)			hybrid	aloin (PCA)					
		carbon black	TPU/CB dissolved			nanofibre	nanofibre					
			in DMF/acetone				membrane					
			(70:30 w/w)									
26	PVDF	PS	DMF: acetone	Negative	CS	Electrospun	Copper film	9	165.9	11.1	0.597	[167]
						PVDF/PS						
27	PVDF	MWCNTs	DMF: acetone	Negative	N/A	PVDF/MWCNT	N/A	N/A	N/A	N/A	N/A	[168]
						nanofibre						
28	PVDF	CNTs	N/A	Negative	CS	Janus	PMMA	9	353	22.4	N/A	[169]
	PVP	Eu(TTA) ₃ (TPPO) ₂				nanofibre	nanobelt array					
						membrane						
						(JNM)						
29	PVDF	PTFE particle	PVDF in DMF:	Negative	Solid-liquid-	PVDF/PDMS/P	Hydrophobic	N/A	150	60	N/A	[170]
		PDMS	acetone		based TENG	TFE	PANI/CNTs/Ag					
			PDMS solution		operating in	electrospun	NWs electrode					
			with PVDF before		a droplet	composite						
			PTFE particles									
			were added									

Chapter 2

	Polymer	Filter	Solvent	Tribo-	Operating	TENG	TENG	Active	V _{oc}	I _{sc}	Peak power	Ref.
				polar	mode	Negative	Positive	Area	(V)	(μΑ)	density	
						layer	layer	(cm²)			(W/m²)	
30	TPU and	BTO particles	DMAc and n-	Positive	CS	PP nonwoven	EC/TPU/BTO	4	125.8	34.1	1.68	[38]
	ethyl		hexane (7:3, v/v)			fabric	composite					
	cellulose						nanofibre					
	(EC)											
31	PVDF and	PTFE	PVDF in DMF	Negative	CS	PTFE/PVA-	PP melt-blown	N/A	58	0.789	N/A	[171]
	PVA		PVA in distilled			PVDF	cloth					
			water and mixed									
			with 60 wt% PTFE									
			emulsion									

2.5.3 Ferroelectret from electrospun hollow fibre

Piezoelectric polymers can be classified as amorphous and semi-crystalline polymers with a permanent molecular dipole moment. The re-orientation of a dipole moment in a material causes the piezoelectric effect to be present due to the polarisation in the material. PVDF is a well-known semi-crystalline piezoelectric material. This material appears to present the most effective piezoelectric property among the polar or piezoelectric polymers through the β and γ phases. The electrospinning technique is the most effective method for enhancing the piezoelectric phase of PVDF. A non-piezoelectric or nonpolar polymer group recently revealed piezoelectric behaviour through the electrospinning process [125], [172-175].

One of the advantages of electrospun fibre is the electret properties caused by the residual charge during the electrospinning process. However, the performance of the electret electrospun fibre has been limited due to the charge decay via the environment. It has been reported that heat, humidity, and solvent affect the deterioration of the fibre, which results in charge decay. Furthermore, the dielectric constant (ε_r) of the material has rarely been associated with the charge decay phenomenon during experimental investigations. There are implications that ε_r is related to charge stability and conductivity [176].

A further simple classification of electrets is homo-electrets and hetero-electrets. Heteroelectret occurs through the internal charging orientation of dipoles, whereas homo-electret generally occurs through excess charge injection into nonpolar materials [176]. Nobeshima et al. (2016) [177], found the piezoelectric-like behaviour in the electrospun fibre of the racemic PLA. This material should not show piezoelectricity in the structure. Generally, a piezoelectric effect is caused by a change in dipole position and/or dipole orientation in a crystal, a ceramic, or a polymer film. The explanation for this behaviour is that the electrospinning process may have induced it. The polymer solution was charged by applying high voltage while the film was stacked on the collector with a unique polarisation-like ferroelectret film in the thickness direction. The strain of the PLA fibre is altered by the applied voltage [177]. The same research group also discovered the same effect with PMMA [178]. In 2017, Nobeshima et al. developed testing techniques by observing displacement changes when loading and unloading forces via a laser displacement sensor. It was shown that the fibre displacement was a key parameter in determining the apparent piezoelectric constant (d_{app}). Figure 2.24 shows the measurement setup for this research group's study. A surface charge potential probe was attached to the fibre during loading and unloading. From 2016 to the present, this group of researchers have developed measurement techniques for investigating the unique properties of a nonpolar electrospun fibre, including PLA, PMMA, PS, and PVA. Electrospun fibres from polar polymers

such as PLLA, PDLLA, and PHB were also compared [172]. In their latest work, the research group published a study of charge potential testing of polar and nonpolar electrospun fibres. It was found that the electrospun fibre from PS revealed the surface charge capacity after 30 days of the electrospinning process. The d_{app} calculation was 1760 pC/N, while PVA seems to have no properties of the electrical charge holding after the electrospinning process.

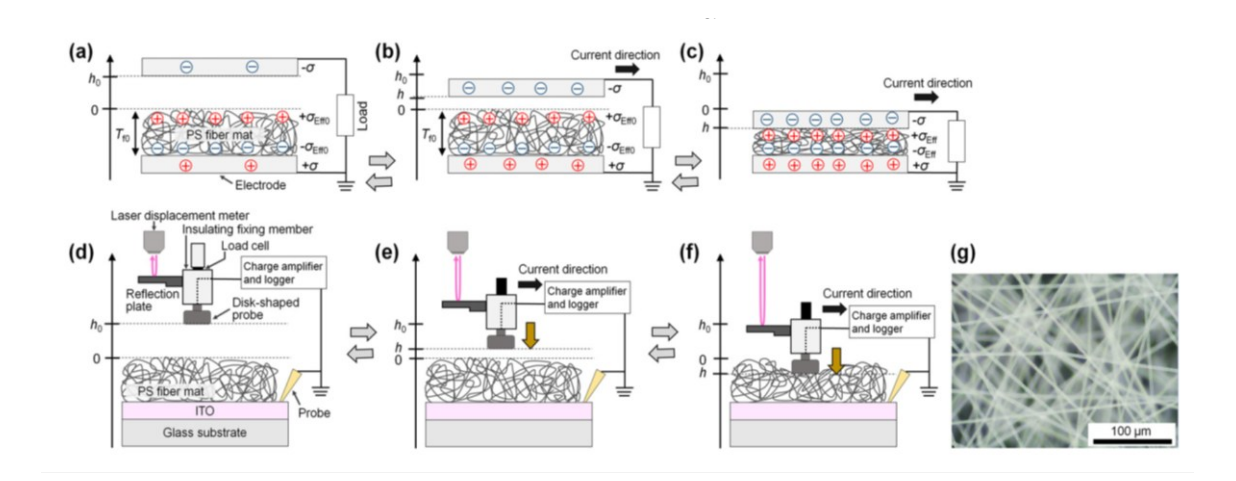


Figure 2. 24 Schematics of the theoretical energy harvesting model of the as-electrospun polystyrene fibre mat setup of Yuya led research group, a) h=h₀, b) h>0, and C) h \leq 0 d)- f) Schematic of the measurement flow of $\Delta Q_{out}(h)$ and h: d) h=h0 e) h>0, and f) h \leq 0, g) Microscope image of the electrospun PS. Reprinted from Ishii and Kurihara, 2019 [175], Copyright 2023 AIP

In 2019, Wang and his team unexpectedly discovered high piezoelectric properties from electrospun PAN. The piezoelectric properties of this material are usually found to be lower than PVDF. PAN is one of the piezoelectric polymers, where the piezoelectric constant is not high when compared with PVDF [179]. A summary of the electrospun nonpolar polymers from the literature is shown in Table 2.7.

Table 2. 7 The comparison of the electrospun fibre of non-polar polymers

Material	Measurement method	Working/testing area	d ₃₃ /output	Ref
РММА	Converse piezoelectric response	Sandwich with gold leaf electrodes 3x5 mm ²	8.5 nm/V	[178]
PS	Calculate the form detected charge due to the applied pressure at 2000 Pa	ITO on glass substrate	1400 pC/N	[125]
PAN PVDF	Compressive impact	5 cm ² Sandwich with Al foil electrode	NA	[179]
PS	Converse piezoelectric response	ITO on glass substrate	>30000pm/V	[174]
PMMA	Calculate the form detected	ITO on glass substrate	1400 pC/N	
PS	charge due to the applied pressure		1760 pC/N	[172]
PVA	at 2000 Pa		Not Found	
PDLLA			750 pC/N	
PLLA			1180 pC/N	
РНВ			310 pC/N	

There is no known report regarding coaxial or hollow fibre of this type for thermoplastic polymer. It is not impossible to fabricate electrospun thermoplastic polymer in hollow fibre form. Furthermore, it could be possible to use bead, lens-like shape fibres that match the requirement of charge storage in ferroelectret materials as a cellular structure mat for charge storage in ferroelectret fibre films (see Figure 2.25).





- a) Bead-less hollow fibre model
- b) Bead lens like shape fibre model

Figure 2. 25 The proposed concept of the bead-like lens hollow fibre for ferroelectret fibre applications a) bead-less fibres with a perfectly rearranged model b) a bead lens-like shape fibre model

Sergey et al. studied the piezoelectric coefficient (d_{33}) of FEP arrays with closed tubular structure air channels with different wall thicknesses of 25 and 50 µm. The tubes had equal air gaps of 250 µm and an outer diameter of 1 mm. The experiment's results corresponded to the analytical model that the same research group suggested in 2018 [180-182]. It was found that the geometry of the arrays and the thickness of the walls and air channels affected the d_{33} coefficient. The model predicted that arrays produced by FEP tubes down to 10 µm-thick walls would exhibit a d_{33} coefficient of up to 600 pC/N. This study showed that the thin-walled tubular geometry enhanced the piezoelectric coefficient of the thermoplastic polymer. With this morphology in the nanoscale, a tubular structure with a bead pocket will have benefits for applications in ferroelectret for confining electrical charges. The higher surface area and higher porous structure of the electrospun fibre will enhance the electric charge transport properties of the ferroelectret.

As mentioned, there are no known reports related to further study on the characteristics or the applications of polymer shells for electrospun hollow fibre. Thus, this research aimed to fabricate the electrospun hollow fibre via a one-step approach. The characteristics of the obtained fibre were challenging at different angles, such as structural, mechanical, electrostatic and electromechanical characteristics. This will lead to the application of energy-harvesting materials for small devices and wearable technology.

2.5.4 Energy harvesting from the core-shell structure fibre

Polystyrene (PS) is utilised to enhance charge retention and minimise charge dissipation under its high electron trap levels resulting from its benzene ring structure. This characteristic enables PS to confine electrons and delay their dissipation rate effectively [183]. Li et al. [184] found high electret performance by combining PS and PVDF using electrospinning techniques. The principle behind the outstanding performance was explained as PS and PVDF, which are classified as weakly and strongly polar polymers, respectively, based on their extremely low and high dielectric constants [185]. The dielectric constant of PS and PVDF is 2.5-2.9 and 6.0, respectively. Both PS and PVDF are widely used as electret materials using the electrospinning technique. Due to its excellent ferroelectric property and high dielectric constant, PVDF is especially common in triboelectric, piezoelectric, ferroelectret, and pyroelectric applications. Luo et al. [167], recently reported the high performance of electrospun PS/PVDF using the mechanical blending of PS and PVDF before the electrospinning process. It was found that the electrospun PS/PVDF increases output performance approximately three times compared to the electrospun fibre of PVDF. The mechanical blending technique before the electrospinning process leads to a single structure of PS and PVDF in the polymeric fibre, which helps the adhesion property of electrospun PS. This can be explained by the lower density of PS when it comes to the lightweight, high porosity obtained from the electrospinning process. Electrospun PS does not get much attention among triboelectric applications, even though it has a high level of eliminated charge retention in a dielectric material. At the same time, PVDF has a higher density than PS; the electrospun PVDF is much denser than PS, resulting in better mechanical properties than electrospun PS. Electrospun PVDF has gained much interest in harvesting energy from friction. In addition, the surface potential of electrospun PS and PVDF have been shown to be positive and negative, respectively [184].

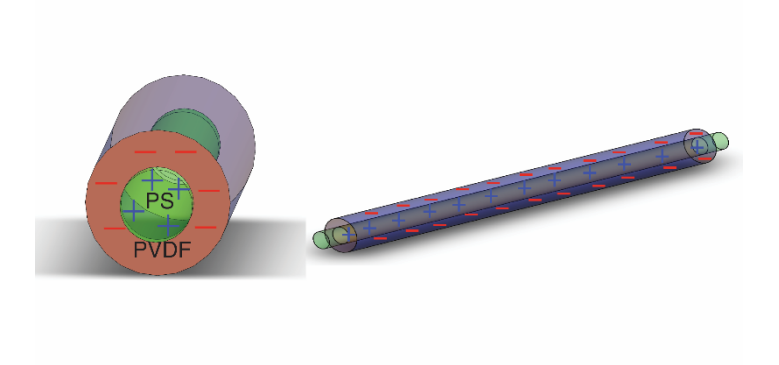


Figure 2. 26 Schematic show the idea of coaxial PS/PVDF electrospun fibre

As far as we know, there have been no reports on the core-shell structure of PS as a core fibre and PVDF as a shell fibre. Electrospun PS has the advantage of having a positive surface

potential, which can cause PVDF to develop a negative surface potential. This results in a large negative surface potential for triboelectric energy harvesters.

2.6 Conclusion

This chapter establishes the theoretical and research background for energy harvesting from electrospun fibres, focusing on the mechanisms, material properties, and structural innovations that enhance performance. The chapter explores key energy harvesting principles, including the piezoelectric, ferroelectret, and triboelectric effects. It reviews the role of polymers such as PVDF, PS, and PTFE in advancing energy harvesting technologies.

Electrospinning is emphasized as a versatile technique for fabricating nanostructured fibres with enhanced surface area and optimized material properties. Significant advancements, including composite, hollow, and core-shell structures, are discussed as transformative approaches to improving energy conversion efficiency and scalability. The potential of these designs for wearable and flexible energy harvesters is highlighted, with core-shell structures showing promising results in combining materials for superior charge retention and triboelectric performance.

The chapter identifies research gaps, such as the need for innovative material combinations, structural optimisation, and durability under environmental conditions. These gaps inform the direction of the experimental studies in later chapters, providing a guide for addressing the limitations of current energy harvesting technologies. This comprehensive review underlines the potential of electrospun fibre technology to enable sustainable, high-performance solutions for next-generation wearable devices.

Chapter 3 Experimental process, materials, and methods

3.1 Introduction

The experimental procedure and the characterisation methodology are discussed. The chapter is divided into two main parts. The first is the experimental design section, which describes the conceptual research framework overview, including materials and equipment used in this research. The materials and characterisation section provides an overview of the equipment for identifying performance/results for material fabrication, divided into geometrical, structural, and electromechanical characteristics.

3.2 Materials, equipment and fabrication

This section presents the details and specifications of the materials used in this work. The details of the electrospinning schematic and its setup are shown. The equipment for characterisation, including testing methodology, is discussed in this section.

3.2.1 Materials and chemicals for electrospinning preparation

1. PVDF

The PVDF solution was prepared from PVDF powder (Sigma Aldrich, Dorset, UK, Mw = 534,000) mixed with N-Dimethylformamide (DMF, Sigma Aldrich, Dorset, UK, 99.8%) and acetone (Fisher Scientific, 99.6%).

2. PS

Polystyrene solution prepared from polystyrene pellet, PS (Mw=280,000, Sigma Aldrich) by stirring in N-Dimethylformamide (DMF), ACS reagent, ≥99.8% (purchased from Sigma Aldrich) as a solvent solution.

3. PTFE

PTFE particles (Sigma Aldrich, Dorset, UK, 1-micron particles) in an 18%wt PVDF solution as a polymer carrier for PTFE.

3.2.2 Electrospinning setup

The electrospinning machine (IME medical electrospinning company EC-DIG) was used to prepare the electrospun fibre. The thermometer and humidity sensor were integrated inside the electrospinning cabinet. Figure 3.1 shows the schematic of the electrospinning setup; the digital wireless optical microscope was placed in the cabinet to observe the Taylor cone formation. The syringe pumps were used to attach a 3 ml PTFE syringe to push the polymer solution through the capillary 21G needle. All syringe pumps were placed outside the cabinet for safety reasons. The bespoke rotation drum, 150 mm in diameter and 200 mm in length, was used as a collector to enhance the electrospun fibre area. The photograph and the schematic of the setup can be seen in Figure 3.1 a) and b), respectively.

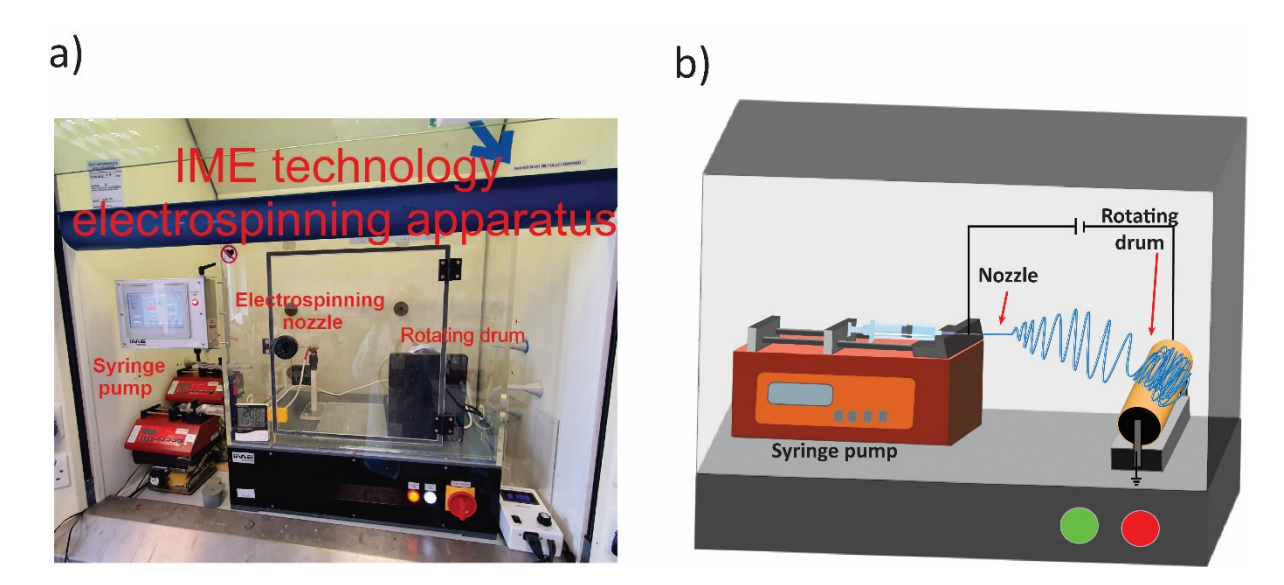


Figure 3. 1 a) The photograph and, b) the schematic of the electrospinning setup used in this work.

3.2.3 Equipment for characterisation

This section has been divided into 2 main areas: equipment for geometrical and structural characterisation and the equipment for electromechanical characterisation. This section provides details in relation to the processes for conducting the experiments.

3.2.3.1 Fourier-transform infrared spectroscopy (FTIR)

Regarding the examination of the solvent residue, a Thermo Scientific^{\mathbb{M}} Nicolet^{\mathbb{M}} iS5 FTIR Spectrometer was deployed to study the chemical bond of the fibre after completion of the electrospinning process. As for the PVDF fibre, the FTIR spectra was applied in order to identify phase fractions between α and β .

The Fourier transform infrared spectrometer (Thermo Scientific ID7, UK) was used to analyse the electrospun fibre's chemical structure.

The preferred technique for infrared spectroscopy is called Fourier Transform InfraRed, or FT-IR. Infrared radiation is passed through a sample during infrared spectroscopy. The sample absorbs some of the infrared light, but some also passes through (transmits). The resulting spectrum serves as a molecular fingerprint of the material by depicting molecular absorption and transmission. No two different molecular configurations create the same infrared spectrum, similar to a fingerprint. As a result, infrared spectroscopy can be used for various analyses. With absorption peaks that match the frequency of vibrations between the bonds of the atoms making up the material, an infrared spectrum becomes a fingerprint of a sample. No two compounds create exactly the same infrared spectrum since every substance is made up of a different combination of atoms. As a result, any kind of substance can be verified (by a qualitative study) using infrared spectroscopy. Additionally, the size of the spectral peaks provides an apparent indication of the amount of material present.

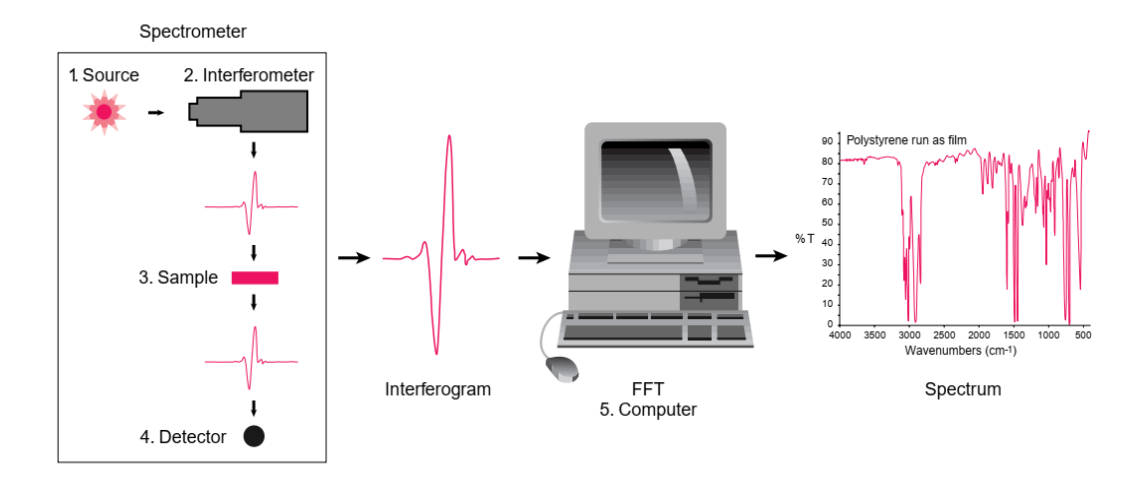


Figure 3. 2 Working principle of FTIR. Reprinted from Introduction to Fourier Transform Infrared Spectrometry (2001) [186]. Copyright 2001 Thermo Nicolet Corporation

3.2.3.2 Scanning electron microscope (SEM)

The scanning electron microscope (SEM, Phenom ProX, Thermo Fisher Scientific) was employed to characterise the morphology and identify the hollow structure form of the fibre mat samples. In the hollow structure fibre study, the fibre mats were frozen in liquid nitrogen before using the SEM and carefully broken in half to investigate the sample's cross-section. In order to eliminate the charging effect from the non-conductive sample during measurement, all samples were coated with silver particles for 2 min, approximately 5-10 nm. The images were performed using the backscattered electron at 15kV with the working distance (WD) between 6 – 8 mm. The

average diameter of the electrospun fibre was characterised using the ImageJ program in the individual strain. The diameter distribution curve was then analysed using Origin Pro software to find the median fibre diameter.

3.2.3.3 Transmission electron microscopy (TEM)

Transmission electron microscopy (Hitachi, HT7700) was utilised to characterise the inner structure of the hollow and coaxial fibre. Also, the embedded PTFE size in PVDF fibre was analysed using a TEM image. The fibre was coated onto the TEM grid located in the middle of the aluminium foil substrate during electrospinning. The average diameter of the core and shell of the electrospun fibre was characterised using the ImageJ program in the individual strain measurement. The diameter distribution curve was then analysed using Origin Pro software to find the median fibre diameter.

3.2.3.4 X-ray diffraction (XRD)

After electrospinning, the middle part of the electrospun fibre was used in the measurement. X-ray diffraction analysis (D8 Advance, Bruker) was used in a grazing angle operating mode to analyse the crystalline phase of the PTFE/PVDF electrospun fibre. It is well known that most polymers do not show the crystalline pattern via the XRD technique. However, this work uses the crystalline PVDF to study mixing in PTFE and PS. Thus, to investigate the phase change in piezoelectric properties of PVDF, the XRD technique is used to distinguish the phase change.

3.2.3.5 Surface potential testing

A surface potential test was designed to examine the electrostatic characteristics of the electrospun fibre. This was carried out by adopting the standard of charge decay of the electret filtration testing method from J. Lee et al. [176]. Figure 3.3 shows the schematic of the surface charge potential test experimental design. Several studies have demonstrated that heat and humidity can deteriorate an electret material. This can result in a loss of charge [176], [184], [187].

The electrostatic field meter (Simco FMX-003) was used to measure the electrospun fibre's surface potential. The electrostatic field meters measure a material's surface potential by detecting the electric field generated by the charge on the material's surface. It measures static voltages by detecting the electric field generated by a charged object. This is done by placing the material in an electrostatic field and measuring the change in the field caused by the presence of the material. The device uses a conductive case and ground snap to facilitate grounding, which is essential for accurate measurements. Proper grounding ensures the electrostatic field meter can accurately reference the potential difference between the charged object and the

ground [188]. The surface potential of the material is directly related to the measured change in the electrostatic field, allowing for the determination of the material's charge state and its interactions with the environment.

Electrostatic field meter has limitations in terms of its spatial resolution, as it measures the average surface potential over a relatively large area. In contrast, traditionally used for triboelectric application, the Kelvin probe atomic force microscope (KPFM) offers a higher spatial resolution for surface potential measurements. This technique uses a vibrating probe tip to detect the contact potential difference between the tip and the sample surface, allowing for surface potential mapping with nanometer-scale resolution. It should be noted that the surface potential measured by KPFM and electrostatic field meter should not be compared, as the working principle is different.

Electrostatic field meter is appropriate to use in measuring the large area of materials used in applications such as facemasks [189], filtration [190-193] or electronic components in general [194]. In addition, several works [163], [195-197] report on energy harvesting using the electrostatic field meter when referring to an overall surface potential. The surface potential can be affected by environmental factors such as temperature, humidity, and adsorbates or contaminants on the surface. Thus, in the surface potential testing experiment, the working environment was kept at 55 ± 5 % RH and a temperature of 21 ± 3 °c during measurement.

After completion of the electrospinning process, the sample was carefully removed from the substrate using anti-static tweezers. The surface charge potential was then measured using an electrostatic field meter. The sample was exposed to the environment for 14 days, and then the surface potential was measured again. After 14 days, the residual charge was removed from all samples using the discharge chamber setup in Figure 3.4. The discharge chamber was closed and grounded, and the bottom layer had an isopropyl (IPA) reservoir under the mesh. The samples were laid on the mesh to discharge electrospun fibre and expose the IPA vapour. The surface potential was measured after discharge to ensure no charge in the fibre mat. The samples were left in the environment, and surface potential was monitored regularly.

In the study of hollow electrospun fibre, the sample was treated using the corona charge technique under the assumption of being ferroelectret-based. Then, the sample was coronacharged and measured for the surface potential charge. The sample was then exposed to the environment for another 14 days. The surface potential was then measured again.

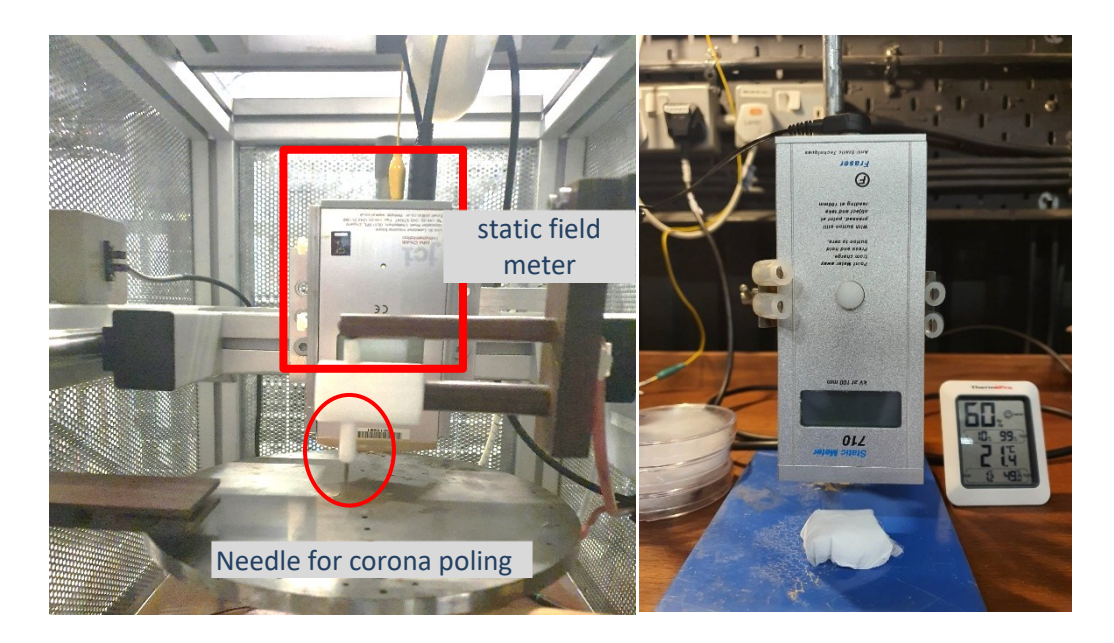


Figure 3. 3 The setup for static potential testing, a) the corona charge equipment, b) the setup of static measurement before and after the corona charge in the study of the hollow PVDF electrospun fibre under the assumption of being ferroelectret-based.

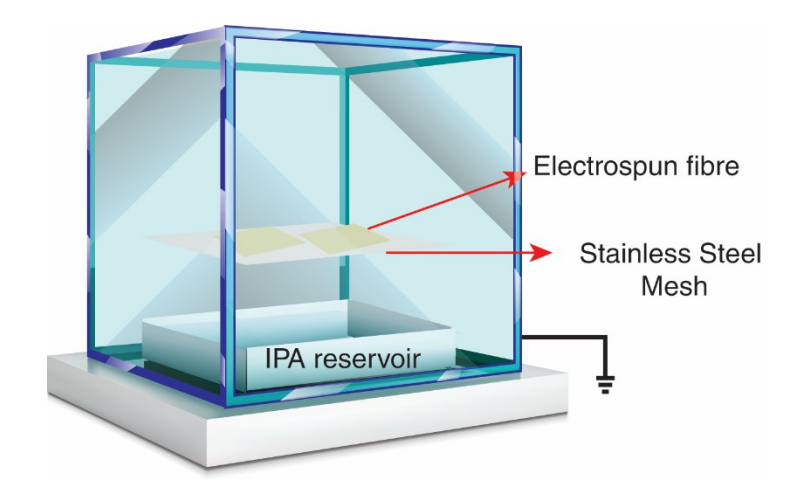


Figure 3. 4 Discharge chamber setup

3.2.3.6 Piezometer

The piezoelectric coefficient (d₃₃) and capacitance (c) of the fibre mat were measured using Piezometer system, PM300. The analysis was conducted using the system's standard measurement as a dynamic force of 0.25 N, static force of 10 N and frequency of 110 Hz. The data was collected from the average value of 5 positions on the sample. The reading was taken 10 seconds after the equipment started reading (when a green light appeared).

The Piezometer system clamps the sample and subjects it to a low-frequency force. Processing of the electrical signals from the sample and comparison with a built-in reference enables the system to give a direct reading of d_{33} values. The method of operation for this type of d_{33} meter is sometimes called the "quasi-static" or "Berlincourt" method [198] A key principle is that the test frequency is low compared to any likely system or sample resonances, yet high enough that a conclusive measurement can be made within a few seconds.

3.2.3.7 Tapping test setup

To test the energy harvesting performance in the piezoelectric and piezoelectret mode, the fibre mat was assembled with a copper electrode and PET adhesion tape as shown in Figure 3.5.

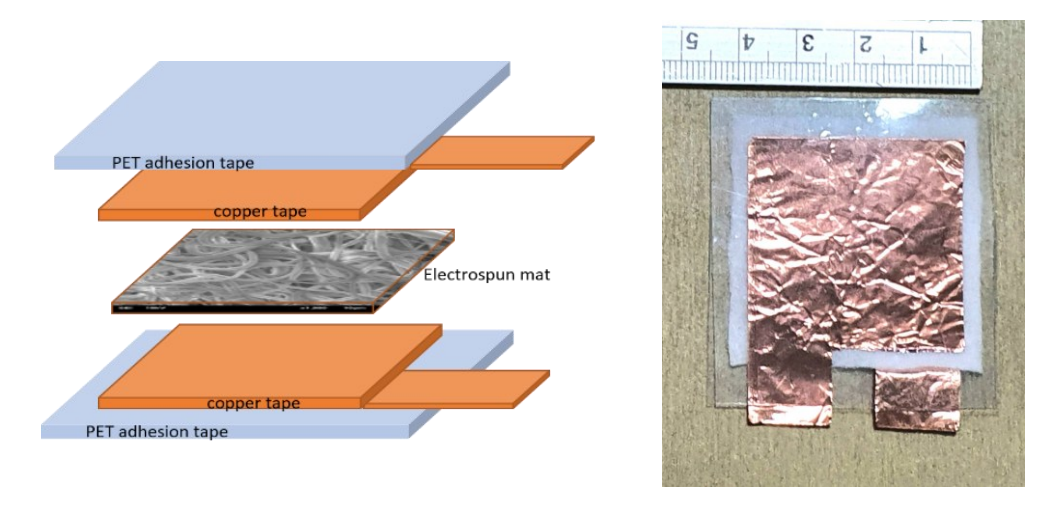


Figure 3. 5 The schematic of assembling the cell for the tapping test

The tapping test rig was developed from previous studies and comes from inserting the sample between 2 electrodes and tapping at a constant rate [199-200]. The tapping test rig was set up using a linear actuator motor to provide a constant rate and pressure. The linear actuator motor has a rated voltage of 12V, 900 rpm. The sample was attached to the oscilloscope to observe changes in voltage induced by the mechanical movement of the rig.

3.2.3.8 Voltage and current measurement for Triboelectric mode

The energy harvesting of the electrospun fibre operating in Triboelectric mode was set up differently compared to piezoelectric and piezoelectret modes. The test was performed using a tapping rig in the vertical contact separate triboelectric generator, as shown in Figure 3.6. The open circuit voltage (V_{oc}) output of the energy harvester was measured using an oscilloscope (MSO7012B, Agilent Technologies) with a 10 M Ω probe resistance. During open circuit voltage measurement, the oscilloscope was connected to the 1 G Ω resistor as a voltage divider circuit due to the large internal impedance of the TENG. Consequently, the measured output voltages

from the oscilloscope were multiplied by a factor of 101 in order to get an accurate open-circuit voltage (V_{oc}) of the triboelectric nanogenerators (TENGs) based on the voltage divider principle, as seen in the circuit diagram in Figure 3.7 b). The DC power analyser (N6705B, Agilent Technologies) measured the short circuit current (I_{sc}). The graph obtained from the current was used to calculate the charge transfer using the relationship of $Q_{transfer} = \int_{t_i}^{t_f} I dt$ in the contact and separation region.

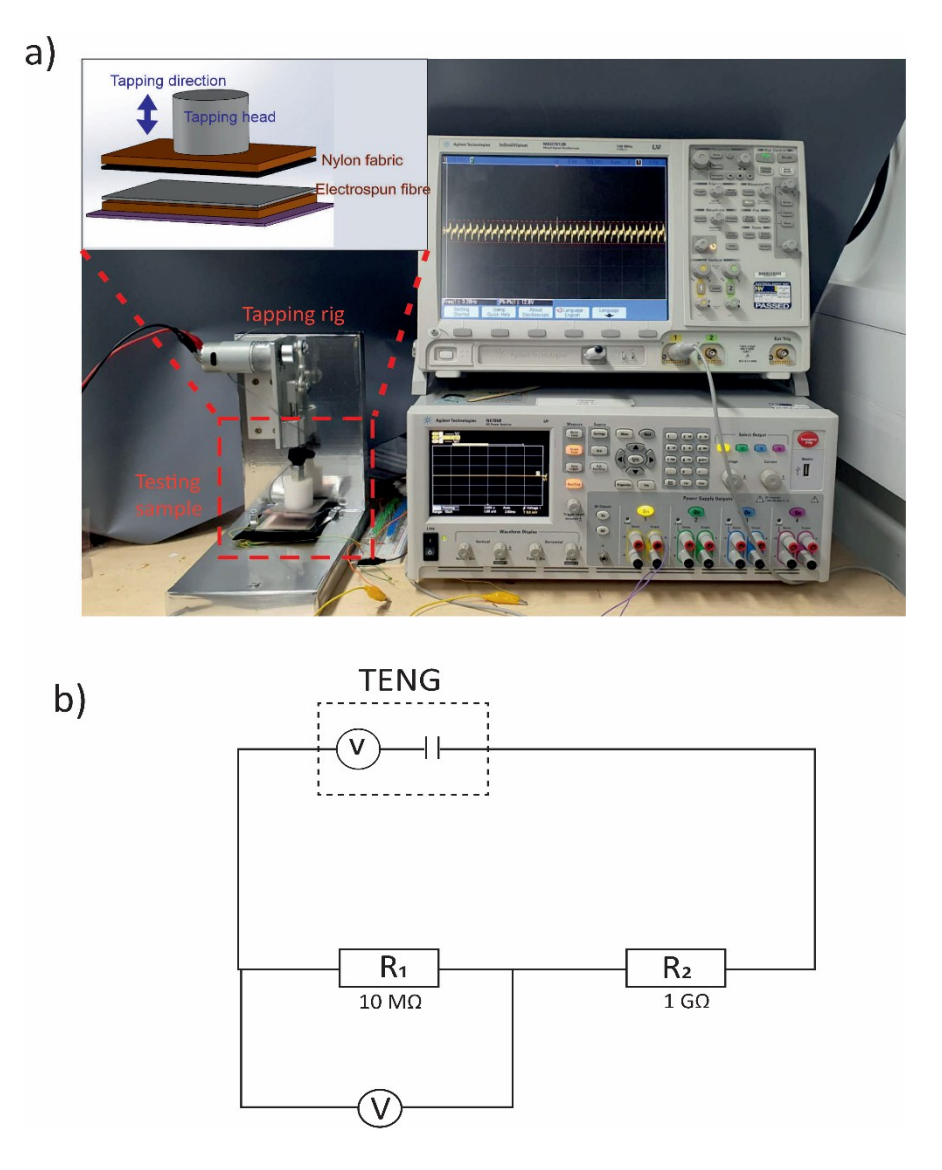


Figure 3. 6 a) The experimental setup for the tapping test b) diagram of voltage divider circuit

3.3 Conclusion

This chapter details the materials, experimental processes, and methods employed in the fabrication and characterisation of electrospun fibres intended for energy harvesting applications. This chapter provides the basis for the study by outlining the processes involved in the preparation of composite, hollow, and coaxial fibres, along with the methods used for their characterisation.

Chapter 3

The effective development of the electrospinning apparatus and the development of parameters for fibre fabrication represent major achievements. Utilising advanced characterisation techniques such as SEM, TEM, FTIR, and XRD resulted in a comprehensive understanding of the morphology, structure, and material properties of the fibres. Furthermore, electromechanical testing methodologies were carefully developed to assess the energy harvesting capabilities of the produced fibres. This chapter presents an experimental framework that ensures both reproducibility and precision in the fabrication and analysis of electrospun fibres. This section provides the basis for the following chapters by providing readers with essential tools and methodologies to investigate the energy harvesting potential of different fibre structures. The thorough methodology in material preparation and testing defines a crucial advancement in the field of electrospun fibre technology, particularly for applications in wearable and flexible energy harvesting devices.

Chapter 4 Energy harvesting performance of composite electrospun fibre

4.1 Introduction

From chapter 2, PTFE is well known as a promising negative triboelectrification in the triboelectric series chart [201-202]. Thus, many researchers utilised the PTFE as a negative material for triboelectric [125-126], [203]. Typically, commercial PTFE from different sources shows various energy harvesting performances depending on its manufacturing technique. Electrospinning techniques can be used to modify the surface morphology. This improves the triboelectric properties as it enhances the surface area of the material. Additionally, a high voltage is applied to the polymer solution in the electrospinning process. This results in a high volume of charged particles being introduced into the solution, which are subsequently captured within the electrospun fibre after solidification. It is acknowledged that electrospun Polyvinylidene Fluoride (PVDF) fibre appears to be a high-performance polymer that exhibits piezoelectric properties and has a negative triboelectric behaviour [202]. Several studies have reported on the energy conversion ability of PVDF in the triboelectric mode. It has been demonstrated that PVDF exhibits significant potential for energy conversion when used as the negative material in the triboelectric mode [204-206]. Interestingly, fabricating PTFE using electrospinning is challenging due to its exceptional physical and chemical characteristics. This makes it extremely difficult to electrospin without chemical or physical modification [207]. Zhao et al. demonstrated energy harvesting from electrospun PTFE fibres by utilising PEO as a carrier [208]. Regarding this attempt, a precursor polymer solution was employed to create the structure of PTFE using an electrospinning technique, resulting in the formation of PTFE fibre mats. In order to remove the precursor polymer as well as restore the trapped charge in the PTFE fibre, a corona charging procedure is necessary if the fibre is intended to be used in an electrostatic device or to improve triboelectric generation. The PTFE fibres made in this approach possess good energy-harvesting properties. However, the material preparation process requires a minimum of two steps.

Combining PVDF and PTFE, which possess the negative triboelectric side, could improve the triboelectrification in the TENG element using the electrospinning technique. The electret characteristic of PVDF, which has been doped with PTFE and produced via an electrospinning method, exhibits a strong surface potential when used in filtration membrane applications [209-210]. However, this literature does not demonstrate the performance of energy harvesting.

In this chapter, the energy harvesting performance and the structure of additive – PTFE in the composite fibre PVDF are investigated. The electrospun fibre was prepared in 2 sets of electrospinning conditions. First, PTFE particles were added to the controlled PVDF at 20% solution. Second, the overall polymer solution was controlled at 20%.

4.2 The additive PTFE in the controlled PVDF fibre

4.2.1 Introduction

The purpose of the initial study on additive PTFE in the PVDF fibre was to fabricate PTFE in the form of fibre using PVDF fibre as a carrier solution. The 1-micron PTFE particle was mixed in the PVDF solution without any treatment. The energy harvesting performance was observed via open-circuit voltage on the book-shaped assembly. The fabrication process and the energy harvesting performance are discussed in this section.

4.2.2 Materials and Methods

4.2.2.1 Electrospinning Preparation

The PTFE/PVDF electrospun fibre was produced by mixing 1-micron PTFE particles in an 18%wt PVDF solution as a polymer carrier for PTFE. The PVDF solution was prepared from PVDF powder mixed with DMF and acetone at a 7:3 ratio and mixed on a magnetic hotplate stirrer at 60 °C for 4 h. Different concentrations (0, 1, 2, 3, and 4%wt.) of the PTFE particles were added to the PVDF solvent solution and blended using the magnetic stirrer at room temperature for 2 h. Electrospinning was performed using a blunt tip (21 G) needle. The distance from the tip to the substrate, the applied voltage, the flow rate, and the rotating drum speed were kept constant at 22 cm, 25 kV, 2 mL/hr, and 150 rpm, respectively, for each concentration. After electrospinning for 90 min, the PTFE/PVDF fibre was collected in the form of a nonwoven fibre mat, as shown in Figure 4.2 a). The energy harvesting performance of the electrospun PTFE/PVDF fibre mats was measured without any further processing steps.

4.2.2.2 Test Assembly and Protocol

The electrospun PTFE/PVDF fibre mats with each concentration of PTFE (0, 1%, 2%, 3%, and 4%) were cut into 5×4 cm samples. Each sample was assembled in a sandwich structure with Cu electrodes using a folded-over (book-shaped) PVC sheet backing, as shown in Figure 4.2 b). This forms a vertical contact separation mode triboelectric harvester. A second generator design with a piece of nylon fabric added to the assembly as a triboelectric donor material was used to

explore the addition of this material to enhance the performance of the triboelectric power generator.

A cyclical compression test system using a linear actuator was set up to apply a controlled pressure of 0.5 N/cm² at different frequencies (3-12 Hz), as shown in Figure 4.2 c). The test sample was attached to the oscilloscope to observe the changes in the voltage induced by the periodic mechanical pressure applied by the rig. The capacitor charging experiment used a full-wave bridge rectifier to charge 0.1, 1, 10, and 100 µF capacitors.

4.2.3 Results and Discussion

The structure of the PTFE/PVDF electrospun fibre prepared by controlling the PVDF percentage was studied using SEM alongside the fibre diameter distribution curve, as shown in Figure 4.1. The SEM image shows the embedding of PTFE particles in the PVDF electrospun fibre. The amount of PTFE particles increases with the increase of PTFE percentage in the observed SEM images. However, the PTFE4 sample shows the mixing of the fibre and the dented region, which indicates that the electrospinning process is not continuing properly due to inappropriate polymer content in the solution.

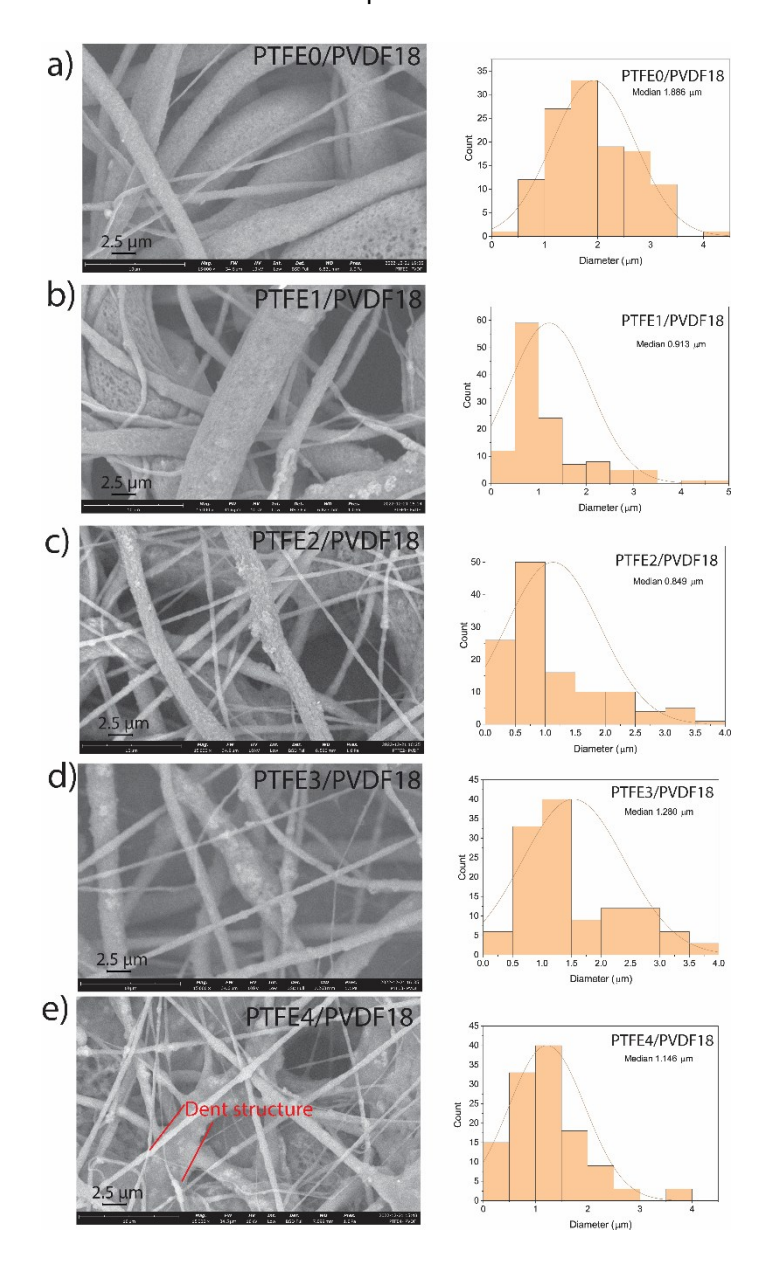


Figure 4. 1 SEM images of the single PTFE/PVDF electrospun fibre with the diameter distribution curve prepared by control PVDF at 18% a) PTFE 0%, b) PTFE 1 %wt, c) PTFE 2 %wt, d) PTFE 3%wt, e) PTFE 4%wt.

The vertical book-shaped structure was chosen for energy harvesting performance testing as it is simple and could be assembled into a multi-layered device. The highest voltage output from compressing at 5 Hz was found to be 30 V for the 4%wt PTFE, which is five times higher than that of the 100% PVDF sample (6 V), as shown in Figure 4.2 d). This clearly shows that introducing the PTFE particles in the PVDF fibre can improve the performance of triboelectric power generators. The output voltage increases with an increasing percentage of PTFE particles. However, 4% PTFE was the highest amount of polymer content that could be processed via electrospinning because the solution conductivity was not strong enough to produce the electrospun fibre.

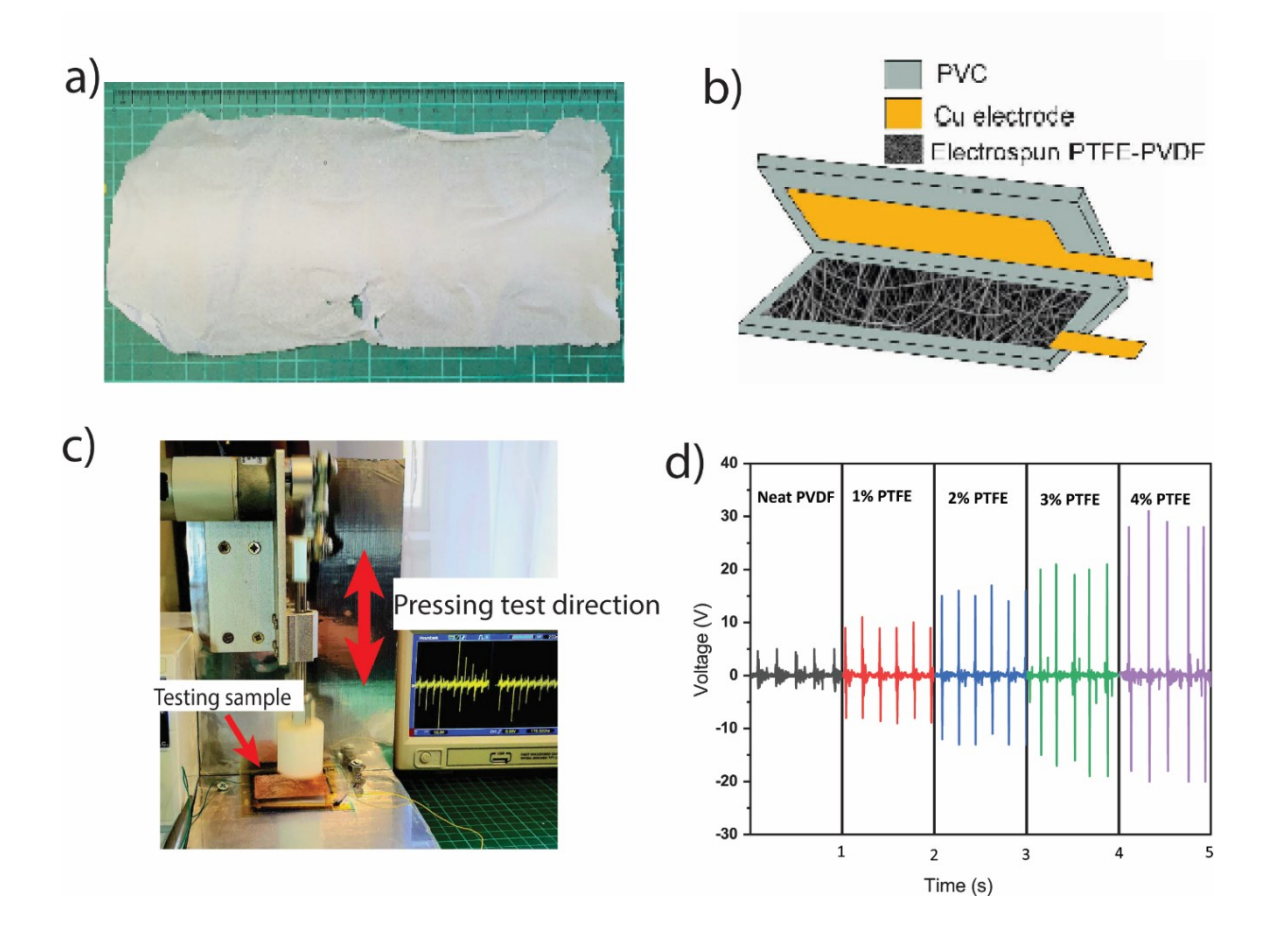


Figure 4. 2 a) PTFE/PVDF fibre mats after the electrospinning process of the 4%wt PTFE in the PVDF sample; b) the schematic of the book-shaped assembly for the testing cell PTFE/PVDF fibre sandwich with electrodes; c) the compression test rig; d) voltage output from constantly tapping the booked-shaped PTFE/PVDF fibre assembly at different PTFE concentrations of 0, 1, 2, 3, and 4%wt., respectively.

The 4% PTFE in the PTFE/PVDF sample was used in the energy harvesting test at different pressing rates of 3-12 Hz. It was found that the output voltage increases with an increasing pressing frequency. The highest output voltage of around 55 V was found at 12 Hz, as shown in Figure 4.3 b). To enhance the energy harvesting performance of the triboelectric power generator, nylon fabric, which exhibits a high positive affinity in the triboelectric material series, was placed on top of the top copper electrode, as shown in Figure 4.3 a). The voltage output of the Nylon-PTFE/PVDF device at the different pressing frequencies is shown in Figure 4.3 c). A small improvement in the voltage output was observed with the highest voltage output, which reached 70 V at 12 Hz.

The charging experiment was further performed to explore and compare the amounts of energy captured by the device and transferred to the capacitor storage. Devices with and without the nylon fabric were tested at 5 Hz with different capacitor values, and the results are shown in Figure 4.3 d), e). Overall, the energy stored in the capacitors is higher for the nylon-PTFE/PVDF

device, with the amounts of energy stored being 0.15, 1.0, 7.2 and 4.5 μ J for 0.1, 1, 10 and 100 μ F, respectively. The maximum energy stored value occurs with the 10 μ F capacitor, nearly reaching its maximum capacity in the 300s charging time. This was 69%, 79%, 94% and 89% larger than those of the device without nylon for 0.1, 1, 10 and 100 μ F, respectively. The energy stored in the 100 μ F capacitor was less than that of the 10 μ F capacitor over the same duration due to the impedance mismatch.

After connecting the optimum harvester structure (4% PTFE with Nylon fabric) to a full-wave bridge rectifier circuit, it was found that 95 LED lights were illuminated when it was compressed at 12 Hz, as can be seen in Figure 4.3 f). The charging experiment and illuminating LED light results demonstrate the promising mechanical energy conversion achieved with the electrospun PTFE/PVDF fibre mat. The lightweight, flexible, and breathable PTFE/PVDF electrospun fibre could be integrated within clothing as an energy source whilst remaining comfortable for the user.

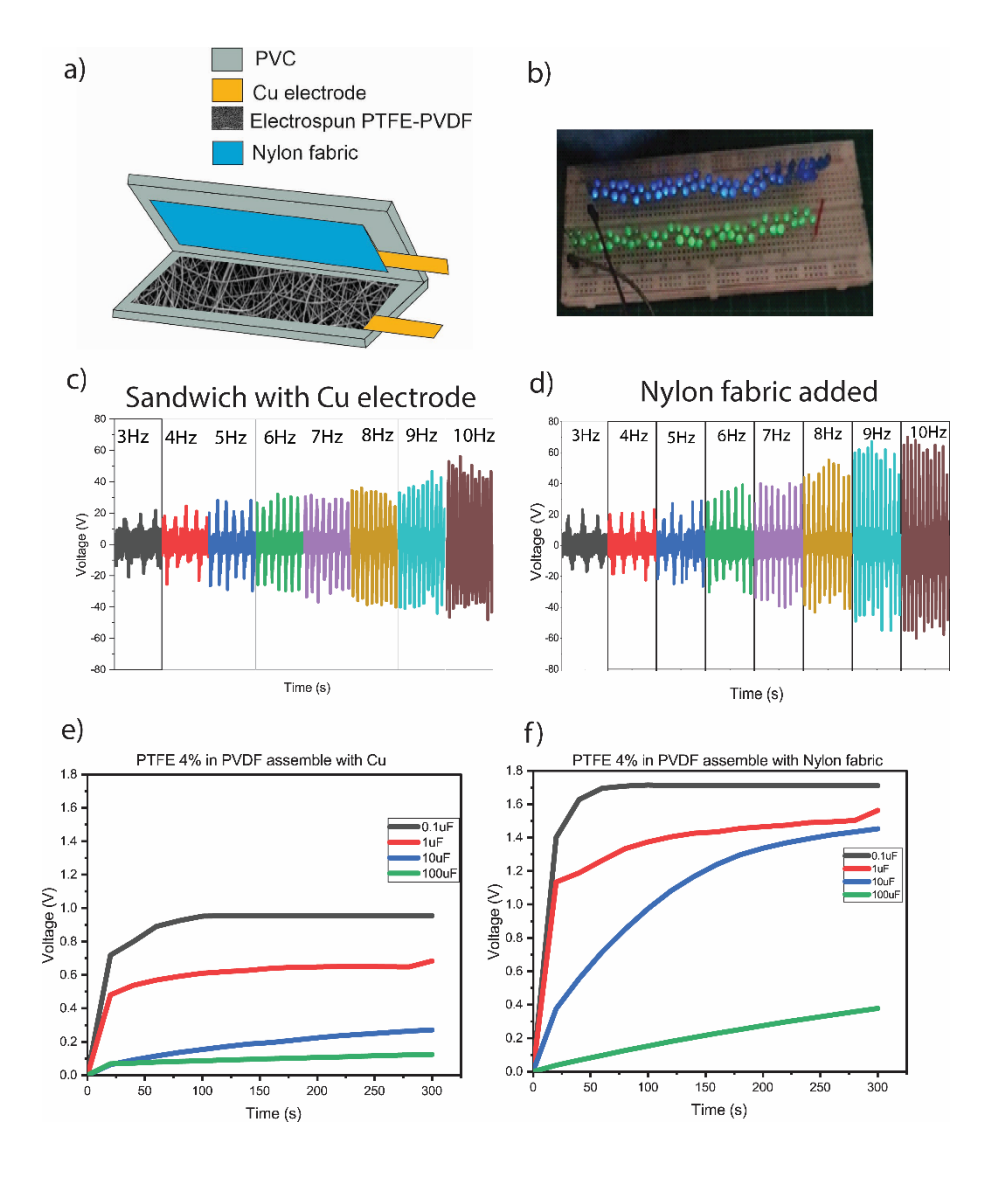


Figure 4. 3 a) The schematic of the improved triboelectric harvester design with added nylon fabric, b) 95 LED lights were illuminated via tapping the harvester with the

PTFE/PVDF electrospun fibres as the acceptor and nylon fabric as the donor material, c) the voltage output of the triboelectric assembly without nylon fabric, d) the voltage output of the triboelectric assembly after introducing nylon fabric the charging profile, e) voltage vs. time of the PTFE/PVDF fibre device without nylon fabric, f) the charging profile after introducing nylon fabric.

4.2.4 Conclusion of the additive PTFE in the controlled PVDF fibre

A flexible Polytetrafluoroethylene (PTFE) fibre was successfully prepared using a one-step electrospinning process using a Polyvinylidene Fluoride (PVDF) solution as a precursor. The energy harvesting performance was first explored using a vertical contact separation mode triboelectric assembly. The electrospun fibres were collected in the form of a non-woven textile mat, which displayed a very promising negative surface potential. The voltage output was increased by a factor of five by adding PTFE to the PVDF electrospun fibre. This was further improved by the addition of a nylon fabric with the triboelectric harvester. The textile harvester was shown to illuminate up to 95 LED lights when it was assembled with nylon fabric as a donor material. However, this experiment did not show the optimised electrospinning conditions. The next section will demonstrate the energy harvesting from the optimised PTFE/PVDF electrospun fibre.

4.3 Controlling the overall polymer concentration experiment

4.3.1 Introduction

The previous attempt in section 4.2, demonstrated the potential voltage output from the electrospun PTFE/PVDF fibre as a preliminary study [40]. However, this work did not provide an optimisation test for the material. In this study, the systematic test of the additive PTFE in PVDF electrospun fibre is demonstrated, and the energy harvesting performance and its fabrication of the electrospun PTFE/PVDF fibre are also investigated.

Even though the results suggest that the percentage of PTFE particles is proportional to the energy-harvesting performance, the percentage of the added PTFE particles to the PVDF fibre was limited to 4% from adding PTFE particles directly to 18% of the PVDF solution. This affected the conductivity of the overall polymer solution, as the percentage of the overall polymer increased while the solvent remained the same. In this section, the systematic study of the optimised PTFE/PVDF, along with its energy harvesting performance, is discussed.

4.3.2 Materials and Methods

4.3.2.1 Electrospinning Preparation

The flow chart for the preparation of PTFE/PVDF electrospun fibre can be seen in Figure 4.4. The PVDF and PTFE particles were combined to produce the PTFE/PVDF electrospun fibre at a controlled overall polymer at 20% in the following ratios: PTFE1% + PVDF 19%, PTFE2% + PVDF 18%, PTFE3% + PVDF 17%, PTFE4% + PVDF 16%, PTFE5% + PVDF 15%, PTFE6% + PVDF 14%, and PTFE7% + PVDF 13%. To prevent the PTFE particle from accumulating, it was sonicated for six hours prior to being mixed with the PVDF and DMF: acetone solvent. Following each mixing ratio of PTFE/PVDF polymer powder, DMF and acetone were blended in a 7:3 ratio. For a total of six hours, the solution was stirred at 60°C using a magnetic hotplate stirrer. The PTFE/PVDF solution was then put in a 3 ml syringe with a blunt tip (21G) needle and attached to the syringe pump of the electrospinning apparatus. For every concentration, the distance between the tip and the substrate, the applied voltage, the flow rate, and the rotational speed of the drum remained constant at 22 cm, 25 kV, 2 ml/hr, and 150 rpm, respectively. In order to assess the energy harvesting efficiency, the PTFE/PVDF fibre was collected as a nonwoven fibre mat and assembled in a triboelectric energy harvester without any additional processing.

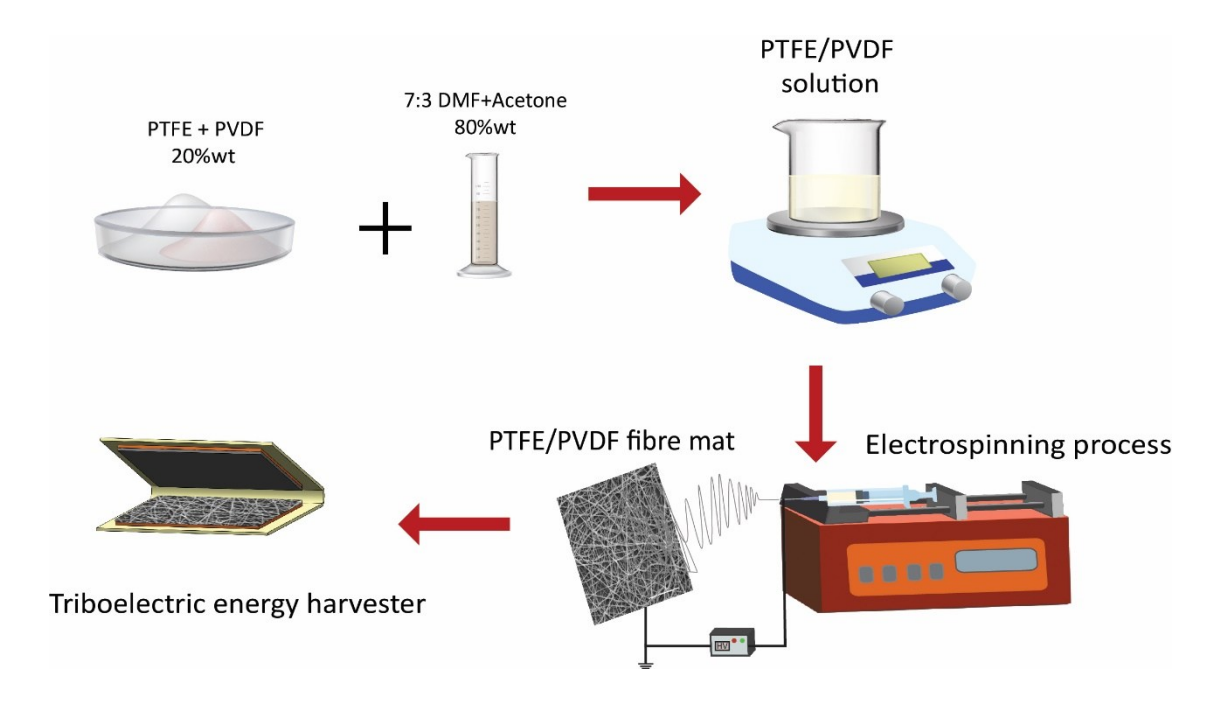


Figure 4. 4 The flow chart describes the PTFE/PVDF electrospun fibre preparation.

4.3.2.2 Fibre characterisation

After electrospinning, the solvent was evaporated; it can be assumed that the percentage of PTFE and PVDF in the solid fibre follows Table 4.1. The morphology and structure of the electrospun PTFE/PVDF were investigated through the scanning electron microscope (SEM) (Phenom ProX, Thermo Fisher Scientific) and tunnelling electron microscope (TEM) (HT7700, Hitachi). The chemical composition and structure of the material were analysed using a Fourier transform infrared (FTIR) spectrometer (Nicolet iS5, Thermo Fisher Scientific), and X-ray diffraction analysis (D8 Advance, Bruker) was used to analyse the crystalline phase of the PTFE/PVDF electrospun fibre.

4.3.2.3 Electromechanical characterisation

The PTFE/PVDF electrospun fibre was cut at 4 cm x 5 cm and then attached with Cu tape, which works as an electrode. The other side of the triboelectric energy harvester, nylon fabric, was used as a positive material. This was attached to the Cu electrode and tested in the vertical contact separation mode with a distance of 1.5 cm, as shown in Figure 4.5 a). A controlled pressure of 0.5 N/cm² (measured by an FSR402 sensor) was applied at different frequencies (3-9 Hz), utilising the cycle compression test system with a linear actuator. As seen in Figure 4.11 a), the 4 cm x 5 cm pieces of PTFE/PVDF electrospun fibre were assembled using a folded-over PVC template (in the book-shaped form) and nylon fabric as triboelectric donor material. The book-shaped assembly was used to test the capacitor charging and LED light illuminating ability.

The energy harvesting performance of the triboelectric energy harvester was measured using a tapping rig. The open circuit voltage (V_{oc}) output of the energy harvester was measured using an oscilloscope (MSO7012B, Agilent Technologies) with the $10M\Omega$ probe resistance. During open circuit voltage measurement, the oscilloscope was connected to the $100~M\Omega$ as a voltage divider circuit due to the large internal impedance of the TENG. The DC power analyser (N6705B, Agilent Technologies) measured the short circuit current (I_{sc}). The high-precision digital multimeter (Keithley 2100 6 1/2) was used to measure the voltage over the capacitor in the charging capability measurement.

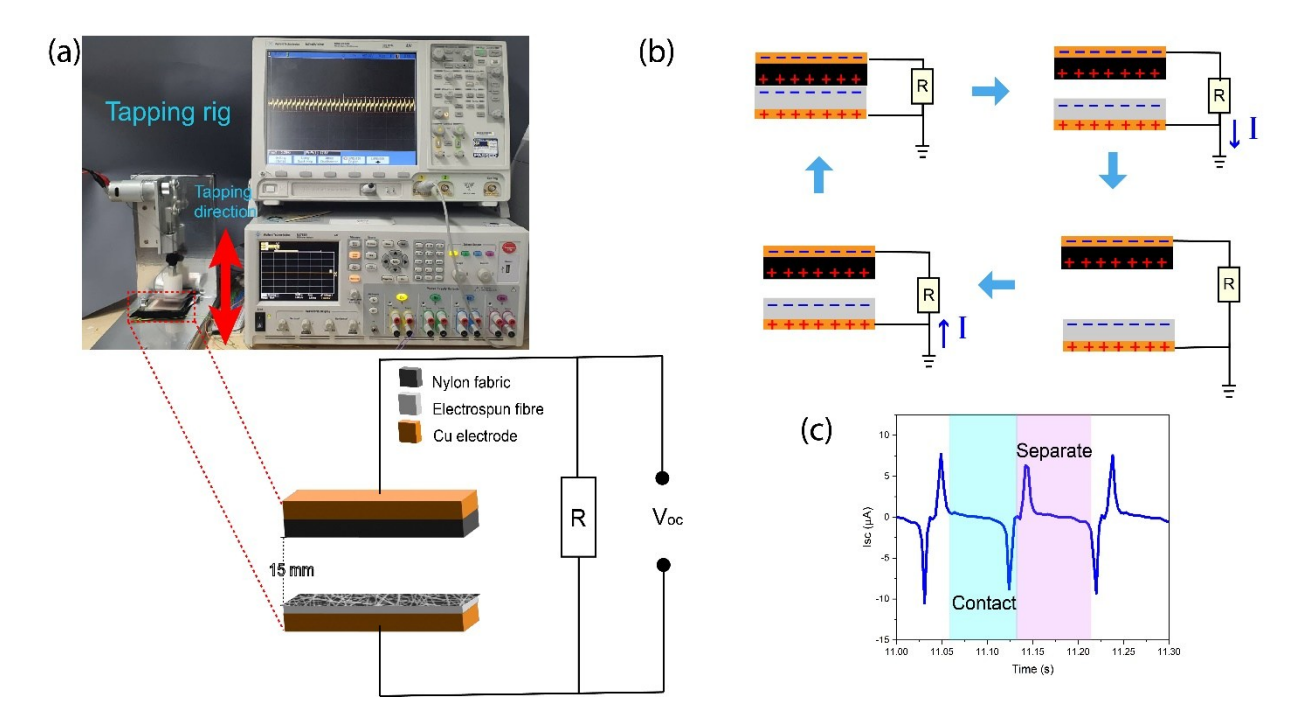


Figure 4. 5 a) Schematic of PTFE/PVDF triboelectric assembly and testing, b) working principle in contact standing mode and c) corresponding with the measurement of short circuit current

4.3.3 Results and discussion

4.3.3.1 Morphological analysis

Figures 4.6 a) – h) show the surface morphologies observed in the SEM of the PTFE/PVDF electrospun fibre at various PTFE and PVDF ratios. The surface of the 100% PVDF fibre (Figure 3a) is smooth without any visible bead-like structures. This is the base fibre material used as a benchmark in the study of the effects of the additive PTFE powder. The addition of the PTFE powder to the base PVDF material can be seen to cause increasing fibre surface roughness with increasing amounts of PTFE microparticles. The PTFE/PVDF solution enabled successful electrospinning of the porous fibre mat up to a concentration of 16% PVDF with 4% of the PTFE particles, see Figure 4.6 e). Beyond this, when more than 5% of PTFE was added to the solution, the electrospinning process could not consistently produce PTFE/PVDF fibres, producing a combination of fibrous and film-like deposits shown in Figure 4.6 f)- h). This was due to the decreased conductivity of the PTFE/PVDF solution, which affects the behaviour of the electrospinning process of the PTFE4/PVDF16 solution yield (the 20/80 PTFE/PVDF fibre). The sample code of the PTFE/PVDF fibre can be found in Table 4.2. The TEM images in Figure 4.7 a) and b) indicate the location of PTFE particles in the PVDF fibre, demonstrating that these have been successfully blended in the starting solution and distributed across the PVDF matrix. The

PTFE particle size embedded in PVDF strain was found to be less than 1 micron due to the sonication process before electrospinning preparation.

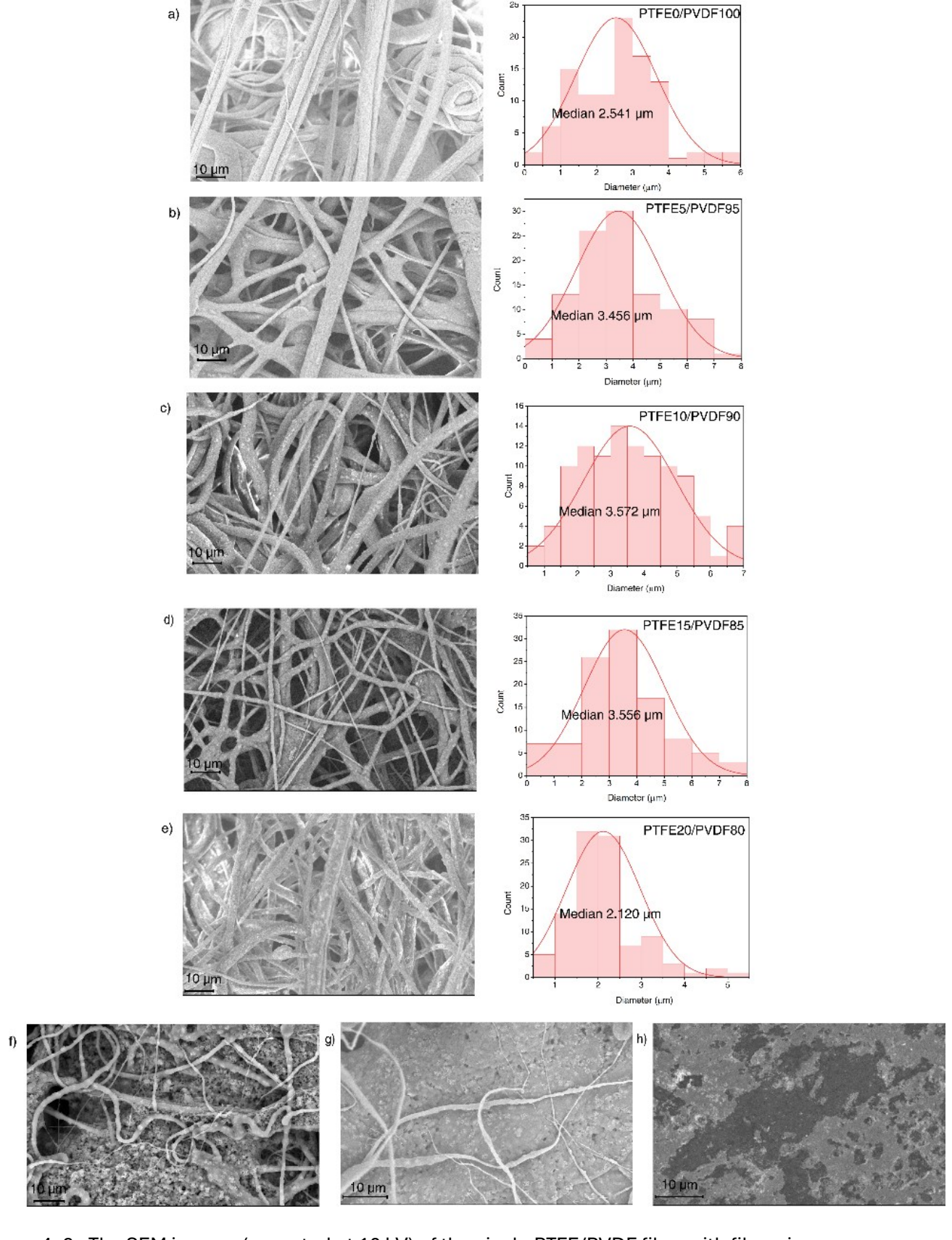


Figure 4. 6 The SEM images (operated at 10 kV) of the single PTFE/PVDF fibre with fibre size distribution curve prepared by different PTFE/PVDF ratios a) PTFE0/PVDF100, b)

PTFE5/PVDF95, c) PTFE10/PVDF90, d) PTFE15/PVDF85, e) PTFE20/PVDF80, f) PTFE25/PVDF75, g) PTFE30/PVDF70 and h) PTFE35/PVDF65

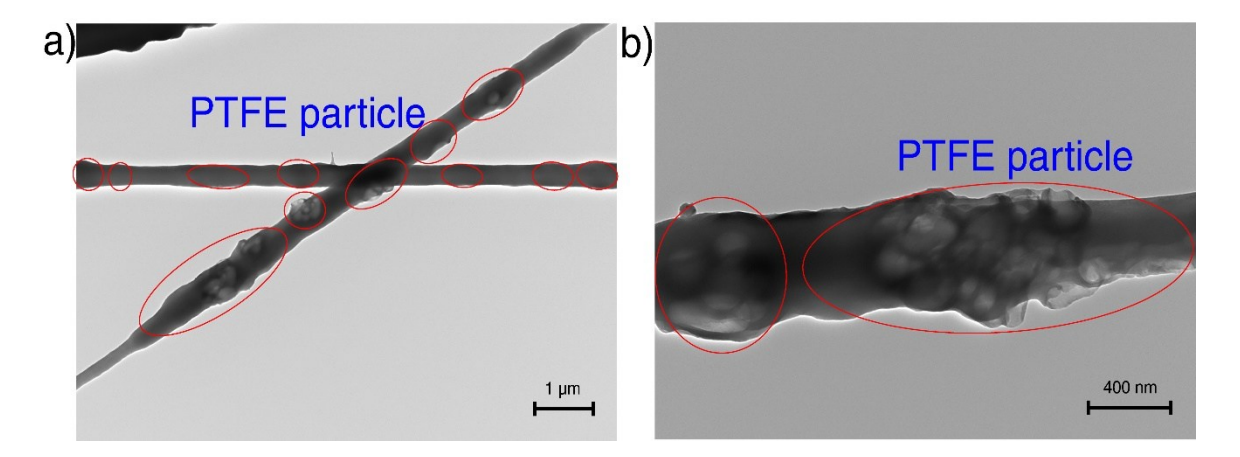


Figure 4. 7 TEM images were measured at acceleration voltage of 100 kV, filament voltage of 25 kV for a single PTFE20/PVDF80 fibre, which was coated on the mesh copper grids at magnification a) 7000x, b) 25000x.

4.3.3.2 Structural analysis

The FTIR measured chemical composition of PTFE/PVDF electrospun fibres are shown in Figure 4.8 a) alongside the results for the PDVF and PTFE powders. All samples of the PTFE/PVDF electrospun fibres exhibit the characteristic peaks at 840 and 877, representing the β - and C-H wagging in the α -phase of PVDF, respectively. When compared with the results obtained from PVDF powder, which shows peaks at 614, 764, 796, 877, 976, and 1170, it is evident the crystalline piezoelectric β -phase has been effectively induced by the electrospinning process [137], [211]. It is well known that the electrospinning process encourages the β -phase of PVDF due to the strong electric field induced in the polymer solution during whipping of the fibres [211-212]. Also, the incorporation of PTFE into the electrospun PVDF can be observed at the peak 1170, representing the perturbation of the C=F bond of PTFE and PVDF, as both consist of carbon and fluorine atoms [213]. The characteristics of the PTFE powder spectrum are represented in the peaks 1201 and 1150, which correspond to the asymmetrical and symmetrical CF2-stretching, whereas peaks 642 and 630 represent the C-F deformation [214-215].

The XRD pattern of the PTFE/PVDF electrospun fibre at different percentages of PTFE is shown in Figure 4.8 b). The pure PVDF electrospun fibre exhibits only one strong peak at 20.6° (110/200), representing the β -phase of the PVDF. After introducing PTFE in the PVDF electrospun fibre, the α -phase at a peak of 18.4° (020) occurred and was related to the amount of PTFE in the PVDF fibre. The intensity of the α -phase at a peak of 18.4° (020) becomes stronger as the percentage

of PTFE increases. Table 4. 1 shows the crystallinity index (CI) obtained from the XRD results, which is calculated by

$$\%Crystallinity = \frac{S_c}{S_t}$$
 (4.1)

Where S_c represents the area under the curve at the peak crystalline alpha and beta phases, and S_t represents the total area under the plot.

This interesting behaviour can be explained by the electric field during the electrospinning process. The β -phase PVDF can be induced by a strong electric field in the electrospinning process. When the PTFE particles are added to the PVDF solution, the dielectric properties of the PTFE/PVDF solution increase, resulting in a reduced electric field to induce β -phase. The α -phase requires less energy than the β -phase to form, and thus, the β -phase decreases while the α -phase increases, as shown in Table 4.1.

Table 4. 1 Crystallinity index obtained from XRD

	Crystallinity index (%)		
	α-Phase	β-Phase	
PTFE0/PVDF100	0	47.50	
PTFE5/PVDF95	12.73	29.64	
PTFE10/PVDF90	16.09	29.42	
PTFE15/PVDF85	18.16	24.63	
PTFE20/PVDF80	23.62	20.03	

In summary, both the FTIR and XRD spectra results indicate that the PTFE/PVDF electrospun fibres have a mix of α - and β -phase PVDF. The amount of the β -Phase decreases, and the α -phase increases with an increase in the percentage of PTFE. In addition, the electromechanical performance of the PTFE/PVDF presented in section 4.3.3 is not related to the piezoelectric phase of the PVDF. It confirms that the β -phase of PVDF (exhibiting piezoelectric properties) is not the key to high energy harvesting performance in the hybrid piezo-triboelectric-based design. The relationship between the number of fluorine atoms, which increases the negative charge, and the surface morphology of the PTFE/PVDF fibre was responsible for the triboelectric effect. When more fluorine atoms at higher PTFE percentages are added, the texture of the fibre becomes non-porous due to unsuitable electrospinning conditions. This results in a change in

surface morphology that leads to a decrease in the electromechanical performance. This relationship is supported by surface potential measurements taken using the electrostatic field meter SIMCO-FX003. These measurements showed wide variations depending upon location on the fibre mat and the corresponding thickness at that point, but the average potential of PVDF and PTFE20/PVDF80 was 1.1 and 1.8 kV, respectively.

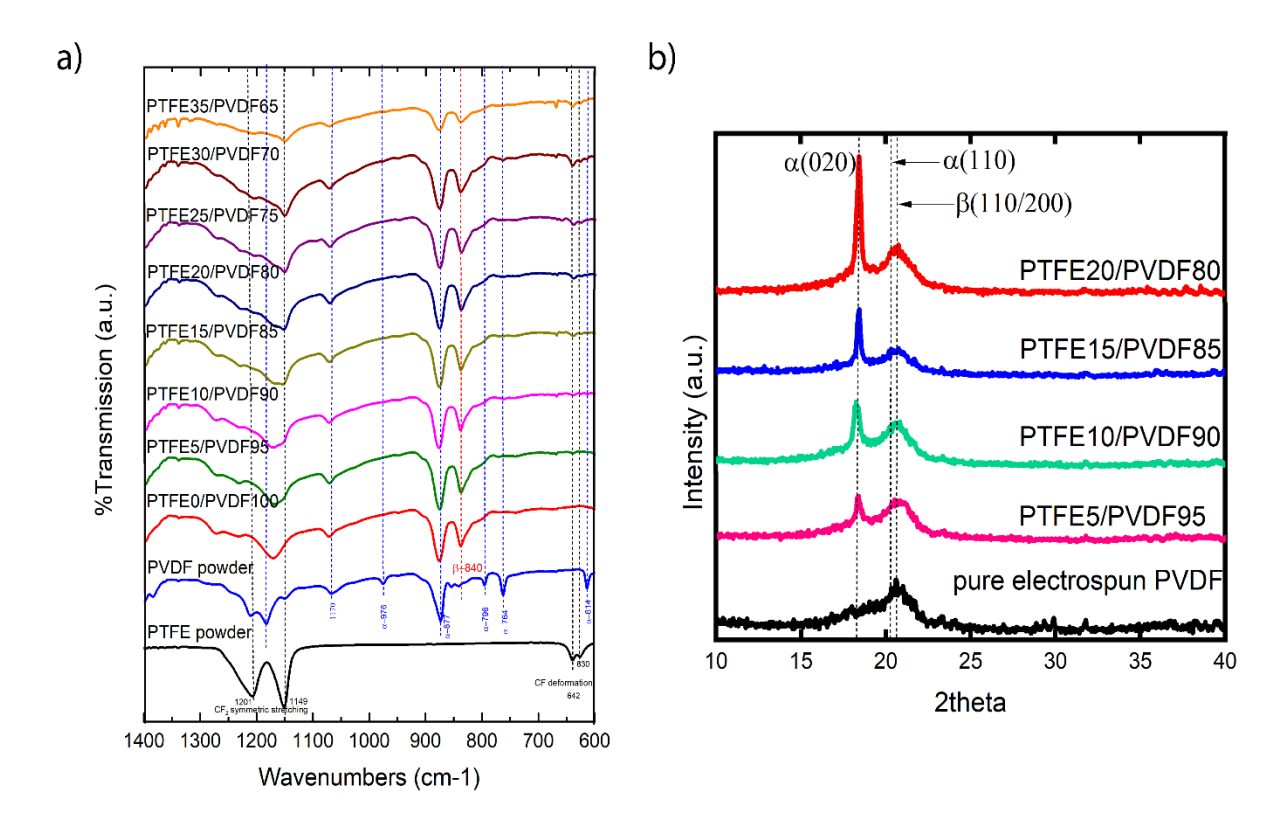


Figure 4. 8 a) FTIR-ATR spectra of PTFE/PVDF electrospun fibre. The measurements were carried out at room temperature over the range of 600-1400 cm⁻¹ b) XRD spectra of the single PTFE/PVDF electrospun fibre. The analyses were conducted on samples using Cu- Kα₁ radiation 1.5406 Å, 40 kV and 25 mA, Step size 0.5.

4.3.3.3 Electromechanical study

The energy harvesting performance was initially tested with the tapping rig to explore the optimum PTFE concentration. The test was performed at 6 Hz using the contact separation triboelectric mode. The $V_{\rm oc}$ and $I_{\rm sc}$ of each sample prepared from different concentrations were read after tapping for approximately 3 min to ensure that the tapping rate and the signal output were consistent. When the surfaces make contact, there is an electron transfer from the positively charged nylon to the negatively charged electrospun PTFE/PVDF. This leads to the nylon surface gaining a positive charge and the electrospun PTFE/PVDF surface developing a negative charge. When the surfaces are separated, an induced potential difference between the electrodes arises, leading to the development of opposite transferred charges on the electrodes through electrostatic induction. Consequently, an electric charge will transfer from the bottom

electrode to the top electrode via an external load in order to balance the potential difference until it reaches a state of equilibrium. As the surfaces approach each other, the potential difference caused by tribo-charging will gradually decrease until it reaches zero. The charges that were transferred are now moving in the opposite direction, from the top to the bottom electrode.

The open circuit voltage (V_{oc}) and short circuit current (I_{sc}) output measured at a 6 Hz tapping rate are shown in Figure 4.9 a) and 4.9 b), respectively. The V_{oc} and I_{sc} obtained from pure PVDF are slightly less than those obtained from other samples that include PTFE particles. The outputs from PTFE5/PVDF95, PTFE10/PVDF90 and PTFE15/PVDF85 were similar, which relates to the similar fibre size, resulting in the PTFE particles being similarly distributed within the fibres. For the PTFE20/PVDF80 sample, as shown in Figure 4.6 e), the fibre size is smaller and, combined with the higher percentage of PTFE particles, there is a greater concentration of PTFE at the surface of the fibres. This increases the triboelectric effect due to the superior triboelectric properties of the PTFE. When the PTFE particles exceed 20% (samples PTFE25/PVDF75, PTFE30/PVDF70, and PTFE35/PVDF65) the electrospinning process could not correctly form the fibres, resulting in poor mixing of PTFE particles and PVDF binder and thus the output is reduced in comparison with the PTFE20/PVDF80 (as seen in Figure 4.9 a) and b)). It was found that the peak-to-peak V_{oc} shows a similar output for pure PVDF and up to PTFE15/PVDF85. The peak-to-peak Voc shows a sharp increase to 390 V for the PTFE20/PVDF80 fibres. The results for the peak-to-peak $I_{\rm sc}$ follow a similar pattern with a maximum peak $I_{\rm sc}$ of 8 μA occurring with the PTFE20/PVDF80. The PTFE20/PVDF80 fibre mat made from the 4% PTFE and 16% PVDF solution gives the highest electrical output and was used in the subsequent analysis to investigate the effectiveness of the contact separation mode triboelectric energy harvesting using the electrospun fibres.

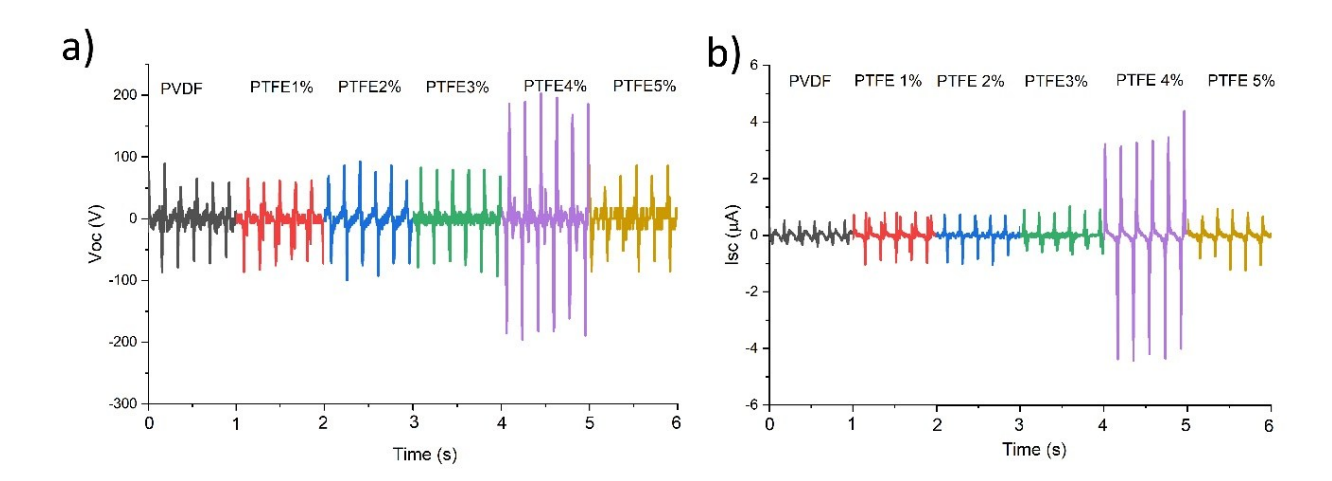


Figure 4. 9 a) open circuit voltage was tested over 100 M Ω resistor and b) short circuit current of the PTFE/PVDF electrospun fibre prepared at different concentrations.

The open circuit voltage (V_{oc}) output and short circuit current (I_{sc}) of the PTFE20/PVDF80 fibre mat were tested at different load resistance ($1k\Omega$ - $6G\Omega$), as shown in Figure 4.10 a). The calculated peak power ($P = \frac{V_p^2}{R}$) and the power density ($P = \frac{V_p^2}{RA}$) from the test are plotted in Figure 4.10 b). The highest power and power density were obtained at an optimal load resistance of 10 M Ω and were found to be 7 mW and 348.5 mW/m², respectively.

The contact-separation mode TENG works with a connected resistor R for this cyclical testing using the tapping rig. The top electrode moves up and down with the separation distance, x(t), from the fixed bottom triboelectric material. According to Ohm's law

$$V(t) = RI(t) = R\frac{dQ(t)}{dt}$$
(4.2)

V is the voltage output, Q is the amount of transferred charge between the two electrodes, I is the current output, and R is the load resistance; the $V_{\rm oc}$ and $I_{\rm sc}$ depend on the frequency of cyclical movement on both sides of triboelectric materials as a sinusoidal function that can be described by,

$$x(t) = A\sin(\omega t + \theta) \tag{4.3}$$

where t, A, ω and θ are the time, amplitude, angular velocity and initial phase angle of the cyclical motion, respectively [216-217].

The V_{oc} and I_{sc} obtained when testing at tapping frequencies of 4 to 9 Hz are shown in Figure 4.10 c) and d), peak V_{oc} and I_{sc} versus tapping frequency are plotted in Figure 4.10 e). As expected, the increased tapping frequency resulted in an increase in the V_{oc} and I_{sc} . When increasing the tapping frequency, the top layer contacts and separates the bottom layer quicker, resulting in the charge transfer reaching the equilibrium quicker through the external load. When the charge transfer reaches equilibrium, the output should reach the saturated point and then plateau, as found in the literature [155] and [218]. However, the tapping rig used in this work has limitations in testing; thus, the results could not show the saturation point. Table 4.2 summarises the results obtained for all samples.

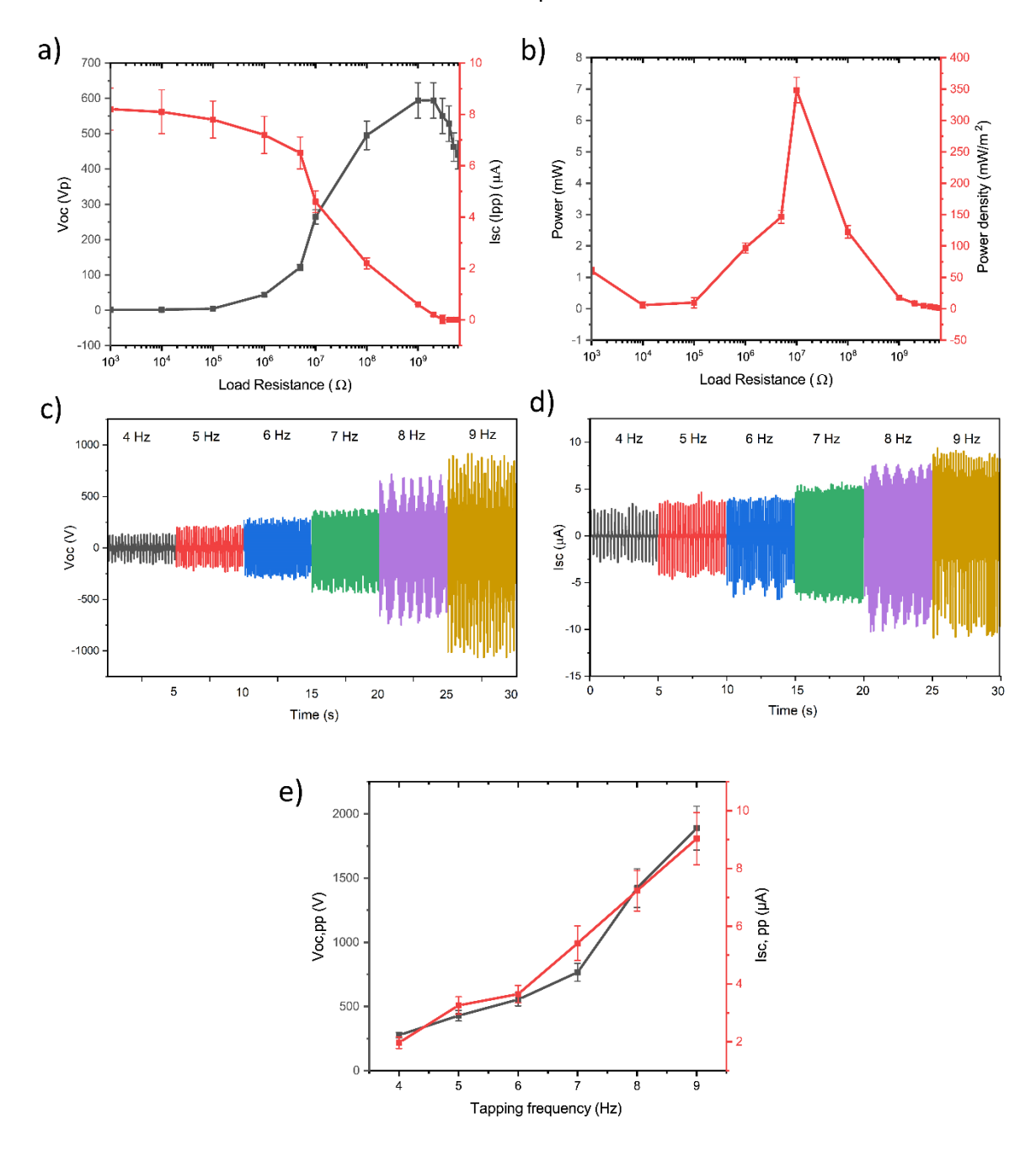


Figure 4. 10 a) peak open circuit voltage (V_{oc}) and peak to peak short circuit current (I_{sc}) v.s. load resistance test, b) calculated power and power density of the PTFE20/PVDF80 over different resistances, c) V_{oc} and, d) I_{sc} of PTFE20/PVDF80 at different tapping frequencies.

Table 4. 2 Summary of the electromechanical characteristics of the sample.

Code	Solution mixing	Percentage	Tapping	V _{oc}	I _{sc}
	condition	of polymer	frequenc	(rms)	(rms)
		in fibre	У	(V)	(μΑ)
			(Hz)		
PVDF	PTFE0/PVDF20	PVDF 100%	6	46	0.4
PTFE5/PVDF95	PTFE1%/PVDF19%	PTFE 5%,	6	48	0.6
		PVDF95%			
PTFE10/PVDF90	PTFE2%/PVDF18%	PTFE10%,	6	59	0.9
		PVDF90%			
PTFE15/PVDF85	PTFE3%/PVDF17%	PTFE15%,	6	54	1.1
		PVDF85%			
PTFE20/PVDF80	PTFE4%/PVDF16%	PTFE20%,	6	196	3.2
		PVDF80%			
PTFE25/PVDF75	PTFE5%/PVDF15%	PTFE25%,	6	60	0.7
		PVDF75%			
PTFE20/PVDF80	PTFE4%/PVDF16%	PTFE20%,	4	98	1.4
		PVDF80%			
			5	152	2.7
			6	196	3.2
			7	271	4.3
			8	503	6.2
			9	668	7.0

To demonstrate the practical utilisation of the PTFE/PVDF fibre, the book-shaped PVC substrate was assembled with the PTFE20/PVDF80 and the nylon fabric. The diode circuit was connected to the TENG to convert AC to DC for the charging capacitor experiment, as shown in Figure 4.11 a). The charging capacitor testing was performed using the tapping rig with a tapping frequency of 6 Hz, which was tested with capacitors of 0.1, 0.47, and 1 μ F, respectively. The calculated energy from charging obtained from $U = \frac{1}{2} CV^2$ was found at the capacitor 0.1, 0.47, and 1 μ F is

1.0, 16.7, and 41.2 μ J, respectively. The book-shaped TENG was further tested by illuminating the LED lights using a hand-tapping method, as shown in Figure 4.11 c). It was found that hand tapping could illuminate 100 LED lights, as shown in Figure 4.11 d).

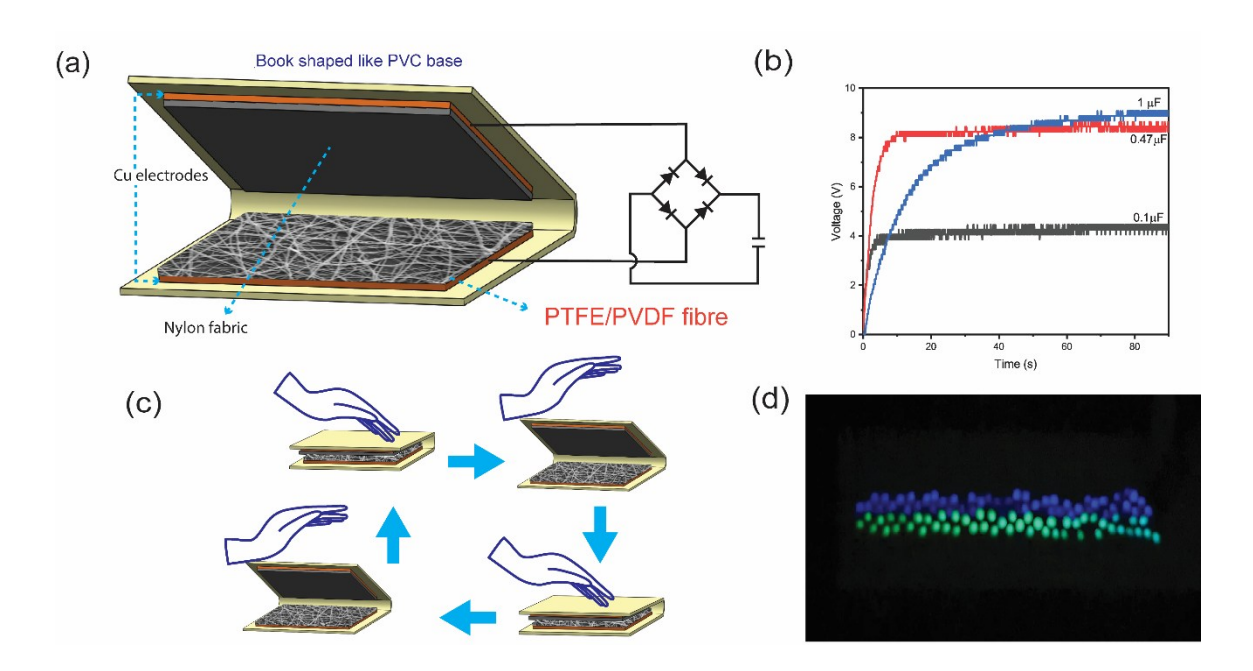


Figure 4. 11 a) Schematic of the book-shaped triboelectric energy harvester used to charge the capacitors; b) the voltage across 0.1, 0.47, and 1, capacitors, when charged by the book-shaped energy harvester at 6 Hz over a 90s period; c) schematic of the hand tapping test during the testing of the 100 LED lights experiment; d) the 100 LED lights illuminated via hand tapping of the book-shaped PTFE/PVDF energy harvester

To demonstrate the potential energy harvesting output in a practical energy harvesting application, the electropun fibre mat was assembled into a modified shoe insole to harvest energy during walking and running. The insole was modified to include four cut-out sections, each 2 cm x 2 cm, placed next to each other, resulting in an active area of 16 cm² located at the heel of the foot. A rib of the insole was left between these sections to ensure the insole remained comfortable to use and to make the active sections imperceptible to the user (see the schematic of the insole in Figure 4.12 a). The harvester operates in the contact separation mode with the electrospun fibre mat making contact with the nylon during the initial contact and loading phases associated with the foot being placed on the ground during the gait cycle, and separating as the heel lifts off during the terminal stance and pressing phases. The harvester was realised from 100% electrospun PVDF fibres and was placed on the left foot insole, and from PTFE20/PVDF80 electrospun fibres and was used in the right insole (as shown in Figure 4.12 a)) enabling a comparison of the PVDF and electrospun PTFE/PVDF fibres. The insole was placed inside an otherwise normal pair of running shoes and connected to the full bridge rectifier circuit consisting of 1N4007 diodes to charge the capacitors. Figure 4.12 c) shows the

voltage across the 0.1, 0.47, and 1.0 μ F capacitors that was measured while running on a treadmill. The calculated energy obtained from running, using the formula $U=\frac{1}{2}$ CV^2 for capacitors 0.1, 0.47, and 1 μ F was found to be 0.7, 15.8, and 100.8 μ J, respectively. Figure 4.12 d) shows the comparison of the voltage across the 1 μ F capacitor between the insole made from pure PVDF and PTFE20/PVDF80 when charging by walking and running. The calculated energy obtained from the PVDF insole from running and walking was 25.9 and 27.4 μ J, respectively. The calculated energy obtained from the PTFE20/PVDF80 insole from running and walking was 69.6 and 100.8 μ J, respectively. The energy obtained from the insole made from PTFE20/PVDF80 was shown to be approximately 3 times greater when walking and 4 times greater when running than the PVDF insole.

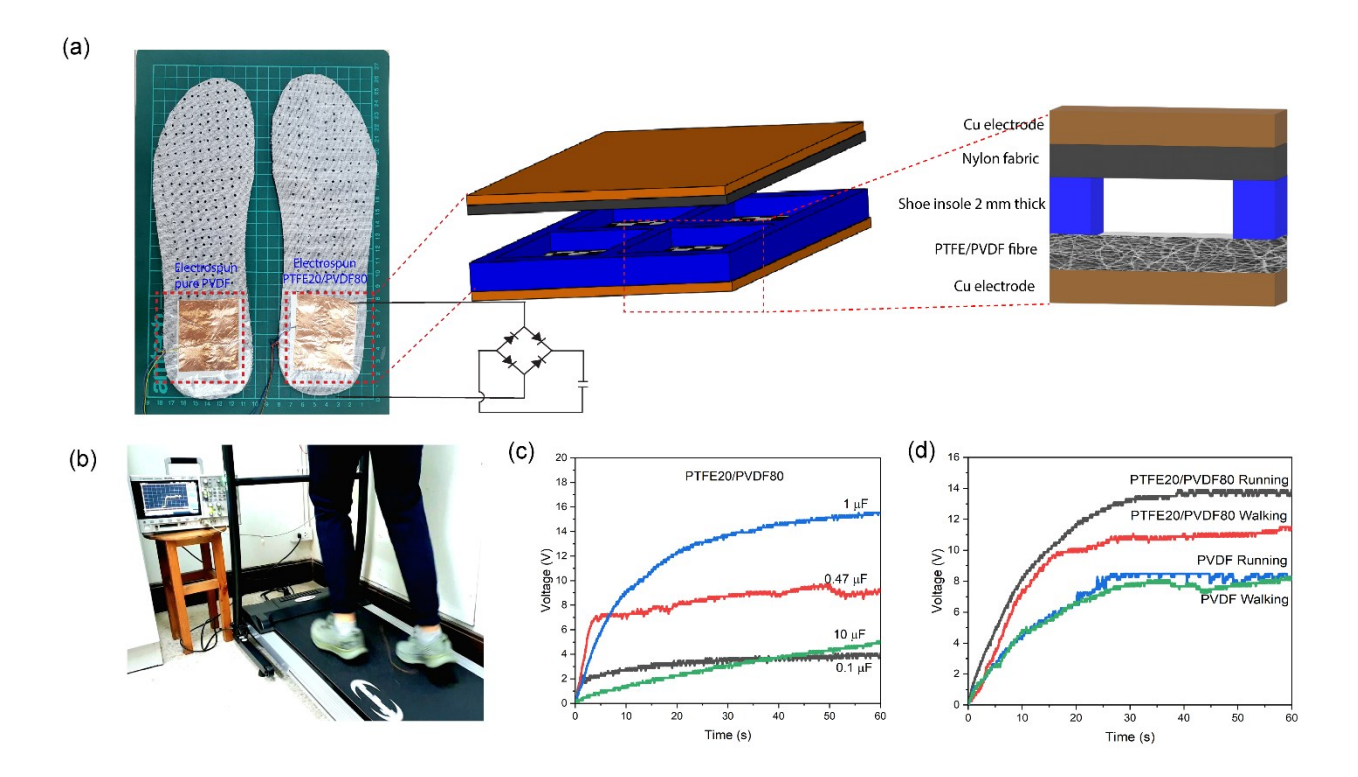


Figure 4. 12 The triboelectric insole for a demonstration of human gait energy harvesting a) the photo and schematic of the shoe insole used in this study b) the photo when charging the capacitor when running on the treadmill c) the voltage across the 1 μF capacitor, when charged by running on the PTFE20/PVDF80 insole over a 60s period d) the comparison of the voltage across the 1 μF capacitor, when running and walking on PTFE20/PVDF80 and PVDF insole over a 60s period

4.3.4 Conclusion of controlling the overall polymer concentration experiment

It was possible to effectively prepare a flexible Polytetrafluoroethylene (PTFE) fibre utilising a one-step electrospinning process with a PVDF solution as a precursor. An examination was conducted on the energy harvesting performance of a triboelectric assembly operating in a

vertical contact separation mode with electrospun fibres with different percentages of PTFE as the negative materials and nylon as the triboelectric positive material. The electrospun fibres created a nonwoven textile mat with a promising negative surface potential, with the optimum percentage being 20% PTFE loading in the PVDF matrix. This percentage of PTFE in the electrospun fibre enhanced the voltage and current output by 4 and 7 times, respectively, but the maximum power density was 348.5 mW/m 2 at a 10 M Ω resistance. Additionally, the application of the electrospun fibres was further demonstrated in book-shaped and shoe insolebased triboelectric harvesters operating in the contact separation mode. The book shaped harvester assembled with the PVDF energy harvester can successfully charge an energy storage capacitor using a full bridge rectifier circuit pointing the way towards energy harvesting powered systems. Electrospinning is a straightforward process for fabricating fibres that can be directly used in a non-woven fibre mat that is entirely compatible with textiles being soft, breathable, and conformable. Fibres could also be used to fabricate triboelectric PTFE/PVDF threads that could be combined within a woven or knitted textile. The improvements in electrical output from the fibres with PTFE certainly merit further investigation for practical energy harvesting applications.

The improvements in electrical output from the fibres with PTFE certainly merit further investigation in practical energy harvesting applications. The influence of the PTFE particles on the surface roughness of the fibres has not been quantified in this study. This surface roughness can affect the output of the TENG, and therefore, this will be studied in future work using an Atomic Force Microscope (AFM).

4.4 Conclusions

Chapter 4 discusses the energy harvesting capabilities of electrospun fibres made from PTFE/PVDF composites. The investigation effectively shows the creation of composite fibres through a single-step electrospinning technique. Optimising the concentration of PTFE particles within the PVDF matrix led to a significant enhancement in the material's triboelectric performance. The findings indicate that the composite containing 20% PTFE produced significantly enhanced energy harvesting results, exhibiting increases in voltage and current by factors of 4 and 7, respectively, when compared to pure PVDF fibres. The triboelectric energy harvester utilising these composite fibres reached a peak power density of 348.5 mW/m², showcasing its potential for real-world applications, including shoe insoles and book-shaped configurations. The materials demonstrated favourable attributes for wearable applications, such as flexibility, breathability, and lightweight features.

The findings show potential; however, optimising electrospinning parameters and refining fibre assembly design could significantly improve energy harvesting efficiency and broaden possible applications. This chapter provides a basis for creating advanced, adaptable, and eco-friendly energy harvesting devices through the use of composite electrospun fibres.

Chapter 5 Energy harvesting performance from the hollow and coaxial electrospun fibres

5.1 Introduction

This chapter discusses the fabrication and energy harvesting performance of the complex structure of electrospun fibre based on the research gap discussed in Chapter 2. The chapter is divided into two main parts: hollow fibre and coaxial fibre fabrication. The investigation of structure, morphology, chemical composition, energy harvesting performance and electrostatic properties of the hollow structure of PVDF and the coaxial structure of PS/PVDF electrospun fibre are discussed.

5.2 The energy harvesting from the hollow structure electrospun fibre

Section 2.5.3 explores the piezoelectric potential of polymers such as PVDF, focusing on enhancing their electromechanical performance through electrospinning. It underscores the significant potential of ferroelectret materials for energy harvesting applications, especially in creating lightweight, flexible, and high-performance structures suitable for wearable technologies. This section sets the stage for advancing energy-harvesting devices using electrospun hollow fibres, emphasising their practical applications and areas for further research. This chapter turns the research gap into the experimental work.

5.2.1 Introduction and research motivation of hollow PVDF electrospun fibre

The tubular structure is of interest to researchers, and several studies have predicted the performance of thin-walled thermoplastic in FEP and PTFE polymers. Studies related to the tubular structures in nonpolar thermoplastic FEP and PTFE polymers have suggested that hollow structures with an outer shell thickness of less than 50 microns may be able to produce higher d₃₃ values than those with a thicker shell [181], [219-220]. The results obtained through these investigations, though, were predicted, and no practical experiments were ever conducted. After a thorough search by the author of this report, no studies related to ultra-thin shell tubular structures were discovered.

Therefore, the challenge of fabricating the hollow structure for a thermoplastic polymer has not yet been achieved. In this regard, an electrospinning technique could be developed to possibly

achieve an ultra-thin tubular structure ferroelectret material. Electrospinning has been widely studied and can be explained in simple terms. During the electrospinning process, polymer in a liquid state is extruded from a needle tip at a constant rate. The resulting droplet of the polymer solution is then turned into a fine fibre which is deposited onto a grounded collector by a high electric force through the needle tip. Electrospinning can generate nanoscale fibres with high porosity and a high surface area. Materials produced by this method have been used in various applications such as wound dressings [73], tissue engineering [84], filters [75], [221], protective wearable devices [76], sensors [78], and batteries [222]. Furthermore, electrospinning parameters can be developed to fabricate polymeric hollow fibre with a shell thickness in the order of a submicron.

To date, hollow fibre structures fabricated by electrospinning techniques have been achieved using two approaches. The first approach is based on the coaxial fibre template. This involves the removal of the core of the fibre after the electrospinning process has been completed. This is achieved through heat treatment or by chemical treatment. This more traditional method requires two steps of preparation and is popular for the fabrication of ceramic or metal shell fibres, where the shell fibre has a much higher melting point than the core fibre. The second approach is a one-step method based on the different evaporation rates of the core and shell solutions. This method works with polymeric shell fibre as its melting point is not much higher than that of the core fibre. Several studies have successfully fabricated a hollow structure thermoplastic polymer such as PCL [98], PVDF [89] through a one-step electrospinning process. However, none of these studies were related to producing fibres for energy harvesting applications. A one-step production approach for the fabrication of hollow structures through electrospinning is beneficial when producing thermoplastic ferroelectret. The fabricated ferroelectret material produced through a one-step electrospinning approach is flexible, lightweight, biocompatible, requires a low processing temperature and produces high piezoelectric efficiency. In addition, ferroelectret materials made in this manner will be easier to recycle as the structure is less complex.

Further investigation is necessary to demonstrate energy harvesting potential from ultra-thin tubular ferroelectret. Therefore, this research aims to fabricate and investigate the energy harvesting potential for the electrospun hollow fibre from thermoplastic polymer by using a coaxial electrospinning technique. The comparison of energy harvesting performance between solid and hollow electrospun fibres is demonstrated.

5.2.2 Experiments

5.2.2.1 Fabrication of electrospun hollow fibre structure

The electrospinning machine (EC-DIG. IME, Netherlands) was used to prepare the electrospun fibre. The thermometer and humidity sensor were integrated inside the electrospinning cabinet. The digital wireless optical microscope was placed in the cabinet for the observation of the Taylor cone formation. The schematic of the electrospinning setup is shown in Figure 5.1.

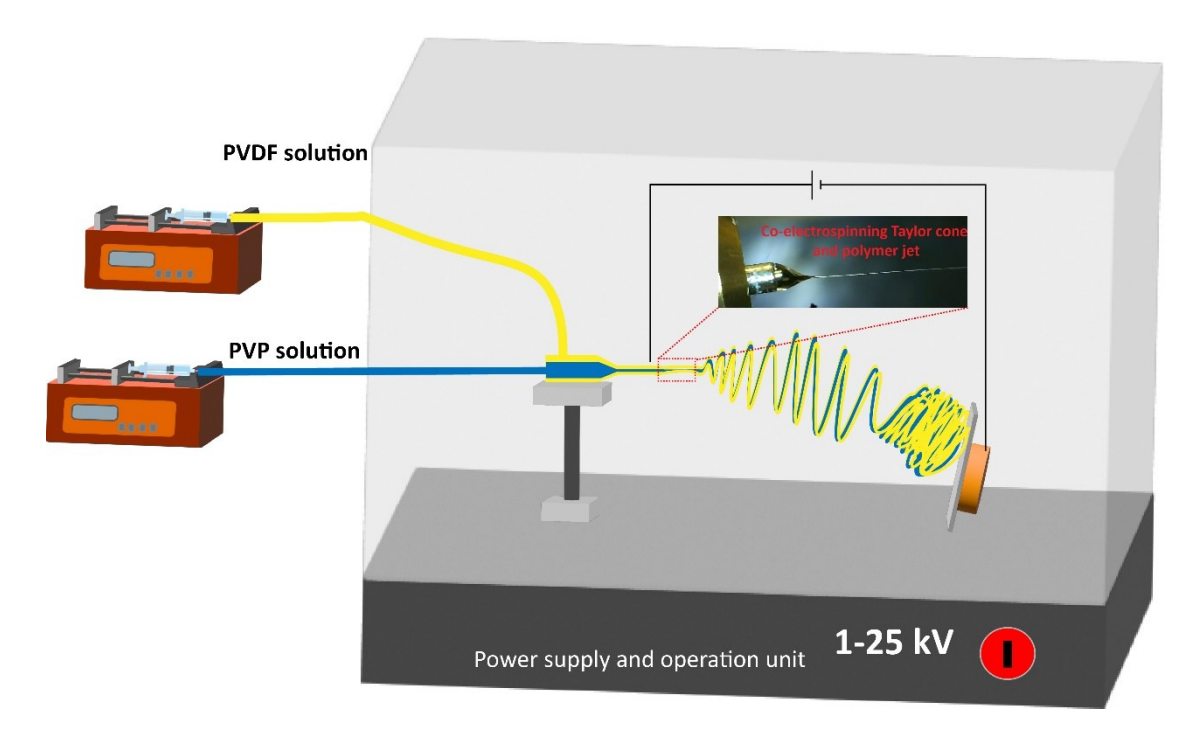


Figure 5. 1 The schematic of electrospinning apparatus to fabricate hollow fibre structure

In order to obtain hollow structure electrospun fibre using one-step electrospinning, the base condition for preparing the solid structure fibre of the selected polymer shell and core needs to be explored. The Polyvinylidene fluoride (PVDF) is selected as a shell polymer, and the Polyvinylpyrrolidone (PVP) is selected as a core polymer. The mechanism plays the main part in the Taylor cone, as shown in Figure 5.2. It works with different core and shell solution evaporation rates while in the liquid stage. Both core and shell solutions should not be mixed with each other. This is because a gel interface layer is formed once they come in contact in the Taylor cone area. The gel interface forms a structure within the shell solution. The shell solution is pulled to the target by an electrostatic force, and the solvent evaporates and then forms a solid state with a hollow structure fibre.

This approach is sensitive to humidity and temperature during electrospinning, and it requires the shell to evaporate quicker than the core so it can form a solid hollow structure before arriving at the target.

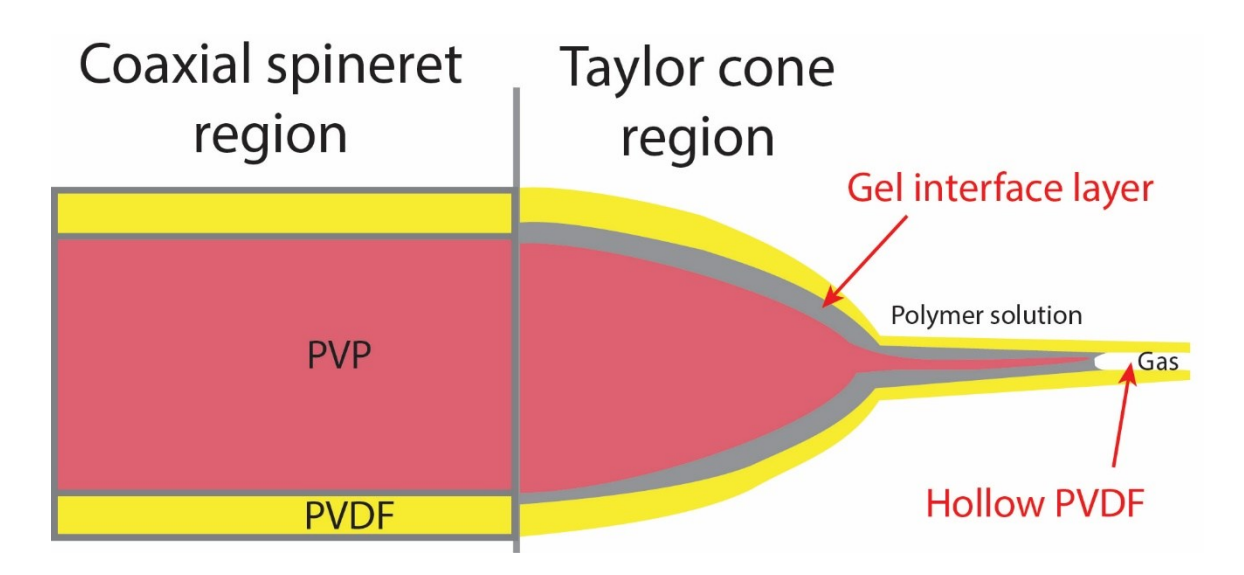


Figure 5. 2 Hollow structure formation in a one-step electrospun hollow fibre technique

For the solid structure of PVDF, the PVDF solutions were prepared at different polymeric concentrations of PVDF powder for mixing with DMF and acetone at a 1:1 ratio. The specifications are as follows: DMF and acetone, The solutions for the PVDF fibre were prepared at different polymer concentrations (15, 17, 18, 20, 22%wt) with the solvent ratio of DMF and acetone at 1:1 (v/v) on the hot plate stirrer for 4 hours at 60 c. The electrospinning experiment was performed by using a blunt tip (21G) needle. The distance from tip to the substrate, the applied voltage, and flow rate were studied at 17, 20, 23 cm, 20, 23, 25 kV and 4, 6 ml/hr, respectively.

To explore the solid fibre condition of PVP, the PVP solutions were prepared from PVP powder at different polymer concentrations (15, 17, and 20%wt) in the mixing solvent of DMF and Ethanol. Each concentration was mixed at different ratios of DMF and Ethanol of 4:6, 6:4, 7:3, 8:2 (v/v). The red dye was added to the solution to assist in the observation of the Taylor cone during the coaxial experiment. The electrospinning experiment was performed using a blunt-tip (21G) needle. The distance between tip to substrate, voltage and flow rate were studied for each solution concentration. If the experiment has been successful, the Taylor cone should form a stable cone jet shape with no dripping, and the substrate should be dry after the fibre hits the target without any residual dye colour remaining [89], [98].

Observation regarding the state of the Taylor cone was recorded in greater detail during the electrospinning process. The stability of the Taylor cone should remain unchanged throughout 4 min of the electrospinning process. If dripping occurs during the electrospinning process, it is considered an unstable Taylor cone state. By keeping the flow rate constant at 0.5 ml/hr, the study focused on examining the working distance and applied voltage in the fine range of 13-27 cm and 13-25 kV, respectively. Based on data gained from solid fibre experiments, PVDF and PVP solutions were chosen and used as the shell and core solutions for coaxial electrospinning, respectively. The condition of PVDF and PVP solutions was selected from the solid fibre experiments when mixing both solutions in the coaxial spinneret. A digital camera was used to observe the compound Taylor cone. The Taylor cone geometry was analysed for each condition from photographs using imaging software (ImageJ). This was done to study the size and angle of the Taylor cone. Although the optimum concentration of PVDF solution for solid fibre was 20 wt%, the polymer concentration that suited the coaxial experiment was 15-17%wt. The one-step hollow electrospun fibre relies on the different evaporation rates of the shell and core solution. This study is designed to use the core solvent, which evaporates quicker than the shell solution during the flight of the polymer jet. Thus, the distance from the tip to the target for preparing PVP solid fibre with the evaporated solvent was studied.

The PVP solid fibre experimentation process data showed the minimum completely evaporated solution state at 0.5 ml/hr at a needle to substrate distance greater than 19 cm and a voltage greater than 20 kV. The PVDF solution reached a minimum evaporated state at a needle to substrate distance of not over 20 cm and an applied voltage above 20 kV. This condition helps to eliminate the distance parameter in the coaxial electrospinning study. Thus, to find the hollow fibre condition, the distance from the needle tip to the substrate was kept constant at 20 cm.

The shell flow rate of the PVDF at 17% mixed with a 1:1 ratio of DMF and acetone was kept constant at 4 ml/hr. The core flow rate of the PVP at 20% mixed with a 4:6 ratio of DMF and EtOH was studied at 3 different levels, these being 0, 0,5 and 1.5 ml/hr. The applied voltage was also studied at 3 levels at 20, 23 and 25 kV. The full-factorial DOE scheme was used to help identify the best condition for hollow structure fibre preparation.

5.2.2.2 Geometrical and structural characteristics

The geometrical characteristics section includes the morphology and structure of the intended hollow fibre for PVDF. The tested samples were prepared from 20% PVP mixed with a 7:3 ratio of DMF and EtOH. The samples were coated onto aluminium foil and were examined with the SEM. In regard to the examination of the solvent residue, a Thermo Scientific™ Nicolet™ iS5 FTIR Spectrometer was deployed to study the chemical bond of the fibre after completion of the electrospinning process. As for the PVDF fibre, the FTIR spectra was applied to identify phase

fractions between α and β . The Benchtop X-ray Powder Diffraction, Bruker D2 PHASER, was used to analyse the crystal structure of the PVDF fibre.

5.2.2.3 Electromechanical characteristics

A surface potential test was designed, for the examination of the electrostatic characteristics of the electrospun fibre. To study the electret characteristic of the fibre, the surface potential data was recorded 3 times as follows: 14 days after electrospinning, after corona discharge and 14 days after corona discharge.

The piezoelectric coefficient (d₃₃) and capacitance (c) of the fibre mat were measured using Piezometer system, PM300. The standard measurements for the system—dynamic force of 0.25 N, static force of 10 N, and frequency of 110 Hz- were used for the analysis. The data was collected from the average value of 5 positions on the sample.

In order to test the energy harvesting performance, the fibre mat (2cm x 2cm) was assembled with a copper electrode and PET adhesion tape as shown in Figure 5.5 a). The tapping test rig was developed from previous studies and comes from inserting the sample between two electrodes and tapping at a constant rate [199], [223]. The tapping test rig was set up to provide a constant rate and pressure using a linear actuator motor. The linear actuator motor has a rated voltage of 12V, 900 rpm. The sample was attached to the oscilloscope to observe changes in voltage induced by the mechanical movement of the rig, as shown in Figure 5.5 b).

5.2.3 Results and discussion

5.2.3.1 The geometrical characteristics

As seen from the SEM image in Figures 5.3 a) and 5.3 b), the hollow PVDF fibres were internally broken. The diameter of the fibre was found to be around 2 microns. As seen in Figure 5.3 b), the obtained hollow fibres exhibit variation in their forms. In this case, solidification of the outer shell occurred at the onset of the instability of the compound jet, thereby departing from a near-perfect cylindrical shape. The shell and core diameters were barely observed from this technique. This may indicate that only part of the sample had formed as a hollow fibre. In addition, this could imply that the chosen condition may not be totally suitable for this technique.

The results from FTIR spectra analysis of the solid PVDF and partial hollow PVDF fibres are shown in Figure 5.3 c). The FTIR spectra analysis of the characteristic transmission band of non-polar α -phase at 762, 795, 853, 975, and 1382 cm⁻¹ was hardly observed. The polar β -phase for the electrospun PVDF fibre was observed at 840, 1234, 1275, and 1431 cm⁻¹. It can be

concluded that the ability of the transform β -phase for the electrospinning technique is of a high standard. However, this cannot explain the differences in the structure of the hollow and solid fibre through using the FTIR spectra.

The structural results obtained from the X-ray diffractometer, were initially determined from the PVDF sample prepared from PVDF 17% mixed with a 5:5 ratio of DMF and acetone as a shell solution and PVP 20 % mixed with a 7:3 ratio of DMF and EtOH and additional red dye for the core solution. This sample was expected to have been a hollow structured PVDF fibre. The fibre, though, appeared to be partially hollow when referring to the results from the SEM images. However, the degree of hollow space for the entire sample has not yet been established. The X-ray pattern, as shown in Figure 5.3 d), shows the dominant peak at 20.6°, corresponding to the β -phase in a single-plane crystal.

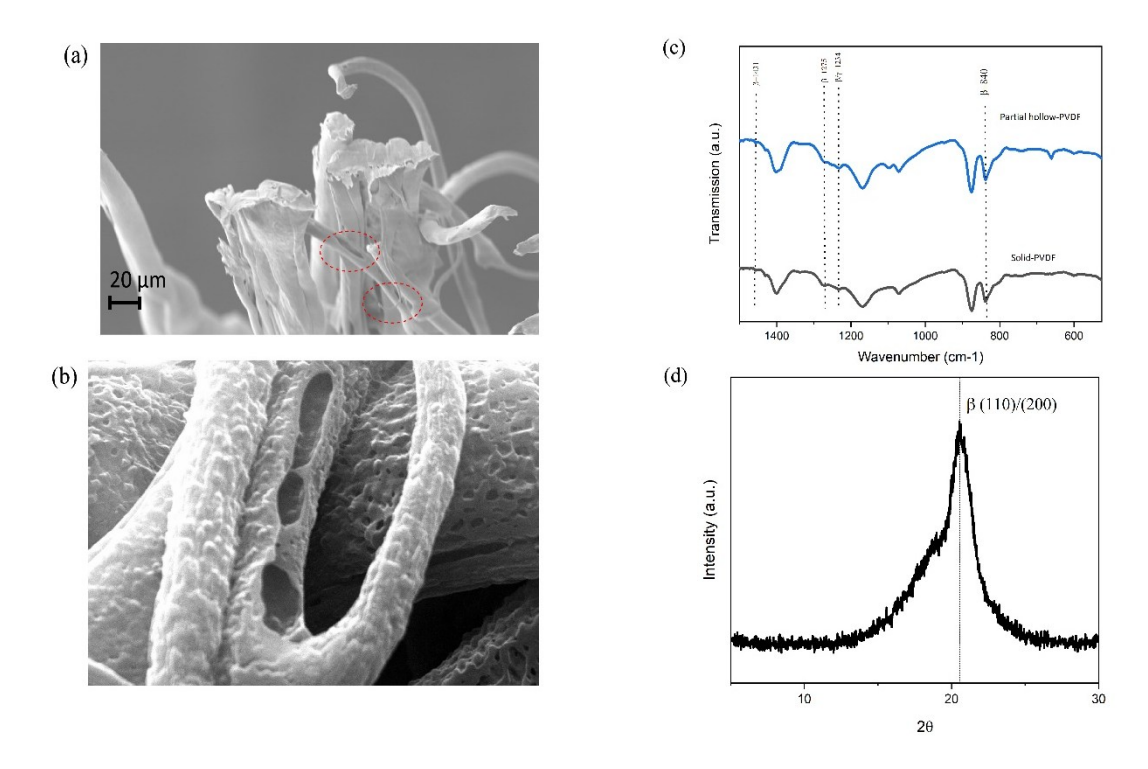


Figure 5. 3 a) and b) the SEM images of the electrospun partial hollow PVDF fibre c) the FTIR spectra of the solid and partial hollow PVDF electrospun fibres d) the XRD pattern of the partial hollow PVDF electrospun fibre

5.2.3.2 The electromechanical characteristics

After completion of the electrospinning process, the samples were carefully removed from the substrate using anti-static tweezers. The surface charge potential was then measured using a static fieldmeter. All samples were weighed after the electrospinning process via a four-digit laboratory scale. The samples were exposed to the environment for 14 days, and then the surface

potential was measured again. After 14 days, the residual charge was removed from all samples using an isopropyl spray. Then, the samples were corona charged and measured for the surface potential charge. The samples were exposed to the environment for another 14 days. The surface potential was then measured again.

The surface potential of the core-shell PVP-PVDF and the partial hollow electrospun fibre were observed after the electrospinning process and corona charge, as shown in Figure 5.4. Overall, the PVDF fibre shows a negative surface potential and engages the negative trapped charge after leaving the environment.

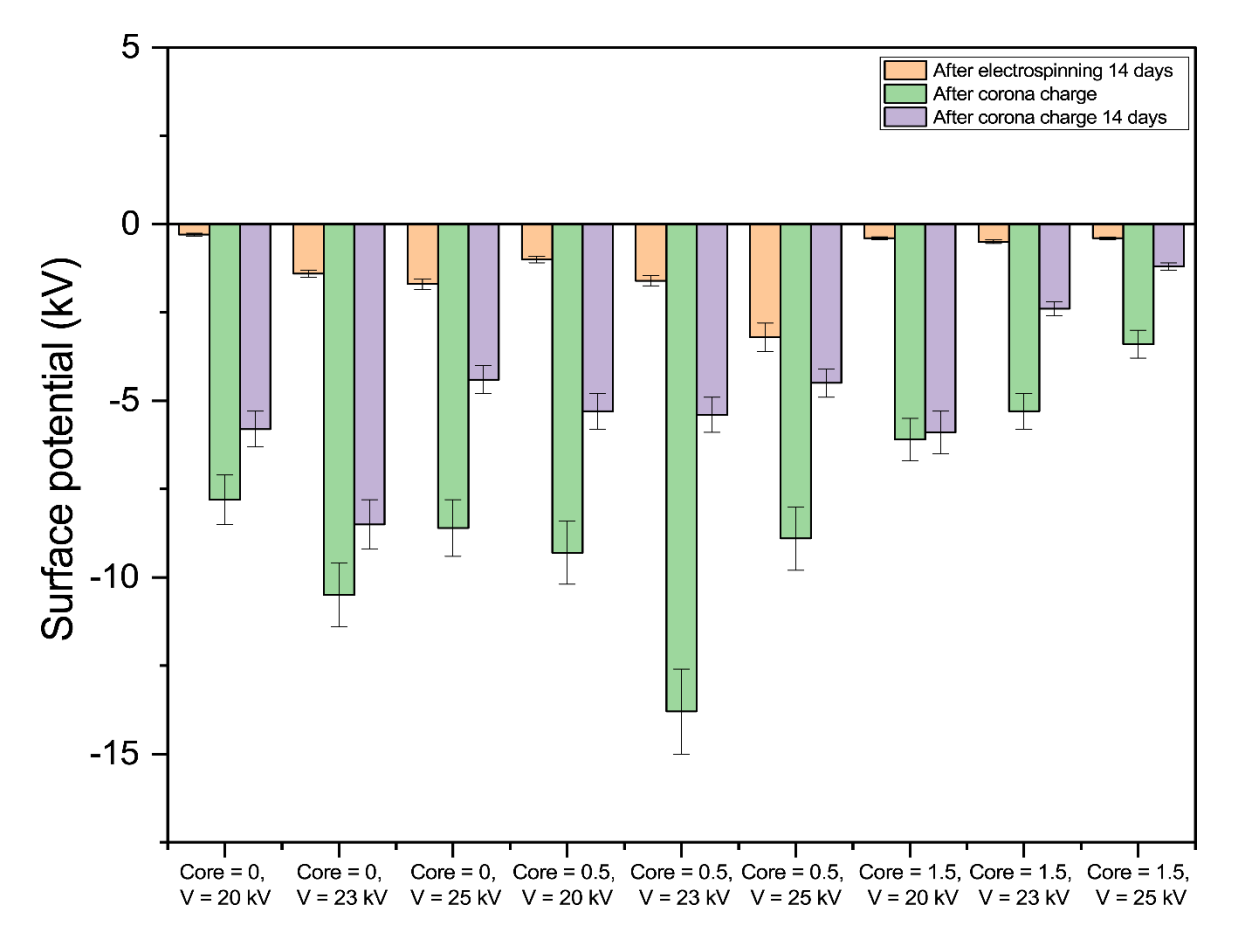


Figure 5. 4 Surface potential of hollow structure PVDF after electrospinning, after left in the environment for 14 days, and after corona charge for 14 days.

As shown in Figure 5.4, the measurement of the d_{33} found that the maximum d_{33} from the partial hollow PVDF fibre is 28.7 pC/N. However, after reading for 10s, the high d_{33} value disappeared. The maximum absolute value piezoelectric coefficient for the PVDF hollow fibre was found to be 28.7 pC/N. After reading for 10s the d_{33} value appeared to disappear. This may be caused by the deformation of the fibre mat structure after the force was applied during the testing procedure. The sample prepared from the PVDF solution 17 wt% and PVP 20% with the core flow rate and the applied voltage is 0 ml/hr, and 23 kV, was used in the further electromechanical test.

Interestingly, during the d_{33} measurement, the d_{33} reading appeared not to be constant. It could be assumed that the hollow structure of the electrospun collapsed due to the external stimulation force, indicating that the nano tubular structure was not stable enough to harvest energy based on the ferroelectret principle. The high reading found in the initial testing period may indicate a triboelectric charge from the high surface area of the hollow structure compared to the solid PVDF structure.

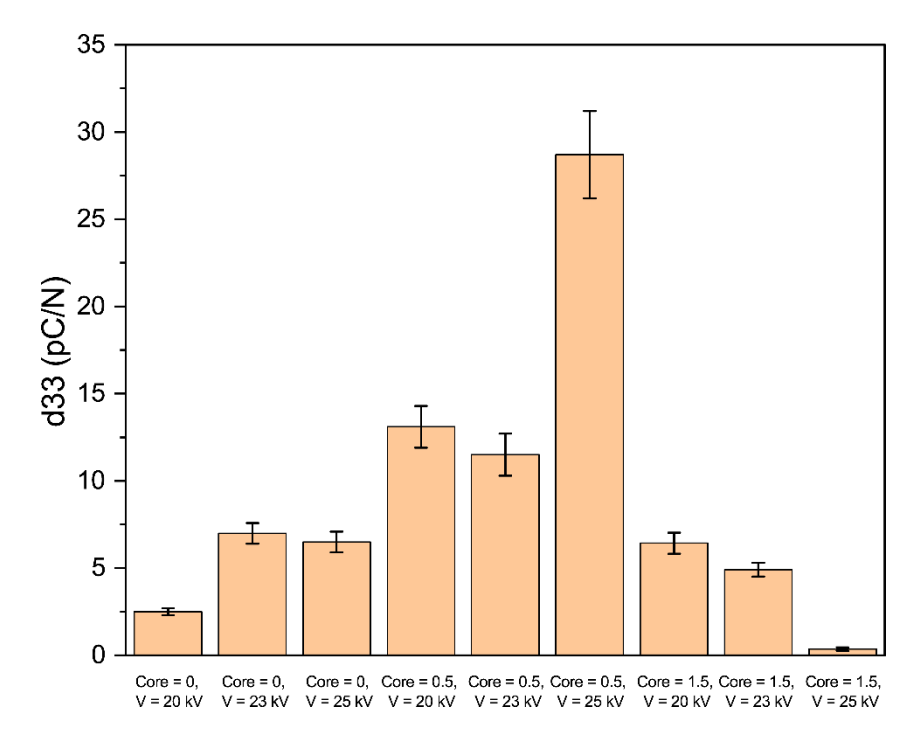


Figure 5. 5 The maximum absolute piezoelectric coefficient value of the coaxial PVDF measured from PiezoMeter PM-300

A tapping test was set up using a linear motor that tapped the sample at a constant rate and pressure in order to study the energy harvesting performance. The output voltage under the compressive force on the PVDF electrospun solid fibre and partial hollow fibre are shown in Figure 5.5 c). The maximum peak-to-peak open circuit voltage obtained from the partial hollow fibre was shown to be 8.7 V, while the solid fibre was 6.4 V. The peak power density output calculated from $P = V_{pp}^2/RA$ where R is the resistance of the oscilloscope (10 M Ω), and A is the active area of the testing sample. The power density from the solid and partial hollow PVDF electrospun fibre was found at 1.60 and 2.18 mW/m², respectively. It was found that the hollow structure had better power output than the solid structure.

As discussed in section 5.2.3.2, the higher power output coming from the hollow structure PVDF is not beneficial from the ferroelectret-based structure due to the weakness of the nano tubular structure under the external force. However, this higher output may be caused by the triboelectric charge. The contact–separation configuration mode may be more suitable for a hollow fibre structure.

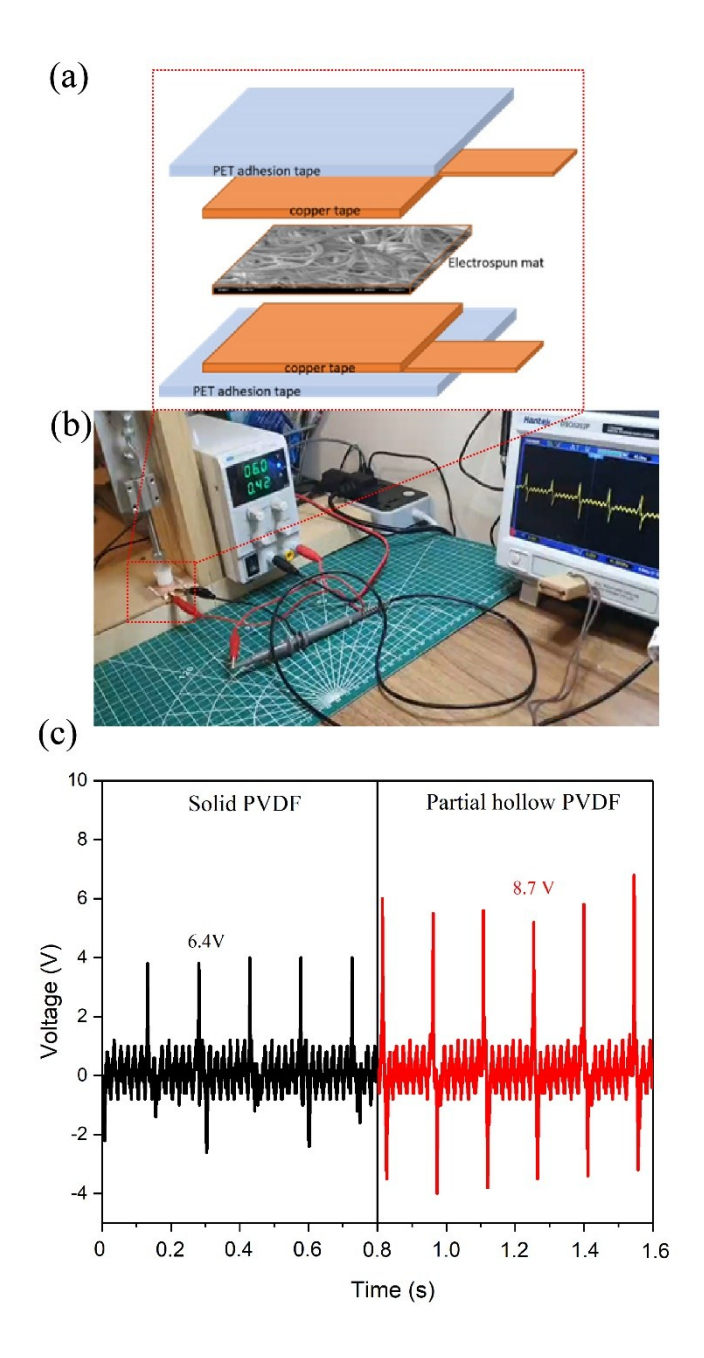


Figure 5. 6 a) Schematic of the testing sample for tapping test, b) the setup of tapping rig during tapping test, c) the open circuit output voltage of solid PVDF and partial hollow PVDF electrospun fibres

5.2.4 Conclusion from the energy harvesting from the hollow fibre structure

This research aims to investigate the energy harvesting potential from the electrospun hollow fibre using a one-step coaxial hollow electrospinning method. PVDF was selected to improve the energy harvesting of the flexible polymer. The investigation of the fibre covers geometrical and electromechanical characteristics. The structure and morphology were examined and investigated through SEM. It was found that the hollow structure of the PVDF sample was

revealed through the burst of the skin in the shell of the fibre. The chemical bonding results from the FTIR spectra indicate a small level of mixing between PVP and PVDF for the partial hollow fibre. The PVDF sample revealed the dominant piezoelectric β -phase spectra, which agreed with the strong peak of β -phase obtained from the XRD result. The electromechanical test results from the solid and partial hollow PVDF samples showed the maximum output voltages at 6.4 and 8.7 V, respectively. The power density from the solid and partial hollow PVDF electrospun fibre was found at 1.60 and 2.18 mW/m², respectively. However, the higher output observed from hollow PVDF structures was not considered to be a benefit of ferroelectret-based assemblies.

5.3 Energy harvesting performance from the coaxial electrospun fibres

Section 2.5.4, the comprehensive review of the theoretical background and state-of-the-art research in energy harvesting from electrospun fibres, specifically focusing on core-shell structures, is discussed. It highlights the advantages of core-shell fibre designs, particularly their ability to combine the complementary properties of different materials. The integration of a PS core and PVDF shell demonstrates significant advancements in energy harvesting capabilities by leveraging PS's high charge retention and PVDF's ferroelectric and triboelectric properties. These fibres exhibit enhanced power densities and practical functionality, making them ideal candidates for scalable, lightweight, and flexible energy harvesting applications. The potential of core-shell fibres could overcome the limitations of single-material fibres, thereby improving efficiency, durability, and adaptability for wearable and portable devices. This chapter discusses the fabrication and investigation of the energy performance of the coaxial structure.

5.3.1 Introduction and research motivation

The working principle of the triboelectric effect relies on the contact between two materials, namely the donor and the acceptor. The triboelectrification of PTFE has been shown to be the best in the triboelectric list as an acceptor, and nylon 6 has been shown to be the best donor [201]. However, to improve the triboelectrification of the triboelectric material, the researcher may need to consider that the top-range material chosen may have limited properties. Keeping the treatment process to a minimum while remaining effective is the key to developing this technology. The main approaches to improve surface triboelectrification are to enhance surface area, embed the dipole material, modify surface morphology, modify surface chemistry, and integrate ferroelectric materials.

In triboelectric generator research and development, the mainstream research focuses on increasing the amount of charge generated using chemical and physical approaches. For chemical approaches, the main work focuses on introducing chemical function groups and high dielectric fillers to the base high triboelectric material, such as barium titanate (BaTiO₃)[72], [224-225], calcium titanate [226], carbon nanotubes [183], Mxene [227]. Several techniques have been reported to enhance the specific surface area of polymers, including physical modification through the use of block copolymer templating [228], moulds [229], electrospinning [230], 3D printing [231], and reactive ion etching [232]. However, little research currently focuses on controlling the charge transfer and storage in triboelectric materials.

There is some interest in using electrospinning techniques to fabricate a combination of PS and PVDF in both electret filters [184], [233-235], and triboelectric energy harvesters [236]. However, none introduce the core-shell structure of PS and PVDF to enhance the charge storage inside the fibre mats.

To the best of our knowledge, there have been no published reports regarding the core-shell structure of PS as a core fibre and PVDF as a shell fibre; the model of core-shell PS/PVDF can be seen in Figure 5.6 b). Electrospun polystyrene (PS) possesses the benefit of exhibiting a positive surface potential, leading to the induction of a negative surface potential in polyvinylidene fluoride (PVDF). As a consequence, triboelectric energy harvesters have a significant negative surface potential. In this work, the core-shell structure of PS and PVDF is prepared using precipitation using a single nozzle electrospinning technique, and the energy performance is investigated for the first time.

5.3.2 Experimental procedure

5.3.2.1 Electrospun fibre preparation

In order to produce the coaxial structure of PS/PVDF using the precipitation method with a single nozzle electrospinning technique, PS and PVDF powder were used to prepare the polymer solution by stirring in DMF as a solvent solution. The different concentrations of each PS and PVDF 10, 12, 14 16 and 18 % were prepared in DMF and stirred at 80 c° for 12 hrs. The PS and PVDF solutions were then mixed by keeping the polymer content at 28%, PS10% +PVDF18%, PS12% +PVDF16%, PS14% +PVDF14%, PS16% +PVDF12%, and PS18% +PVDF10%. The mixing of PS/PVDF solutions was left for three days for the precipitation process to occur. The solution was stirred at room temperature before commencing the electrospinning process. The initial experiment implied that the PS precipitated into a colloid layer by varying the PS and PVDF solution ratio. As the density of PS is lower than PVDF, the PS in DMF floats to the top layer. It was discovered that the colloid layer became thicker when the amount of PS solution was

higher in the mixed solution. It was confirmed by FTIR analysis that the top layer solution is PS, and the bottom layer solution is PVDF in DMF. The flow chart of the core-shell structure of PS/PVDF preparation is shown in Figure 5.6 a).

5.3.2.2 Electrospun fibre characteristics

The obtained fibres were collected as nonwoven fabric and then investigated in physical, chemical and electromechanical studies. After the electrospinning process, the electrostatic field meter (Simco FX-003, Japan) was used to collect the surface potential results. The morphology and structure of the electrospun PTFE/PVDF were examined using the scanning electron microscope (SEM) (Phenom ProX, Thermo Fisher Scientific) and the tunnelling electron microscope (TEM) (HT7700, Hitachi). The chemical composition and structure of the materials were examined using a Fourier transform infrared (FTIR) spectrometer (Nicolet iS5, Thermo Fisher Scientific). Additionally, X-ray diffraction analysis (D8 Advance, Bruker) was employed to evaluate the crystalline phase of the PTFE/PVDF electrospun fibre.

5.3.2.3 The electromechanical study

The coaxial PS/PVDF electrospun fibre was cut to dimensions of 4 cm x 5 cm and subsequently attached using Cu tape, operating as an electrode. The opposite side of the triboelectric energy harvester consisted of nylon fabric, which served as the positive material. This was attached to the Cu electrode and tested in the vertical contact separation mode with a distance of 1.5 cm, as shown in Figure 5.14 a). A controlled pressure of 0.5 N/cm² was applied at different frequencies (3-10 Hz), utilising the cycle compression test system with a linear actuator.

The energy harvesting efficiency of the triboelectric energy harvester was evaluated by utilising a tapping apparatus. The energy harvester's open circuit voltage (V_{oc}) was measured using an oscilloscope (MSO7012B, Agilent Technologies) equipped with a $10M\Omega$ probe resistance. To measure the open-circuit voltage, the oscilloscope was connected to the 1 G Ω resistor as a voltage divider circuit due to the substantial internal impedance of the TENG. The N6705B DC power analyser, manufactured by Agilent Technologies, was utilised to measure the short circuit current (I_{sc}).

Figure 5.14 a) shows the arrangement of PS/PVDF electrospun fibre pieces, measuring $4 \, \text{cm} \times 5 \, \text{cm}$, which were assembled using a folded-over PVC template in the shape of a book. The nylon fabric was utilised as the triboelectric donor material. The book-shaped structure was utilised to evaluate the capacitor charging capacity and the LED light illuminating capability.

Chapter 5

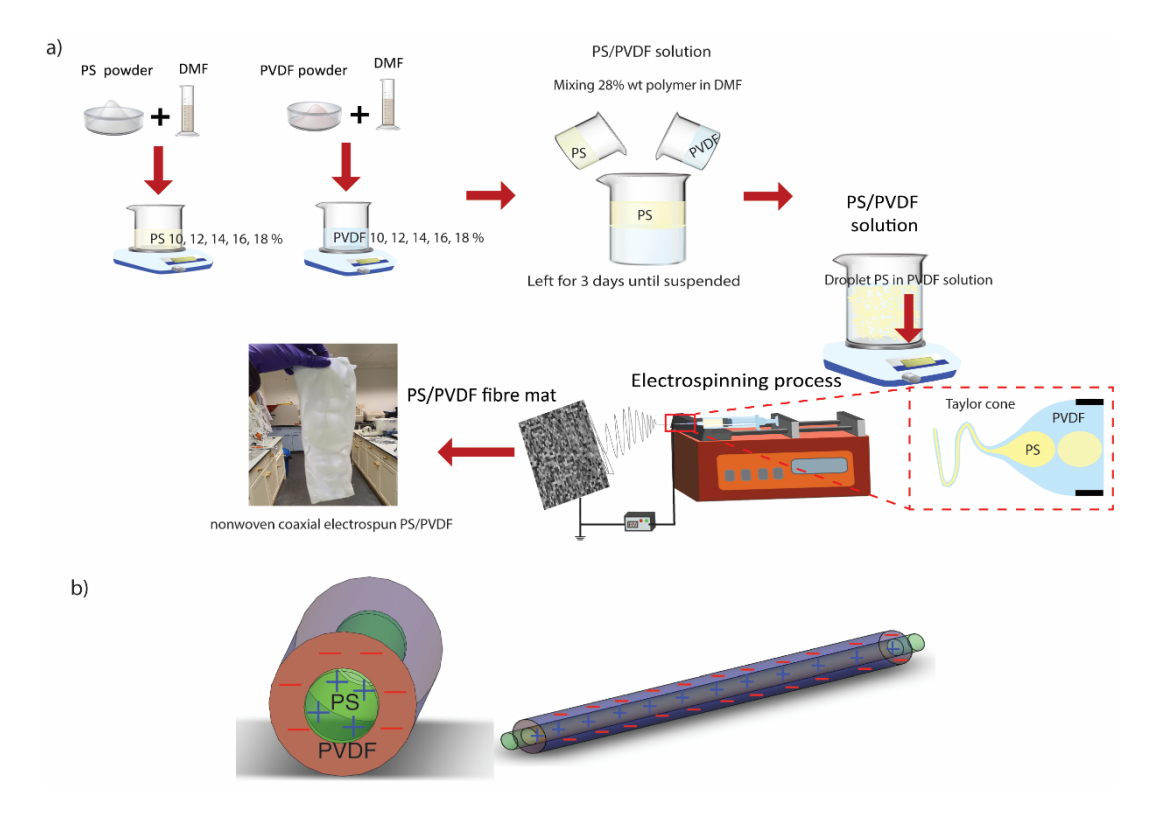


Figure 5. 7 a) The flow chart of coaxial PS/PVDF electrospun fibre preparation, b) model of the coaxial PS/PVDF electrospun fibre where PS is the core and PVDF is the shell fibre.

5.3.3 Results and discussion

In this section, the results from the PS/PVDF coaxial fibre are discussed in the material structure, and its characterisation, including the electromechanical properties and, finally, the electrostatic properties of the obtained fibre, are investigated.

5.3.3.1 Morphology and structure characterisation

The coaxial PS/PVDF fibre morphology was observed using SEM for the whole structure. The skin of the coaxial PS/PVDF was not smooth except for the sample PS14/PVDF14. The rough fibre skin, resulting in the evaporation rate of the solvent, was not dried immediately after the electrospun fibre arrived at the target, resulting in penetration into the solid polymer skin. The overall sample did not observe the bead-like structure, indicating that the concentration of the polymer solution was appropriate for the electrospinning process. With the higher percentage of PS, the sample shows the lower density characteristic of PS fibre. It should be noted that the electron beam from the SEM techniques will not penetrate through the sample. Thus, the coaxial structure was not shown by using this technique. The average diameter of the coaxial PS10/PVDF18, PS12/PVDF16, PS14/PVDF14, PS16/PVDF12, and PS18/PVDF10 electrospun fibre measured from SEM are 2.202, 2.690, 3.404, 2.209, and 2.221 µm, respectively. The average diameter of the SEM increased with the percentage of PVDF core and reached the

maximum at 3.404 μ m for the sample PS14/PVDF14, as shown in Figure 5.8. When the percentage of PVDF was higher for samples PS16/PVDF12 and PS18/PVDF10, the fibre diameter tended to decrease due to the lower dielectric constant of the polymer solution.

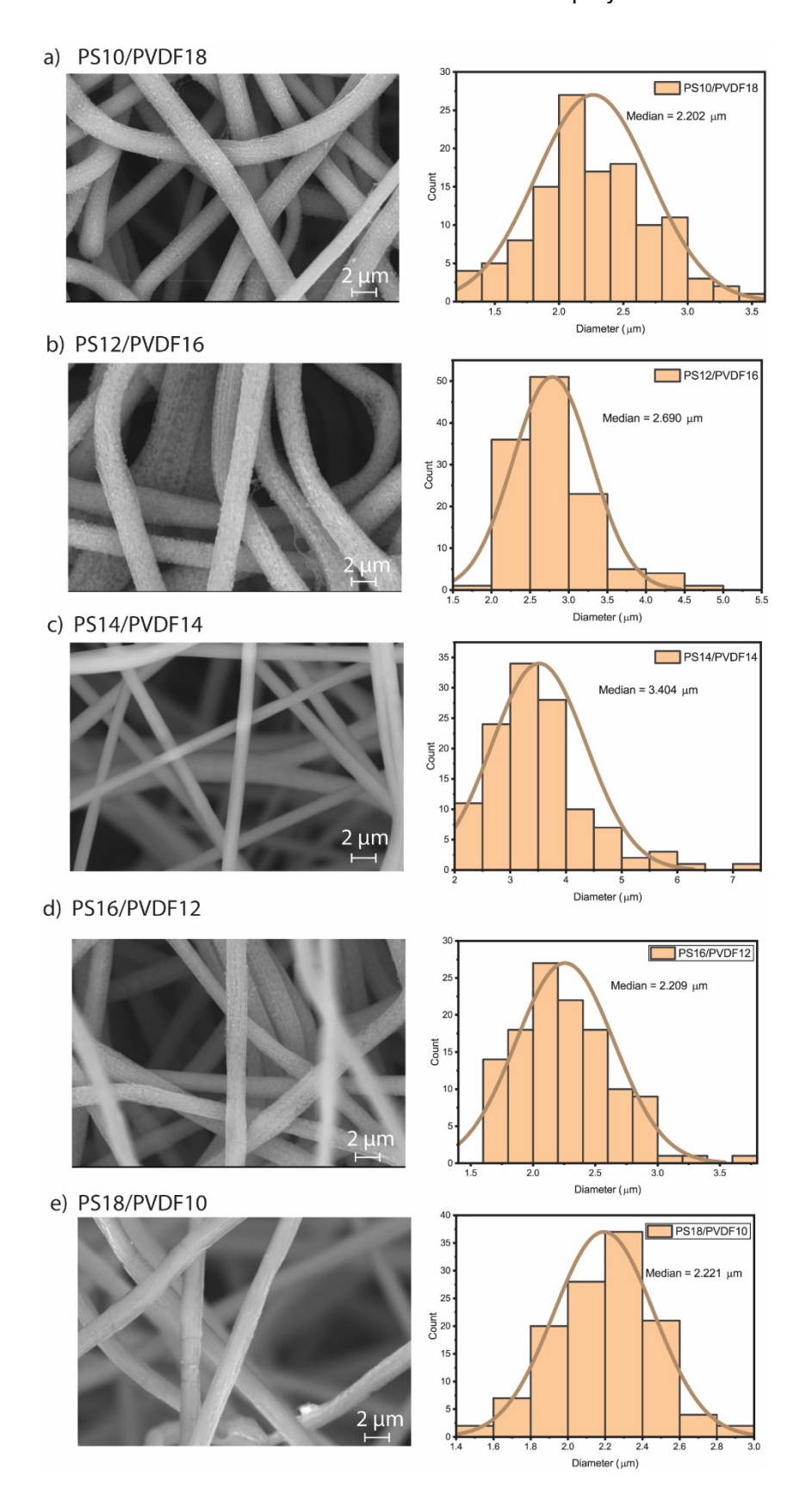


Figure 5. 8 SEM images show the structure and morphology of the PS/PVDF electrospun fibres.

To investigate the core-shell structure of the PS/PVDF fibre, TEM was used to analyse the structure and diameter of the core and shell. Figure 5.9 shows the TEM images along with core and shell diameter distribution. Overall, the structure observed from the TEM analysis exhibited a coaxial structure in all coaxial PS-PVDF samples. However, the PS18/PVDF10 showed the core and shell layer mixing. The TEM images showed the coaxial structure in all PS/PVDF electrospun fibre areas. It was also shown that the core diameter increased with an increase in PS percentage. However, in the PS18/PVDF10 sample, the core appeared to be blended, and the PS shell was nominated for the PS/PVDF fibre structure. This showed similar results to the composite fibre PS/PVDF obtained from Li et al. [184], when using a high percentage of PS in the PVDF matrix.

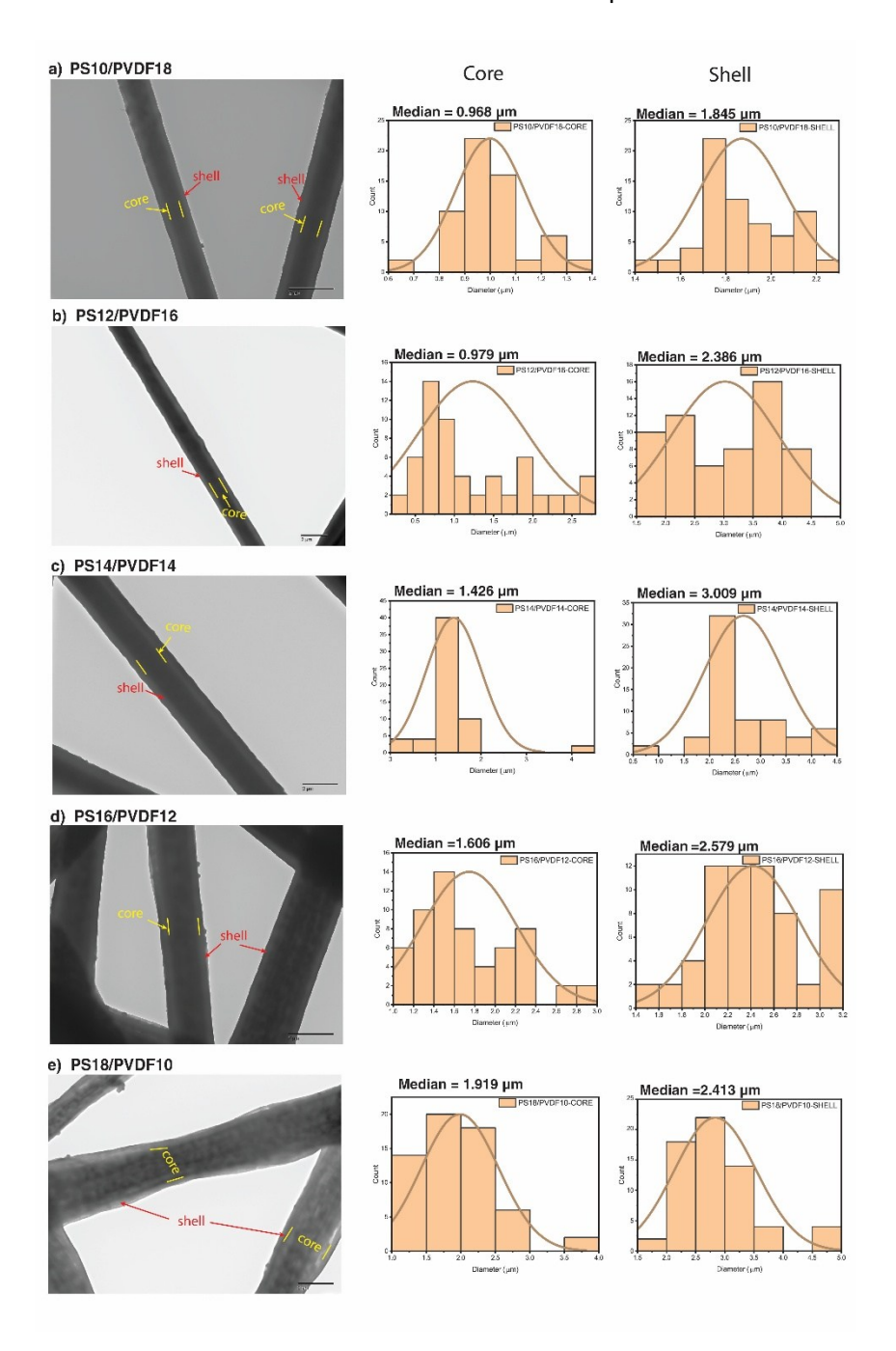


Figure 5. 9 TEM images of the coaxial PS/PVDF electrospun fibre.

The summaries of the average diameter observed from SEM and the shell and core layer observed from TEM of the coaxial PS10/PVDF18, PS12/PVDF16, PS14/PVDF14, PS16/PVDF12, and PS18/PVDF10 electrospun fibre are shown in Table 5.2. The shell diameter measured using the TEM technique was slightly smaller than that obtained using the SEM technique due to the smaller sample size and higher resolution measurement. The shell diameter of the coaxial PS10/PVDF18, PS12/PVDF16, PS14/PVDF14, PS16/PVDF12, and PS18/PVDF10 electrospun fibre were 1.845, 2.386, 3.009, 2.579, and 2.413 µm, respectively. Whereas the average diameter of the core for the coaxial PS10/PVDF18, PS12/PVDF16, PS14/PVDF14, PS16/PVDF12,

and PS18/PVDF10 electrospun fibre were 0.968, 0.979, 1.426, 1.606, and 1.919 µm, respectively. It was found that the core layer increased with an increase in PS percentage.

The variation of the texture from SEM and TEM analysis found that the skin of the coaxial PS/PVDF became smoother when the PS percentage was increased. However, when the maximum PS percentage was added to the sample PS18/PVDF10, the skin of the fibre showed breaking, corresponding to the picture observed from TEM. The diameter of the core fibre increased with an increase in PS percentage, which confirmed that the core of the coaxial PS/PVDF fibre was PS. This corresponds to the results obtained from the FTIR technique, which can be seen in Figures 5.11 and 5.12.

At first, the coaxial structure assumed that the PS formed the fibre's core and PVDF formed the shell of the fibre due to the solution preparation process. The density of PS is less than PVDF. Thus, in the miscible solution, PS was suspended on the top of the solution, as shown in Figure 5.5. After leaving the PS/PVDF to precipitate for three days, the PS/PVDF solutions were stirred on the magnetic stirrer before the electrospinning process. The core-shell structure's working principle lies in the immiscibility of two liquids in the solutions. During the electrospinning process, the electrostatic force stretches the liquid phase of the immiscible solutions and forms the core-shell structure after the solvent has evaporated, as shown in Figure 5.2.

To ensure that PS and PVDF are formed as core and shell fibres in the coaxial PS/PVDF fibre, the suspended layer was investigated using FTIR to confirm that the suspended layer is PS immiscible in the PVDF solution matrix, as shown in Figure 5.10. It shows that the suspended layer became thicker when the percentage of PS increased. The results from the FTIR investigation show that the suspended layer was PS, while the matrix layer was PVDF.

Table 5. 1 Summary of the average diameter, core and shell layer of the coaxial PS/PVDF fibres

Sample	Average diameter from SEM diameter (µm)	Average shell diameter from TEM diameter (µm)	Average core diameter from TEM diameter (µm)
PS10/PVDF18	2.202	1.845	0.968
PS12/PVDF16	2.690	2.386	0.979
PS14/PVDF14	3.404	3.009	1.426
PS16/PVDF12	2.209	2.579	1.606
PS18/PVDF10	2.221	2.413	1.919

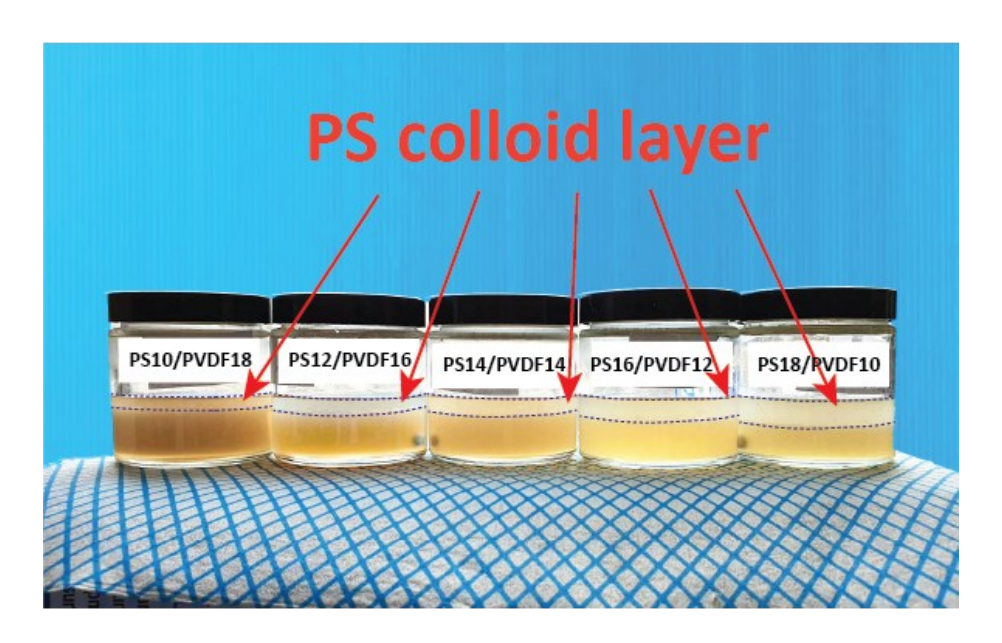


Figure 5. 10 PS-PVDF solutions and colloid layer

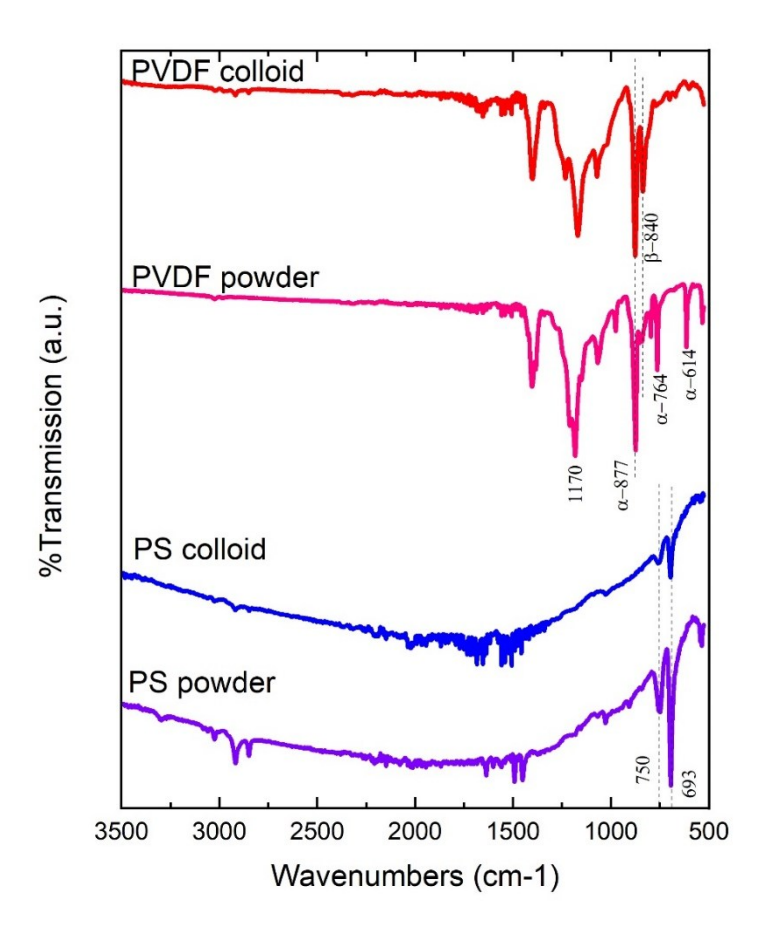


Figure 5. 11 The FTIR result of the suspended layer in PS/PVDF solution

The chemical structure was investigated using the FTIR technique. To investigate the changes in the chemical structure of the PS and PVDF before using the electrospinning process, the powders of PS and PVDF were compared to the FTIR spectra of the coaxial PS/PVDF fibre.

The electrospun pure PVDF peaks at 840 and 876, corresponding to the β - and C-H wagging in the α -phase of PVDF, respectively. Compared with the results obtained from PVDF powder, which showed the peaks at 614, 764, 796, 877, 976, and 1170, the electrospinning technique could effectively induce the crystalline piezoelectric β -phase. On the other hand, pure PS has three distinct transmission bands that are easily noticeable. The transmission intensities at 3200–2800 cm⁻¹ were identified as the symmetric and asymmetric vibrations of C–H bonds. The wavenumber range of 1600–1400 cm⁻¹ corresponds to the bending vibration, while the higher intensities observed around 770–650 cm⁻¹ are attributed to the mono-substituted benzene [120].

In the coaxial PS/PVDF electrospun fibre, the overall sample showed the peak of PVDF at 532, 614, 840, 877, and 1170, which corresponded to α – phase, β – phase, α – phase and the perturbation of the C=F bond, respectively. In contrast, the peak of PS showed the attribution of

Chapter 5

mono-substituted benzene at 535, 693, and 755. The attribution of bending vibration and vibration of C-H bonds were observed in the range of 770 to 3000 cm⁻¹.

From the FTIR result, small β – phase was observed at the peak 840. The content of β – phase (f_{β}) can be calculated from FTIR spectra using the equation [237],

$$f_{\beta} = \frac{I_{\beta}}{1.26I_{\alpha} + I_{\beta}} \tag{5.1}$$

Where I_{α} represents the intensity of α – phase peak and I_{β} represents the intensity of β – phase peak. The result of β – phase content calculated from FTIR spectra is shown in Table 5.3.

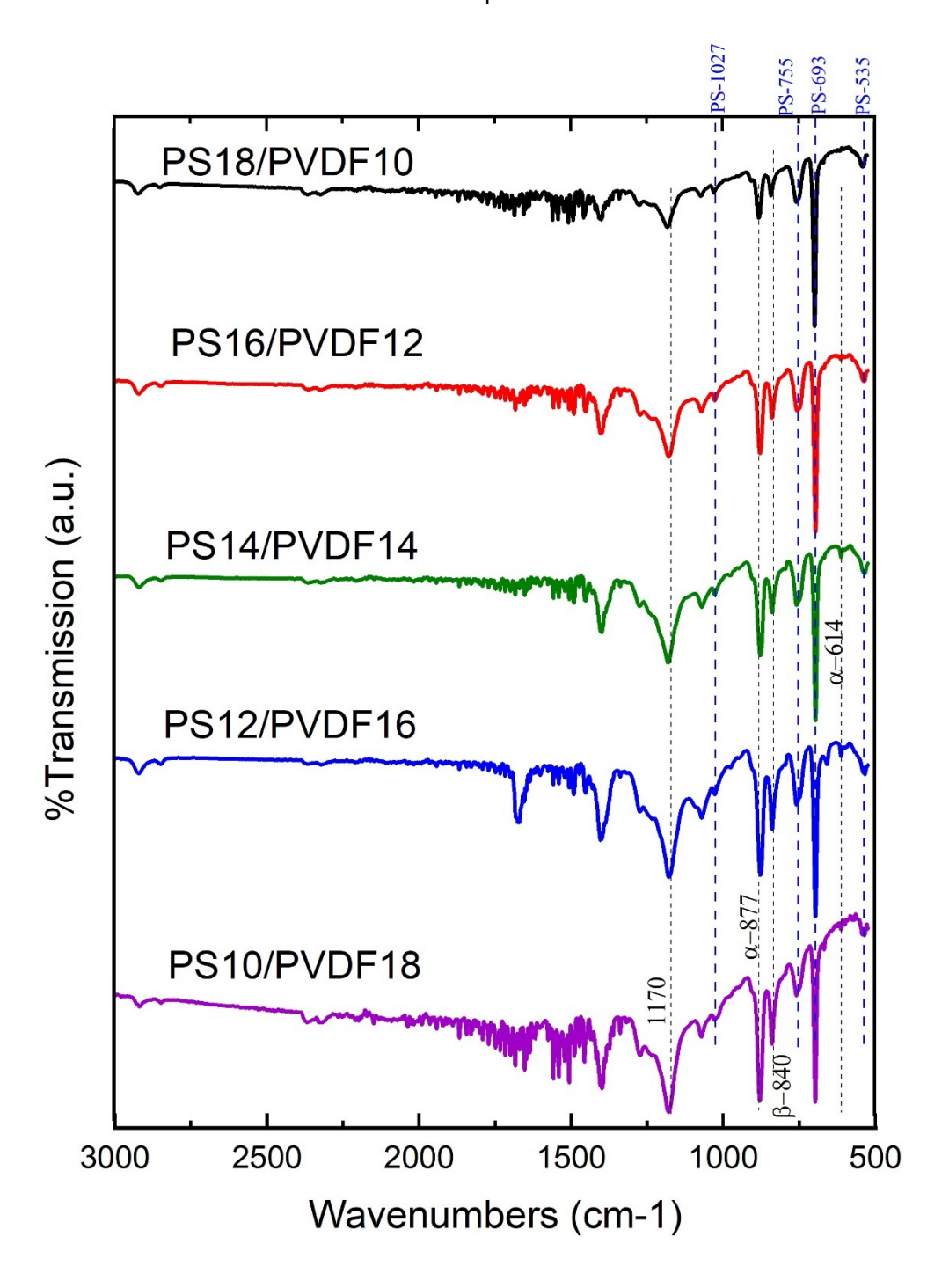


Figure 5. 12 Chemical composition of the Coaxial PS/PVDF fibre.

The X-ray diffraction (XRD) technique was utilised to analyse the phase structure of the coaxial PS/PVDF. The XRD pattern of the coaxial PS/PVDF set is shown in Figure 5.13. The only peak of the piezoelectric β -phase of PVDF was found at 20.6, which indicated a 110/200 plane. The crystallinity of the β -phase decreased when increasing the PS percentage, which was barely observed for the sample PS16/PVDF12 and no peak was found at PS18/PVDF10. The crystallinity index of the β -phase calculated from the XRD peak pattern indicated that the β -phase decreased when increasing the PS, as shown in Table 5.3. Thus, the energy harvesting output

from these two samples is expected to be unrelated to the piezoelectric effect. Meanwhile, the energy harvesting output from PS10/PVDF18, PS12/PVDF16, and PS14/PVDF14 was the mixing of triboelectric and piezoelectric effects.

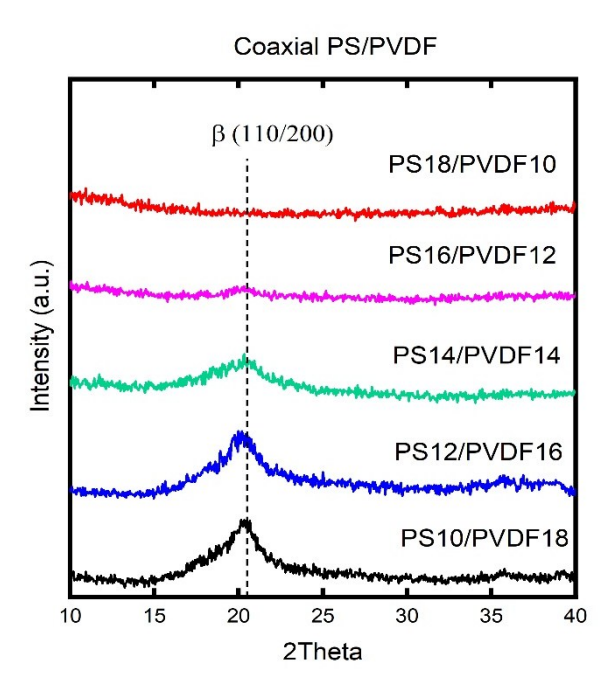


Figure 5. 13 XRD pattern of the coaxial PS/PVDF electrospun fibre at various ratios of polymer solutions.

Table 5. 2 The crystallinity index of β -phase PVDF as calculated from XRD and FTIR spectra.

Sample	Crystallinity index of β-Phase from XRD (%)	β-Phase content calculated from FTIR spectra (%)
PS10/PVDF18	44.476	42.795
PS12/PVDF16	44.408	42.802
PS14/PVDF14	27.041	29.255
PS16/PVDF12	11.754	180677
PS18/PVDF10	0	11.579

5.3.3.2 Electromechanical properties and energy harvesting performance

To explore the optimised concentration, the initial test of the vertical contact separation mode of the triboelectric generator of coaxial PS/PVDF electrospun fibre was performed at 6 Hz using the tapping test setup described in Chapter 3.

The electromechanical testing was initially performed using a tapping test setup described in Chapter 3. Open circuit voltage and short circuit current were collected at 3 – 10 Hz for each polymer concentration, as shown in Figure 5.9 d) and e). The summary of the electromechanical test, including peak-to-peak open circuit voltage, short circuit current, and calculated charge transfer, is shown in Table 5.3.

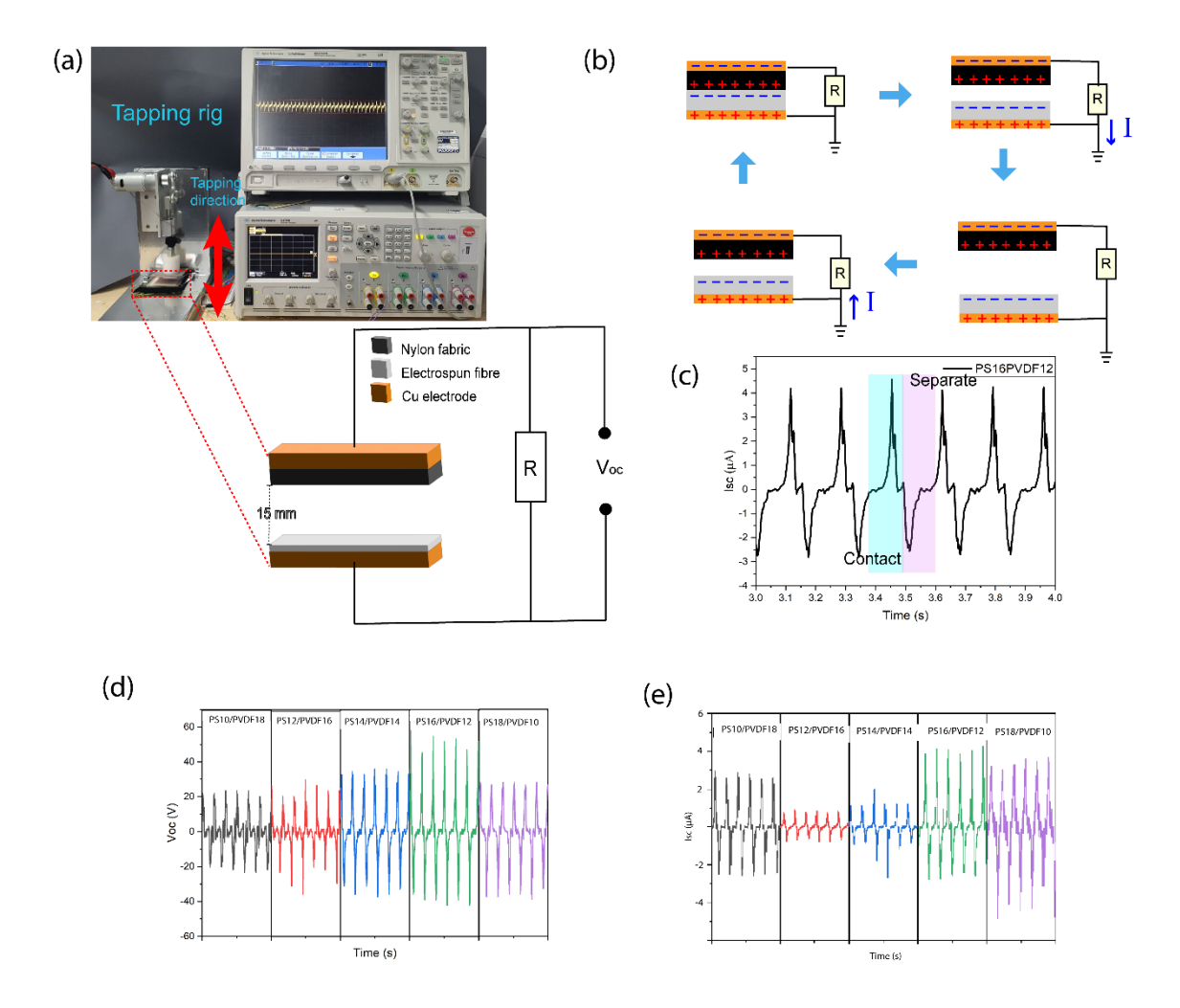


Figure 5. 14 a) Schematic of PS/PVDF triboelectric assembly and testing, b) working principle in contact standing mode, c) corresponding with the measurement of short circuit current, d) open circuit voltage and e) short circuit current of the coaxial PS/PVDF electrospun fibre at various concentrations during the tapping test. The result was collected at the tapping frequency of 6 Hz.

The V_{oc} and I_{sc} of the testing at the different tapping frequencies (3 - 10 Hz) are shown in Figure 5.15 a) and b), whereas Figure 5.15 d) shows the relationship between peak V_{oc} , I_{sc} and tapping frequency. It was found that the increased tapping frequency resulted in an increase of the V_{oc} and I_{sc} . Table 5.4 summarises the V_{oc} and I_{sc} for all testing samples. The effect of frequency can be explained by quicker charge transfer to the equilibrium stage when the tapping test was performed with high frequency.

The open circuit voltage (V_{oc}) output and short circuit current (I_{sc}) of the electrospun fibre prepared from PS16/PVDF12 were tested at different load resistances ($1k\Omega$ -6G Ω), as can be seen in Figure 5.15 c). The highest power and power density were found at 5 M Ω resistance and were found to be 0.125 W and 6.27 W/m², respectively.

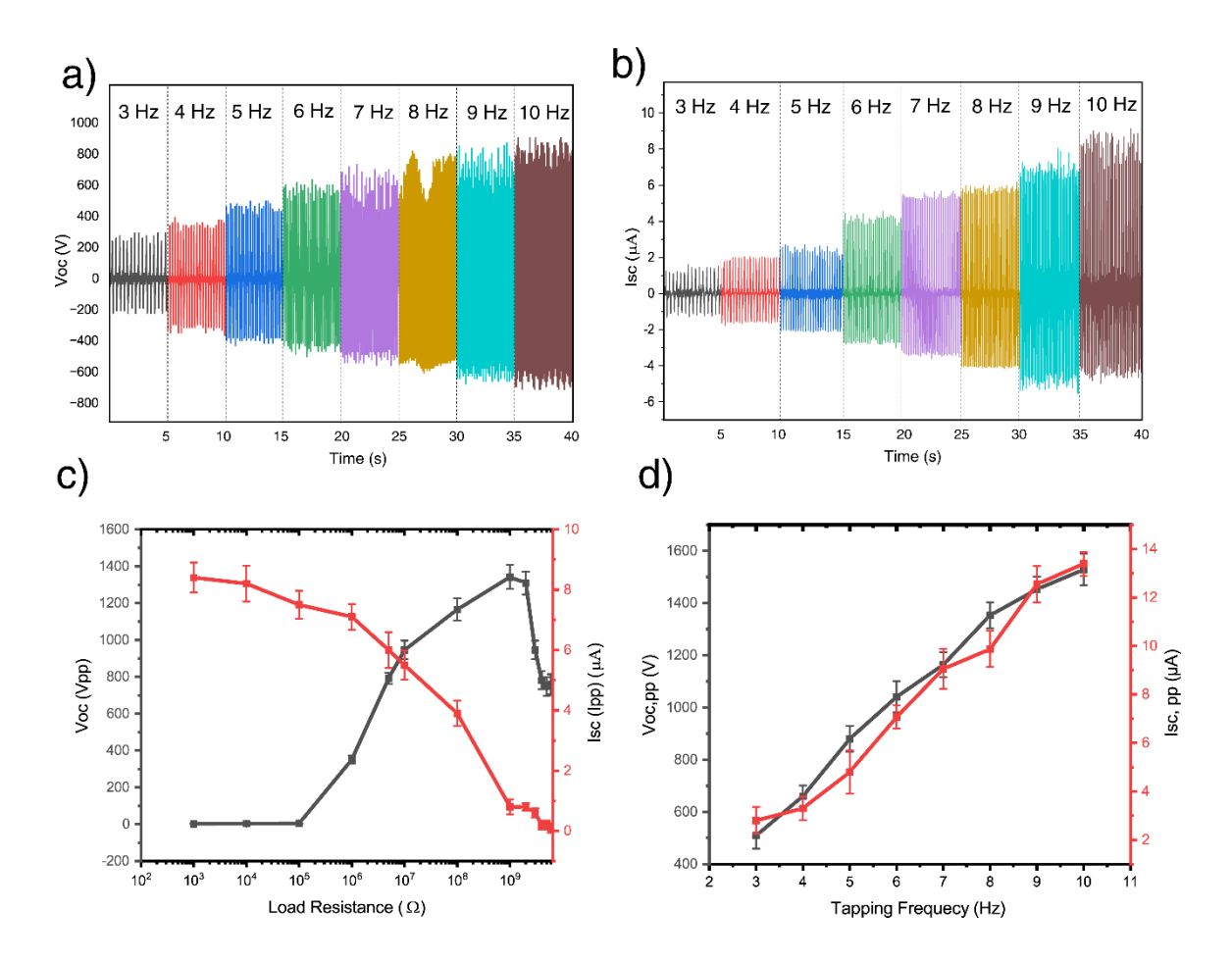


Figure 5. 15 a) open circuit voltage (V_{oc}) and b) short circuit current (I_{sc}) obtained from the bookshaped PS16/PVDF12 assembly c) V_{oc} and I_{sc} v.s. load resistance test, d)) V_{oc} and I_{sc} of the book-shaped PS16/PVDF12 assembly at different tapping frequencies.

Table 5. 3 Summary of the electromechanical characteristics of the samples

Code	Tapping frequency (Hz)	V _{oc} (rms) (V)	Ι _{sc} (rms) (μΑ)	Q _{transfer} (nC)	
				Contact	Separate
PS10/PVDF18	6	176	1.9	304	265
PS12/PVDF16	6	183	0.5	87	93
PS14/PVDF14	6	256	0.7	159	92
PS16/PVDF12	6	366	2.5	514	226
PS18/PVDF10	6	250	3.0	304	532
PS16/PVDF12	3	183	0.9	382	252
	4	231	1.3	404	221
	5	305	1.5	350	227
	6	366	2.5	514	226
	7	414	3.0	548	280
	8	408	3.5	547	298
	9	512	4.3	518	341
	10	554	4.5	597	338

The coaxial PS16/PVDF12 was further tested using the book-shaped PVC template on charging performance with the capacitors 0.22, 0.47, 1, 10, 33, and 100 μ F. The energy stored in the capacitor was calculated from $E=\frac{1}{2}CV^2$, is 8.91, 9.7, 21.1, and 125 μ J for the capacitors 0.22, 0.47, 1, and 10 μ F, respectively. The energy stored in the 10 μ F capacitor was less than that of the 10 μ F capacitor over the same duration due to the impedance mismatch.

The tapping was performed with the book-shaped template to test the ability to charge the capacitor. It was found to fully charge small capacitors at 0.22, 0.47 and $1\mu F$ within 50 seconds.

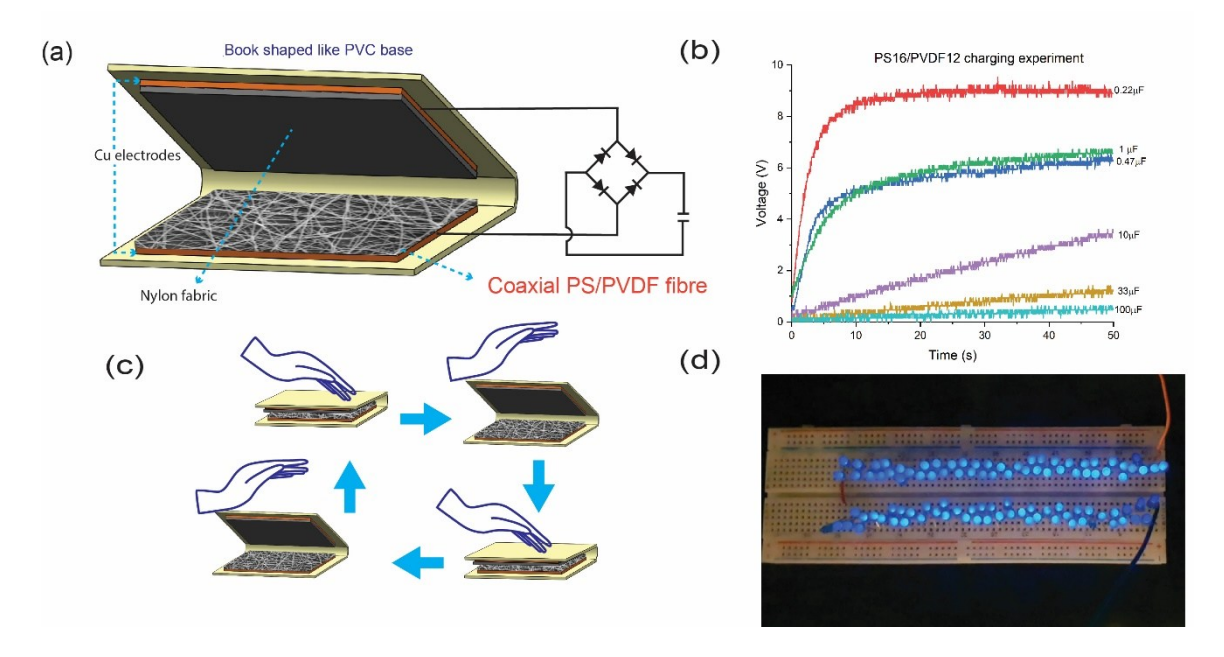


Figure 5. 16 a) Schematic of book-shaped triboelectric energy harvester on charging capacitor testing b) the voltage output over the capacitor 0.22, 0.47, 1, 10, 33 and 100 μ F, respectively, during the charging capacitor testing of the PS16/PVDF12 assembled with the book shaped energy harvester c) the schematic of the hand tapping test during the testing of the 100 LED lights experiment d) the 100 LED lights illuminated via hand tapping of the book shaped like PS16/PVDF12 energy harvester.

5.3.3.3 Surface potential results from the distinguished charges experiment

The physical appearance of the sample PS16/PVDF12 shows a high level of trapped charge density, as seen in Figure 5.17. The PS16/PVDF12 shows promising energy harvesting performance, corresponding to the appearance of high surface charge density. Thus, the electrostatic field meter was used to investigate the electrostatic behaviour of the PS16/PVDF12. The experimental setup is shown in Figure 5.17 b). The PS16/PVDF12 sample was grounded during the measurement.

It should be noted that the limitation of using the static field meter to measure the surface potential of the complex fabric structure depends on the thickness and the position of the trapped charge. Thus, the results obtained from different position measurements vary depending on the thickness and trapped charge. The surface potential distribution curve after the electrospinning process is shown in Figure 5.13. The surface potential obtained from samples PS10/PVDF18, PS12/PVDF16, and PS14/PVDF14 showed similar patterns with negative surface potential with the median of approximately 8-10 kV. In contrast, the sample obtained from PS16/PVDF12 and PS18/PVDF10 showed a high negative surface potential of over 15 kV.

However, the physical appearance of sample PS18/PVDF10 exhibited poor physical quality, so it could not be used in wearable devices.

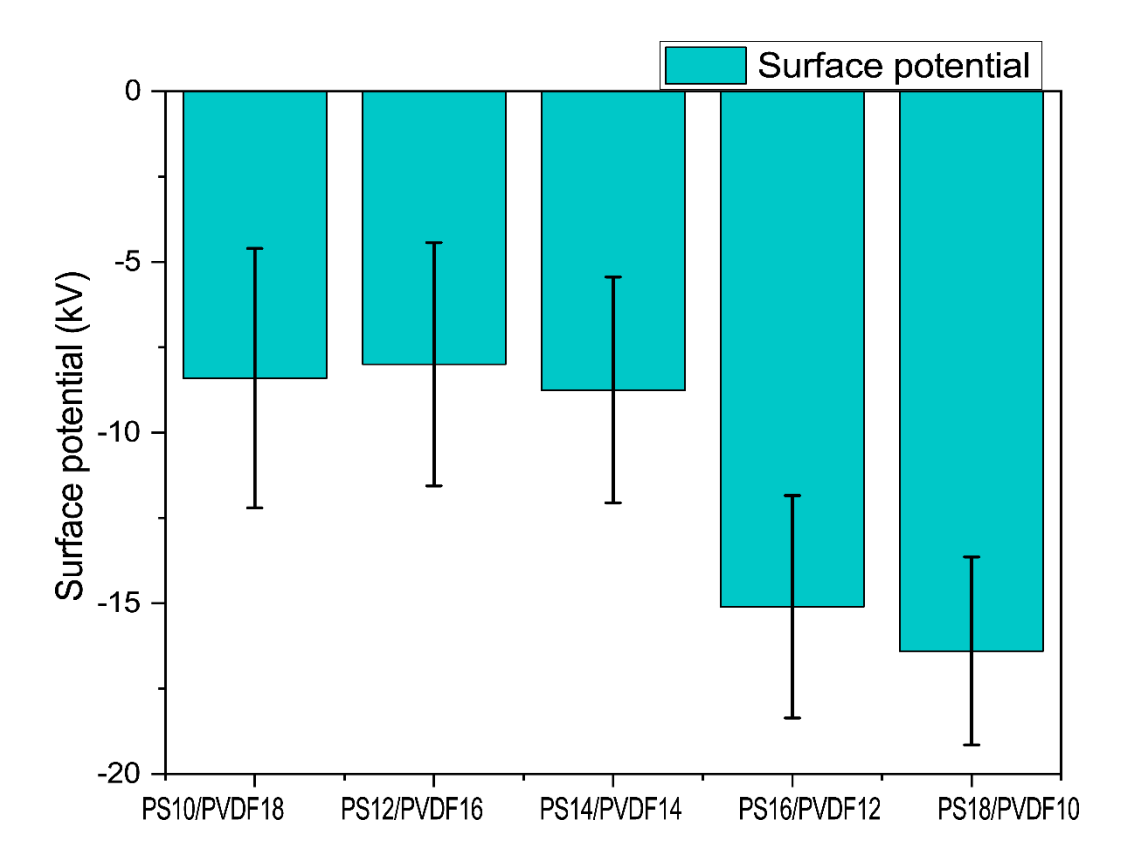


Figure 5. 17 the bar charge presents the surface potential after electrospinning of sample PS10/PVDF18, PS12/PVDF16, PS14/PVDF14, PS16/PVDF12, and PS18/PVDF10

The electrostatic discharge chamber in Figure 5.18 was set up to expose the sample during the surface potential study and to identify the type of surface potential obtained from the electrospun fibre. The electrospun fibre samples of PVDF, PS and PS16/PVDF12 were cut into 5 x 5 cm dimensions. The surface potential was measured before exposing the sample on top of the stainless-steel mesh, which was placed over the IPA reservoir. Each sample was left overnight to ensure the surface potential was 0 kV. The samples were then rubbed with a PET rod to build up the triboelectric charge. The surface potential results were collected to compare the type of surface potential, as shown in Figure 5.15.

The electrospun fibre for PS showed positive surface potential results before discharge and after the triboelectric charge was built up at +2.9 and + 1.1, respectively. In contrast, the electrospun PVDF fibre exhibited negative surface potential before discharge and after rubbing at -2.9 and -0.68, respectively. The surface potential obtained from this experiment confirmed that the PS16/PVDF12 showed a negative surface potential approximately 3 and 9 times higher

than the PVDF electrospun fibre before discharge and after rubbing, respectively. The core-shell structure model could support the excellent surface potential obtained from this technique.

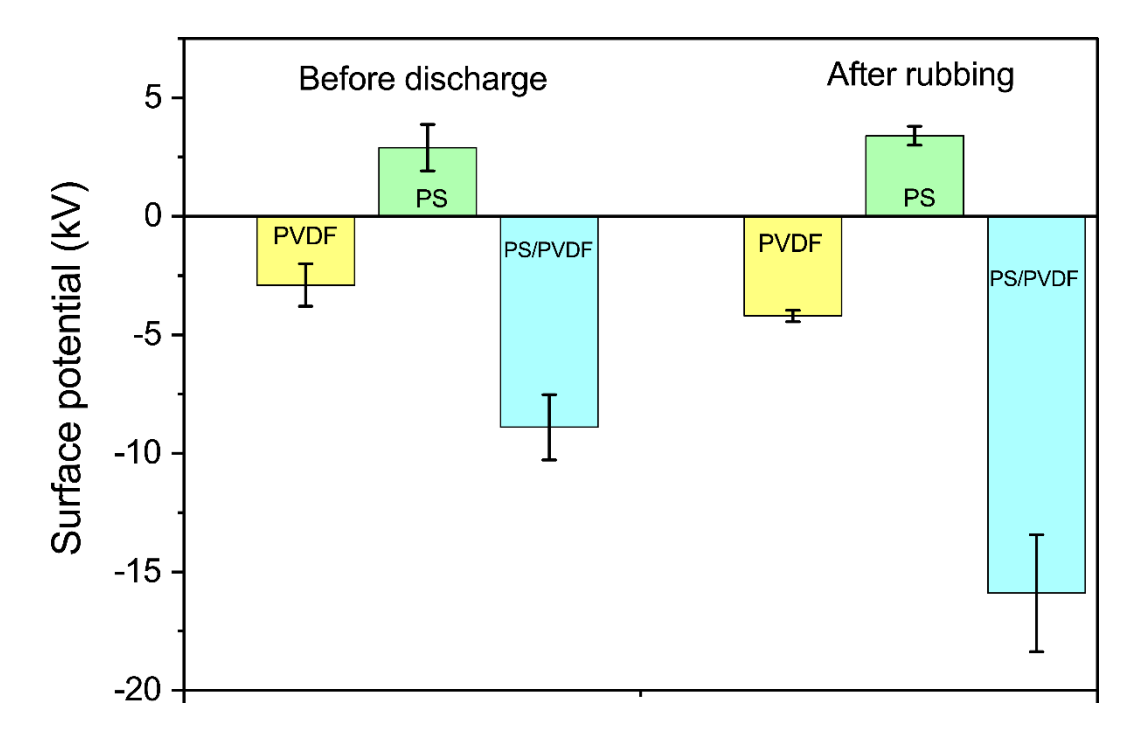


Figure 5. 18 The bar chart presents the surface potential before discharge in the discharge chamber and after the rubbing test to build up a triboelectric charge of the electrospun PVDF, PS and coaxial PS/PVDF, respectively.

5.3.4 Conclusion of the energy harvesting performance from the core-shell structure PS/PVDF electrospun fibre

The core-shell structure of PS/PVDF electrospun fibre was successfully fabricated using the precipitation of an immiscible solution in a single-nozzle electrospinning technique. The study from FTIR and TEM indicated that PS was formed as a core layer, and PVDF formed as a shell layer. The energy harvesting performance was demonstrated in terms of V_{oc} and I_{sc} under the testing of vertical contact separated triboelectric generator mode. The tapping was performed using the book-shaped template to test the ability of charging capacitors. The highest power and power density were found at 5 M Ω resistance and were found to be 0.125 W and 6.27 W/m², respectively. Small capacitors of 0.22, 0.47 and 1 μ F could be fully charged within 50 seconds. The energy stored was 8.91, 9.7, 21.1, and 125 μ J for the capacitors 0.22, 0.47, 1, and 10 μ F, respectively.

The surface potential measurement after electrospinning and discharge using the discharge cabinet experiment found that the coaxial electrospun fibre was capable of inducing the electrostatic charge as a negative material in the triboelectric series.

5.4 Conclusion

This chapter draws on the innovation of using the complex structure of electrospun fibre. It explores the energy-harvesting capabilities of hollow and coaxial electrospun fibres, highlighting their promise as effective materials for energy harvesting in wearable technology. The investigation presented innovative fabrication methods, featuring a one-step coaxial electrospinning technique for hollow PVDF fibres and a single-nozzle strategy for coaxial PS/PVDF fibres.

The hollow PVDF fibres demonstrated superior piezoelectric performance relative to solid fibres, reaching a maximum power density of 2.18 mW/m^2 and a piezoelectric coefficient (d_{33}) of 28.7 pC/N. The advancements highlight the efficiency of the hollow fibre configuration in boosting energy harvesting potential for ferroelectret uses. However, from the results of piezoelectric coefficient testing, the improvement of voltage output might not be concluded that it is based on the ferroelectret effect.

The coaxial PS/PVDF fibres exhibited impressive capabilities in triboelectric energy harvesting, reaching a power density of 6.27 W/m². A book-shaped energy harvester model was constructed with these fibres and effectively charged capacitors and powered 100 LEDs, demonstrating its practicality and potential for scalability in real-world applications.

The results validate the effectiveness of hollow and coaxial fibre structures for energy harvesting, especially in the context of wearable and flexible devices. Future investigations may explore enhanced optimisation of material combinations, fibre geometries, and their integration into more intricate wearable systems. This chapter enhances the comprehension of electrospun fibre structures and their utilisation in sustainable energy harvesting technologies.

Chapter 6 Conclusion and Future Works

6.1 Conclusion

This thesis demonstrates the novel potential of electrospun fibres in energy harvesting applications, especially in wearable technologies. The study achieves significant improvements in the performance and usability of PTFE/PVDF composites, hollow PVDF, and coaxial PS/PVDF fibres by the utilisation of new fabrication procedures. Significant discoveries include increased power densities, feasible integration into wearable devices, and improved material characteristics. The results emphasise the feasibility of electrospun fibres as a sustainable energy harvesting alternative, providing solutions to issues related to device miniaturisation, flexibility, and biocompatibility. These contributions offer a basis for continued innovation in smart textiles and self-powered systems, promoting a more sustainable and energy-efficient future when combined with biocompatible electrodes.

Chapter 2 reviews the literature on energy harvesting mechanisms, the role of polymers in mechanical energy harvesting, and the advancements in electrospinning techniques for fabricating energy harvesting materials. It provides a theoretical foundation by discussing piezoelectric, ferroelectret, and triboelectric effects, highlighting their potential for wearable technology applications. The chapter identifies the advantages of polymer-based energy harvesters, such as flexibility, lightweight properties, and scalability, while noting their relatively lower performance compared to ceramic counterparts. It emphasises the significance of electrospinning in creating nanostructured fibres with high surface areas, which are important for enhancing charge transfer and energy conversion efficiency in triboelectric and piezoelectric applications. A research gap was identified that showed the need for innovative material combinations and fibre structures, such as composites, hollow fibres, and coaxial fibres, to improve energy harvesting performance. This provides the basis for the experimental investigations in subsequent chapters, which aim to address these gaps. Overall, this chapter establishes the context and necessity for the research, providing a basis for developing advanced electrospun fibres as efficient, scalable, and practical energy-harvesting solutions for wearable devices.

Chapter 3 outlines the materials, experimental processes, and methods used to fabricate and characterise electrospun fibres for energy harvesting applications. The chapter establishes the foundation for the research by detailing the preparation of composite, hollow, and coaxial fibres, as well as the techniques employed for their characterisation.

The successful setup of the electrospinning apparatus and the optimisation of parameters for fibre fabrication are critical achievements. Advanced characterisation techniques, including SEM, TEM, FTIR, and XRD, provided comprehensive insights into the morphology, structure, and material properties of the fibres. Additionally, electromechanical testing methodologies were effectively designed to evaluate the energy-harvesting performance of the fabricated fibres. The experimental framework developed in this chapter ensures reproducibility and accuracy in fabricating and analysing electrospun fibres. It sets the stage for subsequent chapters by providing the necessary tools and methodologies to explore the energy harvesting capabilities of the various fibre structures. The rigorous approach to material preparation and testing represents a significant step toward advancing electrospun fibre technology for wearable and flexible energy harvesting devices.

Chapter 4 presents the energy harvesting performance of PTFE/PVDF composite electrospun fibres. The study successfully demonstrates the fabrication of composite fibres using a onestep electrospinning process. By optimising the concentration of PTFE particles within the PVDF matrix, the material's triboelectric performance was significantly enhanced. The results reveal that the composite with 20% PTFE achieved superior energy harvesting outputs, with voltage and current increases of 4 and 7 times, respectively, compared to pure PVDF fibres.

The triboelectric energy harvester using these composite fibres achieved a maximum power density of 348.5 mW/m² and demonstrated its applicability in practical settings such as shoe insoles and book-shaped assemblies. The materials also exhibited desirable properties for wearable applications, including flexibility, breathability, and lightweight characteristics. While the findings are promising, further optimisation of electrospinning parameters and fibre assembly design could enhance energy harvesting efficiency and expand potential applications. This chapter establishes a foundation for developing high-performance, flexible, and sustainable energy harvesting devices using composite electrospun fibres.

Chapter 5 investigates the energy-harvesting performance of hollow and coaxial electrospun fibres, demonstrating their potential as efficient energy-harvesting materials for wearable technology. The study introduced novel fabrication techniques, including a one-step coaxial electrospinning method for hollow PVDF fibres and a single-nozzle approach for coaxial PS/PVDF fibres.

The hollow PVDF fibres exhibited enhanced piezoelectric performance compared to solid fibres, achieving a maximum power density of 2.18 mW/m^2 and a piezoelectric coefficient (d_{33}) of 28.7 pC/N. However, the d_{33} results do not align with the working principle based on ferroelectret. The observed enhancement in voltage output during the initial test suggests a potential

contribution from triboelectric charge, attributed to the increased surface area provided by the hollow structure.

The coaxial PS/PVDF fibres demonstrated remarkable triboelectric energy harvesting performance, achieving a power density of 6.27 W/m². The book-shaped energy harvester assembled using these fibres efficiently charged capacitors and illuminated 100 LEDs, showcasing its practicality and scalability for real-world applications.

Overall, the findings show the energy harvesting ability of composite PTFE/PVDF, hollow PVDF and coaxial PS/PVDF fibre structures. They can be particularly used in wearable and flexible devices when integrated with wearable elements such as fabric electrodes and conductive yarn.

6.2 Future works

This research was conducted during the pandemic. Consequently, there exists an insufficiency in the evaluation of the fundamental apparatus necessary to explore the various critical elements of the manufactured materials. The future work could be carried out in 2 parts: further investigation of the energy harvesting performance and fabrication for wearable devices.

6.2.1 Further investigation of the energy harvesting performance

The analysis of the composite PTFE/PVDF, hollow PVDF, and coaxial PS/PVDF fibre structure was completed without an examination of surface roughness, a critical element in the energy harvesting capabilities of triboelectric devices. The investigation of the surface roughness could be done by using the Atomic Force Microscope (AFM).

The findings presented in Chapter 5 indicate remarkable surface potential characteristics for the coaxial PS/PVDF fibre. Nonetheless, the electrostatic field meter employed in this study exhibits certain limitations regarding the precision of its outcomes. This could be investigated using the Kelvin Probe mode in AFM, discussed in Chapter 3.

For material surface improvement, using PTFE particles as an additive material in other electrospinning polymers such as PS, PVP, PVA, or coaxial PS/PVDF should be further studied in electromechanical properties.

The enhanced electrical output achieved by the fibres containing PTFE justifies the need for additional research in practical energy harvesting applications. This study did not quantify the impact of PTFE particles on the surface roughness of the fibres. The effect of surface roughness

on the performance of the TENG will be investigated in future research utilising an Atomic Force Microscope (AFM).

6.2.2 Further work on wearable devices

The composite PTFE/PVDF, hollow structure PVDF, and coaxial PS/PVDF electrospun fibres can be used as an alternative energy harvesting part in wearable devices when assembled with fabric electrodes. Therefore, from a materials perspective, further exploration of electrospinning parameters such as voltage polarity and flow rate could be conducted to adjust the surface chemistry and enhance the proportion of polar β -phase in PVDF fibres, thereby optimising the triboelectric output based on the result from Szewczyk et al. (2020) [90].

For wearable devices, the fabric electrode could be integrated with the composite PTFE/PVDF, hollow structure PVDF, and coaxial PS/PVDF electrospun fibres to test the wearable devices. In a further study, the single PTFE/PVDF electrospun fibre could be used in the harvesting energy application in various assemblies and implemented with wearable devices.

The coaxial PS/PVDF fibre could be used for an electret air filtration application based on Lue et al. [167]. The particle filtration could be tested for the electret filtration performance.

Appendix A Publications

Smart Materials and Structures



PAPER • OPEN ACCESS

The investigation of the energy harvesting performance using electrospun PTFE/PVDF based on a triboelectric assembly

To cite this article: Pattarinee White et al 2024 Smart Mater. Struct. 33 075010

View the article online for updates and enhancements.

You may also like

- Lithium Dendrite Growth Suppression in Anode-Free Lithium Battery Using Bifunctional Electrospun Gel Polymer Electrolyte Membrane Yosef Nikodimos, Wel-Nien Su and Bing-June Hawane
- Enhanced ferro-actuator with a porositycontrolled membrane using the solved process and the HF etching method
 Kilsu Kim, Seong Young Ko, Jong-Oh Park et al.
- Enhanced Electrochemical Performance of NCM811 Cathodes with Functionalized PVDF Graft Copolymer Binders Tong Llu, Rohan Parekh, Plott Mocny et al.



This content was downloaded from IP address 152.78.0.24 on 01/01/2025 at 07:11

IOP Publishing

Smart Materials and Structures

https://doi.org/10.1088/1361-665X/ad50

Smart Mater. Struct. 33 (2024) 075010 (12pp)

The investigation of the energy harvesting performance using electrospun PTFE/PVDF based on a triboelectric assembly

Pattarinee White 1.2.* , Piyapong Pankaew , Dmitry Bavykin , M Moshrefi-Torbati and Stephen Beeby 6

E-mail: p.white@soton.ac.uk, piyapong.p@rmutp.ac.th, d.bavykin@soton.ac.uk, m.m.torbati@soton.ac.uk and spb@ecs.soton.ac.uk

Received 1 April 2024, revised 3 May 2024 Accepted for publication 24 May 2024 Published 6 June 2024



Abstract

This work presents an investigation into the energy harvesting performance of a combination of polytetrafluoroethylene (PTFE) and polyvinylidene fluoride (PVDF) materials prepared using a one-step electrospinning technique. Before electrospinning, different percentages of the 1 micron PTFE powder were added to a PVDF precursor. The surface morphology of the electrospun PTFE/PVDF fibre was investigated using a scanning electron microscope and tunnelling electron microscope. The structure was investigated using Fourier-transform infrared spectroscopy and x-ray diffraction analysis (XRD). A highly porous structure was observed with a mix of the α - and β -phase PVDF. The amount of β -phase was found to reduce when increasing the percentage of PTFE. The maximum amount of PTFE that could be added and still be successfully electrospun was 20%. This percentage showed the highest energy harvesting performance of the different PTFE/PVDF combinations. Electrospun fibres with different percentages of PTFE were deployed in a triboelectric energy harvester operating in the contact separation mode and the open circuit voltage and short circuit current were obtained at frequencies of 4–9 Hz. The 20% PTFE fibre showed 4 (51–202 V) and 7 times (1.3–9.04 μ A) the voltage and current output respectively when compared with the 100% PVDF fibre. The $V_{\rm oc}$ and I_{sc} were measured for different load resistances from 1 k Ω to 6 G Ω and achieved a maximum power density of 348.5 mW m⁻² with a 10 MΩ resistance. The energy stored in capacitors 0.1, 0.47, 1, and 10 μ F from a book shaped PTFE/PVDF energy harvester were 1.0, 16.7, 41.2 and 136.8 μ J, respectively. The electrospun fibre is compatible with wearable and e-textile applications as it is breathable and flexible. The electrospun PTFE/PVDF was assembled into shoe insoles to demonstrate energy harvesting performance in a practical application.

Original content from this work may be used under the terms of the Creative Commons Attribution 4.0 licence. Any further distribution of this work must maintain attribution to the author(s) and the title of the work, journal citation and DOI.

© 2024 The Author(s). Published by IOP Publishing Ltd

¹ Centre for Flexible Electronics and E-Textiles, University of Southampton, Southampton, United Kingdom

² Division of Physics, Rajamangala University of Technology Krungthep, Bangkok, Thailand

³ Division of Industrial Materials Science, Rajamangala University of Technology Phra Nakhon, Bangkok, Thailand

⁴ Energy Technology Group, University of Southampton, Southampton, United Kingdom

Mechatronics Research Group, University of Southampton, Southampton, United Kingdom

Author to whom any correspondence should be addressed.

Smart Mater. Struct. 33 (2024) 075010 P White et al.

Supplementary material for this article is available online

Keywords: textile triboelectric nanogenerator, wearable devices, electrospinning, PTFE, PVDF

1. Introduction

From 2023 to 2030, the market for wearable smart technology is predicted to grow by 14.6% [1]. A rapidly developing platform for wearable technology is electronic textiles (e-textiles or smart fabrics). E-textile manufacturing technologies enable wearables to be integrated within garments providing a comfortable and familiar platform. The use of conventional rigid batteries is incompatible with such platforms, and these also need to be regularly charged and replaced and are environmentally harmful [2, 3]. Therefore alternative textile compatible energy harvesting and self-powered sensing technologies powered by ambient energy sources are of considerable interest [4]. The ability to transform human motion-based mechanical energy into electrical energy has been demonstrated utilising piezoelectric materials [5-7] electromagnetic devices [8], electrostatic mechanisms (via the electret/ferroelectret [9, 10] and triboelectric effects [11-13]), and electroactive polymers [14-16] transduction mechanisms.

The triboelectric effect, whereby electrical energy is generated from the triboelectrification of materials during cyclical physical contact [17], has been exploited in many example energy harvesting devices [18]. The first a triboelectric nanogenerator (TENG) demonstrated the potential of electrostatic charge transfer in energy harvesting technologies [19]. Textiles are attractive materials for realising TENGs due to their affinity to gain or lose ions during contact and many examples have been demonstrated [20–22]. Novel textile TENGs have also been used in self-powered biomonitoring applications, for example, in wearable cardiovascular and respiratory monitoring [23].

The approaches to enhance the contact-electrification within TENGs and therefore increase the electrical output typically involve three basic methods: modifying surface morphology, modifying surface chemistry, and utilising ferroelectric materials [24]. There are various mechanisms by which the use or addition of ferroelectric materials can improve triboelectrification. Early theories based upon the change in work function of the ferroelectric polymer which enhances electron transfer [25] have been superseded by research that demonstrates it is due to the piezoelectric effect whereby charge is generated within the material during contact that increase electrostatic induction [26]. Polyvinylidene fluoride (PVDF) is one such ferroelectric polymer commonly used in TENGs [27-30]. Electrospun PVDF fibres have demonstrated effective energy conversion when used as the negative triboelectric material [31-33] and the electrical output of PVDF fibres has been further increased by the addition of other fibrous materials within the generator. For example, the combination of PVDF and polyamide 6 fibres produces a 25% increase in peak voltage compared with PVDF fibres alone [34]. Electrospun fibres are inherently compatible with textiles being virtually identical in nature to the fibres used in yarns or non-woven fabrics. Electrospun fibre mats possess the desirable characteristics associated with textiles of breathability, flexibility and feel. Electrospun functional fibres have been used to create smart textiles with advanced functionality. For example, electrospun PVDF nanofibre membranes have been evaluated in face masks and shown to significantly improve the filtration efficiency [35].

Polytetrafluoroethylene (PTFE) has amongst the strongest electron affinity amongst the triboelectric materials placing it at the negative end of the triboelectric series [34, 36]. It is also an excellent electret material being a dielectric material able to quasi-permanently trap surface charge typically generated by ion irradiation [37]. Thus, many TENGs have been demonstrated with PTFE as a negative material [13, 38, 39]. Typically, the PTFE is obtained from commercial sources and the energy harvesting performance is influenced by the manufacturing process. Electrospinning techniques can be used to improve the triboelectric properties by modifying the surface morphology and increasing the surface area of the material. Additionally, during the electrospinning process, a high voltage is applied to the polymer solution which results in a high volume of charged particles being introduced into the solution, which are subsequently trapped within the electrospun fibre after solidification. However, fabricating PTFE using electrospinning is challenging due to its extremely stable chemical and thermal properties making it extremely difficult to obtain a solution suitable for electrospinning without chemical modification [40]. Zhao et al investigated energy harvesting from electrospun PTFE fibres by utilising polyethene oxide (PEO) water solution as a carrier [41]. Here the precursor polymer solution was employed to create a PTFE/PEO structure using emulsion electrospinning. A sintering step at over 350 °C is required to remove the carrier leaving PTFE

This paper presents an evaluation of the energy harvesting performance of an electrospun PTFE/PVDF composite TENG. This combination exploits the extremely strong negative affinity of the PTFE with the piezoelectric charge generation properties of the PVDF ferroelectric polymer. The work builds upon a preliminary study [42] that investigated composite materials up to 4% PTFE. Here the systematic evaluation of the percentage of PTFE in the PVDF fibre is presented and the PTFE 20%/PVDF 80% composite fibre achieved a 4 times increase in open circuit voltage (51–202 V) and a 7 times increase in short circuit current (1.3–9.04 μ A) when compared with the 100% PVDF fibre. The paper also presents the application of the electrospun PTFE/PVDF fibre mat combined with a nylon fabric in a shoe insole where the composite material again produces a significant increase in

the power output when compared with a pure PVDF fibre

2. Experimental section

2.1. Electrospun fibre preparation

The fabrication of the electrospun PTFE/PVDF fibres is illustrated in figure 1. PVDF (Sigma Aldrich, Dorset, UK, Mw = 534 000) and PTFE (Sigma Aldrich, 1 mm mean diameter particles) powders were blended together in the following ratios: PTFE1% + PVDF 19%, PTFE2% + PVDF 18%, PTFE3% + PVDF 17%, PTFE4% + PVDF 16%, PTFE5% + PVDF 15%, PTFE6% + PVDF 14%, and PTFE7% + PVDF 13%. Each PTFE/PVDF powder blend was then combined with a solvent solution of N-Dimethylformamide (DMF, Sigma Aldrich, Dorset, UK, 99.8%) and acetone (Fisher Scientific, Waltham, MA, USA, 99.6%) mixed in a 7:3 ratio. The solvent solution was stirred at 60 °C using a magnetic hotplate stirrer for a total of six hours before adding the powder blend at a ratio of 20% powder 80% solvent by weight. To prevent the PTFE particles from agglomerating, the solution was sonicated for six hours prior to mixing with the PVDF and DMF: acetone solvent [43].

The PTFE/PVDF solution was put in a 3 ml syringe with a blunt tip (21 G) needle and attached to the syringe pump of the electrospinning apparatus (EC-DIC, IME Technologies, Netherlands). For each concentration, the distance between the tip and the substrate, the applied voltage, the flow rate, and the rotational speed of the drum remained constant at 22 cm, 25 kV, 2 ml hr⁻¹, and 150 rpm, respectively. The PTFE/PVDF fibre was collected as a nonwoven fibre mat and assembled into a triboelectric energy harvester without any additional processing.

2.2. Fibre characterisation

After electrospinning, the solvent was fully evaporated, and it can be assumed that the percentages of PTFE in the solid fibre are as stated in table 2. The morphology and structure of the electrospun PTFE/PVDF fibres were investigated through the scanning electron microscope (SEM) (Phenom ProX, Thermo Fisher Scientific) and tunnelling electron microscope (TEM) (HT7700, Hitachi). The chemical composition and structure of the material were analysed using a Fourier transform infrared (FTIR) spectrometer (Nicolet iS5, Thermo Fisher Scientific), and x-ray diffraction analysis (XRD) (D8 Advance, Bruker) was used to analyse the crystalline phase of the PTFE/PVDF electrospun fibre.

2.3. Electromechanical characterisation

The PTFE/PVDF electrospun fibre mat was cut down to 4 cm × 5 cm and then bonded to Cu tape, which works as an electrode. The copper electrodes are fabricated from a single-sided adhesive copper tape, and the fibres are simply attached to the adhesive layer. The other side of the triboelectric test set up used nylon fabric as the triboelectric donor material. This was similarly bonded to a Cu electrode, and the materials were tested with a separation distance of 1.5 cm. A controlled pressure of approximately 0.5 N cm⁻² (measured using force sensor FSR402) applied at different frequencies (3–9 Hz) using the cyclical compression test system ('tapping rig') shown in figure 2(a). This tested the materials in the vertical contact separation mode (figure 2(b)) resulting in voltage and current pulses as shown in figure 2(c).

As illustrated in figure 8(a), the 4 cm × 5 cm PDVF/PTFE electrospun fibre mat was also assembled alongside the nylon fabric into a folded-over book-shaped triboelectric harvester using a PVC substrate. The book shaped assembly was used to demonstrate the illumination of an LED array and test the ability to charge a capacitor.

The open circuit voltage (V_{oc}) output of the energy harvester was measured using an oscilloscope (MSO7012B, Agilent Technologies) with the 10 M Ω probe resistance. During open circuit voltage measurement, the oscilloscope was connected to the 1 G Ω as a voltage divider circuit due to the large internal impedance of the TENG. The DC power analyser (N6705B, Agilent Technologies) was used to measure the short circuit current (I_{sc}).

3. Results and discussion

3.1. Morphological analysis

Figure 3 show the surface morphologies observed in the SEM of the PTFE/PVDF electrospun fibre at the various PTFE and PVDF ratios. The surface of the 100% PVDF fibre (figure 3(a)) is smooth without any visible bead-like structures. This is the base fibre material used as a benchmark in the study of the effects of the additive PTFE powder. The addition of the PTFE powder to the base PVDF material can be seen to cause increasing fibre surface roughness with increasing amounts of PTFE microparticles. The PTFE/PVDF solution enabled successful electrospinning of the porous fibre mat up to a concentration of 16% PVDF with 4% of the PTFE particles (figure 3(e)). Beyond this, when more than 5% of PTFE was added to the solution, the electrospinning process could not consistently produce PTFE/PVDF fibres producing a combination of fibrous and film like deposits shown in figures 3(f)-(h). This was due to the decreased conductivity of the PTFE/PVDF solution which affects the behaviour of the electrospinning process. The PTFE4/PVDF16 solution yield the 20/80 PTFE/PVDF fibre which were investigated in the TEM, the sample code of the PTFE/PVDF fibre can be found in the table 2. The TEM images in figures 4(a) and (b) indicate the location of PTFE particles in the PVDF fibre demonstrating these have been successfully blended in the starting solution and distributed across the PVDF matrix. The PTFE particle size embedded in PVDF strain was found to be less than 1 µm due to the sonication process before electrospinning preparation.

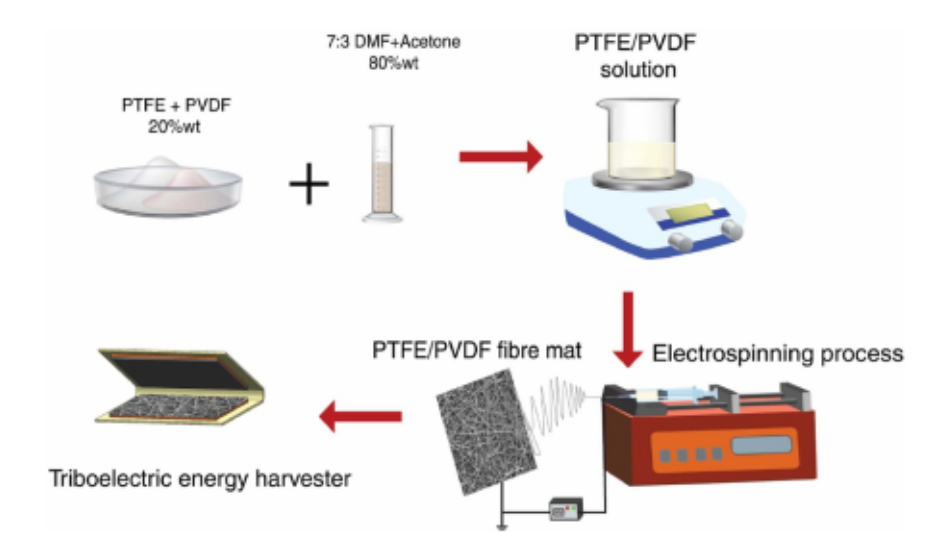


Figure 1. The flow chart describes the PTFE/PVDF electrospun fibre preparation.

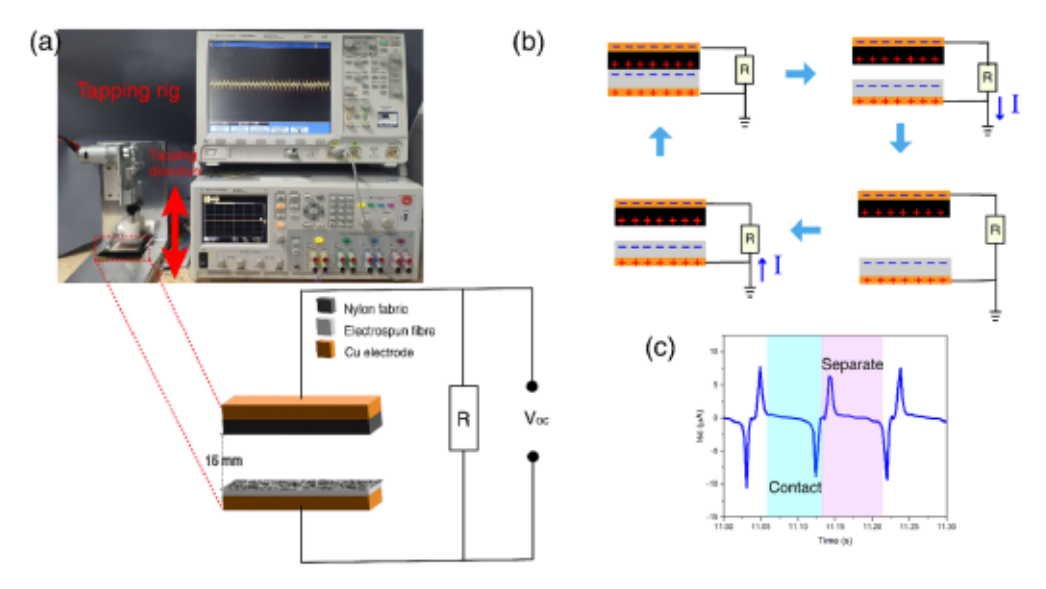


Figure 2. (a) Schematic of PTFE/PVDF triboelectric assembly and photograph of the tapping test rig; (b) working principle in the contact separation mode; (c) example plot of the short circuit current.

3.2. Structural analysis

The FTIR measured chemical composition of PTFE/PVDF electrospun fibres are shown in figure 5(a) alongside the results for the PDVF and PTFE powders. All samples of the PTFE/PVDF electrospun fibres exhibit the characteristic peaks at 840 and 877, representing the β - and C–H wagging in the α -phase of PVDF, respectively. When compared with the results obtained from PVDF powder, which shows peaks at 614, 764, 796, 877, 976, and 1170, it is evident the crystalline piezoelectric β -phase has been effectively induced by

the electrospinning process [44, 45]. It is well known that the electrospinning process encourages the β -phase of PVDF due to the strong electric field induced in the polymer solution during whipping of the fibres [44, 46]. Also, the incorporation of PTFE into the electrospun PVDF can be observed at the peak 1170, representing the perturbation of the C=F bond of PTFE and PVDF, as both consist of carbon and fluorine atoms. The characteristics of the PTFE powder spectrum is represented in the peaks 1201 and 1150, which correspond to the asymmetrical and symmetrical CF₂-stretching [47], whereas peaks 642 and 630 represent the C-F deformation [48, 49].

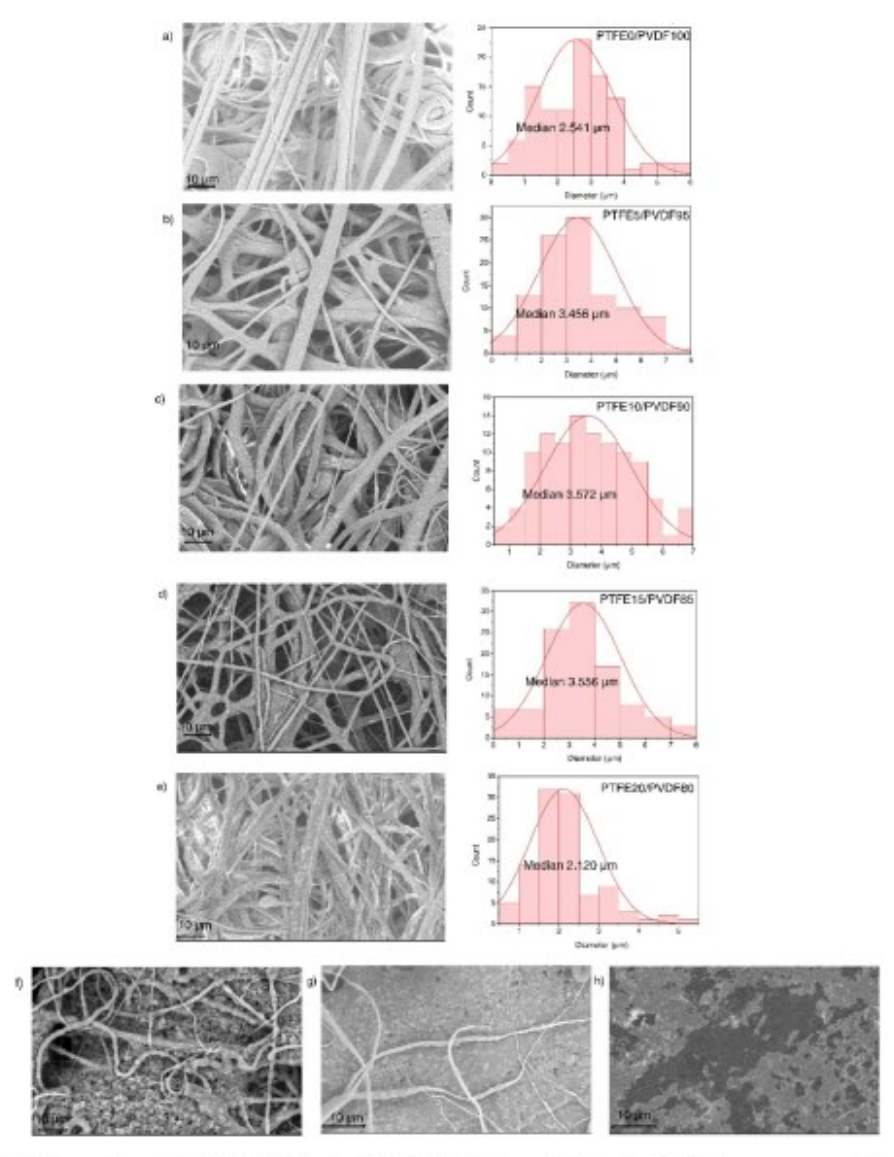


Figure 3. The SEM images (operated at 10 kV) of the single PTFE/PVDF fibre with fibre size distribution curve prepared by different PTFE/PVDF ratios (a) PTFE0/PVDF100, (b) PTFE5/PVDF95, (c) PTFE10/PVDF90, (d) PTFE15/PVDF85, (e) PTFE20/PVDF80, (f) PTFE25/PVDF75, (g) PTFE30/PVDF70 and (h) PTFE35/PVDF65.

The XRD pattern of the PTFE/PVDF electrospun fibre at different percentages of PTFE are shown in figure 5(b). The pure PVDF electrospun fibre exhibits only one strong peak at 20.6° (110/200), representing the β -phase of the PVDF. After introducing PTFE in the PVDF electrospun fibre, the α -phase at a peak of 18.4° (020) occurred and was related to the amount of PTFE in the PVDF fibre. The intensity of the α -phase at a peak of 18.4° (020) becomes stronger as the percentage of PTFE increases. Table 1 shows the crystallinity index (CI) obtained from the XRD results which is calculated by

$$%Crystallinity = \frac{S_c}{S_t}$$
 (1)

where S_c represents the area under the curve at the peak crystalline alpha and beta phases and S_t represent the total area under the plot [50].

This interesting behaviour can be explained by the electric field during the electrospinning process. The β -phase PVDF can be induced by a strong electric field in the electrospinning process. When the PTFE particles are added to the PVDF

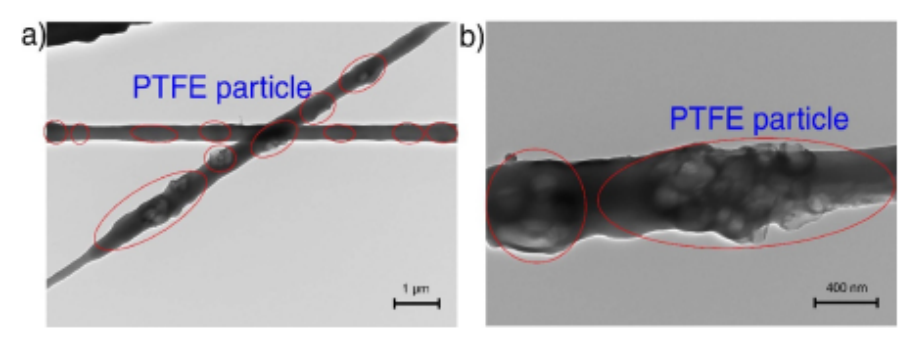


Figure 4. TEM images were measured at acceleration voltage 100 kV, filament voltage 25 kV for a single PTFE20/PVDF80 fibre which was coated on the mesh copper grids at magnification (a) 7000x (b) 25000x.

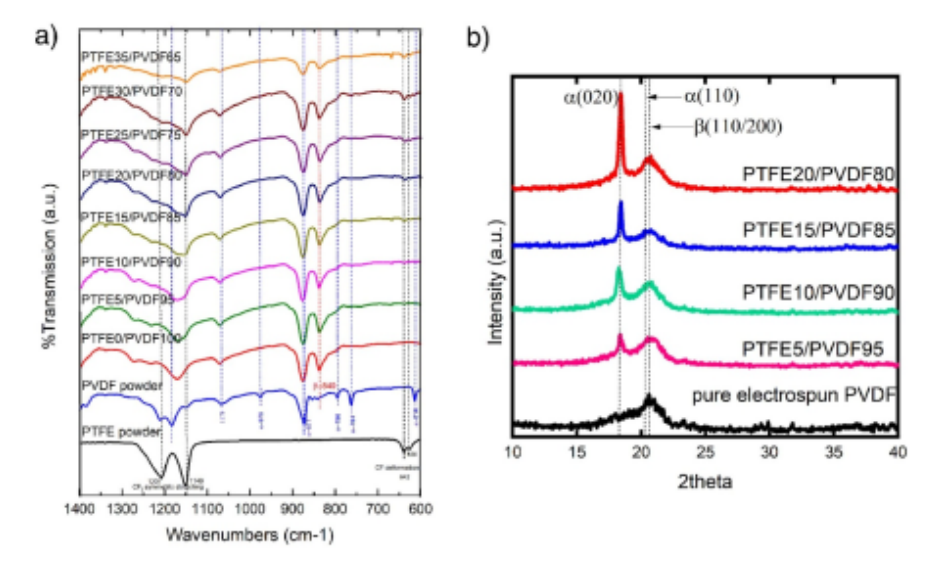


Figure 5. (a) FTIR-ATR spectra of PTFE-PVDF electrospun fibre. The measurements were carried out at room temperature over the range of $600-1400 \, \mathrm{cm}^{-1}$ (b) XRD spectra of the single PTFE-PVDF electrospun fibre. The analyses were conducted on samples using Cu -K α_1 radiation 1.5406 Å, 40 kV and 25 mA, Step size 0.5.

Table 1. Crystallinity index obtained from XRD.

	Crystallinity index (%)	
	α -Phase	β -Phase
PTFE0/PVDF100	0	47.50
PTFE5/PVDF95	12.73	29.64
PTFE10/PVDF90	16.09	29.42
PTFE15/PVDF85	18.16	24.63
PTFE20/PVDF80	23.62	20.03

solution, the dielectric properties of the PTFE/PVDF solution increase, resulting in a reduced electric field to induce β -phase. The α -phase requires less energy than the β -phase to form and thus, the β -phase decreases while the α -phase increases as shown in table 1.

In summary, both the FTIR and XRD spectra results indicate that the PTFE/PVDF electrospun fibres have a mix of α -

and β -phase PVDF. The amount of the β -Phase decreases, and the α -phase increases with an increase in percentage of PTFE. In addition, the electromechanical performance of the PTFE/PVDF presented in section 3.3 is not related to the piezoelectric phase of the PVDF. It confirms that the β -phase of PVDF (exhibiting piezoelectric properties) is not the key to high energy harvesting performance in the hybrid piezotriboelectric-based design. The relationship between the number of fluorine atoms which increases the negative charge and the surface morphology of the PTFE/PVDF fibre was responsible for the triboelectric effect. When more fluorine atoms at higher PTFE percentages are added, the texture of the fibre becomes non-porous due to unsuitable electrospinning conditions. This results in a change in surface morphology that leads to a decrease in the electromechanical performance. This relationship is supported by surface potential measurements taken using the static fieldmeter SIMCO-FX003. These measurements showed wide variations depending upon location on

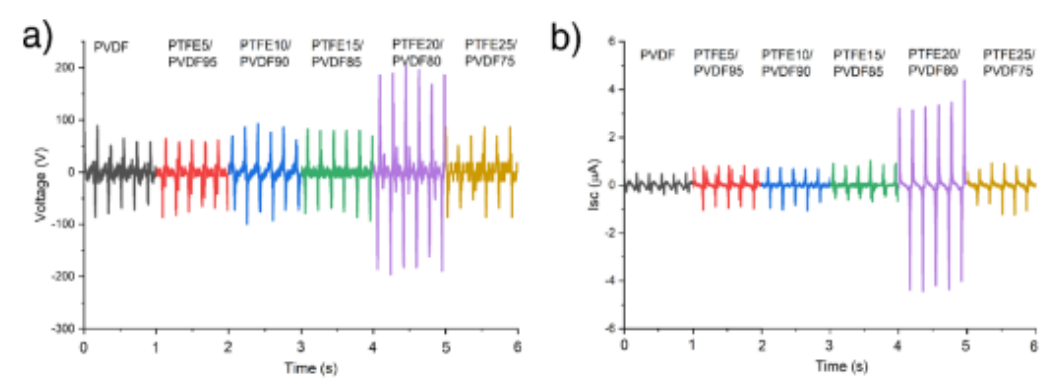


Figure 6. (a) open circuit voltage was tested across a 1 G Ω load resistor and (b) short circuit current of the PTFE/PVDF electrospun fibre prepared at different concentrations.

the fibre mat and the corresponding thickness at that point, but the average potential of PVDF and PTFE20/PVDF80 were 1.1 and 1.8 kV, respectively.

3.3. Electromechanical study

The energy harvesting performance was initially tested with the tapping rig in order to explore the optimum PTFE concentration. The test was performed at 6 Hz using the contact separation triboelectric mode (figures 2(a) and (b)). The V_{oc} and Isc of each sample prepared from different concentrations were read after tapping for approximately 3 min to ensure that the tapping rate and the signal output were consistent. When the surfaces make contact, there is an electron transfer from the positively charged nylon to the negatively charged electrospun PTFE/PVDF. This leads to the nylon surface gaining a positive charge and the electrospun PTFE/PVDF surface developing a negative charge. When the surfaces are separated, an induced potential difference between the electrodes arises, leading to the development of opposite transferred charges on the electrodes through electrostatic induction. Consequently, an electric charge will transfer from the bottom electrode to the top electrode via an external load in order to balance the potential difference until it reaches a state of equilibrium. As the surfaces approach each other, the potential difference caused by tribo-charging will gradually decrease until it reaches zero. The charges that were transferred are now moving in the opposite direction, from the top to the bottom electrode.

The open circuit voltage (V_{oc}) and short circuit current (I_{sc}) output measured at a 6 Hz tapping rate are shown in figures 6(a) and (b) respectively. The V_{oc} and I_{sc} obtained from pure PVDF are slightly less than those obtained from other samples that include PTFE particles. The output from PTFE5/PVDF95, PTFE10/PVDF90 and PTFE15/PVDF85 were similar which relates to the similar fibre size which results in the PTFE particles being similarly distributed within the fibres. For the PTFE20/PVDF80 sample, as shown in figure 3(e), the fibre size is smaller and, combined with the higher percentage of PTFE particles, there is a greater concentration of PTFE at the surface of the fibres. This increases the

triboelectric effect due to the superior triboelectric properties of the PTFE. When the PTFE particles exceed 20% (samples PTFE25/PVDF75, PTFE30/PVDF70, and PTFE35/PVDF65) the electrospinning process could not correctly form the fibres, resulting in poor mixing of PTFE particles and PVDF binder and thus the output is reduced in comparison with the PTFE20/PVDF80 (as seen in figures 6(a) and (b)). It was found that the peak-to-peak V_{oc} shows a similar output for pure PVDF and up to PTFE15/PVDF85. The peak-to-peak Voc shows a sharp increase to 390 V for the PTFE20/PVDF80 fibres. The results for the peak-to-peak Isc follow a similar pattern with a maximum peak I_{sc} of 8 μ A occurring with the PTFE20/PVDF80. The PTFE20/PVDF80 fibre mat made from the 4% PTFE and 16% PVDF solution gives the highest electrical output and was used in the subsequent analysis to investigate the effectiveness of the contact separation mode triboelectric energy harvesting using the electrospun fibres.

The open circuit voltage (V_{∞}) output and short circuit current (I_{sc}) of the PTFE20/PVDF80 fibre mat were tested at different load resistance $(1 \text{ k}\Omega - 6 \text{ G}\Omega)$, as shown in figure 7(a). The calculated peak power $(P = \frac{V_p^2}{R})$ and the power density $(P = \frac{V_p^2}{RA})$ from the test are plotted in figure 7(b). The highest power and power density were obtained at an optimal load resistance of 10 M Ω and were found to be 7 mW and 348.5 mW m $^{-2}$, respectively.

The contact-separation mode TENG works with a connected resistor R for this cyclical testing using the tapping rig. The top electrode moves up and down with the separation distance, x(t), from the fixed bottom triboelectric material. According to Ohm's law

$$V(t) = RI(t) = R \frac{dQ(t)}{dt}$$
(2)

V is the voltage output, Q is the amount of transferred charge between the two electrodes, I is the current output, and R is the load resistance; the $V_{\rm oc}$ and $I_{\rm sc}$ depend on the frequency of cyclical moving on both sides of triboelectric materials as a sinusoidal function that can be described by

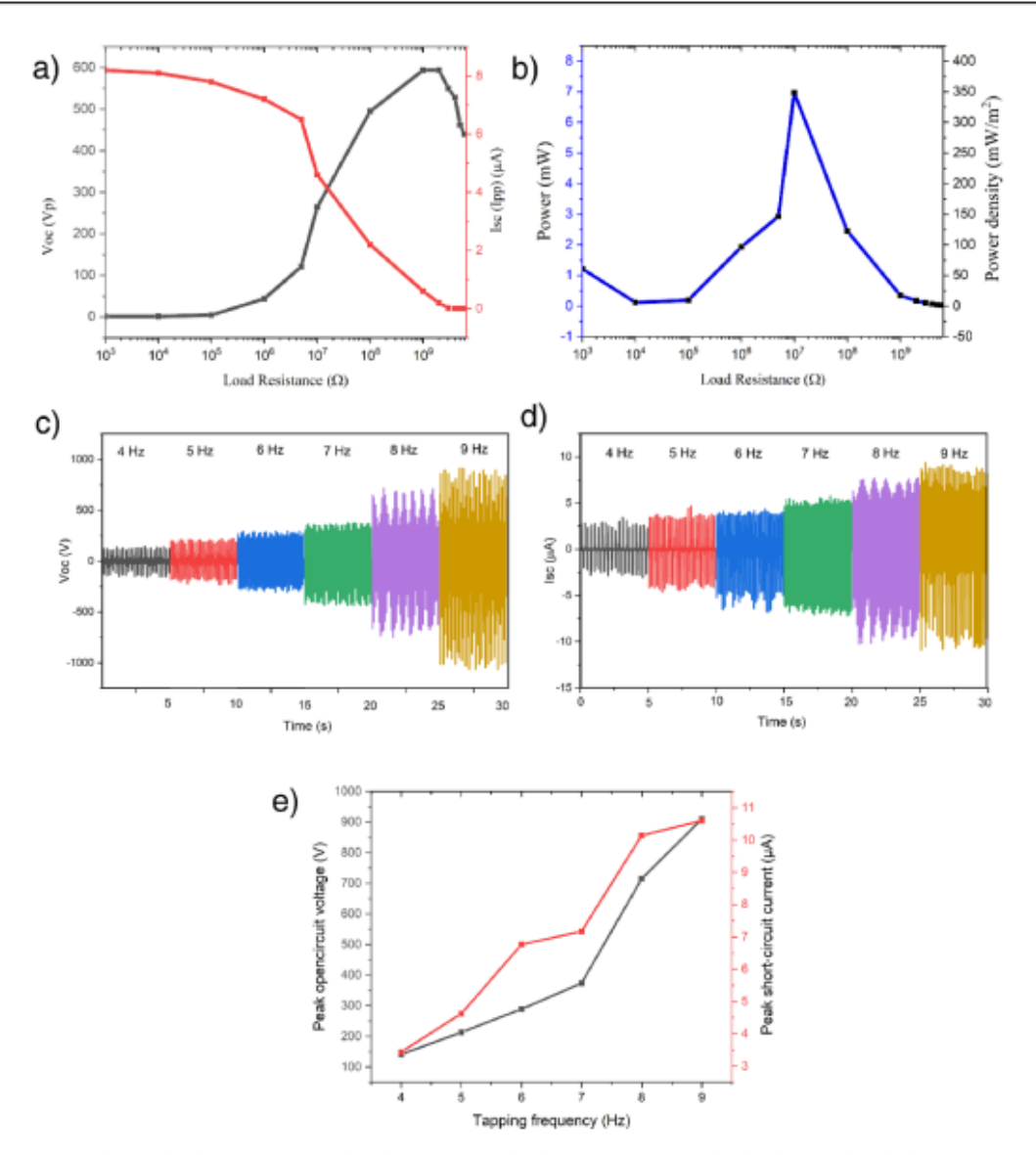


Figure 7. (a) peak open circuit voltage (V_{∞}) and peak to peak short circuit current (I_{sc}) versus load resistance; (b) calculated power and power density of the PTFE4/PVDF16 versus load resistances; (c) V_{∞} and (d) I_{sc} of PTFE4/PVDF16 at different tapping frequencies; (e) peak values of V_{∞} and I_{sc} as a function of tapping frequency.

 $x(t) = A\sin(\omega t + \theta)$, where t, A, ω and θ are the time, amplitude, angular velocity and initial phase angle of the cyclical motion, respectively [51, 52].

The V_{oc} and I_{sc} obtained when testing at tapping frequencies of 4–9 Hz are shown in figures 7(c) and (d), peak V_{oc} and I_{sc} versus tapping frequency is plotted in figure 7(e). As expected, the increased tapping frequency resulted in an increase of the V_{oc} and I_{sc} . When increasing the tapping frequency, the top layer contacts and separates the bottom layer quicker, resulting in the charge transfer reaching the equilibrium quicker through the external load. When the charge transfer reaches

equilibrium, the output should reach the saturated point and then plateau, as found in the literature [53, 54]. However, the tapping rig used in this work has limitations in testing; thus, the results could not show the saturating point. Table 2 summarizes the results obtained for all samples.

To demonstrate the practical utilisation of the PTFE/PVDF fibre, the book-shaped PVC substrate was assembled with the PTFE20/PVDF80 and the nylon fabric and connected to a full bridge rectifier to convert the AC output to DC to enable the energy to be stored on a capacitor as shown in figure 8(a). This experiment provides an accurate practical assessment of

Table 2. Summary of the electromechanical characteristics of the sample.

Code	Solution mixing condition	Percentage of polymer in fibre	Tapping frequency (Hz)	V _{oc} (peak to peak) (V)	I_{sc} (peak to peak) (μ A)
PVDF	PTFE0/PVDF20	PVDF 100%	6	130	1.23
PTFE5/PVDF95	PTFE1%/PVDF19%	PTFE 5%, PVDF95%	6	136	1.63
PTFE10/PVDF90	PTFE2%/PVDF18%	PTFE10%, PVDF90%	6	167	2.45
PTFE15/PVDF85	PTFE3%/PVDF17%	PTFE15%, PVDF85%	6	154	3.11
PTFE20/PVDF80	PTFE4%/PVDF16%	PTFE20%, PVDF80%	6	555	9.04
PTFE25/PVDF75	PTFE5%/PVDF15%	PTFE25%, PVDF75%	6	171	2.10
PTFE20/PVDF80	PTFE4%/PVDF16%	PTFE20%, PVDF80%	4	277	3.95
			5	429	7.68
			6	555	9.04
			7	766	12.24
			8	1422	17.36
			9	1889	19.72

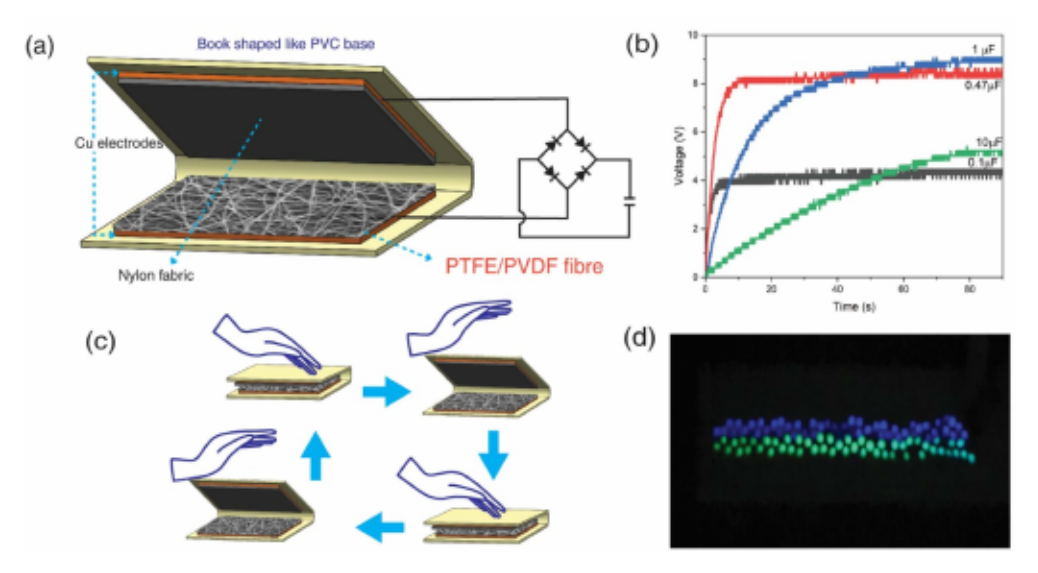


Figure 8. (a) Schematic of the book-shaped triboelectric energy harvester used to charge the capacitors; (b) the voltage across 0.1, 0.47, 1, and $10~\mu\text{F}$ capacitors, when charged by the book shaped energy harvester at 6 Hz over a 90 s period; (c) schematic of the hand tapping test during the testing of the 100 LED lights experiment; (d) the 100 LED lights illuminated via hand tapping of the book shaped PTFE/PVDF energy harvester.

the energy that can be harvested and delivered to the energy storage device and includes the losses that occur in the conditioning circuit. The capacitor charging test was performed using the tapping rig with a frequency of 6 Hz with capacitors of 0.1, 0.47, 1, and 10 μ F. The calculated energy from charging obtained from $U=\frac{1}{2}\,CV^2$ was found at the capacitor 0.1, 0.47, 1, and 10 μ F is 1.0, 16.7, 41.2 and 136.8 μ J, respectively. The book-shaped TENG was further tested by illuminating an LED array using manual tapping method, as illustrated in figure 8(c). It was found that hand tapping could illuminate 100 LEDs, as shown in figure 8(d). The blue and green LEDs used in this work require at least 3.4 V in order to light one LED bulb. In this case, it can be assumed that the hand tapping TENGs prepared using PTFE/PVDF fibre with a frequency of approximately 6 Hz can generate more than 340 V in order to

illuminate 100 LED light bulbs. The illuminated LED bulbs can be seen in the supporting data S1.

To demonstrate the potential energy harvesting output in a practical energy harvesting application, the electropun fibre mat was assembled into a modified shoe insole to harvest energy during walking and running. The insole was modified to include four cut-out sections each $2 \text{ cm} \times 2 \text{ cm}$ placed next to each other resulting in an active area of 16 cm^2 located at the heal of the foot. A rib of insole was left between these sections to ensure the insole remained comfortable to use and to make the active sections imperceptible to the user (see the schematic of insole in figure 9(a)). The harvester operates in the contact separation mode with the electrospun fibre mat making contact with the nylon during the initial contact and loading phases associated with the foot being placed on the

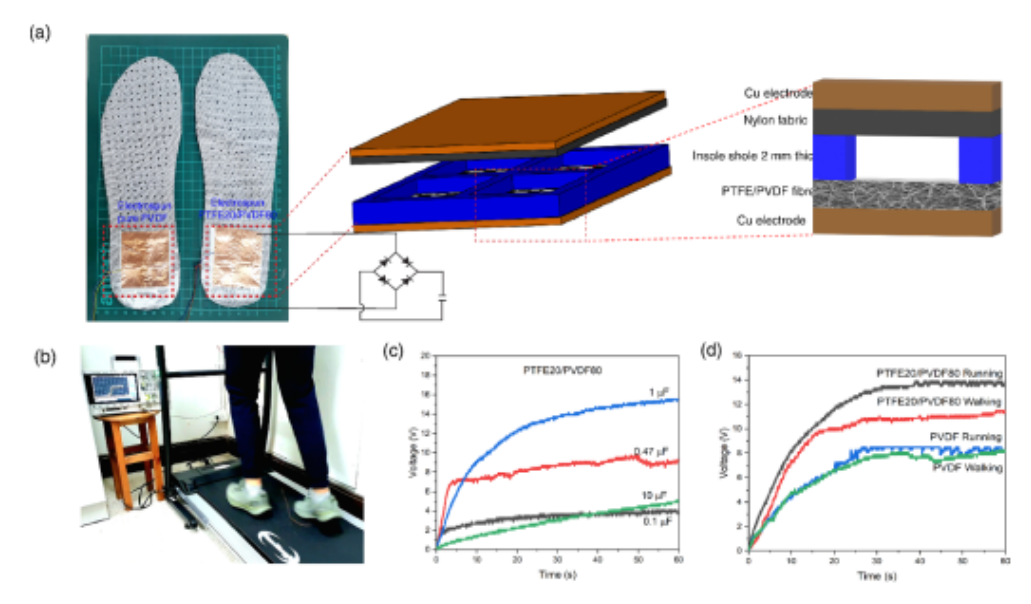


Figure 9. The triboelectric insole for a demonstration of human gait energy harvesting (a) the photo and schematic of the shoe insole used in this study (b) the photo when charging the capacitor when running on the treadmill (c) the voltage across the 1 μ F capacitor, when charged by running on the PTFE20/PVDF80 insole over a 60 s period (d) the comparison of the voltage across the 1 μ F capacitor, when running and walking on PTFE20/PVDF80 and PVDF insole over a 60 s period.

ground during the gait cycle and separating as the heal lifts off during the terminal stance and pressing phases. The harvester was realised from 100% electrospun PVDF fibres which was placed on the left foot insole, and from PTFE20/PVDF80 electrospun fibre which was used in the right insole (as shown in figure 9(a)) enabling a comparison of the PVDF and electrospun PTFE/PVDF fibres. The insole was placed inside an otherwise normal pair of running shoes and connected to the full bridge rectifier circuit consisting of 1N4007 diodes to charge the capacitors. Figure 9(c) shows the voltage across the 0.1, 0.47, 1.0 and 10 μF capacitors that was measured during running on treadmill, as can be seen in the supporting data S2. The calculated energy obtained from running using the formula $U = \frac{1}{5}CV^2$ at capacitors 0.1, 0.47, 1, and 10 μ F was found to be 0.7, 15.8, 100.8 and 105.8 μ J, respectively. Figure 9(d) shows the comparison of the voltage across the 1 μ F capacitor between the insole made from the pure PVDF and PTFE20/PVDF80 when charging by walking and running. The calculated energy obtained from the PVDF insole from running and walking was 25.9 and 27.4 μJ, respectively. While the calculated energy obtained from the PTFE20/PVDF80 insole from running and walking was 69.6 and 100.8 μJ, respectively. The energy obtained from the insole made from PTFE20/PVDF80 was shown to be approximately 3 times greater when walking and 4 times greater when running than the PVDF insole

4. Conclusion

It was possible to effectively prepare a flexible PTFE fibre utilising a one-step electrospinning process with a PVDF

solution as a precursor. An examination was conducted on the energy harvesting performance of a triboelectric assembly operating in a vertical contact separation mode with electrospun fibres with different percentages of PTFE as the negative materials and nylon as the triboelectric positive material. The electrospun fibres created a nonwoven textile mat with promising negative surface potential with the optimum percentage being 20% PTFE loading in the PVDF matrix. This percentage of PTFE in the electrospun fibre enhanced the voltage and current output by 4 and 7 times, respectively but it, was found that the maximum power density was 348.5 mW m-2 at a 10 MΩ resistance. Additionally, the application of the electrospun fibres was further demonstrated in book-shaped and shoe insole based triboelectric harvesters operating in the contact separation mode. The book shaped harvester assembled with the PVDF energy harvester can successfully charge an energy storage capacitor using a full bridge rectifier circuit pointing the way towards energy harvesting powered systems. Electrospinning is a straightforward process for fabricating fibres that can be directly used in a non-woven fibre mat that is entirely compatible with textiles being soft, breathable, and conformable. Fibres could also be used to fabricate triboelectric PTFE/PVDF threads that could be combined within a woven or knitted textile. The improvements in electrical output from the fibres with PTFE certainly merit further investigation in practical energy harvesting applications. The influence of the PTFE particles on the surface roughness of the fibres has not been quantified in this study. This surface roughness can affect the output of the TENG and therefore this will be studied in future work using an atomic force microscope.

Data availability statement

All data that support the findings of this study are included within the article (and any supplementary files).

Acknowledgments

Pattarinee White expresses her gratitude to the Royal Thai Government Scholarship for kindly providing support for her research. Under the Chairs in Emerging Technologies Scheme, the U.K. Royal Academy of Engineering provided support for Stephen Beeby's study.

Conflict of interest

The authors declare no conflict of interest.

CRediT authorship contribution statement

Pattarinee White: Review, Investigation, Writing—original draft, Validation, Methodology. Piyapong Pankaew: Investigation, Formal analysis, Resources. Dmitry Bavykin: Supervision, Resources, Formal analysis. Mohamed Moshrefi-Torbati: Supervision, Resources, Conceptualization, Stephen Beeby: Supervision, Conceptualization, Resources, Writing—review & editing

Funding

This research received no external funding.

ORCID iDs

Pattarinee White https://orcid.org/0000-0001-6341-6378 Piyapong Pankaew https://orcid.org/0000-0001-5099-403X

M Moshrefi-Torbati https://orcid.org/0000-0003-3112-6354

Stephen Beeby https://orcid.org/0000-0002-0800-1759

References

- Research G V 2023 Wearable technology market share & trends report (available at: www.grandviewresearch.com/ industry-analysis/wearable-technology-market)
- [2] Melchor-Martínez E M, Macias-Garbett R, Malacara-Becerra A, Iqbal H M N, Sosa-Hernández J E and Parra-Saldívar R 2021 Environmental impact of emerging contaminants from battery waste: a mini review Case Stud. Chem. Environ. Eng. 3 100104
 [3] Islam M T, Huda N, Baumber A, Hossain R and Sahajwalla V
- [3] Islam M T, Huda N, Baumber A, Hossain R and Sahajwalla V 2022 Waste battery disposal and recycling behavior: a study on the Australian perspective Environ. Sci. Pollut. Res. 29 58980–9001
- [4] Komolafe A, Zaghari B, Torah R, Weddell A S, Khanbareh H and Tsikriteas Z M 2021 E-textile technology review-from materials to application IEEE Access 9 97152–79
- Zeyrek Ongun M et al 2020 Aligned PVDF-TrFE nanofibers with high-density PVDF nanofibers and PVDF core-shell

- structures for endovascular pressure sensing J. Mater. Sci., Mater. Electron. 31 188–95
- [6] Kim S, Towfeeq I, Dong Y, Gorman S, Rao A and Koley G 2018 P(VDF-TrFE) film on PDMS substrate for energy harvesting applications Appl. Sci. 8 213
- [7] Ghosh S K, Sinha T K, Xie M, Bowen C R, Garain S and Mahanty B 2021 Temperature-pressure hybrid sensing all-organic stretchable energy harvester ACS Appl. Electron. Mater. 3, 248–59
- [8] Halim M A, Cho H, Salauddin M and Park J Y 2016 A miniaturized electromagnetic vibration energy harvester using flux-guided magnet stacks for human-body-induced motion Sens. Actuators A 249 23–31
- [9] Shi J, Yong S and Beeby S 2018 An easy to assemble ferroelectret for human body energy harvesting Smart Mater. Struct. 27 084005
- [10] Wan H, Cao Y, Lo L W, Zhao J, Sepúlveda N and Wang C 2020 Flexible carbon nanotube synaptic transistor for neurological electronic skin applications ACS Nano 14 10402–12
- [11] Busolo T, Ura D P, Kim S K, Marzec M M, Bernasik A and Stachewicz U 2019 Surface potential tailoring of PMMA fibers by electrospinning for enhanced triboelectric performance Nano Energy 57 500-6
- [12] Paosangthong W, Wagih M, Torah R and Beeby S 2019 Textile-based triboelectric nanogenerator with alternating positive and negative freestanding grating structure Nano Energy 66 104148
- [13] Paosangthong W, Wagih M, Torah R and Beeby S 2022 Textile-based triboelectric nanogenerator with alternating positive and negative freestanding woven structure for harvesting sliding energy in all directions Nano Energy 92, 106739
- [14] Due J, Munk-Nielsen S and Nielsen R 2010 Energy harvesting with di-electro active polymers *IET Conf. Publ* vol 2010 (563 CP)
- [15] McKay T G, Rosset S, Anderson I A and Shea H 2013 An electroactive polymer energy harvester for wireless sensor networks J. Phys.: Conf. Ser. 476 0–5
- [16] Elbarmaki J, EL Jouad M, Belhora F and Hajjaji A 2022 Wave energy harvesting using Silicone as Electro-active Polymers Mater. Today 66 22–25
- [17] Pan S and Zhang Z 2019 Fundamental theories and basic principles of triboelectric effect: a review Friction 7 2–17
- [18] Munirathinam P, Anna Mathew A, Shanmugasundaram V, Vivekananthan V, Purusothaman Y, Kim S J and Chandrasekhar A 2023 A comprehensive review on triboelectric nanogenerators based on real-time applications in energy harvesting and self-powered sensing Mater. Sci. Eng. B 297 116762
- [19] Fan F R, Tian Z Q and Lin Wang Z 2012 Flexible triboelectric generator Nano Energy 1 328–34
- [20] Lai Y C, Hsiao Y C, Wu H M and Wang Z L 2019 Waterproof fabric-based multifunctional triboelectric nanogenerator for universally harvesting energy from raindrops, wind, and human motions and as self-powered sensors Adv. Sci. 6 1801883
- [21] He T, Shi Q, Wang H, Wen F, Chen T, Ouyang J and Lee C 2019 Beyond energy harvesting—multi-functional triboelectric nanosensors on a textile *Nano Energy* 57 338–52
- [22] He M, Du W, Feng Y, Li S, Wang W, Zhang X, Yu A, Wan L and Zhai J 2021 Flexible and stretchable triboelectric nanogenerator fabric for biomechanical energy harvesting and self-powered dual-mode human motion monitoring Nano Energy 86 106058
- [23] Lama J, Yau A, Chen G, Sivakumar A, Zhao X and Chen J 2021 Textile triboelectric nanogenerators for self-powered biomonitoring J. Mater. Chem. A 9 19149–78

Smart Mater. Struct. 33 (2024) 075010 P White et al.

- [24] Šutka A, Lapčinskis L, He D, Kim H, Berry J D, Bai J, Knite M, Ellis A V, Jeong C K and Sherrell P C 2023 Engineering polymer interfaces: a review toward controlling triboelectric surface charge Adv. Mater. Interfaces 10 2300323
- [25] Lee K Y, Kim S K, Lee J-H, Seol D, Gupta M K, Kim Y and Kim S-W 2016 Controllable charge transfer by ferroelectric polarization mediated triboelectricity Adv. Funct. Mater. 26 3067–73
- [26] Šutka A, Malnieks K, Linarts A, Timusk M, Jurkans V, Gornevs I, Blüms J, Berzina A, Joost U and Knite M 2018 Inversely polarised ferroelectric polymer contact electrodes for triboelectric-like generators from identical materials Energy Environ. Sci. 11 1437–43
- [27] Lee J P, Lee J W and Baik J M 2018 The progress of PVDF as a functional material for triboelectric nanogenerators and self-powered sensors Micromachines 9 30–33
- [28] Garcia C, Trendafilova I, Guzman de Villoria R and Sanchez Del Rio J 2018 Self-powered pressure sensor based on the triboelectric effect and its analysis using dynamic mechanical analysis Vano Finero 50 4(1) -9
- mechanical analysis Nano Energy 50 401–9
 [29] Garcia C and Trendafilova I 2019 Real-time diagnosis of small energy impacts using a triboelectric nanosensor Sens.

 Actuators A 291 196–203
- [30] Garcia C, Trendafilova I and Sanchez Del Rio J 2019 Detection and measurement of impacts in composite structures using a self-powered triboelectric sensor *Nano Energy* 56 443-53
- [31] Hao Y, Bin Y, Tao H, Cheng W, Hongzhi W and Meifang Z 2015 Preparation and optimization of Polyvinylidene fluoride (PVDF) triboelectric nanogenerator via electrospinning *IEEE-NANO 2015–15th Int. Conf. Nanotechnology* vol 1 pp 1485–8
 [32] Guo Y, Zhang H, Zhong Y, Shi S, Wang Z, Wang P and
- [32] Guo Y, Zhang H, Zhong Y, Shi S, Wang Z, Wang P and Zhao Y 2023 Triboelectric nanogenerator-based near-field electrospinning system for optimizing PVDF fibers with high piezoelectric performance ACS Appl. Mater. Interfaces 15 5242–52
- [33] Shaikh M O, Huang Y B, Wang C C and Chuang C H 2019 Wearable woven triboelectric nanogenerator utilizing electrospun PVDF nanofibers for mechanical energy harvesting *Micromachines* 10 438
- [34] Tofel P, Částková K, Říha D, Sobola D, Papež N, Kaštyl J, Ţálu Ş and Hadaš Z 2022 Triboelectric response of electrospun stratified PVDF and PA structures Nanomaterials 12 349
- [35] Al-Attabi R et al 2023 Durable and comfortable electrospun nanofiber membranes for face mask applications Sep. Purif. Technol. 322 124370
- [36] Lee J W, Ye B U and Baik J M 2017 Research update: recent progress in the development of effective dielectrics for high-output triboelectric nanogenerator APL Mater. 5 073802
- [37] Schröder S, Strunskus T, Rehders S, Gleason K K and Faupel F 2019 Tunable polytetrafluoroethylene electret films with extraordinary charge stability synthesized by initiated chemical vapor deposition for organic electronics applications Sci. Rep. 9 1–7
- [38] Kang D, Lee H Y, Hwang J-H, Jeon S, Kim D, Kim S M and Kim S-W 2022 Deformation-contributed negative triboelectric property of polytetrafluoroethylene: a density functional theory calculation *Nano Energy* 100 107531
- [39] Lin S, Cheng Y, Mo X, Chen S, Xu Z, Zhou B, Zhou H, Hu B and Zhou J 2019 Electrospun polytetrafluoroethylene nanofibrous membrane for high-performance self-powered sensors Nanoscale Res. Lett. 14 251

- [40] Xiong J, Huo P and Ko F K 2009 Fabrication of ultrafine fibrous polytetrafluoroethylene porous membranes by electrospinning J. Mater. Res. 24 2755–61
- [41] Zhao P, Soin N, Prashanthi K, Chen J, Dong S and Zhou E 2018 Emulsion electrospinning of polytetrafluoroethylene (PTFE) nanofibrous membranes for high-performance triboelectric nanogenerators ACS Appl. Mater. Interfaces 10 5880-91
- [42] White P, Bavykin D, Moshrefi-Torbati M and Beeby S 2023 The energy harvesting performance of a flexible triboelectric-based electrospun PTFE/PVDF fibre Eng. Proc. 30 3–7
- [43] Windey R, AhmadvashAghbash S, Soete J, Swolfs Y and Wevers M 2023 Ultrasonication optimisation and microstructural characterisation for 3D nanoparticle dispersion in thermoplastic and thermosetting polymers Composites B 264 110920
- [44] Medeiros K A R, Rangel E Q, Sant'Anna A R, Louzada D R, Barbosa C R H and D'Almeida J R M 2018 Evaluation of the electromechanical behavior of polyvinylidene fluoride used as a component of risers in the offshore oil industry Oil Gas Sci. Technol. 73 48
- [45] Bairagi S, Khandelwal G, Karagiorgis X, Gokhool S, Kumar C, Min G and Mulvihill D M 2022 High-performance triboelectric nanogenerators based on commercial textiles: electrospun nylon 66 nanofibers on silk and pvdf on polyester ACS Appl. Mater. Interfaces 14 44591–603
- [46] Lee B-S, Park B, Yang H S, Han J W, Choong C and Bae J 2014 Effects of substrate on piezoelectricity of electrospun poly(vinylidene fluoride)-nanofiber-based energy generators ACS Appl. Mater. Interfaces 6 3520-7
- [47] Piwowarczyk J, Jedrzejewski R, Moszy'nski D, Kwiatkowski K, Niemczyk A and Baranowska J 2019 XPS and FTIR studies of polytetrafluoroethylene thin films obtained by physical methods *Polymers* 11 1–13
- [48] Mihály J, Sterkel S, Ortner H M, Kocsis L, Hajba L and Furdyga É 2006 FTIR and FT-Raman spectroscopic study on polymer based high pressure digestion vessels Croat. Chem. Acta 79 497–501 (available at: https://hrcak.srce.hr/ file/8817)
- [49] Barylski A, Aniolek K, Swinarew A S, Kaptacz S, Gabor J, Waśkiewicz Z and Stanula A 2020 Novel organic material induced by electron beam irradiation for medical application *Polymers* 12 1–11
- [50] Rotaru R, Savin M, Tudorachi N, Peptu C and Samoila P 2018 Ferromagnetic iron oxide-cellulose nanocomposites prepared by ultrasonication polymer chemistry nanocomposites prepared by ultrasonication *Polym. Chem.* 9 860–8
- [51] Yang B, Zeng W, Peng Z H, Liu S R, Chen K and Tao X M 2016 A fully verified theoretical analysis of contact-mode triboelectric nanogenerators as a wearable power source Adv. Energy Mater. 6 1–8
- [52] Zhao H, Wang H, Yu H, Xu Q, Li X, Guo J, Shao J, Wang Z L, Xu M and Ding W 2024 Theoretical modeling of contact-separation mode triboelectric nanogenerators from initial charge distribution *Energy Environ. Sci.* 17 2228–47
- [53] Rana S M S, Rahman M T, Salauddin M, Sharma S, Maharjan P, Bhatta T, Cho H, Park C and Park J Y 2021 Electrospun PVDF-TrFE/MXene nanofiber mat-based triboelectric nanogenerator for smart home appliances ACS Appl. Mater. Interfaces 13 4955–67
- [54] Xiong J, Cui P, Chen X, Wang J, Parida K, Lin M-F and Lee P S 2018 Skin-touch-actuated textile-based triboelectric nanogenerator with black phosphorus for durable biomechanical energy harvesting Nat. Commun. 9 1–9





Proceeding Paper

The Energy Harvesting Performance of a Flexible Triboelectric-Based Electrospun PTFE/PVDF Fibre †

Pattarinee White 1,* 0, Dmitry Bavykin 2, Mohamed Moshrefi-Torbati 3 and Stephen Beeby 100

- Centre for Flexible Electronics and E-Textiles, University of Southampton, Southampton SO17 1BJ, UK
- Energy Technology Research Group, University of Southampton, Southampton SO17 1BJ, UK
- Mechatronics Research Group, University of Southampton, Southampton SO17 1BJ, UK
- Correspondence: p.white@soton.ac.uk
- † Presented at the 4th International Conference on the Challenges, Opportunities, Innovations and Applications in Electronic Textiles, Nottingham, UK, 8-10 November 2022.

Abstract: A triboelectric power generator/energy harvester is an attractive option for mechanical energy harvesting for smart, wearable applications. This paper reports on the fabrication and evaluation of the energy harvesting performance of Polytetrafluoroethylene/Polyvinylidene Fluoride (PTFE/PVDF) fibre prepared using a one-step electrospinning technique. Different concentrations (0, 1, 2, 3, and 4%wt.) of the 1 µm PTFE powder in the electrospun PVDF fibre were investigated. The electrospun fibre was assembled into a nonwoven fabric mat and tested in the vertical contact separation triboelectric mode by constructing a sandwich structure with electrodes in a book-shaped assembly. The voltage output from the cyclical compressive test for fibres with 4%wt. PTFE in PVDF was five times greater than it was for the 100% PVDF electrospun fibres. The influence of adding nylon fabric as a triboelectric donor material within the assembly was explored. The output of the 4%wt. PTFE/PVDF sample was then tested with and without nylon fabric at different frequencies (3–12 Hz). The results show a further 80% increase in the output voltage with the additional nylon fabric included, and the harvester was able to illuminate up to 95 LEDs.

Keywords: triboelectric; textile energy harvester; electrospinning; electrospun fibre



Citation: White, P.; Bavykin, D.; Moshrefi-Torbati, M.; Beeby, S. The Energy Harvesting Performance of a Flexible Triboelectric-Based Electrospun PTFE/PVDF Fibre. Eng. Proc. 2023, 30, 8. https://doi.org/ 10.3390/engproc2023030008

Academic Editors: Kai Yang, Russel Torah and Theodore Hughes-Riley

Published: 20 January 2023



Copyright: © 2023 by the authors. Licensee MDPI, Basel, Switzerland. This article is an open access article distributed under the terms and conditions of the Creative Commons. Attribution (CC BY) license (https:// creativecommons.org/licenses/by/

1. Introduction

Polytetrafluoroethylene (PTFE) has good thermal stability, and is the most negative triboelectric material listed in the triboelectric series that are used for energy harvesting applications [1]. Increasing the surface area of the PTFE within a triboelectric harvester is one approach to improve the output of the harvester. Previous attempts to prepare PTFE fibre mats using the electrospinning process involve the use of a precursor polymer solution in order to structure the shape of the PTFE. This requires a subsequent thermal treatment to eliminate the precursor polymer and, if it is used in an electrostatic device or to enhance the triboelectric generation, a corona charging process to restore the trapped charge in the PTFE fibre. The PTFE fibres produced in this manner show good energy harvesting performances, but they require two or more steps in the material preparation [2-5]. Electrospun Polyvinylidene Fluoride (PVDF) fibre has been recognised as a high-performance piezoelectric polymer [6], which also exhibits negative triboelectric properties [1]. PTFE and PVDF can be combined during electrospinning, and this avoids the requirement for the precursor polymer and the subsequent additional processes. The use of electrostatically charged electrospun PTFE/PVDF has been demonstrated in air filtration [7], but its energy harvesting performance has not yet been reported.

The combined PTFE/PVDF fibres can be readily assembled into a non-woven textile, allowing the material to be used in various triboelectric operating modes, such as the lateral sliding mode demonstrated by Paosangthong et al. [8]. The fabrication and testing of the energy harvesting performance of PTFE/PVDF fibre is reported.

Eng. Proc. 2023, 30, 8. https://doi.org/10.3390/engproc2023030008

https://www.mdpi.com/journal/engproc

Eng. Proc. 2023, 30, 8

2. Materials and Methods

2.1. Electrospinning Preparation

The PTFE/PVDF electrospun fibre was produced by mixing PTFE particles (Sigma Aldrich, Dorset, UK, 1 micron particles) in an 18%wt PVDF solution as a polymer carrier for PTFE. The PVDF solution was prepared from PVDF powder (Sigma Aldrich, Dorset, UK, Mw = 534,000) mixed with N-Dimethylformamide (DMF, Sigma Aldrich, Dorset, UK, 99.8%) and acetone (Fisher Scientific, Waltham, MA, USA, 99.6%) at a 7:3 ratio and mixed on a magnetic hotplate stirrer at 60 °C for 4 h. Different concentrations (0, 1, 2, 3, and 4%wt.) of the PTFE particles were added to the PVDF solvent solution and blended using the magnetic stirrer at room temperature for 2 h. The electrospinning process was performed using a blunt tip (21 G) needle. The electrospinning apparatus EC-DIG produced by IME Technologies, Netherlands was used in this study. The distance from the tip to the substrate, the applied voltage, the flow rate, and the rotating drum speed were kept constant at 22 cm, 25 kV, 2 mL/hr, and 150 rpm, respectively, for each concentration. After electrospinning for 90 min, the PTFE/PVDF fibre was collected in the form of a nonwoven fibre mat, as shown in Figure 1a. The energy harvesting performance of the electrospun PTFE/PVDF fibre mats were measured without any further processing steps.

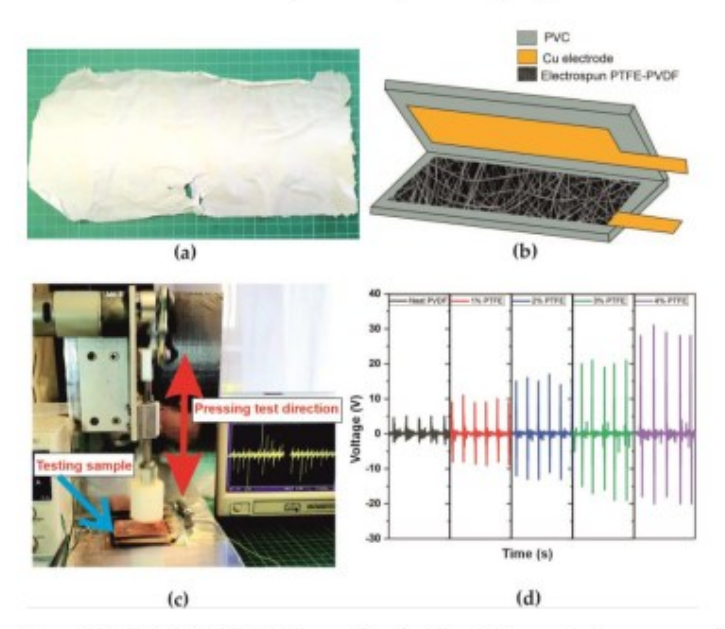


Figure 1. (a) PTFE/PVDF fibre mats after the electrospinning process of the 4%wt PTFE in the PVDF sample; (b) the schematic of the booked shape assembly for the testing cell PTFE/PVDF fibre sandwich with electrodes; (c) the compression test rig; (d) voltage output from constantly tapping the booked shape PTFE/PVDF fibre assembly at different PTFE concentrations of 0, 1, 2, 3, and 4%wt., respectively.

2.2. Test Assembly and Protocol

The electrospun PTFE/PVDF fibre mats with each concentration of PTFE (0, 1%, 2%, 3%, and 4%) were cut into 5×4 cm samples. Each sample was then assembled in a sandwich structure with Cu electrodes using a folded over (book-shaped) PVC sheet backing, as shown in Figure 1b. This forms a vertical contact separation mode triboelectric harvester. A second generator design with a piece of nylon fabric added to the assembly as a triboelectric donor material was used to explore the addition of this material for the enhancement of the performance of the triboelectric power generator.

A cyclical compression test system using a linear actuator was set up to apply a controlled pressure of 0.5 N/cm² at different frequencies (3–12 Hz), as shown in Figure 1c.

Eng. Proc. 2023, 30, 8

The test sample was attached to the oscilloscope to observe the changes in the voltage induced by the periodic mechanical pressure applied by the rig. The capacitor charging experiment was performed using a full-wave bridge rectifier to charge 0.1, 1, 10, and $100~\mu F$ capacitors.

3. Results and Discussion

The vertical book-shaped structure was chosen for energy harvesting performance testing as it is a simple structure and could be assembled into a multi-layered device. The highest voltage output from compressing at 5 Hz was found to be 30 V for the 4%wt PTFE, which is five times higher than that of the 100% PVDF sample (6 V), as shown in Figure 1d. This clearly shows that introducing the PTFE particles in the PVDF fibre can improve the performance of triboelectric power generators. The output voltage increases with an increasing percentage of PTFE particles. However, 4% PTFE is the highest amount of polymer content that can be processed via electrospinning because the solution conductivity is not strong enough to produce the electrospun fibre.

The 4% PTFE in the PTFE/PVDF sample was used in the energy harvesting test at different pressing rates of 3–12 Hz. It was found that the output voltage increases with an increasing pressing frequency. The highest output voltage of around 55 V was found at 12 Hz, as shown in Figure 2b. To enhance the energy harvesting performance of the triboelectric power generator, nylon fabric, which exhibits a high positive affinity in the triboelectric material series, was placed on top of the top copper electrode as shown in Figure 2a. The voltage output of the Nylon-PTFE/PVDF device at the different pressing frequencies is shown in Figure 2c. A small improvement in the voltage output was observed with the highest voltage output, which reached at 70 V at 12 Hz.

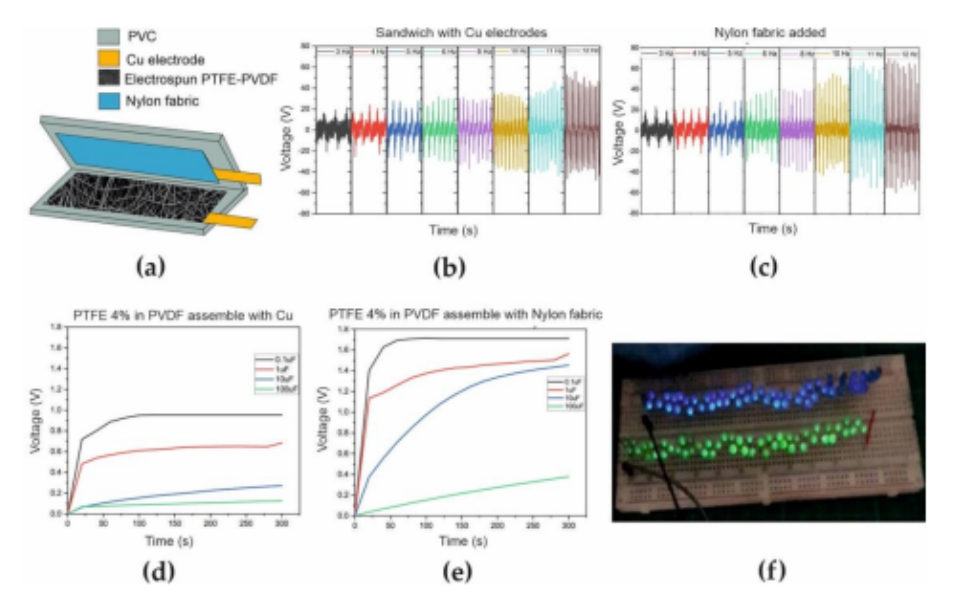


Figure 2. (a) The schematic of the improved triboelectric harvester design with added nylon fabric, (b) the voltage output of the triboelectric assembly without nylon fabric, (c) the voltage output of the triboelectric assembly after introducing nylon fabric, (d) the charging profile, voltage vs. time of the PTFE/PVDF fibre device without nylon fabric, (e) the charging profile after introducing nylon fabric and (f) 95 LED lights were illuminated via tapping the harvester with the PTFE/PVDF electrospun fibres as the acceptor and nylon fabric as the donor material.

The charging experiment was further performed to explore and compare the amounts of energy captured by the device and transferred to the capacitor storage. Devices with Eng. Proc. 2023, 30, 8

and without the nylon fabric were tested at 5 Hz with the different capacitor values, and the results are shown in Figure 2d,e. Overall, the energy stored in the capacitors is higher for the nylon-PTFE/PVDF device, with the amounts of energy stored being 0.15, 1.0, 7.2 and 4.5 μJ for 0.1, 1, 10 and 100 μF , respectively. The maximum energy stored value occurs with the 10 μF capacitor, which nearly reached its maximum capacity in the 300 s charging time. This is 69%, 79%, 94% and 89% larger than those of the device without nylon for 0.1, 1, 10 and 100 μF , respectively. The energy stored in the 100 μF capacitor is less than that of the 10 μF capacitor over the same duration due to the impedance mismatch.

After connecting the optimum harvester structure (4% PTFE with Nylon fabric) to a full-wave bridge rectifier circuit, it was found that 95 LED lights were illuminated when it was compressed at 12 Hz. The charging experiment and illuminating LED light results demonstrate the promising mechanical energy conversion that was achieved with the electrospun PTFE/PVDF fibre mat. The lightweight, flexible, and breathable PTFE/PVDF electrospun fibre could be integrated within clothing as an energy source, whilst remaining comfortable for the user.

4. Conclusions

A flexible Polytetrafluoroethylene (PTFE) fibre was successfully prepared using a one-step electrospinning process using a Polyvinylidene Fluoride (PVDF) solution as a precursor. The energy harvesting performance was first explored using a vertical contact separation mode triboelectric assembly. The electrospun fibres were collected in the form of a non-woven textile mat, which displayed a very promising negative surface potential. The voltage output was increased by a factor of five by adding PTFE to the PVDF electrospun fibre. This was further improved by the addition of a nylon fabric with the triboelectric harvester. The textile harvester was shown to illuminate up to 95 LED lights when it was assembled with nylon fabric as a donor material.

Author Contributions: Conceptualization, P.W. and S.B.; methodology, P.W.; formal analysis, P.W.; investigation, P.W.; resources, D.B., M.M.-T. and S.B.; data curation, P.W.; writing—original draft preparation, P.W., M.M.-T., D.B. and S.B.; writing—review and editing, P.W., M.M.-T., D.B. and S.B.; visualization, P.W.; supervision, M.M.-T., D.B. and S.B.; project administration, S.B.; funding acquisition, S.B. All authors have read and agreed to the published version of the manuscript.

Funding: This research received no external funding.

Institutional Review Board Statement: Not applicable.

Informed Consent Statement: Not applicable.

Data Availability Statement: The data presented in this study are available upon request from the corresponding author.

Acknowledgments: Pattarinee White would like to thank the Royal Thai Government Scholarship and Rajamangala University of Technology Krungthep for kindly supporting this research. The work of Stephen Beeby was supported by the U.K. Royal Academy of Engineering under the Chairs in Emerging Technologies Scheme.

Conflicts of Interest: The authors declare no conflict of interest.

References

- Diaz, A.F.; Felix-Navarro, R.M. A Semi-Quantitative Tribo-Electric Series for Polymeric Materials: The Influence of Chemical Structure and Properties. J. Electrost. 2004, 62, 277–290. [CrossRef]
- Su, C.; Li, Y.; Cao, H.; Lu, C.; Li, Y.; Chang, J.; Duan, F. Novel PTFE Hollow Fiber Membrane Fabricated by Emulsion Electrospinning and Sintering for Membrane Distillation. J. Membr. Sci. 2019, 583, 200–208. [CrossRef]
- Lin, S.; Cheng, Y.; Mo, X.; Chen, S.; Xu, Z.; Zhou, B.; Zhou, H.; Hu, B.; Zhou, J. Electrospun Polytetrafluoroethylene Nanofibrous Membrane for High-Performance Self-Powered Sensors. Nanoscale Res. Lett. 2019, 14, 251. [CrossRef] [PubMed]
- Zhao, P.; Soin, N.; Prashanthi, K.; Chen, J.; Dong, S.; Zhou, E.; Zhu, Z.; Narasimulu, A.A.; Montemagno, C.D.; Yu, L.; et al. Emulsion Electrospinning of Polytetrafluoroethylene (PTFE) Nanofibrous Membranes for High-Performance Triboelectric Nanogenerators. ACS Appl. Mater. Interfaces 2018, 10, 5880–5891. [CrossRef] [PubMed]

Eng. Proc. 2023, 30, 8 5 of 5

 Lu, Y.; Amroun, D.; Leprince-Wang, Y.; Basset, P. A Paper-Based Electrostatic Kinetic Energy Harvester with Stacked Multiple Electret Films Made of Electrospun Polymer Nanofibers. J. Phys. Conf. Ser. 2016, 773, 012032. [CrossRef]

- Lam, T.N.; Wang, C.C.; Ko, W.C.; Wu, J.M.; Lai, S.N.; Chuang, W.T.; Su, C.J.; Ma, C.Y.; Luo, M.Y.; Wang, Y.J.; et al. Tuning Mechanical Properties of Electrospun Piezoelectric Nanofibers by Heat Treatment. *Materialia* 2019, 8, 100461. [CrossRef]
- Dong, Z.Q.; Ma, X.H.; Xu, Z.L.; You, W.T.; Li, F.B. Superhydrophobic PVDF-PTFE Electrospun Nanofibrous Membranes for Desalination by Vacuum Membrane Distillation. Desalination 2014, 347, 175–183. [CrossRef]
- Paosangthong, W.; Wagih, M.; Torah, R.; Beeby, S. Textile-Based Triboelectric Nanogenerator with Alternating Positive and Negative Freestanding Grating Structure. Nano Energy 2019, 66, 104148. [CrossRef]

Disclaimer/Publisher's Note: The statements, opinions and data contained in all publications are solely those of the individual author(s) and contributor(s) and not of MDPI and/or the editor(s). MDPI and/or the editor(s) disclaim responsibility for any injury to people or property resulting from any ideas, methods, instructions or products referred to in the content.

2024 12th International Electrical Engineering Congress (FECON) | 979-8-3503-8359-1/24/531.00 © 2024 IEEE | DOI: 10.1109/IEECON60677.2024.10537826

2024 International Electrical Engineering Congress (iEECON 2024)

March 6-8, 2024, Pattaya Chonburi, THAILAND

The fabrication of the electrospun Polyvinylidene fluoride (PVDF) hollow structure fibre for energy harvesting applications

ls Pattarinee White
Rajamangala University of Technology
Krungthep
Bangkok, Thailand

Centre for Flexible Electronics and E-Textiles University of Southampton Southampton, UK pattarinee.w@rmutk.ac.th

4th Mohamed Moshrefi-Torbati Mechatronics Research Group University of Southampton Southampton, UK m.m.torbati@soton.ac.uk 2nd Piyapong Pankaew Rajamangala University of Technology Phra Nakhon Bangkok, Thailand piyapong.p@rmutp.ac.th

5th Stephen Beeby
Centre for Flexible Electronics and
E-Textiles
University of Southampton
Southampton, UK
sub@ecs.soton.ac.uk

3rd Dmitry Bavykin
Energy Technology group
University of Southampton
Southampton, UK
d.bavykin@soton.ac.uk

Abstract-In order to develop ferroelectret material, this research aims to produce and investigate energy harvesting performance from a hollow structure polymers using a one-step hollow electrospinning technique. In this study, PVDF (Polyvinylidene fluoride) is used to represent the polar polymer. The obtained hollow and solid structure were characterised in terms of their structural and electromechanical characteristics. The design of the experiment method for producing a hollow fibre structure through electrospinning is discussed in this paper. An SEM (scanning electron microscope) was used to characterise the geometry of the obtained fibres. The geometrical results from the SEM images demonstrate a partial hollow structure for the PVDF electrospun fibres. The partial hollow structure PVDF fibre showed a diameter of around 2 microns. FTIR (Fourier-transform infrared spectroscopy) was used to characterise the structural and chemical bonding of the fibres. The FTIR spectra reveal the piezoelectric β-phase in the solid and partially hollow PVDF samples. This agreed with the dominant peak observed from the XRD (X-ray diffractometry) analysis results. In this study, it can be concluded that electrospinning is an effective technique to induce the piezoelectric β-phase of PVDF. The electromechanical characteristics were studied for the solid and partial hollow structure fibres for the PVDF. A tapping test was used to check the obtained samples. The maximum output voltage from the solid PVDF, and partial hollow PVDF were at 6.4 and 8.7 V, respectively. The power density from the solid and partial hollow PVDF electrospun fibre was found at 1.60 and 2.18 mW/m², respectively. The maximum absolute value piezoelectric coefficient for the PVDF hollow fibre group was

Keywords—PVDF, electrospinning, electret, ferroelectret, sollow fibre

I. Introduction

Wearable technology devices are a rapidly growing market that is predicted to be worth \$62.82 billion (51.1 billion GBP) by 2025. [1] This rapid adoption amongst users has placed wearable technology at the cutting edge of the Internet of Things (IoT). The term wearable technology relates to a type of electronic device that can be worn, embedded, or implanted in the user. Such technology can include clothing, watches, hats, and glasses. These devices work through the cooperation and relationship between materials, electronics, and computers. Advances in technology, resulting in greater functionality, has created a situation whereby various mobile devices require charging on an almost daily basis. Smart electronic devices with a self-powered sensor or their own energy source can make life easier for the user by avoiding the need to recharge in the absence of a power outlet. The alternative of a larger battery may cause issues for users that need to carry various electronic devices for a long time. For example, military personnel, hikers, climbers, and trail runners need to keep weight to a minimum and may find larger batteries to be an added burden. Therefore, energy harvesting devices have been studied as an energy substitute for batteries or other primary energy sources for self-powered sensors. [2] Mechanical energy appears to be a suitable source of power for wearable devices that are connected to the human body. Energy captured from mechanical movement has been shown to be an effective source for conversion to electrical energy. This type of energy creation is possible through foot, knee, hip, and elbow movements in active people.

For wearable devices, a suitable material is required. Research and development of polymer piezoelectric material has played a significant role in harvesting energy from mechanical movement. Piezoelectric polymer is flexible, lightweight, and easier to recycle when compared to ceramic piezoelectric materials. Furthermore, user comfort is a crucial part of the development of wearable technology devices. In this regard, piezoelectric polymer can be easily produced in a breathable and flexible form making it suitable for wearable technology applications. Greater levels of comfort come at a

979-8-3503-8359-1/24/\$31.00 ©2024 IEEE

2024 International Electrical Engineering Congress (iEECON 2024)
March 6-S, 2024, Pattaya Chonburi, THAILAND

cost though with a lower piezoelectric coefficient (d33) for natural piezoelectric polymers such as PVDF when compared to ceramic piezoelectric materials. Various studies have attempted to enhance the efficiency of PVDF by restructuring and blending with composite piezoelectric ceramic and its copolymers. [3], [4]

The recent development of nonpolar cellular polymer film has resulted in improvements to the piezoelectric effect of polymers. This type of cellular piezoelectric polymer is known as "Ferroelectret" and is similar to piezoelectric materials. However, the mechanism for producing electricitic somewhat different. The internal structure of a ferroelectret material is usually made up of randomly arranged cellular voids that include positive and negative charges. The behaviour of the confined charges in the voids show piezoelectric-like properties similar to the dipole moment in ferroelectric materials. Depending on the structural design, ferroelectric material can deliver the performance of piezoelectric coefficient (d33) in the range of thousands of pC/N. In comparison, PVDF, a piezoelectric polymer material shows d33 values of about 20 pC/N. [5]

The tubular structure is of interest to researchers and several studies have predicted the performance of thin wall thermoplastic of FEP and PTFE polymers. Studies related to the tubular structures in nonpolar thermoplastic FEP and PTFE polymers have suggested hollow structures with an outer shell thickness of less than 50 microns may be able to produce higher d33 values than for those with a thicknes shell.[6]-[8] The results obtained through these investigations though were predicted and no practical experiments were ever conducted. After a thorough search by the author of this report, no studies related to ultra-thin shell tubular structures were discovered.

Therefore, the challenge of fabricating the hollow structure for a thermoplastic polymer has not yet been achieved. In this regard, an electrospinning technique could be developed to possibly achieve an ultra-thin tubular structure ferroelectret material. Electrospinning has been widely studied and can be explained in simple terms. During the electrospinning process, polymer in a liquid state is extruded from a needle tip at a constant rate. The resulting droplet of the polymer solution is then turned into a fine fibre which is deposited onto a grounded collector by a high electric force through the needle tip. Electrospinning can generate nanoscale fibres with high porosity and a high surface area. Materials produced by this method have been used in various applications such as wound dressings [9], tissue engineering [10], filters [11], [12], protective wearable devices [13], sensors[14] and batteries [15]. Furthermore, electrospinning parameters can be developed to fabricate polymeric hollow fibre with a shell thickness in the order of a submicron.

To date, hollow fibre structures fabricated by electrospinning techniques have been achieved using two approaches. The first approach is based on the coaxial fibre template. This involves the removal of the core of the fibre after the electrospinning process has been completed. This is achieved through heat treatment or by chemical treatment. This more traditional method requires two steps of preparation and is popular for the fabrication of ceramic or metal shell fibres where shell fibre has a much higher melting point than for the core fibre. The second approach is a one-step method based on the different evaporation rates of the core and shell

solutions. This method works with polymeric shell fibre as its melting point is not much higher than for the core fibre. Several studies have successfully fabricated a hollow structure thermoplastic polymer such as PCL[16], PVDF [17] through a one-step electrospinning process. However, none of these studies were related to producing fibres for energy harvesting applications. A one-step production approach for the fabrication of hollow structures through electrospinning is beneficial when producing thermoplastic ferroelectret. The fabricated ferroelectret material produced through a one-step electrospinning approach is flexible, light weight, biocompatible and requires a low processing temperature and produces high piezoelectric efficiency. In addition, ferroelectret materials made in this manner will be easier to recycle as the structure is less complex.

Further investigation is necessary to demonstrate energy harvesting potential from ultra-thin tubular ferroelectret. Therefore, this research aims to fabricate and investigate the energy harvesting potential for the electrospun hollow fibre from thermoplastic polymer by using a coaxial electrospinning technique. The comparison of energy harvesting performance between solid and hollow electrospun fibres will be demonstrated. This research will aid the study of energy harvesting for wearable technology where a flexible, lightweight, biocompatible, and environmentally friendly material is required.

II. EXPERIMENT

A. Fabrication electrospun hollow structure

The electrospinning machine (EC-DIG. IME, Netherlands) was used to prepare the electrospun fibre. The thermometer and humidity sensor were integrated inside the electrospinning cabinet. The digital wireless optical microscope was placed in the cabinet for the observation of the Taylor cone formation. The schematic of the electrospinning setup is shown in Fig. 1.

In order to obtain hollow structure electrospun fibre using one step electrospinning, the base condition for preparing the solid structure fibre of the selected polymer shell and core need to be explored. The Polyvinylidene fluoride (PVDF) is selected to be a shell polymer and the Polyvinylpyrrolidone (PVP) is selected to be a core polymer.

For solid structure of PVDF, the PVDF solutions were prepared at different polymeric concentrations of PVDF powder (Sigma Aldrich, Dorset, UK, Mw = 534,000), for mixing with DMF and acetone at a 1:1 ratio. The specifications are as follows: N-Dimethylformamide (DMF, Sigma Aldrich, Dorset, UK, 99.8%) and acetone, (Fisher Scientific, Waltham, MA, USA, 99.6%). The solutions for the PVDF fibre were prepared at different polymer concentrations (15, 17, 18, 20, 22%wt) with the solvent ratio of DMF and acetone at 1:1 (v/v) on the hot plate stirrer for 4 hours at 60 c. The electrospinning experiment was performed by using a blunt tip (21G) needle. The distance from tip to the substrate, the applied voltage, and flow rate were studied at 17, 20, 23 cm, 20, 23, 25 kV and 4, 6 ml/hr, respectively.

To explore the solid fibre condition of PVP, the PVP solutions were prepared from PVP powder (Sigma Aldrich, Dorset, UK, Mw = 1,300,000) at different polymer concentrations (15, 17, and 20%wt) in the mixing solvent of DMF and Ethanol. Each concentration was mixed at different

2024 International Electrical Engineering Congress (iEECON 2024)
March 6-8, 2024, Pattaya Chonburi, THAILAND

ratios of DMF and Ethanol (Fisher Scientific, Waltham, MA, USA, 99.9%). of 4:6, 6:4, 7:3, 8:2 (v/v). The red dye was added to the solution to assist in the observation of the Taylor cone during the coaxial experiment. The electrospinning experiment was performed by using the blunt tip (21G) needle. The distance between tip to substrate, voltage and flow rate were studied for each solution concentration. If the experiment has been successful, the Taylor cone should form a stable cone jet shape with no dripping, and the substrate should be dry after the fibre hits the target without any residue dye colour remaining. [16], [17]

Observation regarding the state of the Taylor cone was recorded in greater detail during the electrospinning process. The stability of the Taylor cone should remain unchanged throughout 4 min of the electrospinning process. If dripping occurs during the electrospinning process, it is considered an unstable Taylor cone state. By keeping the flow rate constant at 0.5 ml/hr, the study focused on examining the working distance and applied voltage in the fine range of 13-27 cm and 13-25 kV, respectively. Based on data gained from solid fibre experiments, PVDF and PVP solutions were chosen and used as the shell and core solutions for coaxial electrospinning, respectively. The condition of PVDF and PVP solutions was selected from the solid fibre experiments when mixing both solutions in the coaxial spinneret. A digital camera was used to observe the compound Taylor cone. The Taylor cone geometry was analysed for each condition from photographs using imaging software (ImageJ). This was done to study the size and angle of the Taylor cone. Although the optimum concentration of PVDF solution for solid fibre was 20 wt%. the polymer concentration that suited the coaxial experiment was 15-17%wt. The one-step hollow electrospun fibre relies on the different evaporation rates of the shell and core solution. This study is designed to use the core solvent, which evaporates quicker than the shell solution during the flight of the polymer jet. Thus, the distance from the tip to the target for preparing PVP solid fibre with the evaporated solvent was

The PVP solid fibre experimentation process data showed the minimum completely evaporated solution state at 0.5 ml/hr at a needle to substrate distance greater than 19 cm and a voltage greater than 20 kV. The PVDF solution reached a minimum evaporated state at a needle to substrate distance not over 20 cm and an applied voltage above 20 kV. This condition helps to eliminate the distance parameter in the coaxial electrospinning study. Thus, to find the hollow fibre condition, the distance from the needle tip to the substrate was kept constant at 20 cm.

The shell flow rate of the PVDF at 17% mixed with a 1:1 ratio of DMF and acetone was kept constant at 4 ml/hr. The core flow rate of the PVP at 20% mixed with a 4:6 ratio of DMF and EtOH was studied at 3 different levels, these being 0, 0,5 and 1.5 ml/hr. The applied voltage was also studied at 3 levels at 20, 23 and 25 kV. The full-factorial DOE scheme was used to help identify the best condition for hollow structure fibre preparation.

B. Geometrical and structural characteristics

The geometrical characteristics section includes the morphology and structure of the intended hollow fibre for PVDF. The tested samples were prepared from 20% PVP mixed with a 7:3 ratio of DMF and EtOH. The samples were coated on to aluminium foil and were examined with the SEM. In regard to the examination of the solvent residue, a Thermo ScientificTM NicoletTM iS5 FTIR Spectrometer was deployed to study the chemical bond of the fibre after completion of the electrospinning process. As for the PVDF fibre, the FTIR spectra was applied in order to identify phase fractions between α and β . The Benchtop X-ray Powder Diffraction, Bruker D2 PHASER, was used to analyse the crystal structure of the PVDF fibre.

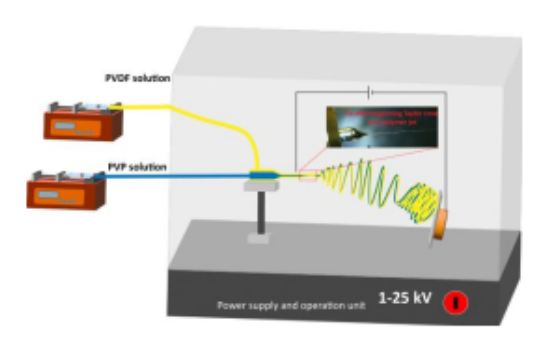


Fig. 1. The schematic of the electrospinning setup.

C. Electromechanical characteristics

A surface potential test was designed, for the examination of the electrostatic characteristics of the electrospun fibre. To study the electret characteristic of the fibre, the surface potential data was recorded 3 times as follows: 14 days after electrospinning, after corona discharge and 14 days after corona discharge.

The piezoelectric coefficient (d33) and capacitance (c) of the fibre mat were measured using Piezometer system, PM300. The standard measurements for the system—dynamic force of 0.25 N, static force of 10 N, and frequency of 110 Hz—were used for the analysis. The data was collected from the average value of 5 positions on the sample.

In order to test the energy harvesting performance, the fibre mat (2cm x2cm) was assembled with a copper electrode and PET adhesion tape as shown in Fig. 4 a). The tapping test rig was developed from previous studies and comes from inserting the sample between two electrodes and tapping at a constant rate. [18], [19] The tapping test rig was set up to provide a constant rate and pressure using a linear actuator motor. The linear actuator motor has a rated voltage of 12V, 900 rpm. The sample was attached to the oscilloscope to observe changes in voltage induced by the mechanical movement of the rig, as shown in Fig. 4 b).

III. RESULTS AND DISCUSSION

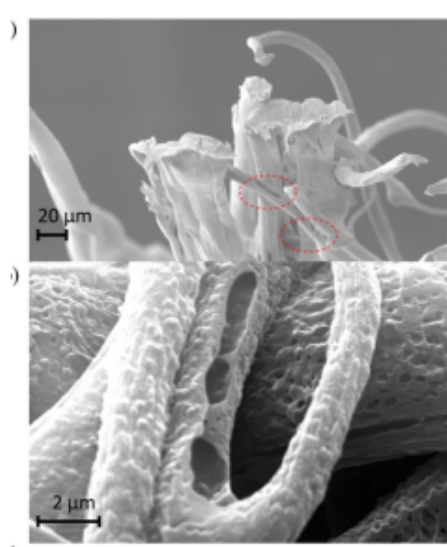
A. The geometrical characteristics

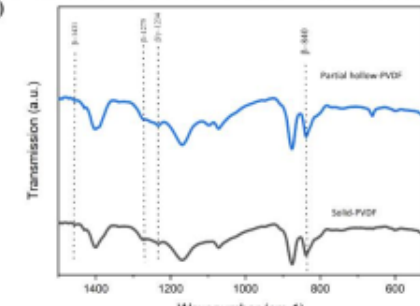
As can be seen from the SEM image in Fig. 2a) and 2b), the hollow PVDF fibres were internally broken. The diameter of the fibre was found to be around 2 microns. As seen in Fig. 2b), the obtained hollow fibres exhibit variation in forms. In this case, solidification of the outer shell occurred at the onset of the instability of the compound jet, thereby departing from a near perfect cylindrical shape. The shell and core diameters were barely observed from this technique. This may indicate that only part of the sample had formed as a hollow fibre. In

2024 International Electrical Engineering Congress (iEECON 2024) March 6-8, 2024, Pattaya Chonburi, THAILAND

addition, this could imply that the chosen condition may not be totally suitable for this technique.

The results from FTIR spectra analysis of the solid PVDF and partial hollow PVDF fibres are shown in Fig. 2 c). The FTIR spectra analysis of the characteristic transmission band of non-polar α -phase at 762, 795, 853, 975, and 1382 cm⁻¹ was hardly observed. The polar β -phase for the electrospun PVDF.





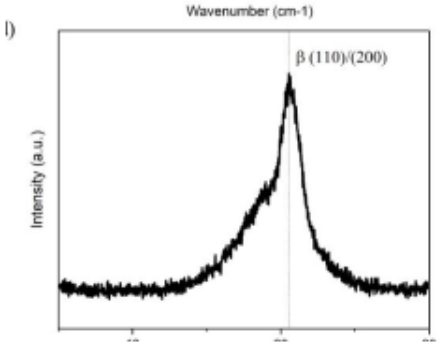


Fig. 2. a) and b) the SEM images of the electrospun partial hollow PVDF fibre c) the FTIR spectra of the solid and partial hollow PVDF electrospun fibres d) the XRD pattern of the partial hollow PVDF electrospun fibre

fibre was observed at 840, 1234, 1275, and $1431~cm^{-1}$. It can be concluded that the ability of the transform β -phase for the electrospinning technique is of a high standard. However, this cannot explain the differences in structure of the hollow and solid fibre through using the FTIR spectra.

The structural results obtained from the X-ray diffractometer, were initially determined from the PVDF sample prepared from PVDF 17% mixed with a 5:5 ratio of DMF and acetone as a shell solution and PVP 20 % mixed with a 7:3 ratio of DMF and EtOH and additional red dye for the core solution. This sample was expected to have been a hollow structured PVDF fibre. The fibre though appeared to be partially hollow when referring to the results from the SEM images. However, the degree of hollow space for the entire sample has not yet been established. The X-ray pattern, as shown in Fig. 2 d), shows the dominant peak at 20.6°, corresponding to the β -phase in a single plane crystal.

B. The electromechanical characteristics

After completion of the electrospinning process, the samples were carefully removed from the substrate using antistatic tweezers. The surface charge potential was then measured using a static fieldmeter. All samples were weighed after the electrospinning process via a four-digit laboratory scale. The samples were exposed to the environment for 14 days, and then the surface potential was measured again. After 14 days, the residual charge was removed from all samples using an isopropyl spray. Then, the samples were corona charged and measured for the surface potential charge. The samples were exposed to the environment for another 14 days. The surface potential was then measured again.

The surface potential of the core-shell PVP-PVDF and the partial hollow electrospun fibre were observed after the electrospinning process and corona charge, as shown in Table 1. Overall, the PVDF fibre shows a negative surface potential and engages the negative trapped charge after leaving the environment. The samples prepared from the core flow rate and the applied voltage is 0 ml/lr and 23 kV, respectively, show the highest surface potential at – 111.6 kV/g.

TABLE I. THE SURFACE POTENTIAL MEASUREMENT OF THE PVDF HOLLOW STRUCTURE FIBRE

Prepared	Surf	Surface		
condition (Core flow rate (ml/hr), applied voltage(kV))	After electrospi nning 14 days	After corona charge	After corona charge 14 days	potential per weight (kV/g)
0, 20	0.3	-7.8	-5.8	-98.2
0, 23	-1.4	-10.5	-8.5	-111.6
0, 25	1.7	-8.6	-4.4	-101.1
0.5, 20	1.0	-9.3	-5.3	-72.1
0.5, 23	1.6	-13.8	-5.4	-106.7
0.5, 25	3.2	-8.9	-4.5	-81.9
1.5, 20	-0.4	-6.1	-5.9	-50.2
1.5, 23	0.5	-5.3	-2.4	-32.3
1.5, 25	0.4	-3.4	-1.2	-21.7

2024 International Electrical Engineering Congress (iEECON 2024)
March 6-8, 2024, Pattaya Chonburi, THAILAND

As shown in Fig. 3, the measurement of the d33 found that the maximum d33 from the partial hollow PVDF fibre is 28.7 pC/N. However, after reading for 10s the high d33 value appeared to disappear. The maximum absolute value piezoelectric coefficient for the PVDF hollow fibre was found to be 28.7 pC/N. After reading for 10s the d33 value appeared to disappear. This may be caused by the deformation of the fibre mat structure after the force was applied during the testing procedure. The sample prepared from the PVDF solution 17 wt% and PVP 20% with the core flow rate and the applied voltage is 0 ml/hr, and 23 kV, was used in the further electromechanical test.

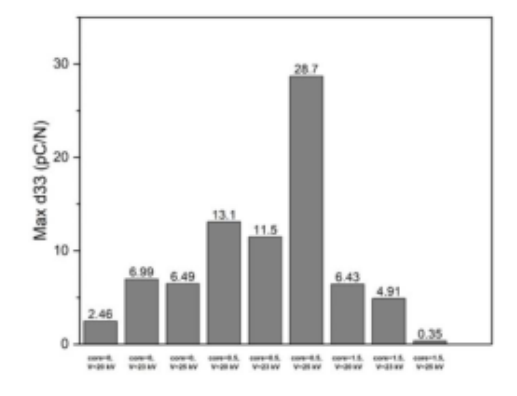


Fig. 3. The maximum absolute piezoelectric coefficient value of the coaxial PVDF measured from PiezoMeter PM-300

IV. CONCLUSION

This research aims to investigate the energy harvesting potential from the electrospun hollow fibre using a one-step coaxial hollow electrospinning method. PVDF was selected to improve the energy harvesting of the flexible polymer. The investigation of the fibre covers geometrical and electromechanical characteristics. The structure and morphology were examined and investigated through SEM. It was found that the hollow structure of the PVDF sample was revealed through the burst of the skin in the shell of the fibre. The chemical bonding results from the FTIR spectra

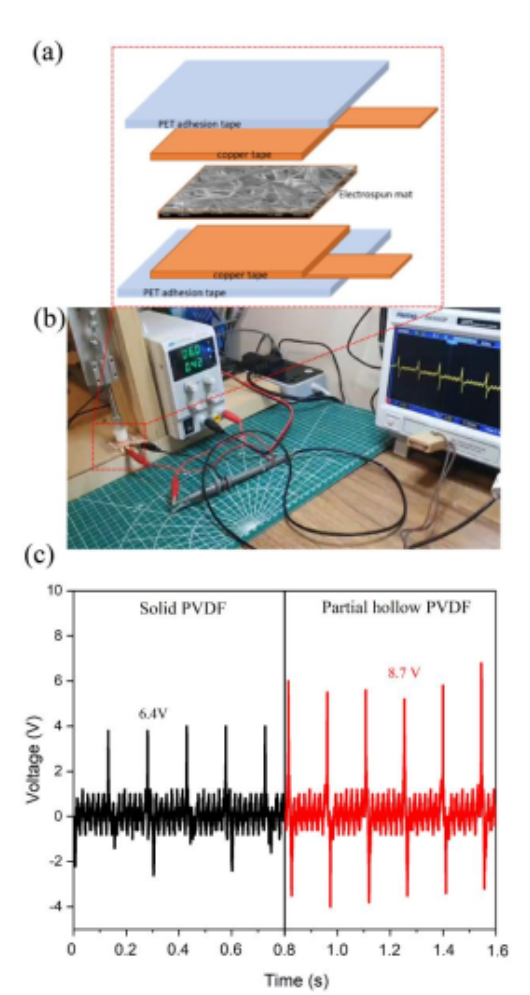


Fig. 4. a) Schematic of the testing sample for tapping test, b) the set up of tapping rig during tapping test, c) the open circuit output voltage of solid PVDF and partial hollow PVDF electrospun fibres

indicate a small level of mixing between PVP and PVDF for the partial hollow fibre. The PVDF sample revealed the dominant piezoelectric β -phase spectra, which agreed with the strong peak of β -phase obtained from the XRD result. The electromechanical test results from the solid and partial hollow PVDF samples showed the maximum output voltages at 6.4 and 8.7 V, respectively. The power density from the solid and partial hollow PVDF electrospun fibre was found at 1.60 and 2.18 mW/m², respectively.

ACKNOWLEDGMENT

Pattarinee White would like to thank the Royal Thai Government Scholarship and the Rajamangala University of Technology Krungthep for kindly supporting this research. The U.K. Royal Academy of Engineering supported the work of Stephen Beeby under the Chairs in Emerging Technologies Scheme.

Appendix A

2024 International Electrical Engineering Congress (IEECON 2024)
March 6-8, 2024, Pattaya Chonburi, THAILAND

REFERENCES

- Meticulous, "Wearable Devices Market Global Opportunity Analysis and Industry Forecast (2019-2025)," Dec. 2019.
- [2] H. Tang et al., "Ferroelectret nanogenerator with large transverse piezoelectric activity," Nano Energy, vol. 50, no. 5, pp. 52–61, 2018.
- [3] V. Bhavanasi, V. Kumar, K. Parida, J. Wang, and P. S. Lee. "Enhanced Piezoelectric Energy Harvesting Performance of Flexible PVDF-TrFE Bilayer Films with Graphene Oxide," ACS Appl. Mater. Interfaces, vol. 8, no. 1, pp. 521–529, 2016.
- [4] K. Uchino, "The development of piezoelectric materials and the new perspective," Adv. Piezoelectric Mater. Sci. Technol., pp. 1–85, 2010.
- [5] Z. Li, Y. Wang, and Z. Y. Cheng, "Electromechanical properties of poly(vinylidene-fluoride- chlorotrifluoroethylene) copolymer," Applied Physics Letters, vol. 88, no. 6. American Institute of Physics, p. 062904, 06-Feb-2006.
- [6] S. Bauer et al., "Template-based fluoroethylenepropylene piezoelectrets with tubular channels for transducer applications," Nano Energy, vol. 7, no. 1, pp. 845–869, 2019.
- [7] S. Zhukov et al., "Biodegradable cellular polylactic acid ferroelectrets with strong longitudinal and transverse piezoelectricity," Appl. Phys. Lett., vol. 117, no. 11, 2020.
- [8] S. Zhukov, D. Eder-Goy, C. Biethan, S. Fedosov, B. X. Xu, and H. Von Seggern, "Tubular fluoropolymer arrays with high piezoelectric response," Smart Mater. Struct., vol. 27, no. 1, p. 15010, 2018.
- [9] Y. Liu, S. Zhou, Y. Gao, and Y. Zhai, "Electrospun nanofibers as a wound dressing for treating diabetic foot ulcer," Asian J. Pharm. Sci., vol. 14, no. 2, pp. 130–143, 2019.
- [10] J. Lanmutti, D. Reneker, T. Ma, D. Tomasko, and D. Farson, "Electrospinning for tissue engineering scaffolds," Mater. Sci. Eng.

- C, vol. 27, no. 3, pp. 504-509, 2007.
- [11] D. Lolla, M. Lolla, A. Abutaleb, H. U. Shin, D. H. Reneker, and G. G. Chase, "Fabrication, polarisation of electrospun polyvinylidene fluoride electret fibers and effect on capturing nanoscale solid aerosols," Materials (Basel)., vol. 9, no. 8, 2016.
- [12] D. Lv et al., "Green Electrospun Nanofibers and Their Application in Air Filtration," Macromol. Mater. Eng., vol. 303, no. 12, pp. 1–18, 2018.
- [13] H. Wu et al., "Electrospun metal nanofiber webs as high-performance transparent electrode," Nano Lett., vol. 10, no. 10, pp. 4242–4248, 2010.
- [14] O. Y. Kweon, S. J. Lee, and J. H. Oh, "Wearable high-performance pressure sensors based on three-dimensional electrospun conductive nanofibers," NPG Asia Mater., vol. 10, no. 6, pp. 540–551, 2018.
- [15] T. Zhao et al., "Electrospun anatase-phase TiO2 nanofibers with different morphological structures and specific surface areas," J. Solid State Chem., vol. 20, no. 3, pp. 3008–3013, 2013.
- [16] Y. Dror et al., "One-step production of polymeric microtubes by coelectrospinning," Small, vol. 3, no. 6, pp. 1064–1073, 2007.
- [17] H. Na, P. Chen, S. C. Wong, S. Hague, and Q. Li, "Fabrication of PVDF/PVA microtubules by coaxial electrospinning," Polymer (Guildf)., vol. 53, no. 13, pp. 2736–2743, 2012.
- [18] S. K. Ghosh et al., "Electrospun gelatin nanofiber based self-powered bio-e-skin for health care monitoring," Nano Energy, vol. 36, no. April, pp. 166–175, 2017.
- [19] N. A. Hoque et al., "Er3+/Fe3+ Stimulated Electroactive, Visible Light Emitting, and High Dielectric Flexible PVDF Film Based Piezoelectric Nanogenerators: A Simple and Superior Self-Powered Energy Harvester with Remarkable Power Density," ACS Appl. Mater. Interfaces, vol. 9, no. 27, pp. 23048–23059, 2017.

Glossary of Terms

Mxene A family of two-dimensional (2D) inorganic compounds made of
transition metal carbides, nitrides, and carbonitrides with the
general formula of $M_{n+1}X_nT_X$, where M is a transition metal, X
represents carbon or nitrogen and T_{X} refers to surface termination
molecules
d ₃₃ Piezoelectric constant

Bibliography

- [1] R. Das and G. Holland, "Wearable Technology 2015-2025: Technologies, Markets, Forecasts." Accessed: Dec. 22, 2024. [Online]. Available: https://www.idtechex.com/en/research-report/wearable-technology-2015-2025-technologies-markets-forecasts/427
- [2] S. P. Beeby, M. J. Tudor, and N. M. White, "Energy harvesting vibration sources for microsystems applications," Meas Sci Technol, vol. 17, no. 12, Dec. 2006, doi: 10.1088/0957-0233/17/12/R01.
- [3] N. Gao et al., "β-Cyclodextrin functionalized coaxially electrospun poly(vinylidene fluoride)@ polystyrene membranes with higher mechanical performance for efficient removal of phenolphthalein," React Funct Polym, vol. 141, pp. 100–111, Aug. 2019, doi: 10.1016/j.reactfunctpolym.2019.05.001.
- [4] Y. Hu and Z. L. Wang, "Recent progress in piezoelectric nanogenerators as a sustainable power source in self-powered systems and active sensors," Nano Energy, vol. 14, pp. 3–14, Oct. 2014, doi: 10.1016/j.nanoen.2014.11.038.
- [5] A. Almusallam et al., "Flexible piezoelectric nano-composite films for kinetic energy harvesting from textiles," Nano Energy, vol. 33, pp. 146–156, Mar. 2017, doi: 10.1016/j.nanoen.2017.01.037.
- [6] H. Zhou et al., "Dual Mode Rotary Triboelectric Nanogenerator for Collecting Kinetic Energy from Bicycle Brake," Advanced Energy and Sustainability Research, vol. 2, no. 6, Jun. 2021, doi: 10.1002/aesr.202000113.
- [7] Y. Lu, D. Amroun, Y. Leprince-Wang, and P. Basset, "A paper-based electrostatic kinetic energy harvester with stacked multiple electret films made of electrospun polymer nanofibers," in Journal of Physics: Conference Series, Institute of Physics Publishing, Dec. 2016. doi: 10.1088/1742-6596/773/1/012032.
- [8] P. Dong et al., "A flexible solar cell/supercapacitor integrated energy device," Nano Energy, vol. 42, pp. 181–186, Dec. 2017, doi: 10.1016/j.nanoen.2017.10.035.
- [9] A. Gupta, D. V. Nandanwar, and S. R. Dhakate, "Electrospun self-assembled ZnO nanofibers structures for photocatalytic activity in natural solar radiations to degrade acid fuchsin dye," Adv Mater Lett, vol. 6, no. 8, pp. 706–710, 2015, doi: 10.5185/amlett.2015.5834.

- [10] H. K. Cho, D. H. Kim, H. S. Sin, C. H. Cho, and S. Han, "Flexible thermoelectric device using thick films for energy harvesting from the human body," Journal of the Korean Ceramic Society, vol. 54, no. 6, pp. 518–524, Nov. 2017, doi: 10.4191/kcers.2017.54.6.07.
- [11] Y. C. Hu, W. L. Hsu, Y. T. Wang, C. T. Ho, and P. Z. Chang, "Enhance the pyroelectricity of polyvinylidene fluoride by graphene-oxide doping," Sensors (Switzerland), vol. 14, no. 4, pp. 6877–6890, Apr. 2014, doi: 10.3390/s140406877.
- [12] G. S. Neugschwandtner, R. Schwödiauer, S. Bauer-Gogonea, S. Bauer, M. Paajanen, and J. Lekkala, "Piezo- and pyroelectricity of a polymer-foam space-charge electret," J Appl Phys, vol. 89, no. 8, pp. 4503–4511, Apr. 2001, doi: 10.1063/1.1355719.
- [13] S. Zhang, Z. Liu, X. Zhang, Z. Wu, and Z. Hu, "Sustainable thermal energy harvest for generating electricity," Mar. 04, 2024, Cell Press. doi: 10.1016/j.xinn.2024.100591.
- [14] Y. Zhang, M. Xie, V. Adamaki, H. Khanbareh, and C. R. Bowen, "Control of electrochemical processes using energy harvesting materials and devices," Dec. 21, 2017, Royal Society of Chemistry. doi: 10.1039/c7cs00387k.
- [15] V. Pecunia et al., "Roadmap on energy harvesting materials," JPhys Materials, vol. 6, no. 4, Oct. 2023, doi: 10.1088/2515-7639/acc550.
- [16] H. Elahi, M. Eugeni, and P. Gaudenzi, "A review on mechanisms for piezoelectric-based energy harvesters," 2018, MDPI AG. doi: 10.3390/en11071850.
- [17] Z. He et al., "Piezoelectric-Driven Self-Powered Patterned Electrochromic Supercapacitor for Human Motion Energy Harvesting," ACS Sustain Chem Eng, vol. 7, no. 1, pp. 1745–1752, Jan. 2019, doi: 10.1021/acssuschemeng.8b05606.
- [18] P. Glynne-Jones, M. J. Tudor, S. P. Beeby, and N. M. White, "An electromagnetic, vibration-powered generator for intelligent sensor systems," in Sensors and Actuators, A: Physical, Feb. 2004, pp. 344–349. doi: 10.1016/j.sna.2003.09.045.
- [19] S. P. Beeby et al., "A micro electromagnetic generator for vibration energy harvesting,"

 Journal of Micromechanics and Microengineering, vol. 17, no. 7, pp. 1257–1265, Jul. 2007,

 doi: 10.1088/0960-1317/17/7/007.
- [20] A. Šutka et al., "Inversely polarised ferroelectric polymer contact electrodes for triboelectric-like generators from identical materials," Energy Environ Sci, vol. 11, no. 6, pp. 1437–1443, Jun. 2018, doi: 10.1039/c8ee00550h.

- [21] C. Hao et al., "Two-dimensional triboelectric-electromagnetic hybrid nanogenerator for wave energy harvesting," Nano Energy, vol. 58, pp. 147–157, Apr. 2019, doi: 10.1016/j.nanoen.2019.01.033.
- [22] C. Hao et al., "Two-dimensional triboelectric-electromagnetic hybrid nanogenerator for wave energy harvesting," Nano Energy, vol. 58, pp. 147–157, Apr. 2019, doi: 10.1016/j.nanoen.2019.01.033.
- [23] Y. Ra et al., "Direct Electrospinning of Reconstructable PVDF-TrFE Nanofibrous Mat 2 onto Conductive Cement Nanocomposite for Triboelectricity-assisted Net Zero Energy Structure." [Online]. Available: https://ssrn.com/abstract=4681259
- [24] S. Wang, L. Lin, and Z. L. Wang, "Nanoscale triboelectric-effect-enabled energy conversion for sustainably powering portable electronics," Nano Lett, vol. 12, no. 12, pp. 6339–6346, Dec. 2012, doi: 10.1021/nl303573d.
- [25] T. V. Reddy, R. A. Reddy, C. Ramprasad, C. Abinay, K. S. Prasanna, and V. S. Kumar, "Design and Modelling of Nano Electric Generators for Energy Harvesting in Smart Wearable Devices," in 3rd International Conference on Innovative Mechanisms for Industry Applications, ICIMIA 2023 - Proceedings, Institute of Electrical and Electronics Engineers Inc., 2023, pp. 1384–1389. doi: 10.1109/ICIMIA60377.2023.10426559.
- [26] X. Li, X. Zeng, J. Li, B. Li, Y. Chen, and X. Zhang, "Biomechanical energy harvesting technologies for wearable electronics: Theories and devices," Aug. 01, 2024, Tsinghua University. doi: 10.1007/s40544-023-0817-8.
- [27] W. Zeng, L. Shu, Q. Li, S. Chen, F. Wang, and X. M. Tao, "Fiber-based wearable electronics: A review of materials, fabrication, devices, and applications," Aug. 20, 2014, Wiley-VCH Verlag. doi: 10.1002/adma.201400633.
- [28] W. Lin, Y. Wei, X. Wang, K. Zhai, and X. Ji, "Study on Human Motion Energy Harvesting Devices: A Review," Oct. 01, 2023, Multidisciplinary Digital Publishing Institute (MDPI). doi: 10.3390/machines11100977.
- [29] M. U. Anjum, A. Fida, I. Ahmad, and A. Iftikhar, "A broadband electromagnetic type energy harvester for smart sensor devices in biomedical applications," Sens Actuators A Phys, vol. 277, pp. 52–59, Jul. 2018, doi: 10.1016/j.sna.2018.05.001.
- [30] B. Alavikia, T. S. Almoneef, and O. M. Ramahi, "Complementary split ring resonator arrays for electromagnetic energy harvesting," Appl Phys Lett, vol. 107, no. 3, Jul. 2015, doi: 10.1063/1.4927238.

- [31] R. Yu et al., "Ambient energy harvesters in wearable electronics: fundamentals, methodologies, and applications," Dec. 01, 2024, BioMed Central Ltd. doi: 10.1186/s12951-024-02774-0.
- [32] Y. Zou, L. Bo, and Z. Li, "Recent progress in human body energy harvesting for smart bioelectronic system," May 01, 2021, KeAi Communications Co. doi: 10.1016/j.fmre.2021.05.002.
- [33] E. Cho et al., "Surface modification of electrospun polyvinylidene fluoride nanofiber membrane by plasma treatment for protein detection," J Nanosci Nanotechnol, vol. 13, no. 1, pp. 674–677, Jan. 2013, doi: 10.1166/jnn.2013.6925.
- [34] Y. Yu and X. Wang, "Chemical modification of polymer surfaces for advanced triboelectric nanogenerator development," Dec. 01, 2016, Elsevier Ltd. doi: 10.1016/j.eml.2016.02.019.
- [35] Y. Guo et al., "Triboelectric Nanogenerator-Based Near-Field Electrospinning System for Optimizing PVDF Fibers with High Piezoelectric Performance," ACS Appl Mater Interfaces, vol. 15, no. 4, pp. 5242–5252, Feb. 2023, doi: 10.1021/acsami.2c19568.
- [36] Y. Tai, S. Yang, S. Yu, A. Banerjee, N. V. Myung, and J. Nam, "Modulation of piezoelectric properties in electrospun PLLA nanofibers for application-specific self-powered stem cell culture platforms," Nano Energy, vol. 89, Nov. 2021, doi: 10.1016/j.nanoen.2021.106444.
- [37] Y. Z. Liu et al., "Review of Electrospinning in the Fabrication of Nanogenerators," Mar. 08, 2024, American Chemical Society. doi: 10.1021/acsanm.4c00306.
- [38] J. Yan et al., "Triboelectric Nanogenerators Based on Membranes Comprised of Polyurethane Fibers Loaded with Ethyl Cellulose and Barium Titanate Nanoparticles," ACS Appl Nano Mater, vol. 6, no. 7, pp. 5675–5684, Apr. 2023, doi: 10.1021/acsanm.3c00124.
- [39] D. Alexeev, N. Goedecke, J. Snedeker, and S. Ferguson, "Mechanical evaluation of electrospun poly(ε-caprolactone) single fibers," Mater Today Commun, vol. 24, Sep. 2020, doi: 10.1016/j.mtcomm.2020.101211.
- [40] P. White, D. Bavykin, M. Moshrefi-Torbati, and S. Beeby, "The Energy Harvesting Performance of a Flexible Triboelectric-Based Electrospun PTFE/PVDF Fibre †," Engineering Proceedings, vol. 30, no. 1, 2023, doi: 10.3390/engproc2023030008.
- [41] P. White, P. Pankaew, D. Bavykin, M. Moshrefi-Torbati, and S. Beeby, "The Fabrication of the Electrospun Polyvinylidene Fluoride (PVDF) Hollow Structure Fibre for Energy

- Harvesting Applications," in Proceeding 12th International Electrical Engineering Congress: Smart Factory and Intelligent Technology for Tomorrow, iEECON 2024, Institute of Electrical and Electronics Engineers Inc., 2024. doi: 10.1109/iEECON60677.2024.10537826.
- [42] P. White, P. Pankaew, D. Bavykin, M. Moshrefi-Torbati, and S. Beeby, "The investigation of the energy harvesting performance using electrospun PTFE/PVDF based on a triboelectric assembly," Smart Mater Struct, vol. 33, no. 7, Jul. 2024, doi: 10.1088/1361-665X/ad508d.
- [43] A. Šutka et al., "Contact electrification between identical polymers as the basis for triboelectric/flexoelectric materials," Physical Chemistry Chemical Physics, vol. 22, no. 23, pp. 13299–13305, Jun. 2020, doi: 10.1039/d0cp01947j.
- [44] K. Uchino, "The development of piezoelectric materials and the new perspective," Woodhead Publishing Limited, 2010, ch. 1.
- [45] S. Kim and H. Lee, "Piezoelectric ceramics with high d33 constants and their application to film speakers," Materials, vol. 14, no. 19, Oct. 2021, doi: 10.3390/ma14195795.
- [46] K. Ahmad, R. Boudville, S. Alam, S. Malaysia, A. Manaf, and N. Abdullah, "Design of Piezoelectric based Pressure Sensors for Gait Rehabilitations using D33 Mode Polarization," in Twelfth International Conference on Sensing Technology (ICST), 2018, pp. 149–153.
- [47] H. Kueppers et al., "PZT thin "lms for piezoelectric microactuator applications," Sensors and Actuators A, no. 97–98, p. 680684, 2002.
- [48] M. Acosta et al., "BaTiO3-based piezoelectrics: Fundamentals, current status, and perspectives," Dec. 01, 2017, American Institute of Physics Inc. doi: 10.1063/1.4990046.
- [49] H. Gullapalli et al., "Flexible piezoelectric zno-paper nanocomposite strain sensor," Small, vol. 6, no. 15, pp. 1641–1646, Aug. 2010, doi: 10.1002/smll.201000254.
- [50] K. S. Ramadan, D. Sameoto, and S. Evoy, "A review of piezoelectric polymers as functional materials for electromechanical transducers," Mar. 2014. doi: 10.1088/0964-1726/23/3/033001.
- [51] Z. Luo et al., "Energy Harvesting Study on Single and Multilayer Ferroelectret Foams under Compressive Force", doi: 10.1109/TDEI.2014.004912.

- [52] Z. Yang, H. Peng, W. Wang, and T. Liu, "Crystallization behavior of poly(ε-caprolactone)/layered double hydroxide nanocomposites," J Appl Polym Sci, vol. 116, no. 5, pp. 2658–2667, Jun. 2010, doi: 10.1002/app.31787.
- [53] S. Bauer, R. Gerhard-Multhaupt, and G. M. Sessler, "Ferroelectrets: Soft Electroactive Foams for Transducers," Phys Today, vol. 57, no. 2, pp. 37–43, 2004, doi: 10.1063/1.1688068.
- [54] O. Hamdi, F. Mighri, and D. Rodrigue, "Piezoelectric cellular polymer films: Fabrication, properties and applications," 2018, AIMS Press. doi: 10.3934/MATERSCI.2018.5.845.
- [55] A. Mohebbi, F. Mighri, A. Ajji, and D. Rodrigue, "Cellular Polymer Ferroelectret: A Review on Their Development and Their Piezoelectric Properties," Advances in Polymer Technology, vol. 37, no. 2, pp. 468–483, Mar. 2018, doi: 10.1002/adv.21686.
- [56] Y. Zhang et al., "Ferroelectret materials and devices for energy harvesting applications," Nano Energy, vol. 57, pp. 118–140, Mar. 2019, doi: 10.1016/j.nanoen.2018.12.040.
- [57] A. Šutka et al., "Engineering Polymer Interfaces: A Review toward Controlling Triboelectric Surface Charge," Sep. 13, 2023, John Wiley and Sons Inc. doi: 10.1002/admi.202300323.
- [58] S. K. Ghosh, T. K. Sinha, B. Mahanty, and D. Mandal, "Self-poled Efficient Flexible 'Ferroelectretic' Nanogenerator: A New Class of Piezoelectric Energy Harvester," Energy Technology, vol. 3, no. 12, pp. 1190–1197, Dec. 2015, doi: 10.1002/ente.201500167.
- [59] H. Yan, L. Yayan, and Y. Yifei, "Simultaneous stretching and static electric field poling of poly(vinylidene fluoride-hexafluoropropylene) copolymer films," in Polymer Engineering and Science, John Wiley and Sons Inc., 2007, pp. 1630–1633. doi: 10.1002/pen.20843.
- [60] Y. Zhang et al., "Ferroelectret materials and devices for energy harvesting applications," Nano Energy, vol. 57, no. December, pp. 118–140, 2019, doi: 10.1016/j.nanoen.2018.12.040.
- [61] S. Wang, L. Lin, and Z. L. Wang, "Nanoscale triboelectric-effect-enabled energy conversion for sustainably powering portable electronics," Nano Lett, vol. 12, no. 12, pp. 6339–6346, Dec. 2012, doi: 10.1021/nl303573d.
- [62] J. Mort, "Polymers, Electronic Properties," 2001.
- [63] H. Zou et al., "Quantifying the triboelectric series," Nat Commun, vol. 10, no. 1, Dec. 2019, doi: 10.1038/s41467-019-09461-x.

- [64] A. F. Diaz and R. M. Felix-Navarro, "A semi-quantitative tribo-electric series for polymeric materials: The influence of chemical structure and properties," J Electrostat, vol. 62, no. 4, pp. 277–290, Nov. 2004, doi: 10.1016/j.elstat.2004.05.005.
- [65] Y. Zi, S. Niu, J. Wang, Z. Wen, W. Tang, and Z. L. Wang, "Standards and figure-of-merits for quantifying the performance of triboelectric nanogenerators," Nat Commun, vol. 6, no. May, 2015, doi: 10.1038/ncomms9376.
- [66] H. Zhang, L. Yao, L. Quan, and X. Zheng, "Theories for triboelectric nanogenerators: A comprehensive review," Jan. 01, 2020, De Gruyter. doi: 10.1515/ntrev-2020-0049.
- [67] I. Logothetis, S. Vassiliadis, and E. Siores, "Triboelectric effect in energy harvesting," in IOP Conference Series: Materials Science and Engineering, Institute of Physics Publishing, Nov. 2017. doi: 10.1088/1757-899X/254/4/042021.
- [68] J. Chung, S. Lee, H. Yong, H. Moon, D. Choi, and S. Lee, "Self-packaging elastic bellows-type triboelectric nanogenerator," Nano Energy, vol. 20, pp. 84–93, Feb. 2016, doi: 10.1016/j.nanoen.2015.12.006.
- [69] C. Xu et al., "On the Electron-Transfer Mechanism in the Contact-Electrification Effect," Advanced Materials, vol. 30, no. 15, Apr. 2018, doi: 10.1002/adma.201706790.
- [70] O. Verners et al., "Smooth polymers charge negatively: Controlling contact electrification polarity in polymers," Nano Energy, vol. 104, Dec. 2022, doi: 10.1016/j.nanoen.2022.107914.
- [71] H. T. Baytekin, B. Baytekin, J. T. Incorvati, and B. A. Grzybowski, "Material transfer and polarity reversal in contact charging," Angewandte Chemie International Edition, vol. 51, no. 20, pp. 4843–4847, May 2012, doi: 10.1002/anie.201200057.
- [72] L. Lapčinskis et al., "Hybrid Tribo-Piezo-Electric Nanogenerator with Unprecedented Performance Based on Ferroelectric Composite Contacting Layers," ACS Appl Energy Mater, vol. 2, no. 6, pp. 4027–4032, Jun. 2019, doi: 10.1021/acsaem.9b00836.
- [73] Y. Liu, S. Zhou, Y. Gao, and Y. Zhai, "Electrospun nanofibers as a wound dressing for treating diabetic foot ulcer," Mar. 01, 2019, Shenyang Pharmaceutical University. doi: 10.1016/j.ajps.2018.04.004.
- [74] Y. Zhang, H. Ouyang, T. L. Chwee, S. Ramakrishna, and Z. M. Huang, "Electrospinning of gelatin fibers and gelatin/PCL composite fibrous scaffolds," J Biomed Mater Res B Appl Biomater, vol. 72, no. 1, pp. 156–165, Jan. 2005, doi: 10.1002/jbm.b.30128.

- [75] D. Lv et al., "Green Electrospun Nanofibers and Their Application in Air Filtration," Dec. 01, 2018, Wiley-VCH Verlag. doi: 10.1002/mame.201800336.
- [76] H. Wu et al., "Electrospun metal nanofiber webs as high-performance transparent electrode," Nano Lett, vol. 10, no. 10, pp. 4242–4248, Oct. 2010, doi: 10.1021/nl102725k.
- [77] S. Lin et al., "Electrospun Polytetrafluoroethylene Nanofibrous Membrane for High-Performance Self-Powered Sensors," Nanoscale Res Lett, vol. 14, no. 1, Dec. 2019, doi: 10.1186/s11671-019-3091-y.
- [78] O. Y. Kweon, S. J. Lee, and J. H. Oh, "Wearable high-performance pressure sensors based on three-dimensional electrospun conductive nanofibers," NPG Asia Mater, vol. 10, no. 6, pp. 540–551, Jun. 2018, doi: 10.1038/s41427-018-0041-6.
- [79] M. Liu et al., "A Review: Electrospun Nanofiber Materials for Lithium-Sulfur Batteries," Dec. 01, 2019, Wiley-VCH Verlag. doi: 10.1002/adfm.201905467.
- [80] D. Han and A. J. Steckl, "Coaxial Electrospinning Formation of Complex Polymer Fibers and their Applications," Oct. 01, 2019, Wiley-VCH Verlag. doi: 10.1002/cplu.201900281.
- [81] A. Haider, S. Haider, and I. K. Kang, "A comprehensive review summarizing the effect of electrospinning parameters and potential applications of nanofibers in biomedical and biotechnology," Dec. 01, 2018, Elsevier B.V. doi: 10.1016/j.arabjc.2015.11.015.
- [82] S. Megelski, J. S. Stephens, D. Bruce Chase, and J. F. Rabolt, "Micro- and nanostructured surface morphology on electrospun polymer fibers," Macromolecules, vol. 35, no. 22, pp. 8456–8466, Oct. 2002, doi: 10.1021/ma020444a.
- [83] S. Zhang, C. Campagne, and F. Salaün, "Influence of solvent selection in the electrospraying process of polycaprolactone," Jan. 24, 2019, MDPI AG. doi: 10.3390/app9030402.
- [84] J. Lannutti, D. Reneker, T. Ma, D. Tomasko, and D. Farson, "Electrospinning for tissue engineering scaffolds," Materials Science and Engineering C, vol. 27, no. 3, pp. 504–509, Apr. 2007, doi: 10.1016/j.msec.2006.05.019.
- [85] S. Chen, R. Li, X. Li, and J. Xie, "Electrospinning: An enabling nanotechnology platform for drug delivery and regenerative medicine," Adv Drug Deliv Rev, vol. 132, pp. 188–213, Jul. 2018, doi: 10.1016/j.addr.2018.05.001.

- [86] S. Yuan, F. Lei, Z. Liu, Q. Tong, T. Si, and R. X. Xu, "Coaxial electrospray of curcumin-loaded microparticles for sustained drug release," PLoS One, vol. 10, no. 7, Jul. 2015, doi: 10.1371/journal.pone.0132609.
- [87] W. Liu, C. Huang, and X. Jin, "Tailoring the grooved texture of electrospun polystyrene nanofibers by controlling the solvent system and relative humidity," Nanoscale Res Lett, vol. 9, no. 1, pp. 1–10, 2014, doi: 10.1186/1556-276X-9-350.
- [88] W. Liu, C. Huang, and X. Jin, "Electrospinning of Grooved Polystyrene Fibers: Effect of Solvent Systems," Nanoscale Res Lett, vol. 10, no. 1, Dec. 2015, doi: 10.1186/s11671-015-0949-5.
- [89] H. Na, P. Chen, S. C. Wong, S. Hague, and Q. Li, "Fabrication of PVDF/PVA microtubules by coaxial electrospinning," Polymer (Guildf), vol. 53, no. 13, pp. 2736–2743, Jun. 2012, doi: 10.1016/j.polymer.2012.04.021.
- [90] P. K. Szewczyk et al., "Enhanced Piezoelectricity of Electrospun Polyvinylidene Fluoride Fibers for Energy Harvesting," ACS Appl Mater Interfaces, vol. 12, no. 11, pp. 13575–13583, Mar. 2020, doi: 10.1021/acsami.0c02578.
- [91] A. K. Moghe and B. S. Gupta, "Co-axial electrospinning for nanofiber structures: Preparation and applications," Polymer Reviews, vol. 48, no. 2, pp. 353–377, Apr. 2008, doi: 10.1080/15583720802022257.
- [92] D. Li and Y. Xia, "Direct fabrication of composite and ceramic hollow nanofibers by electrospinning," Nano Lett, vol. 4, no. 5, pp. 933–938, May 2004, doi: 10.1021/nl049590f.
- [93] I. G. Loscertales, A. Barrero, M. Márquez, R. Spretz, R. Velarde-Ortiz, and G. Larsen, "Electrically Forced Coaxial Nanojets for One-Step Hollow Nanofiber Design," J Am Chem Soc, vol. 126, no. 17, pp. 5376–5377, May 2004, doi: 10.1021/ja049443j.
- [94] Y. Cheng et al., "Preparation of TiO2 hollow nanofibers by electrospining combined with sol-gel process," CrystEngComm, vol. 12, no. 7, pp. 2256–2260, Jul. 2010, doi: 10.1039/b922564a.
- [95] T. Zhao et al., "Multichannel TiO2 hollow fibers with enhanced photocatalytic activity," J Mater Chem, vol. 20, no. 24, pp. 5095–5099, 2010, doi: 10.1039/c0jm00484g.
- [96] J. Zhang, S. W. Choi, and S. S. Kim, "Micro- and nano-scale hollow TiO2 fibers by coaxial electrospinning: Preparation and gas sensing," J Solid State Chem, vol. 184, no. 11, pp. 3008–3013, Nov. 2011, doi: 10.1016/j.jssc.2011.09.014.

- [97] G. H. Lee, J. C. Song, and K. B. Yoon, "Controlled wall thickness and porosity of polymeric hollow nanofibers by coaxial electrospinning," Macromol Res, vol. 18, no. 6, pp. 571–576, Jun. 2010, doi: 10.1007/s13233-010-0607-9.
- [98] Y. Dror et al., "One-step production of polymeric microtubes by co-electrospinning," Small, vol. 3, no. 6, pp. 1064–1073, Jun. 2007, doi: 10.1002/smll.200600536.
- [99] A. V. Bazilevsky, A. L. Yarin, and C. M. Megaridis, "Co-electrospinning of core-shell fibers using a single-nozzle technique," Langmuir, vol. 23, no. 5, pp. 2311–2314, Feb. 2007, doi: 10.1021/la063194q.
- [100] C. Wang, L. Wang, and M. Wang, "Evolution of core-shell structure: From emulsions to ultrafine emulsion electrospun fibers," Mater Lett, vol. 124, pp. 192–196, Jun. 2014, doi: 10.1016/j.matlet.2014.03.086.
- [101] M. Wang, Q. Gao, J. Gao, C. Zhu, and K. Chen, "Core-shell PEDOT:PSS/SA composite fibers fabricated: Via a single-nozzle technique enable wearable sensor applications," J Mater Chem C Mater, vol. 8, no. 13, pp. 4564–4571, Apr. 2020, doi: 10.1039/c9tc05527d.
- [102] S. A. Mirmohammad Sadeghi, S. Borhani, A. Zadhoush, and M. Dinari, "Single nozzle electrospinning of encapsulated epoxy and mercaptan in PAN for self-healing application," Polymer (Guildf), vol. 186, Jan. 2020, doi: 10.1016/j.polymer.2019.122007.
- [103] S. D. A. Zaidi et al., "Single-nozzle electrospun core-shell MoS2@FexOy@CNF anodes for lithium and potassium-ion batteries," J Alloys Compd, vol. 848, Dec. 2020, doi: 10.1016/j.jallcom.2020.156531.
- [104] A. Patanaik, V. Jacobs, and R. D. Anandjiwala, "Performance evaluation of electrospun nanofibrous membrane," J Memb Sci, vol. 352, no. 1–2, pp. 136–142, Apr. 2010, doi: 10.1016/j.memsci.2010.02.009.
- [105] Z. X. Huang et al., "Electrospun polyvinylidene fluoride containing nanoscale graphite platelets as electret membrane and its application in air filtration under extreme environment," Polymer (Guildf), vol. 131, pp. 143–150, Nov. 2017, doi: 10.1016/j.polymer.2017.10.033.
- [106] R. R. Cai, L. Z. Zhang, and A. B. Bao, "PM collection performance of electret filters electrospun with different dielectric materials-a numerical modeling and experimental study," Build Environ, vol. 131, pp. 210–219, Mar. 2018, doi: 10.1016/j.buildenv.2017.12.036.

- [107] Y. Liao, C. H. Loh, M. Tian, R. Wang, and A. G. Fane, "Progress in electrospun polymeric nanofibrous membranes for water treatment: Fabrication, modification and applications," Feb. 01, 2018, Elsevier Ltd. doi: 10.1016/j.progpolymsci.2017.10.003.
- [108] G. M. Sessler and J. Hillenbrand, "Electromechanical Response of Cellular Electret Films."
- [109] G. Collins, J. Federici, Y. Imura, and L. H. Catalani, "Charge generation, charge transport, and residual charge in the electrospinning of polymers: A review of issues and complications," J Appl Phys, vol. 111, no. 4, Feb. 2012, doi: 10.1063/1.3682464.
- [110] D. Mandal, S. Yoon, and K. J. Kim, "Origin of piezoelectricity in an electrospun poly(vinylidene fluoride-trifluoroethylene) nanofiber web-based nanogenerator and nanopressure sensor," Macromol Rapid Commun, vol. 32, no. 11, pp. 831–837, Jun. 2011, doi: 10.1002/marc.201100040.
- [111] L. H. Catalani, G. Collins, and M. Jaffe, "Evidence for molecular orientation and residual charge in the electrospinning of poly(butylene terephthalate) nanofibers,"

 Macromolecules, vol. 40, no. 5, pp. 1693–1697, Mar. 2007, doi: 10.1021/ma061342d.
- [112] H. Gao, W. He, Y. B. Zhao, D. M. Opris, G. Xu, and J. Wang, "Electret mechanisms and kinetics of electrospun nanofiber membranes and lifetime in filtration applications in comparison with corona-charged membranes," J Memb Sci, vol. 600, Apr. 2020, doi: 10.1016/j.memsci.2020.117879.
- [113] Z. A. Alhasssan, Y. S. Burezq, R. Nair, and N. Shehata, "Polyvinylidene difluoride piezoelectric electrospun nanofibers: Review in synthesis, fabrication, characterizations, and applications," 2018, Hindawi Limited. doi: 10.1155/2018/8164185.
- [114] G. Kalimuldina et al., "A review of piezoelectric pvdf film by electrospinning and its applications," Sep. 02, 2020, MDPI AG. doi: 10.3390/s20185214.
- [115] P. Hu, D. Zheng, C. Zhao, Y. Zhang, and J. Niu, "Linear dependence between content of effective piezo-phase and mechanical-to-electrical conversion in electrospun poly(vinylidene fluoride) fibrous membrane," Mater Lett, vol. 218, pp. 71–75, May 2018, doi: 10.1016/j.matlet.2018.01.142.
- [116] D. Sengupta, A. Michael, C. Y. Kwok, J. Miao, and A. G. P. Kottapalli, "Optimized Polyvinylidene Fluoride Nanofiber Webs for Flexible Energy Harvesters," MDPI AG, Nov. 2018, p. 857. doi: 10.3390/proceedings2130857.

- [117] M. Forouharshad, S. G. King, W. Buxton, P. Kunovski, and V. Stolojan, "Textile-Compatible, Electroactive Polyvinylidene Fluoride Electrospun Mats for Energy Harvesting," Macromol Chem Phys, vol. 220, no. 24, Dec. 2019, doi: 10.1002/macp.201900364.
- [118] "Henry C. Savage Chapter 6 Piezoelectric and Pyroelectric Calculations."
- [119] X. Wang, F. Sun, G. Yin, Y. Wang, B. Liu, and M. Dong, "Tactile-sensing based on flexible PVDF nanofibers via electrospinning: A review," Feb. 01, 2018, MDPI AG. doi: 10.3390/s18020330.
- [120] S. Huan, L. Bai, G. Liu, W. Cheng, and G. Han, "Electrospun nanofibrous composites of polystyrene and cellulose nanocrystals: Manufacture and characterization," RSC Adv, vol. 5, no. 63, pp. 50756–50766, 2015, doi: 10.1039/c5ra06117b.
- [121] V. Datsyuk et al., "Polystyrene nanofibers for nonwoven porous building insulation materials," Engineering Reports, vol. 1, no. 2, Sep. 2019, doi: 10.1002/eng2.12037.
- [122] S. Rahmani, A. Arefazar, and M. Latifi, "PMMA/PS coaxial electrospinning: Core-shell fiber morphology as a function of material parameters," Mater Res Express, vol. 4, no. 3, Mar. 2017, doi: 10.1088/2053-1591/aa600c.
- [123] C. Huang, H. Niu, J. Wu, Q. Ke, X. Mo, and T. Lin, "Needleless electrospinning of polystyrene fibers with an oriented surface line texture," J Nanomater, vol. 2012, 2012, doi: 10.1155/2012/473872.
- [124] T. Uyar and F. Besenbacher, "Electrospinning of uniform polystyrene fibers: The effect of solvent conductivity," Polymer (Guildf), vol. 49, no. 24, pp. 5336–5343, Nov. 2008, doi: 10.1016/j.polymer.2008.09.025.
- [125] Y. Ishii et al., "High electromechanical response from bipolarly charged as-electrospun polystyrene fiber mat," Smart Mater Struct, vol. 28, no. 8, Jul. 2019, doi: 10.1088/1361-665X/ab2e3a.
- [126] D. Kang et al., "Deformation-contributed negative triboelectric property of polytetrafluoroethylene: A density functional theory calculation," Nano Energy, vol. 100, Sep. 2022, doi: 10.1016/j.nanoen.2022.107531.
- [127] T. Huang, C. Wang, H. Yu, H. Wang, Q. Zhang, and M. Zhu, "Human walking-driven wearable all-fiber triboelectric nanogenerator containing electrospun polyvinylidene fluoride piezoelectric nanofibers," Nano Energy, vol. 14, pp. 226–235, Nov. 2014, doi: 10.1016/j.nanoen.2015.01.038.

- [128] H. J. Kim et al., "Silk Nanofiber-Networked Bio-Triboelectric Generator: Silk Bio-TEG," Adv Energy Mater, vol. 6, no. 8, Apr. 2016, doi: 10.1002/aenm.201502329.
- [129] H. J. Qiu et al., "A calibration-free self-powered sensor for vital sign monitoring and finger tap communication based on wearable triboelectric nanogenerator," Nano Energy, vol. 58, no. January, pp. 536–542, 2019, doi: 10.1016/j.nanoen.2019.01.069.
- [130] N. Wang et al., "Anisotropic Triboelectric Nanogenerator Based on Ordered Electrospinning," ACS Appl Mater Interfaces, vol. 12, no. 41, pp. 46205–46211, Oct. 2020, doi: 10.1021/acsami.0c13938.
- [131] S. C. Kim et al., "Nanofiber filter performance improvement: Nanofiber layer uniformity and branched nanofiber," Aerosol Air Qual Res, vol. 20, no. 1, pp. 80–88, Jan. 2020, doi: 10.4209/aagr.2019.07.0343.
- [132] B. Mahanty, K. Maity, S. Sarkar, and D. Mandal, "Polymer nanofiber based triboelectric nanogenerator for energy harvesting and self-powered electronics," in AIP Conference Proceedings, American Institute of Physics Inc., Nov. 2020. doi: 10.1063/5.0016777.
- [133] L. N. Zhou et al., "High output achieved by sliding electrification of an electrospun nanograting," Nanoscale, vol. 13, no. 41, pp. 17417–17427, Nov. 2021, doi: 10.1039/d1nr04769h.
- [134] D. Treasa Mathew et al., "Surface Area Enhanced Nylon-6,6 Nanofiber Engineered Triboelectric Nanogenerator for Self-Powered Seat Monitoring Applications," ACS Sustain Chem Eng, vol. 10, no. 43, pp. 14126–14135, Oct. 2022, doi: 10.1021/acssuschemeng.2c02834.
- [135] J. Park, S. Jo, Y. Kim, S. Zaman, and D. Kim, "Electrospun Nanofiber Covered Polystyrene Micro-Nano Hybrid Structures for Triboelectric Nanogenerator and Supercapacitor," Micromachines (Basel), vol. 13, no. 3, Mar. 2022, doi: 10.3390/mi13030380.
- [136] Y. Song et al., "Forward polarization enhanced all-polymer based sustainable triboelectric nanogenerator from oriented electrospinning PVDF/cellulose nanofibers for energy harvesting," Sustain Energy Fuels, vol. 6, no. 9, pp. 2377–2386, Apr. 2022, doi: 10.1039/d2se00321j.
- [137] S. Bairagi et al., "High-Performance Triboelectric Nanogenerators Based on Commercial Textiles: Electrospun Nylon 66 Nanofibers on Silk and PVDF on Polyester," ACS Appl Mater Interfaces, vol. 14, no. 39, pp. 44591–44603, Oct. 2022, doi: 10.1021/acsami.2c13092.

- [138] F. R. Fan, Z. Q. Tian, and Z. Lin Wang, "Flexible triboelectric generator," Nano Energy, vol. 1, no. 2, pp. 328–334, Mar. 2012, doi: 10.1016/j.nanoen.2012.01.004.
- [139] J. Yang, J. Chen, Y. Liu, W. Yang, Y. Su, and Z. L. Wang, "Triboelectrification-based organic film nanogenerator for acoustic energy harvesting and self-powered active acoustic sensing," ACS Nano, vol. 8, no. 3, pp. 2649–2657, Mar. 2014, doi: 10.1021/nn4063616.
- [140] K. Xia, J. Fu, and Z. Xu, "Multiple-Frequency High-Output Triboelectric Nanogenerator Based on a Water Balloon for All-Weather Water Wave Energy Harvesting," Adv Energy Mater, vol. 10, no. 28, Jul. 2020, doi: 10.1002/aenm.202000426.
- [141] Z. Lin et al., "Flexible triboelectric nanogenerator toward ultrahigh-frequency vibration sensing," Nano Res, vol. 15, no. 8, pp. 7484–7491, Aug. 2022, doi: 10.1007/s12274-022-4363-x.
- [142] T. Huang, M. Lu, H. Yu, Q. Zhang, H. Wang, and M. Zhu, "Enhanced power output of a triboelectric nanogenerator composed of electrospun nanofiber mats doped with graphene oxide," Sci Rep, vol. 5, Sep. 2015, doi: 10.1038/srep13942.
- [143] S. Cheon et al., "High-Performance Triboelectric Nanogenerators Based on Electrospun Polyvinylidene Fluoride–Silver Nanowire Composite Nanofibers," Adv Funct Mater, vol. 28, no. 2, pp. 1–7, 2018, doi: 10.1002/adfm.201703778.
- [144] J. H. Zhang, Y. Li, J. Du, X. Hao, and Q. Wang, "Bio-inspired hydrophobic/cancellous/hydrophilic Trimurti PVDF mat-based wearable triboelectric nanogenerator designed by self-assembly of electro-pore-creating," Nano Energy, vol. 61, pp. 486–495, Jul. 2019, doi: 10.1016/j.nanoen.2019.04.065.
- [145] C. Jiang et al., "All-electrospun flexible triboelectric nanogenerator based on metallic MXene nanosheets," Nano Energy, vol. 59, pp. 268–276, May 2019, doi: 10.1016/j.nanoen.2019.02.052.
- [146] X. Pu, J. W. Zha, C. L. Zhao, S. B. Gong, J. F. Gao, and R. K. Y. Li, "Flexible PVDF/nylon-11 electrospun fibrous membranes with aligned ZnO nanowires as potential triboelectric nanogenerators," Chemical Engineering Journal, vol. 398, no. 30, p. 125526, 2020, doi: 10.1016/j.cej.2020.125526.
- [147] X. Zhang et al., "Synergistic enhancement of coaxial nanofiber-based triboelectric nanogenerator through dielectric and dispersity modulation," Nano Energy, vol. 75, Sep. 2020, doi: 10.1016/j.nanoen.2020.104894.

- [148] J. H. Bae et al., "Nano-and microfiber-based fully fabric triboelectric nanogenerator for wearable devices," Polymers (Basel), vol. 12, no. 3, Mar. 2020, doi: 10.3390/polym12030658.
- [149] Y. Li et al., "Mechanically interlocked stretchable nanofibers for multifunctional wearable triboelectric nanogenerator," Nano Energy, vol. 78, Dec. 2020, doi: 10.1016/j.nanoen.2020.105358.
- [150] Z. Yu et al., "Nanoporous PVDF Hollow Fiber Employed Piezo-Tribo Nanogenerator for Effective Acoustic Harvesting," ACS Appl Mater Interfaces, vol. 13, no. 23, pp. 26981–26988, Jun. 2021, doi: 10.1021/acsami.1c04489.
- [151] S. M. S. Rana et al., "Electrospun PVDF-TrFE/MXene Nanofiber Mat-Based Triboelectric Nanogenerator for Smart Home Appliances," ACS Appl Mater Interfaces, vol. 13, no. 4, pp. 4955–4967, 2021, doi: 10.1021/acsami.0c17512.
- [152] J. Huang, Y. Hao, M. Zhao, W. Li, F. Huang, and Q. Wei, "All-Fiber-Structured Triboelectric Nanogenerator via One-Pot Electrospinning for Self-Powered Wearable Sensors," ACS Applied Materials and Interfaces, vol. 13, no. 21, pp. 24774–24784, Jun. 2021, doi: 10.1021/acsami.1c03894.
- [153] L. Shi et al., "High-performance triboelectric nanogenerator based on electrospun PVDF-graphene nanosheet composite nanofibers for energy harvesting," Nano Energy, vol. 80, no. November 2020, p. 105599, 2021, doi: 10.1016/j.nanoen.2020.105599.
- [154] Y. Kim, X. Wu, C. Lee, and J. H. Oh, "Characterization of PI/PVDF-TrFE Composite Nanofiber-Based Triboelectric Nanogenerators Depending on the Type of the Electrospinning System," ACS Appl Mater Interfaces, vol. 13, no. 31, pp. 36967–36975, Aug. 2021, doi: 10.1021/acsami.1c04450.
- [155] S. M. S. Rana et al., "Electrospun PVDF-TrFE/MXene Nanofiber Mat-Based Triboelectric Nanogenerator for Smart Home Appliances," ACS Appl Mater Interfaces, vol. 13, no. 4, pp. 4955–4967, Feb. 2021, doi: 10.1021/acsami.0c17512.
- [156] H. Wang et al., "An all-fibrous triboelectric nanogenerator with enhanced outputs depended on the polystyrene charge storage layer," Nano Energy, vol. 90, Dec. 2021, doi: 10.1016/j.nanoen.2021.106515.
- [157] S. Banerjee, S. Bairagi, and S. W. Ali, "A lead-free flexible piezoelectric-triboelectric hybrid nanogenerator composed of uniquely designed PVDF/KNN-ZS nanofibrous web," Energy, vol. 244, Apr. 2022, doi: 10.1016/j.energy.2022.123102.

- [158] M. F. Lin, K. W. Chang, C. H. Lee, X. X. Wu, and Y. C. Huang, "Electrospun P3HT/PVDF-HFP semiconductive nanofibers for triboelectric nanogenerators," Sci Rep, vol. 12, no. 1, Dec. 2022, doi: 10.1038/s41598-022-19306-1.
- [159] C. Sun, G. Zu, Y. Wei, X. Song, and X. Yang, "Flexible Triboelectric Nanogenerators Based on Electrospun Poly(vinylidene fluoride) with MoS2/Carbon Nanotube Composite Nanofibers," Langmuir, vol. 38, no. 4, pp. 1479–1487, Feb. 2022, doi: 10.1021/acs.langmuir.1c02785.
- [160] J. Xia, Z. Zheng, and Y. Guo, "Mechanically and electrically robust, electro-spun PVDF/PMMA blend films for durable triboelectric nanogenerators," Compos Part A Appl Sci Manuf, vol. 157, Jun. 2022, doi: 10.1016/j.compositesa.2022.106914.
- [161] S. Wanwong, W. Sangkhun, and P. Jiamboonsri, "Electrospun Cyclodextrin/Poly(L-lactic acid) Nanofibers for Efficient Air Filter: Their PM and VOC Removal Efficiency and Triboelectric Outputs," Polymers (Basel), vol. 15, no. 722, 2023.
- [162] J. Yin, J. Wang, S. Ramakrishna, and L. Xu, "All-Electrospun Triboelectric Nanogenerator Incorporating Carbon- Black-Loaded Nanofiber Membranes for Self-Powered Wearable Sensors," 2023, doi: 10.1021/acsanm.3c01891.
- [163] C. Lee, C. Cho, and J. H. Oh, "Highly flexible triboelectric nanogenerators with electrospun PVDF-TrFE nanofibers on MWCNTs/PDMS/AgNWs composite electrodes," Compos B Eng, vol. 255, Apr. 2023, doi: 10.1016/j.compositesb.2023.110622.
- [164] X. Shi, W. Si, J. Zhu, and S. Zhang, "Boosting the Electrical Performance of PLA-Based Triboelectric Nanogenerators for Sustainable Power Sources and Self-Powered Sensing," Small, vol. 20, no. 15, Apr. 2024, doi: 10.1002/smll.202307620.
- [165] H. M. Mousa, A. G. Arafat, A. N. M. Omran, and G. T. Abdel-Jaber, "A hybrid triboelectric and piezoelectric nanogenerator with α-Al2O3 NPs/Doku and PVDF/SWCNTs nanofibers," Colloids Surf A Physicochem Eng Asp, vol. 656, Jan. 2023, doi: 10.1016/j.colsurfa.2022.130403.
- [166] J. Yin, J. Li, S. Ramakrishna, and L. Xu, "Hybrid-Structured Electrospun Nanofiber Membranes as Triboelectric Nanogenerators for Self-Powered Wearable Electronics," ACS Sustain Chem Eng, vol. 11, no. 38, pp. 14020–14030, Sep. 2023, doi: 10.1021/acssuschemeng.3c03025.

- [167] C. Luo et al., "Preparation and application of high performance PVDF/PS electrospinning film-based triboelectric nanogenerator," Chem Phys Lett, vol. 813, Feb. 2023, doi: 10.1016/j.cplett.2022.140276.
- [168] B. Lin et al., "Preparation of MWCNTs/PVDF composites with high-content β form crystalline of PVDF and enhanced dielectric constant by electrospinning-hot pressing method," Diam Relat Mater, vol. 131, Jan. 2023, doi: 10.1016/j.diamond.2022.109556.
- [169] Y. Xie et al., "Triboelectric nanogenerator based on flexible Janus nanofiber membrane with simultaneous high charge generation and charge capturing abilities," Chemical Engineering Journal, vol. 452, Jan. 2023, doi: 10.1016/j.cej.2022.139393.
- [170] Y. Zheng, J. Li, T. Xu, H. Cui, and X. Li, "Triboelectric Nanogenerator for Droplet Energy Harvesting Based on Hydrophobic Composites," Materials, vol. 16, no. 15, Aug. 2023, doi: 10.3390/ma16155439.
- [171] L. Kang, C. Ma, J. Wang, X. Gao, and G. An, "PTFE/PVA-PVDF Conjugated Electrospun Nanofiber Membrane with Triboelectric Effect Used in Face Mask," Fibers and Polymers, vol. 24, no. 6, pp. 1975–1982, Jun. 2023, doi: 10.1007/s12221-023-00206-8.
- [172] C. Iumsrivun, T. Yui, A. Yokoyama, and Y. Ishii, "Quasistatic direct electromechanical responses from as-electrospun submicron/micron fiber mats of several polymers," Polymer (Guildf), vol. 224, May 2021, doi: 10.1016/j.polymer.2021.123732.
- [173] Y. Ishii, "Investigation of electromechanical properties of as-electrospun polystyrene fiber mat via sequential approaching/loading technique," Sens Actuators A Phys, vol. 326, Aug. 2021, doi: 10.1016/j.sna.2021.112717.
- [174] Y. Ishii et al., "Electromechanically Active As-Electrospun Polystyrene Fiber Mat:
 Significantly High Quasistatic/Dynamic Electromechanical Response and Theoretical
 Modeling," Macromol Rapid Commun, vol. 41, no. 14, Jul. 2020, doi:
 10.1002/marc.202000218.
- [175] Y. Ishii and S. Kurihara, "Charge generation from as-electrospun polystyrene fiber mat with uncontacted/contacted electrode," Appl Phys Lett, vol. 115, no. 20, Nov. 2019, doi: 10.1063/1.5126777.
- [176] J. Lee and J. Kim, "Material properties influencing the charge decay of electret filters and their impact on filtration performance," Polymers (Basel), vol. 12, no. 3, Mar. 2020, doi: 10.3390/polym12030721.

- [177] T. Nobeshima, Y. Ishii, H. Sakai, S. Uemura, and M. Yoshida, "Actuation behavior of polylactic acid fiber films prepared by electrospinning," J Nanosci Nanotechnol, vol. 16, no. 4, pp. 3343–3348, Apr. 2016, doi: 10.1166/jnn.2016.12296.
- [178] T. Nobeshima, Y. Ishii, H. Sakai, S. Uemura, and M. Yoshida, "Electrospun poly(methyl methacrylate) fibrous mat showing piezoelectric properties," in Japanese Journal of Applied Physics, Japan Society of Applied Physics, May 2018. doi: 10.7567/JJAP.57.05GC06.
- [179] W. Wang et al., "Unexpectedly high piezoelectricity of electrospun polyacrylonitrile nanofiber membranes," Nano Energy, vol. 56, pp. 588–594, Feb. 2019, doi: 10.1016/j.nanoen.2018.11.082.
- [180] S. Zhukov et al., "Microenergy Harvesters Based on Fluorinated Ethylene Propylene Piezotubes," Adv Eng Mater, vol. 22, no. 5, May 2020, doi: 10.1002/adem.201901399.
- [181] S. Zhukov, D. Eder-Goy, C. Biethan, S. Fedosov, B. X. Xu, and H. Von Seggern, "Tubular fluoropolymer arrays with high piezoelectric response," Smart Mater Struct, vol. 27, no. 1, Jan. 2018, doi: 10.1088/1361-665X/aa9a63.
- [182] S. Zhukov, D. Eder-Goy, S. Fedosov, B. X. Xu, and H. Von Seggern, "Analytical prediction of the piezoelectric d 33 response of fluoropolymer arrays with tubular air channels," Sci Rep, vol. 8, no. 1, Dec. 2018, doi: 10.1038/s41598-018-22918-1.
- [183] N. Cui et al., "Dynamic Behavior of the Triboelectric Charges and Structural Optimization of the Friction Layer for a Triboelectric Nanogenerator," ACS Nano, vol. 10, no. 6, pp. 6131–6138, Jun. 2016, doi: 10.1021/acsnano.6b02076.
- [184] Y. Li, X. Yin, Y. Si, J. Yu, and B. Ding, "All-polymer hybrid electret fibers for high-efficiency and low-resistance filter media," Chemical Engineering Journal, vol. 398, Oct. 2020, doi: 10.1016/j.cej.2020.125626.
- [185] X. Y. Zhao, H. J. Liu, and M. Z. Wang, "Polymer dielectric materials," in Recent Advances in Dielectric Materials, Nova Science Publishers, Inc., 2009, pp. 323–368. doi: 10.5772/50638.
- [186] "Introduction to Fourier Transform Infrared Spectrometry," 2001.
- [187] E. Motyl and B. Łowkis, "Effect of Air Humidity on Charge Decay and lifetime of PP electret nonwovens," FIBRES & TEXTILES in Eastern Europe, vol. 14, no. 5 (59), pp. 39–42, Jan. 2006.

- [188] A. I. T. W. C. Simco, "INSTRUCTIONS Operation/Maintenance FMX-003 Electrostatic Fieldmeter," Jun. 2005. [Online]. Available: www.simcolON.biz
- [189] B. D. Bertram, J. H. Agui, R. A. Kelsch, G. M. Berger, and R. D. Green, "Charging Experiments and Filtration Testing on Facemask Materials Towards Goals of Full Performance Restoration of Used N95 Masks and Enhancement of Common-Fabric Facemasks," 2022. [Online]. Available: http://www.sti.nasa.gov
- [190] Z. Shao, J. Jiang, X. Wang, W. Li, L. Fang, and G. Zheng, "Self-powered electrospun composite nanofiber membrane for highly efficient air filtration," Nanomaterials, vol. 10, no. 9, pp. 1–9, Sep. 2020, doi: 10.3390/nano10091706.
- [191] C. Te Wang et al., "Experimental investigation of the filtration characteristics of charged porous fibers," Aerosol Air Qual Res, vol. 18, no. 6, pp. 1470–1482, Jun. 2018, doi: 10.4209/aaqr.2017.12.0582.
- [192] W. Sambaer, M. Zatloukal, and D. Kimmer, "3D air filtration modeling for nanofiber based filters in the ultrafine particle size range," in AIP Conference Proceedings, 2011, pp. 320–323. doi: 10.1063/1.3604492.
- [193] N. Yan, T. Gao, L. Hua, F. Xie, R.-X. Liu, and Z.-Q. Lu, "Highly electrostatic cellulose acetate-based composite electret nanofiber film for air filtration applications," Aug. 12, 2024. doi: 10.21203/rs.3.rs-4741981/v1.
- [194] K. Kakutani et al., "An electric field screen prevents captured insects from escaping by depriving bioelectricity generated through insect movements," J Electrostat, vol. 70, no. 2, pp. 207–211, Apr. 2012, doi: 10.1016/j.elstat.2012.01.002.
- [195] Y. Kim, X. Wu, and J. H. Oh, "Fabrication of triboelectric nanogenerators based on electrospun polyimide nanofibers membrane," Sci Rep, vol. 10, no. 1, Dec. 2020, doi: 10.1038/s41598-020-59546-7.
- [196] J. Jeong, B. Yoo, E. Jang, I. Choi, and J. Lee, "Metal Electrode Polarization in Triboelectric Nanogenerator Probed by Surface Charge Neutralization," Nanoscale Res Lett, vol. 17, no. 1, 2022, doi: 10.1186/s11671-022-03682-8.
- [197] J. Jeong, J. Ko, and J. Lee, "Dual polarity open circuit voltage in triboelectric nanogenerators originated from two states series impedance," Discover Nano, vol. 19, no. 1, Dec. 2024, doi: 10.1186/s11671-024-04056-y.

- [198] M. Stewart, W. Battrick, and M. Cain, "Measurement Good Practice Guide No. 44 Measuring Piezoelectric d 33 coefficients using the Direct Method Measuring Piezoelectric d 33 coefficients using the Direct Method Contents," 2001.
- [199] N. A. Hoque et al., "Er3+/Fe3+ Stimulated Electroactive, Visible Light Emitting, and High Dielectric Flexible PVDF Film Based Piezoelectric Nanogenerators: A Simple and Superior Self-Powered Energy Harvester with Remarkable Power Density," ACS Appl Mater Interfaces, vol. 9, no. 27, pp. 23048–23059, Jul. 2017, doi: 10.1021/acsami.7b08008.
- [200] S. K. Ghosh, M. Xie, C. R. Bowen, P. R. Davies, D. J. Morgan, and D. Mandal, "A hybrid strain and thermal energy harvester based on an infra-red sensitive Er3+ modified poly(vinylidene fluoride) ferroelectret structure," Sci Rep, vol. 7, no. 1, Dec. 2017, doi: 10.1038/s41598-017-16822-3.
- [201] J. W. Lee, B. U. Ye, and J. M. Baik, "Research Update: Recent progress in the development of effective dielectrics for high-output triboelectric nanogenerator," APL Mater, vol. 5, no. 7, Jul. 2017, doi: 10.1063/1.4979306.
- [202] P. Tofel et al., "Triboelectric Response of Electrospun Stratified PVDF and PA Structures," Nanomaterials, vol. 12, no. 3, Feb. 2022, doi: 10.3390/nano12030349.
- [203] X. Zhang, P. Pondrom, G. M. Sessler, and X. Ma, "Ferroelectret nanogenerator with large transverse piezoelectric activity," Nano Energy, vol. 50, pp. 52–61, Aug. 2018, doi: 10.1016/j.nanoen.2018.05.016.
- [204] Y. Hao, Y. Bin, H. Tao, W. Cheng, W. Hongzhi, and Z. Meifang, "Preparation and optimization of Polyvinylidene fluoride (PVDF) triboelectric nanogenerator via electrospinning," in the 15th IEEE International Conference on Nanotechnology, Rome, Italy: IEEE, Jul. 2015, pp. 1485–1488.
- [205] Y. Guo et al., "Triboelectric Nanogenerator-Based Near-Field Electrospinning System for Optimizing PVDF Fibers with High Piezoelectric Performance," ACS Appl Mater Interfaces, vol. 15, no. 4, pp. 5242–5252, Feb. 2023, doi: 10.1021/acsami.2c19568.
- [206] M. O. Shaikh, Y. Bin Huang, C. C. Wang, and C. H. Chuang, "Wearable woven triboelectric nanogenerator utilizing electrospun PVDF nanofibers for mechanical energy harvesting," Micromachines (Basel), vol. 10, no. 7, Jul. 2019, doi: 10.3390/mi10070438.
- [207] J. Xiong, P. Huo, and F. K. Ko, "Fabrication of ultrafine fibrous polytetrafluoroethylene porous membranes by electrospinning," J Mater Res, vol. 24, no. 9, pp. 2755–2761, Sep. 2009, doi: 10.1557/jmr.2009.0347.

- [208] P. Zhao et al., "Emulsion Electrospinning of Polytetrafluoroethylene (PTFE) Nanofibrous Membranes for High-Performance Triboelectric Nanogenerators," ACS Appl Mater Interfaces, vol. 10, no. 6, pp. 5880–5891, Feb. 2018, doi: 10.1021/acsami.7b18442.
- [209] Z. Q. Dong, X. hua Ma, Z. L. Xu, W. T. You, and F. bing Li, "Superhydrophobic PVDF-PTFE electrospun nanofibrous membranes for desalination by vacuum membrane distillation," Desalination, vol. 347, pp. 175–183, Aug. 2014, doi: 10.1016/j.desal.2014.05.015.
- [210] S. Wang, X. Zhao, X. Yin, J. Yu, and B. Ding, "Electret Polyvinylidene Fluoride Nanofibers Hybridized by Polytetrafluoroethylene Nanoparticles for High-Efficiency Air Filtration," ACS Appl Mater Interfaces, vol. 8, no. 36, pp. 23985–23994, Sep. 2016, doi: 10.1021/acsami.6b08262.
- [211] K. Aracélly et al., "Evaluation of the electromechanical behavior of polyvinylidene fluoride used as a component of risers in the offshore oil industry," Oil & Gas Science and Technology, vol. 73, no. Rev. IFP Energies nouvelles 7, 2018, doi: 10.2516/ogst/2018058.
- [212] B. S. Lee et al., "Effects of substrate on piezoelectricity of electrospun poly(vinylidene fluoride)-nanofiber-based energy generators," ACS Appl Mater Interfaces, vol. 6, no. 5, pp. 3520–3527, Mar. 2014, doi: 10.1021/am405684m.
- [213] J. Piwowarczyk, R. Jedrzejewski, D. Moszyński, K. Kwiatkowski, A. Niemczyk, and J. Baranowska, "XPS and FTIR studies of polytetrafluoroethylene thin films obtained by physical methods," Polymers (Basel), vol. 11, no. 10, Oct. 2019, doi: 10.3390/polym11101629.
- [214] J. Mihály et al., "FTIR and FT-Raman Spectroscopic Study on Polymer Based High Pressure Digestion Vessels."
- [215] A. Barylski et al., "Novel organic material induced by electron beam irradiation for medical application," Polymers (Basel), vol. 12, no. 2, Feb. 2020, doi: 10.3390/polym12020306.
- [216] B. Yang, W. Zeng, Z. H. Peng, S. R. Liu, K. Chen, and X. M. Tao, "A Fully Verified Theoretical Analysis of Contact-Mode Triboelectric Nanogenerators as a Wearable Power Source,"

 Adv Energy Mater, vol. 6, no. 16, Aug. 2016, doi: 10.1002/aenm.201600505.
- [217] H. Zhao et al., "Theoretical modeling of contact-separation mode triboelectric nanogenerators from initial charge distribution," Energy Environ Sci, vol. 17, no. 6, pp. 2228–2247, Feb. 2024, doi: 10.1039/d3ee04143c.

- [218] J. Xiong et al., "Skin-touch-actuated textile-based triboelectric nanogenerator with black phosphorus for durable biomechanical energy harvesting," Nat Commun, vol. 9, no. 1, Dec. 2018, doi: 10.1038/s41467-018-06759-0.
- [219] R. A. P. Altafim et al., "Template-based fluoroethylenepropylene piezoelectrets with tubular channels for transducer applications," J Appl Phys, vol. 106, no. 1, 2009, doi: 10.1063/1.3159039.
- [220] S. Zhukov et al., "Biodegradable cellular polylactic acid ferroelectrets with strong longitudinal and transverse piezoelectricity," Appl Phys Lett, vol. 117, no. 11, Sep. 2020, doi: 10.1063/5.0023153.
- [221] D. Lolla, M. Lolla, A. Abutaleb, H. U. Shin, D. H. Reneker, and G. G. Chase, "Fabrication, polarization of electrospun polyvinylidene fluoride electret fibers and effect on capturing nanoscale solid aerosols," Materials, vol. 9, no. 8, Aug. 2016, doi: 10.3390/ma9080671.
- [222] G. He et al., "Electrospun anatase-phase TiO2 nanofibers with different morphological structures and specific surface areas," J Colloid Interface Sci, vol. 398, pp. 103–111, May 2013, doi: 10.1016/j.jcis.2013.02.009.
- [223] S. K. Ghosh et al., "Electrospun gelatin nanofiber based self-powered bio-e-skin for health care monitoring," Nano Energy, vol. 36, pp. 166–175, Jun. 2017, doi: 10.1016/j.nanoen.2017.04.028.
- [224] Z. Li, X. Wang, Y. Hu, L. Li, and C. Wang, "Triboelectric properties of BaTiO3/polyimide nanocomposite film," Appl Surf Sci, vol. 572, Jan. 2022, doi: 10.1016/j.apsusc.2021.151391.
- [225] M. Wang, W. Zhao, X. Shi, T. Sun, J. Ju, and Y. Tang, "Multifunctional Monitoring System Based on BaTiO3@CMC Aerogel-Based Triboelectric Nanogenerator," J Electron Mater, vol. 52, no. 11, pp. 7124–7131, Nov. 2023, doi: 10.1007/s11664-023-10669-3.
- [226] J. Zhou et al., "Enhancing the Output Performance of a Triboelectric Nanogenerator Based on Modified Polyimide and Sandwich-Structured Nanocomposite Film," Nanomaterials, vol. 13, no. 6, Mar. 2023, doi: 10.3390/nano13061056.
- [227] Y. Dong et al., "Metallic MXenes: A new family of materials for flexible triboelectric nanogenerators," Nano Energy, vol. 44, pp. 103–110, Feb. 2018, doi: 10.1016/j.nanoen.2017.11.044.

- [228] D. Kim, S. B. Jeon, J. Y. Kim, M. L. Seol, S. O. Kim, and Y. K. Choi, "High-performance nanopattern triboelectric generator by block copolymer lithography," Nano Energy, vol. 12, pp. 331–338, Mar. 2015, doi: 10.1016/j.nanoen.2015.01.008.
- [229] C. Pinming et al., "Carbon nanotube/polydimethylsiloxane composite micropillar arrays using non-lithographic silicon nanowires as a template for performance enhancement of triboelectric nanogenerators," Nanotechnology, vol. 32, no. 9, Feb. 2021, doi: 10.1088/1361-6528/abcb7c.
- [230] Y. Hao, J. Huang, S. Liao, D. Chen, and Q. Wei, "All-electrospun performance-enhanced triboelectric nanogenerator based on the charge-storage process," J Mater Sci, vol. 57, no. 8, pp. 5334–5345, Feb. 2022, doi: 10.1007/s10853-022-06927-0.
- [231] G. Liu et al., "One-stop fabrication of triboelectric nanogenerator based on 3D printing," EcoMat, vol. 3, no. 5, Oct. 2021, doi: 10.1002/eom2.12130.
- [232] X. Sun et al., "Controlling the triboelectric properties and tribological behavior of polyimide materials via plasma treatment," Nano Energy, vol. 102, Nov. 2022, doi: 10.1016/j.nanoen.2022.107691.
- [233] K. H. Shobana, M. Suresh Kumar, K. S. Radha, and D. Mohan, "Preparation and characterization of pvdf/ps blend ultrafiltration membranes," Scholarly Journal of Engineering Research, vol. 1, no. 3, pp. 37–44, 2012, [Online]. Available: http://www.scholarly-journals.com/SJER
- [234] N. Gao et al., "β-Cyclodextrin functionalized coaxially electrospun poly(vinylidene fluoride)@ polystyrene membranes with higher mechanical performance for efficient removal of phenolphthalein," React Funct Polym, vol. 141, pp. 100–111, Aug. 2019, doi: 10.1016/j.reactfunctpolym.2019.05.001.
- [235] Z. Jiang et al., "Removal of oil from water using magnetic bicomponent composite nanofibers fabricated by electrospinning," Compos B Eng, vol. 77, pp. 311–318, Aug. 2015, doi: 10.1016/j.compositesb.2015.03.067.
- [236] C. Luo et al., "Preparation and application of high performance PVDF/PS electrospinning film-based triboelectric nanogenerator," Chem Phys Lett, vol. 813, Feb. 2023, doi: 10.1016/j.cplett.2022.140276.
- [237] J. Choi et al., "High β-phase Poly(vinylidene fluoride) Using a Thermally Decomposable Molecular Splint," Adv Electron Mater, vol. 9, no. 1, Jan. 2023, doi: 10.1002/aelm.202200279.